Numerical and Experimental Studies on Dynamic Load Testing of Open-ended Pipe Piles and its Applications

開端杭の動的載荷試験に関する解析的・実験的研究とその適用

Phan Ta Le

Sep, 2013

Dissertation

Numerical and Experimental Studies on Dynamic Load Testing of Open-ended Pipe Piles and its Applications

開端杭の動的載荷試験に関する解析的・実験的研究とその適用

Graduate School of
Natural Science and Technology
Kanazawa University

Division of Environmental Science and Engineering
Course: Environment Creation

School registration No.: 1023142420
Name: Phan Ta Le
Chief advisor: Matsumoto Tatsunori

Abstract

Open-ended pipe piles are widely used in practice for foundations of various structures in both on-land and offshore foundations. They transfer loads from a superstructure to a medium or dense stratum through soft soil layers. When driving an open-ended pipe pile into soils, a part of soils around a pile toe intrudes into inside the pile to form a soil column called soil plug. Theoretically, bearing capacity of an open-ended pipe pile can be calculated from outer shaft resistance, toe resistance and soil plug resistance. In practice, the bearing capacity of a pile can be determined from static load test (SLT) or dynamic load test (DLT). Static load tests are regarded as reliable methods but they are costly and time-consuming, compared to dynamic load tests. Due to the high cost and long test period, SLTs are preserved for large-budget and important projects, and the number of the test piles are usually limited to 1 to 2 % of the working piles. Meanwhile dynamic load tests are quick, low cost and very effective in offshore conditions. With the similar budget for testing, we can carry out up to 10% to 20% number of the working piles. Such larger number of test piles results in the high reliability of the whole foundation solution to the construction site in which soil conditions are varied from distance to distance, compared to the case with only a few static load tests.

Additionally, the accurate prediction of the driving response is a key factor to select a suitable hammer system that minimise the damage of the pile during driving. Also, it can help us to find out a suitable pile length with satisfying the requirements of both bearing capacity and settlement. In the dynamic load testing, wave matching analysis (WMA) plays a key role to identify soil properties and then to derive the static load-displacement relation. Conventionally, Smith's method, characteristic solutions of the wave equation and a finite differential scheme have been used for wave matching analysis of the one-dimensional stress wave propagation in a pile. However, when soil stiffness and velocity-dependent resistance have large values, these methods tend to show numerical instability. One of the reasons is that pile responses at current step in these methods are calculated based on the soil resistance mobilised at the previous calculation step. In other words, the pile behaviour and soil resistance are not fully coupled at a time step. More rigorous methods in which soils surrounding pile are regarded as a continuum media using finite element method, or

finite difference methods have been developed, but they are too computational expensive with computational time of several hours or days, resulting in the difficulty in using continuum methods in routine pile dynamic analysis in practice.

Therefore, a matrix form calculation procedure of the one-dimensional stress wave theory is proposed in this thesis to improve the above mentioned shortcomings. In the proposed numerical method, rational soil resistance models introduced by Randolph and Deeks (1992) are implemented. Effect of the wave propagation in the soil plug is modelled and taken into account. Furthermore, nonlinearity of soil stiffness and radiation damping in the soil models are considered. The proposed method can also be used for the analysis of static loading of the pile, if damping and inertia of the pile and the soil are neglected.

In order to verify the proposed numerical method, firstly, an open-ended pipe pile with soil resistance was analysed, and compared with results obtained from the Smith method and the rigorous continuum method, FLAC^{3D}. The analysed results showed that the proposed method has higher accuracy compared to the Smith method and shorter calculation time compared to the rigorous continuum method FLAC^{3D}. Secondly, verification of the proposed method was conducted by analysing the experimental results obtained from two series of static and dynamic load tests of an open-ended pipe pile and a close-ended pipe pile in model ground of dry sand. The proposed method predicted the static response of both piles with reasonable accuracy. Plugging mode of the open-ended pipe pile under static and dynamic loading conditions can also be simulated using the proposed method. Thirdly, the proposed method was used to analyses the static load tests (SLTs) and dynamic load tests (DLTs) of two open-ended steel pipe piles and two spun concrete piles in a construction site in Viet Nam. The analysed results showed that the static load-displacement curves derived from the final WMAs of DLTs were comparable with the results obtained from the SLTs. WMA using the proposed numerical approach well predicted the static load-displacement curves of the non-tested working piles based on the identified soil parameters of the tested piles. Also, from calculated analyses using the proposed method, the piles which have been subjected to cyclic loading had smaller yield and ultimate capacities compared to the piles subjected to monotonic loading. Finally, the proposed method reasonably estimated static cone resistance of the dynamic cone penetration tests with dynamic measurements.

Acknowledgments

This thesis would not have been possible without the great support and cooperation of many individuals during 3 years of study and research in Geotechnical Laboratory of the Kanazawa University. It is an honour for me to express my sincere words here.

First of all, it would like to express my deepest gratitude to my supervisor, Professor Tatsunori Matsumoto, for his sincere support, valuable discussions and experienced guidance on my study. This thesis would not have been possible without his dedicated help. Under his enthusiastic supervision, I have learnt a lot of things from how to prepare and write a technical paper as well as a thesis to how to present effectively in an international conference. I was also very impressed and admired by his profound knowledge and great interest in doing research.

I wish to express my sincere thankfulness to Associate Professor Shun-ichi Kobayashi for his kind guidance, valuable comments and various informative ideas on my research.

I also would like to show my gratitude to Prof. Hiroshi Masuya, Prof. Masakatsu Miyajima and Prof. Shinichi Igarashi for their valuable comments on my thesis and their serving as members of my doctoral examination committee.

Special appreciations are going to Mr Shinya Shimono, technician of the Geotechnical Laboratory, and other students for many supports in my experimental work and my living. I highly appreciate to all the dedicated supports from staff of Kanazawa University.

I am also indebted to the scholarship sponsor, Vietnamese government, who supports all of the expense for my living and studying for 3 years in Japan.

Lastly, from my heart, I would like to express my cordially thanks to my beloved wife, who takes care of my children instead of me and continuously encourage me during my study in Japan. I also highly appreciate to my parents, my brothers and my sisters for all their supports and encouragements at all time.

PHAN TA LE

Contents

List of Figures

List of Tables

Chapter 1

Introduction

In this introduction chapter, the background and motivation of the thesis is explained firstly. Then, the objective of the thesis is presented. Finally, the organization of the thesis is given in the last section of the chapter.

1.1 Background and motivation

Pile foundations are predominantly employed to transfer large superstructure loads to the ground at sites where shallow foundations cannot be used due to the existence of soft clay or loose sand layers. They may be required to carry uplift loads when used to support tall structures subjected to overturning forces from winds. Piles used in offshore conditions are usually subjected to lateral loads from the impact of berthing ships and from waves. Combinations of vertical and horizontal loads are carried where piles are used to support retaining walls, bridge piers and abutments, and machinery foundations. In terms of subjecting to compressive axial load, the capacity of the pile is the sum of two components, namely shaft friction and base resistance. In case of an open-ended pipe pile, the capacity of the pile consists of three components: outer shaft resistance, pile tip resistance and soil plug base resistance. A pile in which the shaft-frictional component predominates is known as a friction pile, while a pile bearing on rock or some other hard incompressible ground is known as an end-bearing pile.

The mobilisation of limit shaft resistance requires small pile head displacements (about 0.2 to 0.5 % of the pile diameter), whereas much larger head displacements (about 2 to 4 %, even up to 5 to 10 % of the pile diameter in case of nonlinear soil response) are required for full mobilisation of base resistance. Depending on the installation method, most piles are

categorised into two main types: non-displacement piles or displacement piles. Non-displacement piles are cast-in-place piles installed by first removing the soil by a drilling process and then constructing the pile by pouring concrete or grout in the created void space. This installation process causes only small disturbance to the surrounding soil, nearly remaining the initial stress state and soil density. Meanwhile, displacement piles are inserted into the ground by driving or jacking without prior removal of the soil from the ground. This process make the soil reduce the void ratio and generate the high excess pore-water pressure, resulting in the remarkable change of the initial stress state and soil density. Generally, displacement piles have larger capacity than non-displacement piles with the same pile configurations.

Regardless of pile types, the methods used for the determination of pile capacity prior to their installations are categorised into two main methods:

1) Methods based on soil properties determined from laboratory tests.

2) Methods based on in situ tests such as SPT, CPT or DCPT

These design methods are regarded as the so-called static methods. Although pile foundations are very common today and usually employed for supporting heavy and important structures, the most popular and well established methods for the determination of the shaft and base resistances in practice still contain a significant degree of uncertainty and base on the empirical equations, which limits their effectiveness and the wideness of their applicability. As a consequence, foundation engineers often rely on dynamic or static pile testing for verifying the pile capacity and re-evaluating the foundation design prior to construction.

At present, the most common pile load test methods are static load tests (SLTs) and dynamic pile load tests (DLTs). Although SLTs are simple in concept, they are costly, time-consuming and usually used for large-budget and important projects. In DLT, pile acceleration and axial strain at the pile head are recorded during driving in a very short period, about 0.1 s. Then, pile head velocity and displacement histories are calculated from the measured acceleration history through numerical integration technique. Meanwhile, the measured strain is used for calculating the axial force history at the pile head. Wave matching analysis is conducted to identify the soil parameters and then to derive the static load-displacement relation. As far as known, determination of the pile capacity from static pile tests is simple, direct and straightforward. However, only about 1 to 2 % of working piles are selected for the SLT, resulting in a low reliability of the whole foundation solution to the construction sites in which soil condition varies from distance to distance. In these situations, number of the test piles has to increase in order to ensure the reliability of the whole foundation solution. In this aspect, DLT is a promising testing method due to its low cost and short test period. With the

similar budget for testing, number of DLTs test can increase up to 10 to 20% of the working piles, resulting in a high reliability of the whole foundation solution. In other words, we can reduce factor of safety or cut down the cost of the project without reduction of safety of the foundation solution. Therefore, research on dynamic analysis of DLTs is essential to seek for an efficient foundation solution to the structure. Although DLT is quick and efficient compared to SLT, pile capacity estimated from dynamic load tests has always been more challenging and require sophisticated dynamic analysis.

Early efforts in pile dynamics with consideration of the propagation of the one-dimensional stress wave in a pile was made by Smith (1960). In this approach, the pile was modelled as a series of lumped masses interconnected by massless linear springs and the problem was solved using numerical integration technique. In the following decades, several improvements were made to the original work by Smith (e.g. Goble and Rausche 1976, Simons and Randolph 1985, Lee et al. 1988, Rausche et al. 1994, Hussein et al. 1995). Alternative techniques were also proposed for analysing pile driving, such as finite element analysis (e.g. Borja 1988, Nath 1990, Deeks 1992, Mabsout et al. 1995, Liyanapathirana et al. 2000, Masouleh and Fakharian 2007), closed-form solutions (e.g. Hansen and Denver 1980, Uto et al. 1985, Wang 1988, Warrington 1997), characteristic solutions (e.g. De Josselin De Jong 1956, Coyle and Gibson 1970, Heerema 1979, Van Koten et al. 1980, Middendorp and van Weele 1986, Matsumoto and Takei 1991, Courage and van Foeken 1992, Foeken et al. 1996) or finite difference scheme (Wakisaka and Matsumoto 2004).

At present, there are some computer programs using different methods developed for pile driving analysis based on the one-dimensional stress-wave propagation in a single pile. For example, CAPWAP (Goble et al 1976, Rausche et al. 1985) uses Smith method, TNOWAVE (Middendorp et al. 1986), KWAVE (Matsumoto et al. 1991) use characteristic solution, KWAVEFD (Wakasaki et al. 2004) uses finite difference scheme. However, they have still limitations because the pile behaviours and soil resistances in these methods are not fully coupled at a time step. Paik et al. (2003) found that although a good matching is obtained from WMA using CAPWAP program, it still underestimates significantly the load capacity of both closed- and open-ended piles for the conditions investigated by these authors. Beside of limitations of the current WMA due to the numerical method, this might also cause by the soil resistance models or numerical modelling of pile-soil system. Hence, it is needed to improve in the numerical approach with appropriate numerical modelling and realistic soil resistance models to enhance the reliability of the current dynamic analysis.

1.2 Objective

The main objectives of this research are provided as follows:

1. Improve the limitations in the current pile dynamic analysis by proposing a numerical method using a matrix form to analyse the phenomenon of wave propagation in an open-ended pipe pile within a framework of one-dimensional stress-wave theory.
2. Reveal the reliability and higher accuracy of the proposed method compared to the conventional methods through verification work which starts from numerical analysis to analyses of small-scale model tests and full-scale tests.
3. Demonstrate the advantage of dynamic cone penetration tests (DCPTs) with dynamic measurements as well as use the proposed numerical method for identifying the soil resistance acting on the driving rod and cone tip of DCPTs.

1.3 Thesis structure

The thesis consists of the following chapters

Chapter 1 is the introduction chapter of this thesis.

Chapter 2 deals with related research works. Section 2.1 briefly summarised the current pile dynamic analysis methods. Then, mechanisms of soil resistance mobilised along pile shaft and at the pile tip were presented. After that, soil resistance models used in pile driving analysis were reviewed and discussed.

Chapter 3 presents a numerical method based on the one-dimensional stress-wave theory using the rational soil models with some modifications proposed by the authors such as non-linearity of soil stiffness and radiation damping. In order to validate the proposed numerical method, some numerical analyses were conducted by comparison the calculated results with those obtained from the theoretical solution, Smith's method and FLAC^{3D} calculation.

In **Chapter 4**, further validation was conducted using a small scale model in laboratory. First, element tests were carried out to determine initial soil parameters that would be used in dynamic analysis. Second, two series of pile load tests of open-ended and close-ended pipe piles were conducted under static and dynamic loading conditions. From the measured dynamic signals, wave matching analyses were performed to identify the soil parameters that are used to derive the static load-displacement curve and then to compare with the measured static response. Influence of the small size of the model ground on pile behaviour is also discussed. Sensitivity analysis was conducted for the case of close-ended pile in order to investigate the variation of the soil response due to variation of the soil parameters.

In **Chapter 5**, the proposed numerical method was used to analyse a case study of dynamic and static load tests of open-ended steel pipe piles and spun concrete piles of a berth structure at Thi Vai International port in Viet Nam. First, the site and test description was briefly presented. Then wave matching analysis was performed for two test piles to identify the soil parameters. The identified values were used to derive the static responses and compared with those obtained from the SLTs. In addition, the identified values were also used to predict the other two test piles having different configurations and soil profiles. The influence of the numbers of loading processes in SLT on the pile capacity of the open-ended steel pipe pile which is reused after the test was investigated through calculated analysis.

Chapter 6 presents an application of the proposed numerical method to the dynamic cone penetration test. Measured dynamic signals of various types of dynamic cone penetration tests (DCPTs) and a standard penetration test (SPT) in Shiga prefecture, Japan were used to demonstrate the advantage of the DCPT and the SPT with dynamic measurement.

Chapter 7 is the conclusions of this research. The main findings of the theses are summarised. Recommendations for further study were also provided.

Reference

Borja R.I. (1988). Dynamics of pile driving by the finite element method. Computers and Geotechnics; 5(11): 39-49.

Courage W.M.G. and Van Foeken R.J. (1992). TNOWAVE automatic signal matching for dynamic load testing. Proceeding of the 4th International Conference on the Application of Stress-Wave Theory to Piles, The Hague, The Netherlands; 241-246.

Coyle H.M. and Gibson G.C. (1970). Empirical damping constants for sands and clays. Journal, Soil Mechanics and Foundations Division; 96(SM3): 949-965.

Deeks A.J. (1992). Numerical analysis of pile driving dynamics. Ph.D. Thesis, University of Western Australia.

De Josselin De Jong G. (1956). Wat gebeurt er in de grond tijdens het heien. De Ingenieur, 25, Breda, The Netherlands.

Foeken van R.J., Daniels B., and Middendorp P. (1996). An improved method for the real time calculation of soil resistance during driving. Proceeding of the 5th International Conference on the Application of Stress-Wave Theory to Piles, Orlando, Florida, USA; 1132-1143.

Goble G.G. and Rausche F. (1976). Wave equation analysis of pile driving, WEAP Program. Federal Highway Administration Report FHWA-IP-76-14.

Hansen B. and Denver H. (1980). Wave equation analysis of a pile - An analytic model. Proceeding of the International Seminar on the Application of Stress-Wave Theory on Piles, Stockholm; 3-22.

Heerema E.P. (1979). Relationships between wall friction, displacement, velocity and horizontal stress in clay and in sand for pile driveability analysis. Ground Engineering; 12(1): 55-61.

Hussein M., Rausche F. and Likins G. (1995). Computer-based wave equation analysis of pile driveability. Proceeding of the Second Congress on Computing in Civil Engineering, Atlanta, Georgia, USA; 2: 915-926.

Lee S.L., Chow Y.K., Karunaratne G.P. and Wong K.Y. (1988). Rational wave equation model for pile driving analysis. Journal of Geotechnical Engineering; 114(3): 306-325.

Liyanapathirana D.S., Deeks A.J. and Randolph M.F. (2000). Numerical modelling of large deformations associated with driving of open-ended piles. International Journal for Numerical and Analytical Methods in Geomechanics; 24: 1079-1101.

Mabsout M., Reese L., and Tassoulas J. (1995). A study of pile driving by the finite element method. Journal of Geotechnical Engineering, ASCE; 121(7): 535-543.

Masouleh S. F. and Fakharian K. (2007). Application of a continuum numerical model for pile driving analysis and comparison with a real case. Computers and Geotechnics; 35(3): 406-418.

Matsumoto T. and Takei M. (1991). Effects of soil plug on behaviour of driven pipe piles. Soils and Foundations; 31(2): 14-34.

Middendorp P. and Van Weele A.F. (1986). Application of characteristic stress wave method in offshore practice. Proceeding of the 3rd International Conference on Numerical Methods in Offshore Piling, Nantes, Supplement; 6-18.

Nath B. (1990). A continuum method of pile driving analysis: Comparison with the wave equation method. Computers and Geotechnics; 10(4): 265-285.

Paikowsky S.G. (1982). Use of dynamic measurements to predict pile capacity under local conditions. M.Sc. Thesis, Department of Civil Engineering, Technion-Israel Institute of Technology.

Paikowsky S.G. and Whitman R.V. (1990). The effects of plugging on pile performance and design. Canadian Geotechincal Journal; 27: 429-440.

Paikowsky S.G. and Chernauskas L.R. (2008). Dynamic analysis of open-ended pipe pile. Proceeding of the 8th International Conference on the Application of Stress Wave Theory to Piles, Lisbon; 59-76.

Paik K., Salgado R., Lee J. and Kim B. (2003). Behaviour of open- and closed-ended piles driven into sand. Journal of Geotechnical and Geo-environmental Engineering, ASCE; 129(4): 296-306.

Randolph M.F. and Deeks A.J. (1992). Dynamic and static soil models for axial response. Proceeding of the 4th International Conference on the Application of Stress Wave Theory to Piles, The Hague; 3-14.

Rausche F., Goble G.G. and Likins G. (1985). Dynamic determination of pile capacity. Journal of Geotechnical Engineering; 111(3): 367-383.

Rausche F., Likins G. and Goble G.G. (1994). A Rational and usable wave equation soil model based on field test correlations. Proceedings, FHWA International Conference on Design and Construction of Deep Foundations, Orlando, Florida, USA.

Simons H.A. and Randolph M.F. (1985). A new approach to one-dimensional pile driving analysis. Proceeding of the 5th International Conference on Numerical. Methods in Geomechanics, Nagoya; 3: 1457-1464.

Smith E.A.L. (1960). Pile driving analysis by the wave equation. Journal, Soil Mechanics and Foundations Division; 86(EM 4): 35-61.

Uto K., Fuyuki M. and Sakurai M. (1985). An equation for the dynamic bearing capacity of a pile based on wave theory. Proceeding of the International Symposium on Penetrability and Drivability of Piles, San Francisco.

Van Koten H., Middendorp P. and Van Brederode P. (1980). An analysis of dissipative wave propagation in a pile. Proceeding of the International Conference on the Application of Stress-Wave Theory to Piles, Stockholm; 23-40.

Wakisaka T., Matsumoto T., Kojima E. and Kuwayama S. (2004). Development of a new computer program for dynamic and static pile load tests. Proceeding of the 7th International Conference on the Application of Stress-Wave Theory to Piles, Selangor, Malaysia; 341-350.

Wang Y.X. (1988). Determination of capacity of shaft bearing piles using the wave equation. Proceeding of the 3rd International Conference on the Application of Stress-Wave Theory to Piles, Vancouver, Canada; 337-342.

Warrington D.C. (1997). Closed form solution of the wave equation for piles. Master's Thesis, University of Tennessee at Chattanooga.

Chapter 2

Literature review

In this chapter, current dynamic pile analysis method is reviewed firstly. Then, the mechanism of soil resistance mobilised along pile shaft and base is briefly presented. After that resistance soil models for dynamic pile analysis are summarised. Finally, information obtained from the related researches encourages the author developing a numerical method to analyse the one-dimensional stress-wave propagation in an open-ended pipe pile.

2.1 Dynamic pile analysis method

The idea of using the observed pile response during driving for estimating the static pile capacity has been in existence for several decades. In term of determination of the pile capacity, static load test considers the most reliable method. However, it requires high cost and long test period, compared to dynamic load test. Hence, the use of dynamic pile analysis is often attractive for this purpose. The observed pile response during driving can be interpreted using either empirical closed-form equations or wave equation analysis.

The early empirical equations are based on a simple concept of conservation of energy: the energy transmitted to the pile head by the hammer is equal to the work done by the total pile capacity for the observed pile head displacement plus the energy dissipated inside the soil and the pile after a single blow. This can be written as below:

$$R_{\mathrm{u,dyn}} = \frac{\eta W_{\mathrm{h}} H}{(S + S_{\mathrm{c}})} \tag{2.1}$$

where W_{h} is the hammer weight, H is the hammer drop height, η is the efficiency of the driving system, $R_{\mathrm{u,dyn}}$ is the total, dynamic pile capacity, S is the observed pile set, and S_{c} is an

empirical constant expressing the energy dissipated in the pile. This above equation has been used as the basis of many empirical dynamic equations.

The Engineering News (ENR) formula, which has been in use for more than a century, assumes a constant S_c to be equal to 2.54 mm for an air, a steam or a diesel hammer, and equal to 25.4 mm for drop hammer. A safety factor of FS = 6.0 is recommended for estimating the allowable capacity or design working load.

Another popular equation used in the United States is Gates' formula:

$$R_{\mathrm{u,dyn}} = 7\sqrt{W_{\mathrm{h}} H}\,\log(10 N_{\mathrm{b}}) - 550 \ \text{(kN)} \tag{2.2}$$

where N_b is number of hammer blows per 25 mm at final penetration. A safety factor of FS = 3.5 is recommended for this formula.

Modified Hiley Formula is also widely used in practice in Asia region for estimation of the dynamic pile capacity.

$$R_{\mathrm{u,dyn}} = \frac{9.81 \times \eta \times W_{\mathrm{h}} \times H}{S + S_{\mathrm{c}}/2} \times \frac{W_{\mathrm{h}} + c_{\mathrm{cor}}^2 W_{\mathrm{p}}}{W_{\mathrm{h}} + W_{\mathrm{p}}} \ \text{(kN)} \tag{2.3}$$

in which η is the efficiency of the driving hammer varying from 0.8 to 1.0, c_{cor} is coefficient of restitution ranging from 0.4 to 0.5 for most cases. W_p is the weight of pile including helmet, anvil and cushion. A safety factor of FS = 3.0 is recommended for this formula.

Although empirical dynamic formulas are easy to use, their predictions are considerably scatter and, in some case, controversial. Hannigan et al. (1996) concluded that "Whether simple or more comprehensive dynamic formulas are used, pile capacities determined from dynamic formulas have shown poor correlations and wide scatter when statistically compared with static load test result. Therefore, except where well supported empirical correlations under a given set of physical and geological conditions are available, dynamic formulas should not be used". New attempts improve the pile driving formulas. For example, Paikowsky and Chernauskas (1992) used an energy approach with dynamic measurement to predict the static capacity and maximum resistance. Based on a study of 14 cases, related to 9 different piles in 3 different sites, the results indicated that this approach was well predicted the pile capacity compared to the results obtained from the static load test. Although the result was good for these particular sites, it was shown to still suffer from drawbacks due to the following reasons. First, the dynamic formulas assume a rigid pile, thus resistance is constant and

instantaneous to the impact force. Second, most formulas only consider the kinetic energy of the driving system which includes many components such as ram, anvil, helmet, and cushion. Third, the soil resistance is assumed untreated that it is a constant force. This assumption neglects variation of the soil response during driving. Dynamic formulas also cannot estimate the deformation of the pile. Besides that, driving problem is a very highly nonlinear wave propagation problem involving complicated physics and mechanics.

Consideration of empirical formulas nowadays offer little benefit to deep foundation design since the factor of safety (*FS*) recommended in these formulas exceeds the values that typically used for designing based on static methods. Therefore, the use of the more accurate method, wave equation, in the field of pile driving analysis is needed for further potential advancements.

The first pile driving analysis is based on measurements of the stress waves occurring in the pile while driving, called Pile Driving Analyser (PDA). The PDA method is used for determining pile capacity based on the temporal variation of pile head force and velocity. The PDA monitors instrumentation attached to the pile head, and measurements of strain and acceleration are recorded with respect to time. Strain measurements are used to calculate pile axial force, and acceleration measurements are converted to velocities using numerical integration approach. A simple dynamic model (CASE model) is applied to estimate the pile capacity using the Eq. (2.4) which was derived from a closed form solution to the one dimensional stress-wave propagation theory. The calculations for the CASE model are simple to estimate static pile capacity during pile driving operations. PDA measurements are used to estimate total pile capacity as:

$$R_{\mathrm{u,dyn}} = \frac{F_{t1} + V_{t1}Z}{2} + \frac{F_{t1+2L/c} - V_{t1+2L/c}Z}{2} \tag{2.4}$$

where $R_{\mathrm{u,dyn}}$ is the total, dynamic pile resistance, F_{t1} is the measured force at the time t_1, $F_{t1+2L/c}$ is the measured force at the time t_1+2L/c, V_{t1} is the measured velocity at the time t_1, $V_{t1+2L/c}$ is the measured velocity at the time t_1+2L/c, L is the length of the pile, c is the speed of wave propagation in the pile, and $Z = EA/c$ is the pile mechanical impedance. The value, 2L/c, is the time required for a wave travelling to the pile tip and back, which is called "return travelling time". Terms for force and velocity are illustrated in Fig. 2.1.

The total pile resistance, $R_{\mathrm{u,dyn}}$, includes a static and dynamic component of resistance. Therefore, the total pile resistance is:

$$R_{\mathrm{u,dyn}} = R_{\mathrm{static}} + R_{\mathrm{dynamic}} \tag{2.5}$$

in which R_{static} and R_{dynamic} are the static and dynamic resistances, respectively. The dynamic resistance is assumed to be viscous and therefore it is velocity dependent. The dynamic resistance is then estimated as:

$$R_{\mathrm{dynamic}} = J_{\mathrm{c}} Z V_{\mathrm{tip}} \tag{2.6}$$

where J_{c} is the CASE damping constant based on soil type near the pile tip as indicated in Table 2.1 and V_{tip} is the velocity of the pile tip which can be estimated from PDA measurements of force and velocity as:

$$V_{\mathrm{tip}} = (F_{t1} + V_{t1} Z - R_{\mathrm{u,dyn}}) / Z \tag{2.7}$$

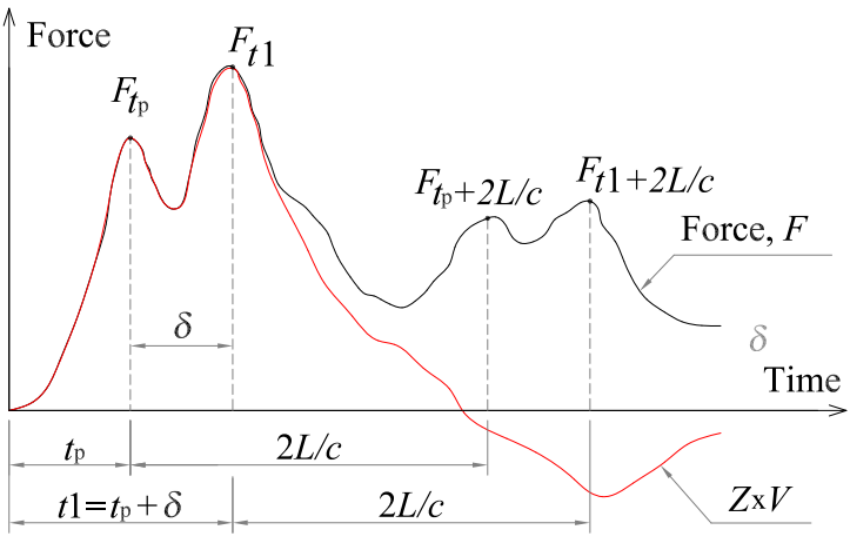

Figure 2.1. Standard, RSP and Maximum, RMX, Case Method Capacity Estimates

Table 2.1. CASE damping factors for estimation of static capacity

Soil type at the pile tip	Original CASE damping (Goble et al. 1975)	Updated CASE damping (Pile Dynamic 1996)
Clean sand	0.05 – 0.20	0.10 – 0.15
Silty sand or Sand silt	0.15 – 0.30	0.15 – 0.25
Silt	0.20 – 0.45	0.25 – 0.40
Silty clay or Clayey silt	0.40 – 0.70	0.40 – 0.70
Clay	0.60 – 1.10	> 0.70

Substituting Eqs. (2.6) and (2.7) into Eq. (2.5) and rearranging terms results in the expression for static load capacity of the pile as:

$$R_{\text{static}} = R_{\text{u,dyn}} - J_{\text{c}}(F_{t1} + V_{t1}Z - R_{\text{u,dyn}}) \tag{2.8}$$

The calculated value of $R_{\text{u,dyn}}$ can vary depending on the selection of t_1 which can occur at some time after initial impact:

$$t_1 = t_{\text{p}} + \delta \tag{2.9}$$

where t_{p} is the time of impact peak, and δ is the time delay for obtaining the maximum value of R_{static}. The two most common CASE methods are the RSP method and the RMX method. The RSP method uses the time of impact as t_1 (corresponds to $\delta = 0$ in Eq. (2.9)). The RMX method varies δ to obtain the maximum value of R_{static}.

The RMX and RSP Case Method equations are the two most commonly used solutions for field evaluation of pile capacity, however, it still remain some drawbacks due to assumptions of uniform pile and the constant value of the empirical damping factor, J_{c}. Hence, a more rigorous numerical analysis procedure based on the wave equation with the use of measured dynamic records is needed to identify the soil parameters through wave matching analysis, and then to derive the static load-displacement relation which is used for pile foundation design.

Following this line, the first method employed in wave equation analysis for pile dynamics was the method of characteristics (De Josselin De Jong 1956). This method is a semi-analytical method, in which the pile is treated as an un-discretised continuum media. Early application of the method of characteristics in pile driving analysis assumed that all soil reactions are concentrated at the pile tip. Later, reaction along the shaft was introduced as a fixed analytical function independent of displacement or velocity. The software TNOWAVE developed by the research organisation TNO (Middendorp et al. 1986) in Netherlands and the software KWAVE developed by Masumoto et al. (1991) in Japan uses the method of characteristics. In these programs the shaft resistance is assumed to be concentrated at given points along the pile shaft. These points are considered as internal boundaries to the problem. The method of characteristics provides the solution of the wave equation inside each pile segment defined by consecutive internal boundaries.

The calculation procedure of the characteristic solution is as follow. The pile is divided into equally spaced intersections. The spaces between the intersections are often called elements. The set of intersections common to each pair of spaces is to be considered as a coordinate system. The waves arriving at the intersections are determined from the waves

calculated at the previous time-step. Between the intersections the pile is frictionless and so the propagation of a wave will be undisturbed. Arriving at the intersection a part of the wave will be transmitted and another part reflected. The magnitude of transmitted and reflected waves depends on the pile properties and the shaft friction. Force, velocity, displacement and accelerations can be calculated from the waves and allow the calculation of energy and friction.

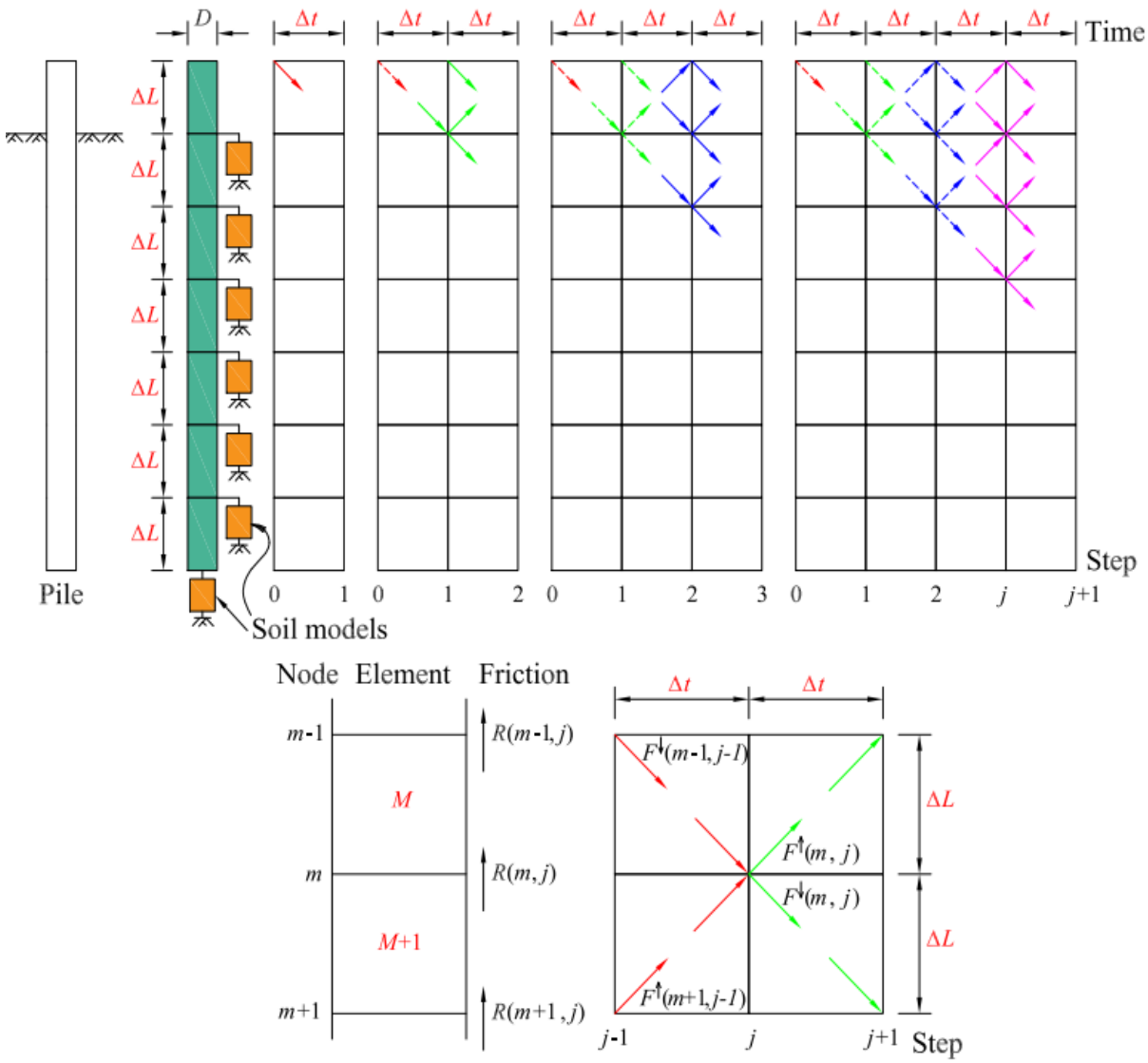

Figure 2.2. Numerical modelling and notation used in characteristic solution

1. Displacement at the pile node *m*, and at the step *j*

$$u(m,j) = u(m,j-1) + v(m,j-1)\times\Delta t = \sum_{0}^{j-1} v(m,j)\times\Delta t \qquad (2.10)$$

2. Downward travelling force, $F^{\downarrow}_{m,j}$, upward travelling force, $F^{\uparrow}_{m,j}$ and axial force, $F(m, j)$, at the pile node *m*, and at the step *j*

$$F^{\downarrow}_{m,j} = F^{\downarrow}_{m\text{-}1,j\text{-}1} - R(m, j)/2 \tag{2.11}$$

$$F^{\uparrow}_{m,j} = F^{\uparrow}_{m+1,j\text{-}1} + R(m, j)/2 \tag{2.12}$$

$$F(m, j) = F^{\downarrow}_{m\text{-}1,j\text{-}1} + F^{\uparrow}_{m+1,j\text{-}1} \tag{2.13}$$

3. Velocity at the pile node *m*, and at the step *j*

$$v(m, j) = \frac{\left[F^{\downarrow}_{m,j} - F^{\uparrow}_{m,j}\right]}{Z(m)} = \frac{\left[F^{\downarrow}_{m\text{-}1,j\text{-}1} - F^{\uparrow}_{m+1,j\text{-}1} - R(m, j)\right]}{Z(m)} \tag{2.14}$$

Here,

Δt is the time interval given by a ratio of pile element length, ΔL, to the wave speed, *c*,

$F^{\downarrow}_{m\text{-}1,j\text{-}1}$ is incident downward travelling force wave at pile node *m*-1 and at step *j*-1,

$F^{\uparrow}_{m+1,j\text{-}1}$ is incident upward travelling force wave at pile node *m*+1 and at step *j*-1,

$Z(m)$ is the impedance of the pile elements *M* between two nodes *m*-1 and *m*,

R(*m*, *j*) is the frictional force acting on the pile node *m* and at step *j*. Calculation of this value depends on the soil resistance models which will discuss in later part.

There are also a number of methods for pile dynamic analysis that are based on semi-analytical approaches other than the method of characteristics: (1) solutions for piles of semi-infinite length (Van Koten et al. 1980, Warrington 1987, Deeks 1992), (2) solutions using the method of images (Hansen and Denver 1980, Uto et al. 1985), (3) solutions by Fourier series (Wang 1988). The main disadvantage of the semi-analytical methods, including the method of characteristics, is that they involve complex mathematics that obstructs the implementation of realistic soil resistance models.

A major advance in pile driving analysis was the work done by Smith in the late 1950s. Smith (1960) developed an entirely numerical method to analyse pile driving without the use of complex mathematics. The pile is discretised into a series of lumped masses connected with linear springs (see Fig. 2.3). The global system of equations of motion (dynamic equilibrium equations) was solved in the time domain by dividing the analysis time into small time

increments. Smith's approach is often called the one-dimensional approach since the effect of the surrounding soil is accounted for through soil resistance models consisting of springs, dashpots and sliders connected to each other in various combinations.

The calculation procedure of the Smith's method is as follow. The pile was first divided into *n* elements from 1 to *n* and *n* +1 nodes from 0 to *n* as shown in Figure 2.3. Soil reactions acting on the pile shaft and at the pile tip were located at each pile node. Pile response including displacement, velocity and axial force are then calculated.

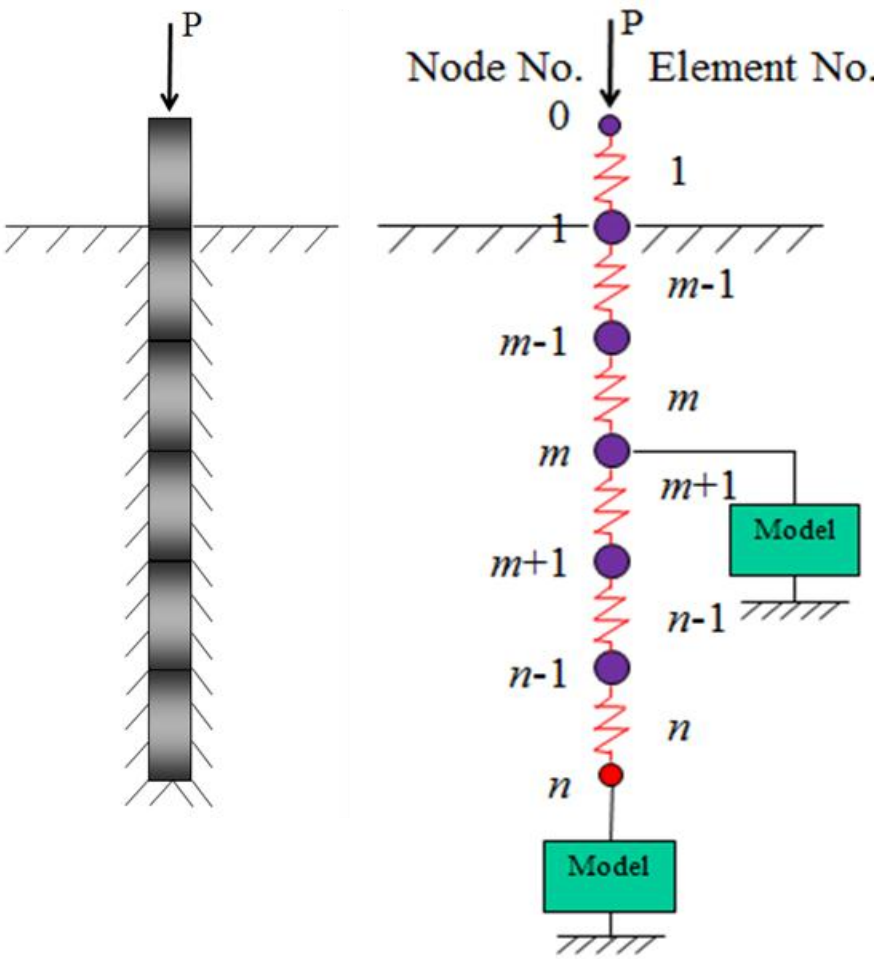

Figure 2.3. Numerical modelling in Smith's method

1. Displacement at the pile node, *m*, during a time step, Δ*t*, at current step *j*

$$u(m, j) = u(m, j-1) + v(m, j-1) \times \Delta t \tag{2.15}$$

2. Force in pile at element, *m*, having an equivalent stiffness *K*(*m*) at current step *j*

$$F(m, j) = u(m\text{-}1, j) - u(m, j) \times K(m) \tag{2.16}$$

3. Velocity at the pile node, m, having an equivalent concentrated mass, $M(m)$ at current step j

$$v(m, j) = v(m, j\text{-}1) + \frac{F(m, j) - F(m+1, j) - R(m, j)}{M(m)} \times \Delta t \qquad (2.17)$$

in which $u(m, j - 1)$ and $v(m, j - 1)$ are the pile displacement and velocity at node m, at previous step, $j - 1$, respectively. $R(m, j)$ is the soil resistance at the pile shaft or at the pile tip calculated from soil responses at previous step, $j - 1$. This value depends on the soil resistance models which will discuss in later part.

The discretisation of the pile and soil in Smith's method is actually based on a finite difference approximation to the governing differential equation. The other solution to the one-dimensional wave propagation in a pile with soil friction was proposed by Wakisaka et al. (2004) by means of a finite difference method (FDM) in the computer program KWAVE-FD. The wave equation with soil resistance is shown in Eq. (2.18)

$$\frac{\partial^2 w}{\partial t^2} = c^2 \frac{\partial^2 w}{\partial x^2} - \frac{1}{\rho} \frac{\tau \times U}{A \times \Delta x} \qquad (2.18)$$

Here, t is the time, x is the coordinate along the pile axis, c is the wave speed, τ is skin friction, U is the circumferential area of a pile element having a length of Δx, w and ρ are the displacement and the density of the pile, respectively.

Finite difference approximation for above equation is expressed by Eq. (2.19) with taking into account a change in pile section properties shown in Fig. 2.4.

$$\begin{aligned} w_{m,j+1} &= 2w_{m,j} - w_{m,j-1} + \frac{2}{A_m\rho_m + A_{m+1}\rho_{m+1}} \left(\frac{\Delta t}{\Delta x}\right)^2 \times \\ &(A_{m+1}E_{m+1}w_{m+1,j} - A_m E_m w_{m,j} - A_{m+1}E_{m+1}w_{m,j} + A_m E_m w_{m-1,j}) - \\ &\frac{U_m + U_{m+1}}{A_m\rho_m + A_{m+1}\rho_{m+1}} \times \frac{\tau_{m,j}}{\Delta x} \times (\Delta t)^2 \end{aligned} \qquad (2.19)$$

where Δt is the time interval, A and E are the cross-sectional area and Young's modulus of the pile. Subscription 'm' and 'j' denote pile node number and time step, respectively.

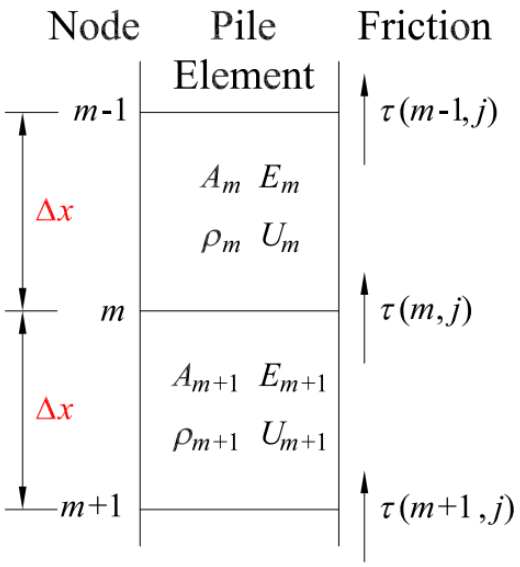

Figure 2.4. Notation used in finite difference scheme.

The finite element method (FEM) has also been used in recent years for the simulation of the pile driving problem (e.g. Smith et al. 1982, Borja 1988, Mabsout et al. 1995, Liyanapathirana et al. 2000, Masouleh and Fakharian 2007). In contrast with the 1-D approach, FEM has the advantage that the soil around the pile is treated as a continuum instead of being represented by spring-dashpot-slider resistance models. Among the available methods for pile driving analysis, the finite element method can produce the most accurate results with the condition that realistic and advanced constitutive models are used for modelling the soil and the analysis domain is properly discretised. In the case of large pile settlement, a large strain formulation is also needed for the correct prediction of the development of limit base resistance. All these requirements result in very computationally expensive simulations, with runtimes of the order of several hours or days. Therefore it is currently impossible to use FEM in routine pile dynamic analysis in design practice.

2.2 Mechanism of soil resistance mobilised along pile shaft and base

Pile driving is a highly nonlinear dynamic problem. Stress waves are transmitted from the pile to the soil, and there are also regions where the soil reaches to failure state. Driven piles penetrate the soil due to the hammer impact on the pile head. As a result, the motion of the pile and the cyclic loading in the soils is transient in nature. The soil in the immediate vicinity of the pile can store energy (elastic deformation) and absorb energy because of plastic and hysteretic dissipation. Plastic dissipation occurs in the highly strained zones adjacent to the

pile in which soil undergoes post-failure plastic deformation. Hysteretic dissipation (hysteretic damping) originates from the nonlinear response of the soil even at the small strain level. It is related to the energy that is absorbed in the soils during a full stress cycle. Energy is also radiated in the far field (radiation damping).

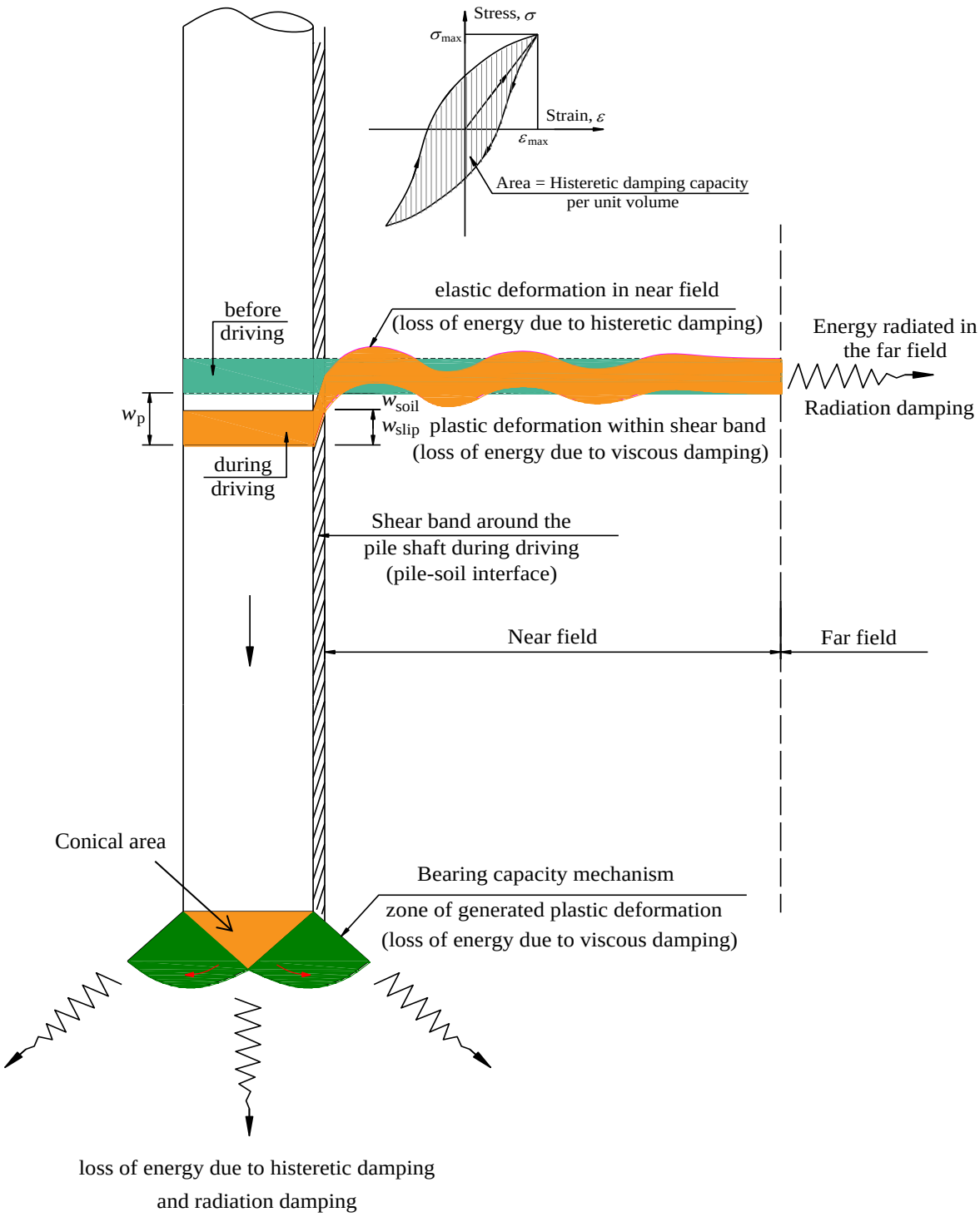

Figure 2.5. Energy transmission and absorption, and deformation mechanism in the soil around the pile shaft and at the pile base during pile driving.

Figure 2.5 shows a schematic representation of the deformation and energy absorption around the pile shaft. As the pile moves downward, it induces shear stress in the soil along its shaft. Limit shaft resistance, τ_{max}, is reached with relatively small pile displacement. Under static conditions, the pile displacement, w_p, required to mobilise τ_{max} is about 1% of the pile diameter, D, or width, B. Under dynamic conditions, w_p is even smaller because of the short wave length of the shear waves radiating outwards from the pile shaft. A thin shear band is formed around the pile at the moment that the limit shaft resistance is reached. All plastic deformation happens inside that shear band. The soil outside the shear band remains in a "pre-failure" state and undergoes predominantly cyclic vertical shearing. The magnitude of the cyclic shear stress reduces dramatically with radial distance from the shaft. The soil region closer to the pile (near field) absorbs most of the energy, with the remaining energy propagating to the far field (radiation damping). If the pile were perfectly rigid, only vertical shear waves would radiate from the pile shaft. In reality, compressive waves are also generated because the pile is deformable and the upper sections of the pile are settled earlier than the lower sections as the hammer pulse travels downwards. However, the effect of compressive waves is much less significant, and the vertical shear wave dominates the mode of deformation around the pile shaft.

Because of the high velocity of pile motions and the large induced strain rates in the soil, the strength of the soil inside the plasticity zones might be higher than that under static conditions. Therefore, the limit shaft resistance and base resistance are expected to be dependent on the pile velocity (rate effect). This means that, in addition to hysteretic damping and radiation damping, driving energy will be absorbed due to the viscous damping inside the plastic zones.

In the case of the pile tip, the plastic deformation is radiated in a region that extends from the pile base to roughly 1 to 2 times the pile width or diameter. The plastic mechanism is similar to the bearing capacity mechanism of shallow footings. During installation a 'rigid' conical area (see Fig 2.5 at the pile tip) is formed under the pile base. This area remains elastic and can be considered as an extension of the pile. The plastic deformation occurs in the fan zone that surrounds the 'rigid' conical area. The soil outside the plastic mechanism provides lateral reaction to the expansion and rotation of the fan zone. As shear and compressive waves propagate through the outer soil region, energy is lost due to hysteretic and radiation damping. Most of the energy radiated from the pile base travels downwards, but a certain small amount of energy is also transmitted towards the ground surface.

2.3 Soil resistance models

The first soil resistance models in pile driving analysis were introduced by Smith (1960). The soil resistance in Smith's model depends on both pile displacements, w_s at pile shaft and w_b at pile tip, and pile velocity, $\dot{w}_s$ at pile shaft and $\dot{w}_b$ at pile tip. It consists of a dashpot that is connected in parallel with a combination of a linear spring and a plastic slider connected in series (Figure 2.6).

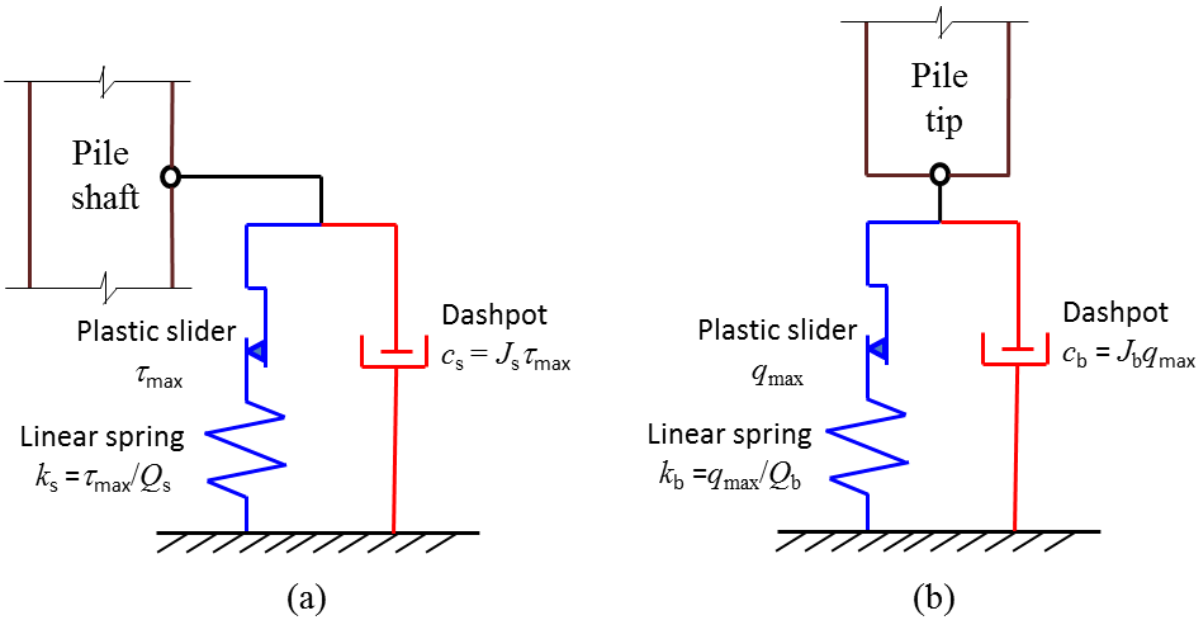

Figure 2.6. Smith's resistance soil models: (a) for pile shaft and (b) for pile base.

The soil resistance in terms of stress on the pile shaft can be written as

$$\tau_s = \min(k_s w_s, \tau_{max}) + c_s \dot{w}_s \tag{2.20}$$

where k_s is the spring stiffness coefficient, c_s is the dashpot coefficient, and τ_{max} is the unit limit shaft resistance. The spring stiffness is given by the following equation:

$$k_s = \tau_{max} / Q_s \tag{2.21}$$

where Q_s is an input parameter called the soil 'quake', having units of length. The quake represents the displacement at which perfect plasticity starts. If the pile displacement, w_s, exceeds the quake, then slider motion is activated and spring deformation stops. The dashpot coefficient is given by equation:

$$c_s = J_s \tau_{max} \tag{2.22}$$

where J_s is a damping input parameter.

Similarly for the base, we have soil resistance in terms of stress expressed as

$$q_{\mathrm{b}} = \min(k_{\mathrm{b}} w_{\mathrm{b}}, q_{\max}) + c_{\mathrm{b}} \dot{w}_{\mathrm{b}} \tag{2.23}$$

where $q_{\max}$ is the unit limit base resistance. The spring and dashpot coefficients are given by the following equations, respectively:

$$k_{\mathrm{b}} = q_{\max} / Q_{\mathrm{b}} \tag{2.24}$$

$$c_{\mathrm{b}} = J_{\mathrm{b}}\, q_{\max} \tag{2.25}$$

The proposed soil quakes and damping constants in the above equations are not standard soil parameters. They are empirical constants determined from back-analyses of pile driving records and pile load tests. Smith (1960) proposed the values $Q_{\mathrm{s}} = Q_{\mathrm{b}} = 2.5$ mm, $J_{\mathrm{s}} = 0.16$ s/m, and $J_{\mathrm{b}} = 0.492$ s/m. Updated empirical damping coefficients were later proposed for sands and clays based on laboratory impact tests (e.g., Forehand and Reese 1964, Coyle and Gibson 1970, Liang and Sheng 1992), and correlations with soil type (e.g. Likins et al. 1992, Paikowsky et al. 1994) or SPT data (e.g. Liang 2000) were established. Generally, the values of damping constants for clays and silts are higher than those for sands. This is apparently due to the higher-viscosity cohesive soils. However, the proposed values of J and Q exhibit a large scatter, making it difficult to develop reliable correlations. Aoki and de Mello (1992) found that J and Q also vary not only with the soil properties and types but also with the level of the hammer energy.

There are some inconsistencies of the Smith's models with the mechanics of pile driving. First, due to the connectivity of the model components (Fig. 2.6), the dashpot is always active, producing the same amount of damping before and after sliding. Second, the model does not distinguish between hysteretic, radiation and viscous damping, taking all of them into an entire viscous damping that is proportional to the static limit resistance.

Holeyman (1985) proposed the resistance model shown in Fig. 2.7. It consists of a spring, a viscosity dashpot and a radiation dashpot, all connected in parallel. Slippage initiates once the sum of resistances provided by these elements exceed the slider strength $\tau_{\max}$.

The resistance component due to the spring and viscosity is expressed as follows:

$$\tau_{\text{spring+visc}} = \frac{G_{\max}}{R} \times \frac{w_{\mathrm{p}}}{\ln(R_{\mathrm{m}}/R)} \left[1 + J(\dot{w}_{\mathrm{p}})^{N} \right] \tag{2.26}$$

where J and N are input parameters that control the viscous component. N is close to 0.2, while J varies from about 0.1 for sands to unity for clay soils (note that velocity in Eq. 2.26 is in units of m/s). $R_m = 2L(1 - v)$ proposed by Randolph and Wroth (1978) is the influence radius of the pile having a radius, R, and an embedment pile length, L. G_{max} is maximum or small-strain shear modulus. w_p and $\dot{w}_p$ are the displacement and velocity of the pile.

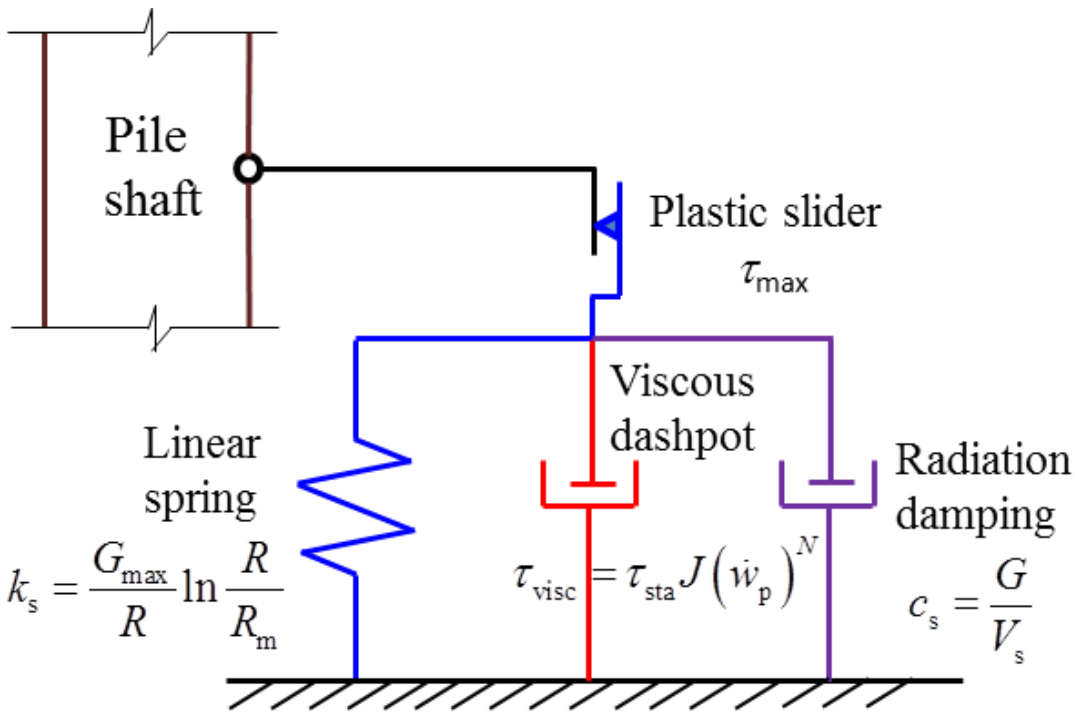

Figure 2.7. Shaft soil resistance model by Holeyman (1985).

The resistance component due to radiation damping is expressed as

$$\tau_{rad} = \frac{G}{V_s} \times \dot{w}_p \tag{2.27}$$

In this model, the spring constant is valid only for static conditions, which leads to values of system's stiffness that are too small. In addition, the soil viscosity is considered active even before sliding.

In 1986, Randolph and Simons proposed a soil resistance model for the pile shaft that has input parameters with clear physical meaning. The model consists of two parts (Fig 2.8): 1) a spring and a dashpot (representing radiation damping) connected in parallel and 2) a plastic slider and a second dashpot (soil viscosity) connected in parallel. The two parts are connected in series. The second part represents the shear band surrounding the pile shaft and the first part represents the rest of the soil, which has not reached a fully plastic state.

The spring and dashpot constants of the first part are based on the solution by Novak et al. (1978). They derived a close-form analytical solution for the soil resistance acting on the shaft of a vertically vibrating, rigid, infinitely long pile by assuming a thin soil disk. The solution is rigorous for an elastic soil and steady-state pile motion. They proposed that the spring, k_s, and radiation dashpot, c_s, constants of the shaft resistance model be expressed as

$$k_s = \frac{2.75 \times G}{\pi \times D} \tag{2.28}$$

$$c_s = \frac{G}{V_s} \tag{2.29}$$

where D is the diameter of the pile, G is the elastic soil shear modulus and V_s is the shear wave velocity of the soil.

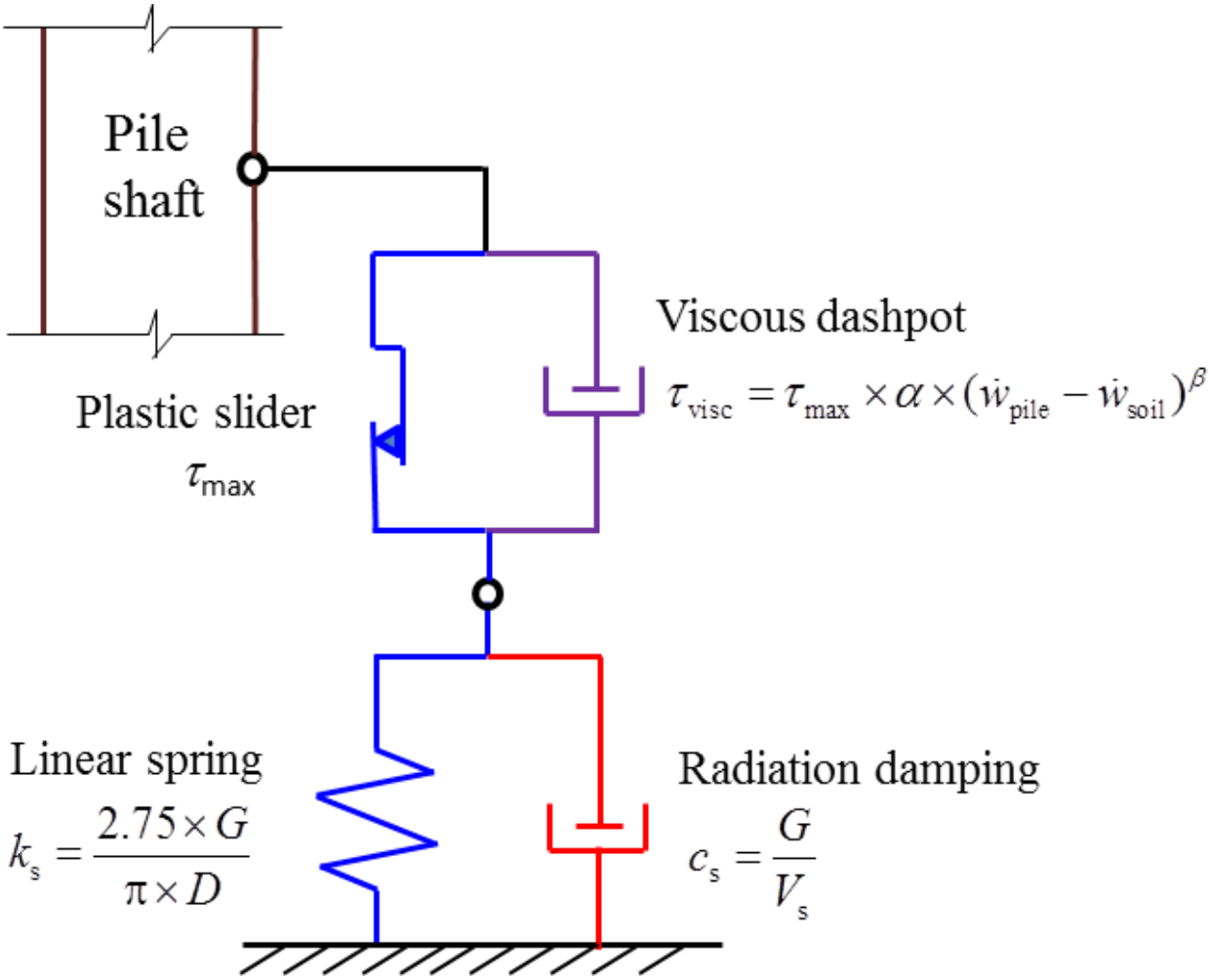

Figure 2.8. Shaft soil resistance model according to Randolph and Simons (1986).

The model part representing the shear band takes into account the rate effect by setting the shear strength, $\tau_{\max}^{\text{dyn}}$, as the sum of two terms: the static resistance, $\tau_{\max}^{\text{sta}}$ and the strength gain due to rate effects (viscosity), τ_{visc}:

$$\tau_{\max}^{\text{dyn}} = \tau_{\max}^{\text{sta}} + \tau_{\text{visc}} = \tau_{\max} + \tau_{\max} \times \alpha \times (\dot{w}_{\text{pile}} - \dot{w}_{\text{soil}})^{\beta} \tag{2.30}$$

where α and β are input parameters similar to the J and N used in Holeyman (1985). As long as the sum of the stresses due to the linear spring and radiation dashpot do not exceed $\tau_{\max}$, the soil and pile move together. If $\tau_{\max}$ gets exceeded, then slippage occurs and the soil on the outer boundary of the shear band moves differently from the pile. The strength gain due to viscosity is a function of the relative velocity between soil and pile. During slippage, the behaviour is controlled by the slider and the viscosity dashpot. This is consistent with the mechanics of shaft resistance described in Section 2.2. The shaft resistance model by Randolph and Simons (1986) has gained recognition in recent years because it uses input parameters that have physical meaning and adheres to the true mechanics of the problem. However, the limitation of the model is that it does not take into account soil nonlinearity and hysteretic damping.

In terms of improvement in the base soil resistance model, Lysmer and Richart (1966) derived a closed-form solution for the motion of a circular rigid footing on the surface of an elastic half-space subjected to vertical transient load in order to estimate the parameters for the base soil resistance model. Their solution gives the total resistance of the soil acting at the footing base as the sum of two components: a spring resistance (displacement-dependent) and a dashpot resistance (velocity-dependent). The spring stiffness per unit area, k_{b}, is estimated from Eq. (2.30) below:

$$k_{\text{b}} = \frac{8 \times G}{\pi(1-\nu) \times D} \tag{2.30}$$

The dashpot in Lysmer's model represents the radiation damping, i.e., the energy loss due to propagation of shear, compressive waves in the elastic half-space. The dashpot coefficient, c_{b}, is given as

$$c_{\text{b}} = \frac{3.4}{\pi(1-\nu)} \rho_{\text{s}} V_{\text{s}} = \frac{3.4}{\pi(1-\nu)} \sqrt{\rho_{\text{s}} G} \tag{2.31}$$

where ρ_{s} is the soil density, ν is the Poisson's ratio of the soil and D is diameter of the circular area.

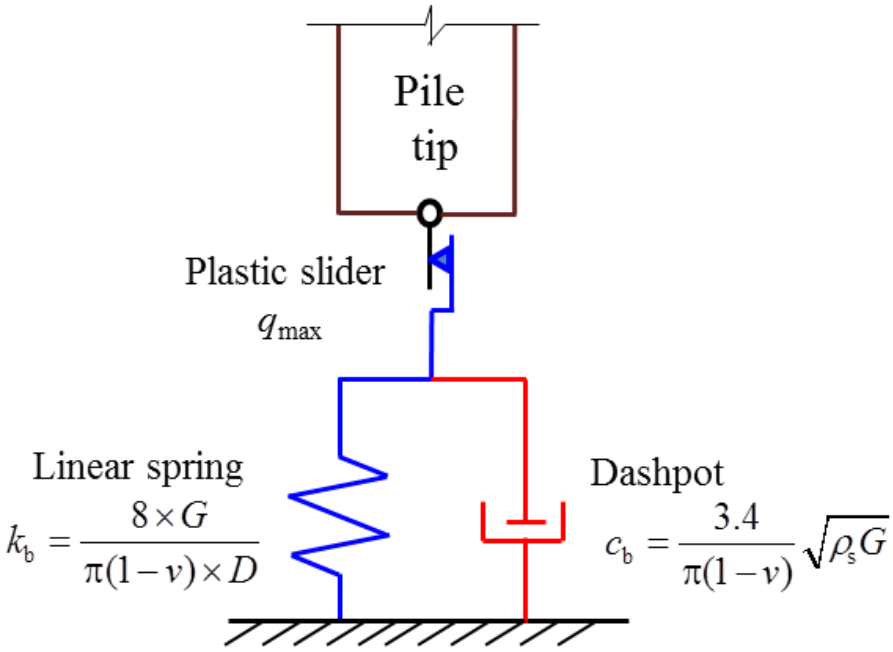

Figure 2.9. Lysmer's base soil resistance model.

Lysmer's analog coefficients can replace Smith's spring and dashpot coefficients (Eqs. 2.24 and 2.25), thus allowing direct association of the base stiffness and damping with actual soil properties (elastic parameters and soil density). Researchers have argued that no waves are transmitted to the soil after the base plastic mechanism has been fully formed, and thus the plastic zone is decoupled from the rest of the soil medium. Based on this consideration, the slider has proposed placing outside the spring-dashpot system, as shown in Fig. 2.9. In that case, the dashpot does not contribute to the soil resistance after base capacity is reached. Since no tension can be transferred from the soil to the pile in reality, the soil resistance at the pile tip is not allowed to take negative values. Instead of tensile force developing at the base, a gap is formed between the pile and soil and the resistance there is zero with the possible exception of a small tensile strength in the case of clays. Compressive forces start developing again only when the gap closes in the course of the analysis.

Such models reduce significantly the empiricism of Smith's model but still miss certain aspects of the response mechanisms of the soil. These are the soil nonlinearity and the corresponding hysteresis damping and the rate dependence of the soil strength inside the failure mechanism on the strain rate (viscous damping).

Wolf (1988) presented a solution to the vibration of a circular rigid footing on the surface of a half-space. However, parameters of this model were valid only for small frequencies in vibration problem which is totally different to the driving problem with high frequency of dynamic signals.

In 1992, Deeks performed finite element approach to validate the base resistance model based on Lysmer's analog. By matching the finite element results with several rheological model configurations, he found that the most accurate resistance model is shown in Fig. 2.10.

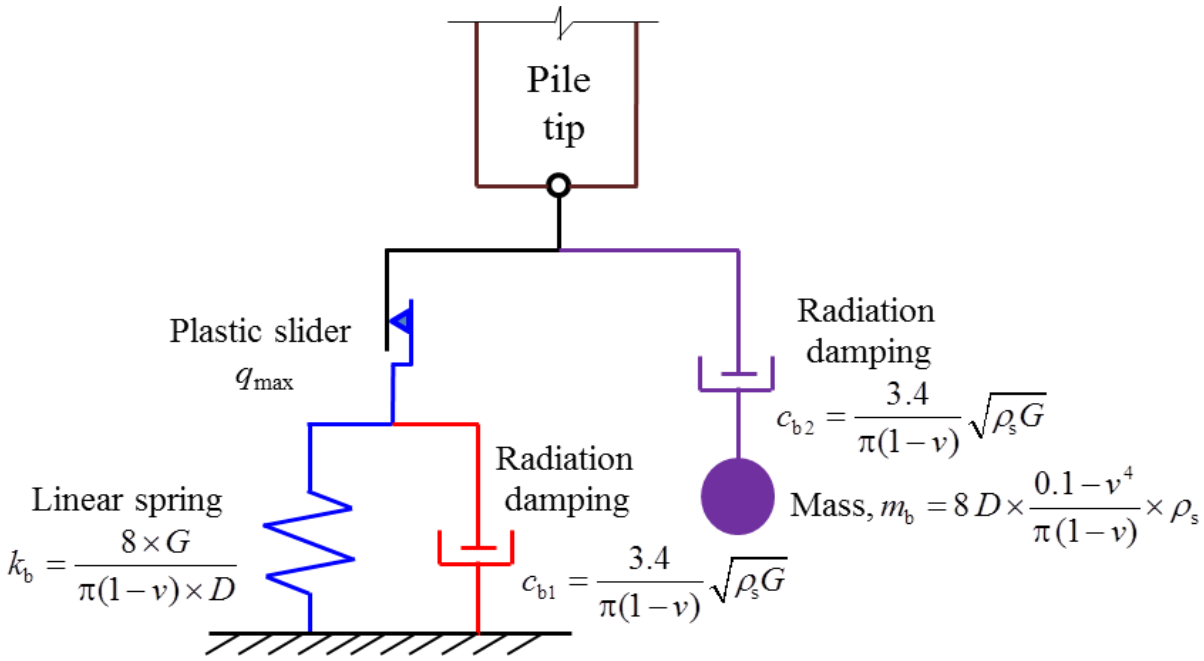

Figure 2.10. Base soil resistance model developed by Deeks and Randolph (1992).

The model consists of two components in parallel. The first component is similar to the base resistance model proposed by Lysmer while the second component contains a dashpot and a mass in series. The mass, m_b, can be seen a representative of the inertia of the soil mass in the failure mechanism. The spring, dashpot coefficients and mass per unit area are given by the following equations:

$$k_b = \frac{8 \times G}{\pi(1-\nu) \times D} \tag{2.32}$$

$$c_{b1} = c_{b2} = \frac{3.4}{\pi(1-\nu)}\sqrt{\rho_s G} \tag{2.33}$$

$$m_b = 8D \times \frac{0.1-\nu^4}{\pi(1-\nu)} \times \rho_s \tag{2.34}$$

This base resistance model performs well in the case of the formation of a plastic mechanism but soil nonlinearity and hysteretic damping still did not taken into account.

2.4 Summary

Research works on the dynamic analysis and the soil resistance models have been briefly reviewed. Several computer programs in pile driving analysis using different analytical methods have been developed. CAPWAP is regarded as a practical tool in pile driving analysis; however, it still has some limitations due to the numerical method and soil resistance model itself. The previous sections demonstrated that significant efforts have been made to develop improved soil resistance models. The improved models show clearly that the spring and dashpot coefficients are not proportional to the limit resistance, as in Smith's model using in CAPWAP, but depend on the soil stiffness, soil density and the pile radius. Among these improved models, rational shaft soil resistance model developed by Simon and Randolph (1986) and rational base soil resistance model proposed by Randolph and Deeks (1992) have input parameters with clear physical meaning; however, soil nonlinearity and hysteretic damping are not considered. Moreover, in the reviewed analytical methods for the one-dimensional wave propagation problem, pile and soil responses are not fully coupled at a time step. This results in numerical instability in case displacement- and velocity- dependent resistances have a large value. Hence, a numerical computer program based on the one-dimensional stress-wave theory using a matrix form and some modifications of the rational soil models has been developed to improve current pile driving analysis. The computer program is verified thoroughly from numerical simulation through small-scale model in laboratory to full-scale test in practice. In addition, the numerical computer program is also used to analyse several DCPTs with dynamic measurement in this research.

References

Aoki N. and de Mello V.F.B (1992). Dynamic loading test curves. Proceeding of the 4th International Conference on the Application of Stress-Wave Theory to Piles, The Hague, The Netherlands; 525-530.

Borja R.I. (1988). Dynamics of pile driving by the finite element method. Computers and Geotechnics; 5(11): 39-49.

Deeks A.J. (1992). Numerical analysis of pile driving dynamics. Ph.D. Thesis, University of Western Australia.

De Josselin De Jong G. (1956). Wat gebeurt er in de grond tijdens het heien (What happens in the soil during pile driving). De Ingenieur, No. 25, Breda, The Netherlands.

Goble G.G., Likins G. and Rausche F. (1975). Bearing capacity of piles from dynamic measurements. Final Report, Department Of Civil Engineering, Case WesternReserve University, Cleveland, Ohio.

Hannigan P.J., Goble G.G., Thendean G., Likins G.E. and Rausche F. (1996). Design and construction of driven pile foundations. Workshop Manual, Publication No. FHWAHI-97-014, 1996.

Hansen B. and Denver H. (1980). Wave equation analysis of a pile - An analytic model. Proceeding of the International Seminar on the Application of Stress-Wave Theory on Piles, Stockholm; 3-22.

Holeyman A.E. (1985). Dynamic non-linear skin friction of piles. Proceeding of the International Symposium on Penetrability and Driveability of Piles, San Francisco, California; 1: 173-176.

Liang R.Y. and Sheng Y. (1992). Theoretical interpretation of Smith's model parameters. Proceeding of the 4th International Conference on the Application of Stress-Wave Theory to Piles, The Hague, The Netherlands; 111-116.

Liang R.Y. (2000). Correlative study of Smith damping coefficient and SPT blow count. Proceeding of the 6th International Conference on the Application of Stress-Wave Theory to Piles, São Paulo, Brazil; 461-467.

Likins G., Rausche F., DiMaggio J. and Teferra W. (1992). A solution for high damping constants in sands. Proceeding of the 4th International Conference on Application of-Stress-Wave Theory to Piles, The Hague, The Netherlands; 117-120.

Liyanapathirana D.S., Deeks A.J. and Randolph M.F. (2000). Numerical modelling of large deformations associated with driving of open-ended piles. International Journal for Numerical and Analytical Methods in Geomechanics; 24: 1079-1101.

Lysmer J. and Richart F.E. (1966). Dynamic response of footing to vertical loading. Journal of Engineering Mechanical Division, ASCE; 92(1): 65-91.

Mabsout M., Reese L. and Tassoulas J. (1995). A Study of pile driving by the finite element method. Journal of Geotechnical Engineering, ASCE; 121(7): 535-543.

Masouleh S. F. and Fakharian K. (2007). Application of a continuum numerical model for pile driving analysis and comparison with a real case. Computers and Geotechnics; 35(3): 406-418.

Matsumoto T. and Takei M. (1991). Effects of soil plug on behaviour of driven pipe piles. Soils and Foundations; 31(2): 14-34.

Middendorp P. and Van Weele A.F. (1986). Application of characteristic stress wave method in offshore practice. Proceeding of the 3rd International Conference on Numerical Methods in Offshore Piling, Nantes, Supplement; 6-18.

Novak M., Nogami T. and Aboul-Ella F. (1978). Dynamic Soil reactions for plane strain case. Journal of Engineering Mechanics Division, ASCE; 104(4): 953-959

Paikowsky S.G. and Chernauskas L.R. (1992). Energy approach for capacity evaluation of driven piles. Proceedings, Fourth International Conference on the Application of Stress-Wave Theory to Piles, The Hague, The Netherlands; 595-601.

Paikowsky S.G., Regan J.E., and McDonnell J.J. (1994). A simplified field method for capacity evaluation of driven piles. Publication No. FHWA-RD-94-042.

Randolph M.F. and Wroth C.P. (1978). Analysis of deformation of vertically loaded piles. Journal of Geotechnical Engineering Division, ASCE; 104(GT12):1-17.

Randolph M.F. and Simons H.A. (1986). An improved soil model for one-dimensional pile driving analysis. Proceeding of the 3rd International Conference of Numerical Methods in Offshore Piling, Nantes, France; 3-17.

Smith I.M. and Y.K. Chow (1982). Three-dimensional analysis of pile drivability. Proceeding of the 2nd International Conference on Numerical Methods in Offshore Pilling, Austin; 1–10.

Uto K., Fuyuki M. and Sakurai M. (1985). An equation for the dynamic bearing capacity of a pile based on wave theory. Proceeding of the International Symposium on Penetrability and Drivability of Piles, San Francisco.

Van Koten H., Middendorp P., and Van Brederode P. (1980). An analysis of dissapative wave propagation in a pile. Proceeding of the International Conference on the Application of Stress-Wave Theory to Piles, Stockholm; 23-40.

Wakisaka T., Matsumoto T., Kojima E. and Kuwayama S. (2004). Development of a new computer program for dynamic and static pile load tests. Proceeding of the 7th International Conference on the Application of Stress-Wave Theory to Piles, Selangor, Malaysia; 341-350.

Wang Y.X. (1988). Determination of capacity of shaft bearing piles using the wave equation. Proceeding of the 3rd International Conference on the Application of Stress-Wave Theory to Piles, Vancouver, Canada; 337-342.

Warrington D.C. (1997). Closed form solution of the wave equation for piles. Master's Thesis, University of Tennessee at Chattanooga.

Wolf J.P. (1988). Soil-Structure Interaction Analysis in Time Domain. Prentice Hall.

Chapter 3

Development of a numerical method for analysing wave propagation in an open-ended pipe pile

This chapter presents a numerical method using a matrix form with Newmark's β method to analyse the phenomenon of wave propagation in an open-ended pipe pile within the framework of one-dimensional stress-wave theory. The proposed numerical method can be used to a fully static problem. In order to verify the proposed method, the calculated results obtained from the proposed method were compared with those obtained from the theoretical solution, the conventional Smith method, and the rigorous continuum method FLAC^{3D}.

3.1 Introduction

Open-ended steel pipe piles have been used for years as the primary solution for constructing foundations for various structures in offshore conditions. Recently, there has been an increasing interest in using spun (pre-stressed concrete) piles for the foundations of many structures, especially residential and industrial buildings. During driving such piles into the ground, a part of the soil around the pile toe enters into the pile to create a soil column called a soil plug. Depending on the relative movement between the pile and the soil plug, the pile is said to be plugged, partially plugged or unplugged. In all three cases, the total resistance of an open-ended pipe pile is the summation of outer shaft resistance, soil plug resistance (or inner shaft resistance) and pile tip resistance.

In pile foundation design, it is common to use the static load-displacement relation of a

single pile to determine its bearing capacity and corresponding displacement. At present, the load-displacement relation is directly obtained from a static load test (SLT) or derived from the interpretation of dynamic load test (DLT) or rapid load test (RLT) signals. While the SLT is considered the most reliable method, it is costly and time-consuming. Rapid pile load testing methods, such as the Statnamic load test method (Bermingham and Janes 1989) and the Spring-hammer load test method (Matsumoto T. et al. 2004), in which the phenomenon of stress-wave propagation in piles is ignored, have been developed. Various methods of interpreting the measured dynamic signals, such as the unloading point method (UPM) (Kusakabe et al. 1995) and the non-linear damping method (NLDM) (Matsumoto et al. 1994) have been proposed to derive the static load-settlement relation of the piles. In DLT, according to the Chapter 2, dynamic analyses have been developed for more than 50 years by many researchers using different analytical approaches with various soil resistance models. For example, the Smith method (Smith 1955, 1960) is employed in WEAP and CAPWAP (Rausche el al. 1972, Goble et al 1976, 1979), characteristic solutions are adopted in TNOWAVE (Middendorp et al. 1986), and KWAVE (Matsumoto et al. 1991), and the explicit finite difference scheme is used in KWAVE-FD (Wakisaka et al. 2004).

In the case of open-ended pipe piles, it is necessary to consider the inner shaft resistance, as well as the wave propagation in the soil plug, in a wave matching analysis. Heerema and de Jong (1979) used the pile-in-pile model with Smith's empirical soil models to analyse the stress wave propagation in an open-ended pile. They were followed by Randolph and Simon (1986), Matsumoto et al. (1991), and Randolph and Deeks (1992), who used rational soil models with linear soil stiffness and a damping coefficient for pile driving analyses.

Considering numerical methods based on the one-dimensional stress-wave propagation theory, their advantage is rapid calculation. Nevertheless, the characteristic solution and the Smith method may have numerical instability when soil stiffness and the velocity-dependent resistance have large values. One of the reasons is that the displacement and velocity of a pile node at the previous calculation time step are used to calculate the soil resistance mobilised at the present calculation step. In other words, the pile behaviour and soil resistance are not fully coupled at each time step. This aspect will be discussed in detail later through a comparison of calculation results using the Smith method and a rigorous numerical method.

More rigorous methods in which the soil surrounding a pile is regarded as a continuum medium using the finite element method (FEM) or the finite difference method (FDM) have been developed. Chow and Smith (1984) performed axisymmetric finite element analyses for solid and pipe piles driven into clay under undrained conditions. Liyanapathirana et al. (2001)

studied the driving responses at the vicinity of the pile tip of thin walled open-ended pipe piles using a two-dimensional axisymmetric FEM. The results indicated that the shear stress reached the maximum magnitude right above the bottom of the soil plug while the vertical stress wave reached the highest magnitude beneath the bottom of the soil plug. Thus, the interaction between the waves travelling in radial and vertical directions at the bottom of the soil plug was considerable. Paikowsky and Chernauskas (2008) employed a two-dimensional finite difference scheme to investigate the spatial stress generated within a soil plug. They suggested that radial wave propagation within the soil plug, as well as compression wave propagation within the pile and the soil plug, should be taken into account. Although such continuum methods are regarded as the most rigorous methods in pile driving analysis, they are relatively slow in calculation, with runtimes of several hours or days. Therefore, it is currently not practical to apply continuum methods in routine pile dynamic analysis.

In order to overcome the above shortcomings of conventional one-dimensional stress-wave propagation analyses as well as those of the rigorous continuum methods, the matrix method of one-dimensional stress-wave propagation analysis in a pile using rational soil models recommended by Randolph and Deeks (1992) is proposed in this chapter. In the proposed method, displacements, velocities and accelerations of the pile, the outer soil and the inner soil at all the nodes are calculated simultaneously, and the soil stiffness- and velocity-dependent resistances are calculated at the same calculation step. Influence of the stress wave propagation on the soil plug is taken into account for an open-ended pile. Furthermore, the non-linearity of soil stiffness and the radiation damping in the soil models are considered. The proposed method can also be used for the analysis of the static loading of a pile, if the damping and inertia of the pile and the soil are ignored. To verify the proposed method, the calculated results obtained from this method were compared with those obtained from a theoretical solution, the conventional Smith method, and a continuum method using a well-known three-dimensional explicit finite-difference computer program, $FLAC^{3D}$.

3.2 Numerical modelling

The numerical model employed for analysing the stress wave propagation in an open-ended pipe pile is shown in Fig. 3.1. In this model, the pile and the soil plug are modelled as a series of massless linear springs with discrete masses at the nodes. Outer frictional forces acting on the pile nodes as well as inner frictional forces acting between the soil plug nodes and the pile nodes are considered. That is, we have four degrees of freedom (pile, soil plug, outer soil and inner soil) at each pile level. In the proposed numerical model, the soil reaction on the pile

annulus and the soil reaction beneath the soil plug are separately considered. The rational soil models proposed by Randolph and Deeks (1992) are implemented for both outer and inner soil resistances.

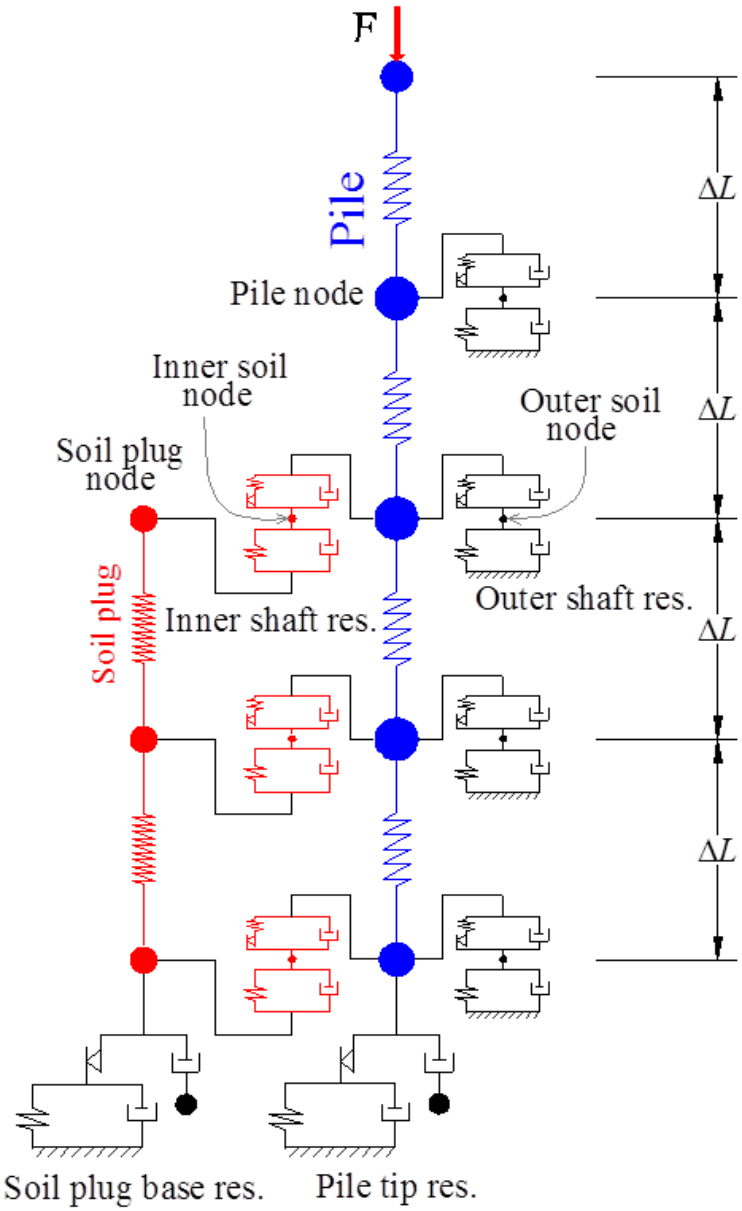

Figure 3.1. Pile – soil system.

Figures 3.2 and 3.3 show the rational soil models employed in the proposed method. In Fig. 2, u_p and v_p are the displacement and the velocity at the pile node, and u_s and v_s are those at the adjacent soil node, respectively. The outer shaft resistance, R_m, at the pile node, m, is calculated as:

$$R_m = (k_s u_s + c_r v_s) \cdot 2\pi r_o \cdot \Delta L \tag{3.1}$$

where k_s and c_r are the soil spring stiffness and the damping, respectively, and r_o is the outer radius of pile. These values can be approximately estimated using the following equations (Randolph and Deeks 1992):

$$k_s = \frac{2.75G}{2\pi r_o} \tag{3.2}$$

$$c_r = \sqrt{\rho_s G} \tag{3.3}$$

in which G and ρ_s are the shear modulus and density of the soil, respectively.

Under static loading conditions, the soil stiffness in the shaft soil model, $k_{s(static)}$, which is lower than that under dynamic loading conditions, is estimated using the following equations provided by Randolph and Deeks (1992).

$$k_{s(static)} = \frac{G}{\zeta r_o} \tag{3.4}$$

$$\zeta = \ln \frac{2.5L_e(1-\nu)}{r_o} \tag{3.5}$$

in which L_e is the embedment pile length.

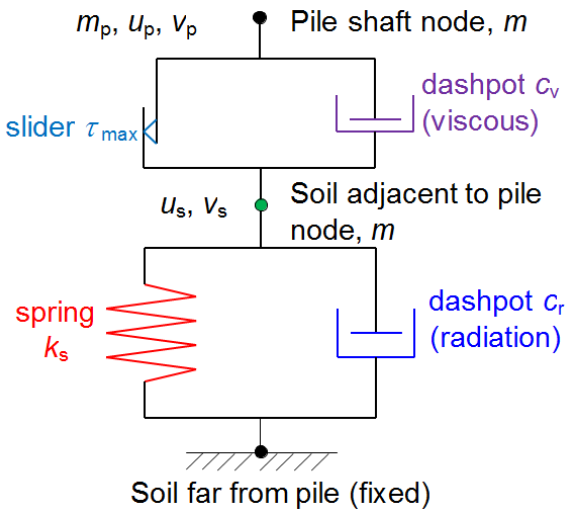

Figure 3.2. Shaft soil model.

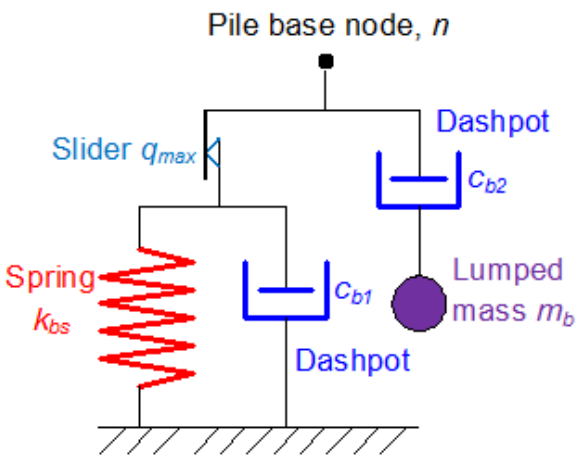

Figure 3.3. Base soil model.

The base resistance beneath the pile tip (annular section), R_p, and beneath the soil plug, R_{sp}, are calculated by the following equations:

$$R_p = \left[(k_{b\text{-}p} u_{bs\text{-}p} + c_{b1} v_{bs\text{-}p}) + c_{b2}(v_p - v_{bw\text{-}p}) \right] \pi (r_o^2 - r_i^2) \tag{3.6}$$

$$R_{\text{sp}} = \left[(k_{\text{b-sp}} u_{\text{bs-sp}} + c_{\text{b1}} v_{\text{bs-sp}}) + c_{\text{b2}} (v_{\text{sp}} - v_{\text{bw-sp}}) \right] \pi r_{\text{i}}^2 \tag{3.7}$$

In Eq. (3.6), $k_{\text{b-p}}$ is the spring stiffness, c_{b1} and c_{b2} are the damping factors, $u_{\text{bs-p}}$ and $v_{\text{bs-p}}$ are the displacement and velocity of the soil beneath the pile tip, $v_{\text{bw-p}}$ is the velocity of the additional soil mass and $m_{\text{bw-p}}$ is the additional soil mass of the soil resistance model beneath the pile tip. Those for the soil resistance beneath the soil plug are indicated with the suffix "sp" in Eq. (3.7). And, r_{o} and r_{i} are the outer and inner radii of the pile. These values are also approximated as follows (Randolph and Deeks 1992):

$$k_{\text{b-p}} = \frac{4G}{\pi (r_{\text{o}} + r_{\text{i}})(1-\nu)} \tag{3.8}$$

$$k_{\text{b-sp}} = \frac{4G}{\pi r_{\text{i}} (1-\nu)} \tag{3.9}$$

$$c_{\text{b1}} = c_{\text{b2}} = \frac{3.2}{\pi (1-\nu)} \sqrt{G \rho_{\text{s}}} \tag{3.10}$$

$$m_{\text{bw-p}} = 16 (r_{\text{o}} - r_{\text{i}}) \frac{0.1 - \nu^4}{\pi\ (1-\nu)} \rho_{\text{s}} \quad \text{(per unit area)} \tag{3.11}$$

$$m_{\text{bw-sp}} = 16 r_{\text{i}} \frac{0.1 - \nu^4}{\pi (1-\nu)} \rho_{\text{s}} \quad \text{(per unit area)} \tag{3.12}$$

where ν is the Poisson's ratio of the base soil.

In the rational shaft resistance model, the maximum dynamic soil resistance at the pile-outer soil interface, $\tau_{\text{max\_out}}^{\text{dyn}}$, and at the pile-inner soil interface, $\tau_{\text{max\_in}}^{\text{dyn}}$, are calculated by the following equations:

$$\tau_{\text{max\_out}}^{\text{dyn}} = \tau_{\text{max\_out}} \left[1 + \alpha \left(\frac{\dot{w}_{\text{p}} - \dot{w}_{\text{so}}}{v_{\text{o}}} \right)^{\beta} \right] \quad \text{(for the outer interface)} \tag{3.13}$$

$$\tau_{\text{max\_in}}^{\text{dyn}} = \tau_{\text{max\_in}} \left[1 + \alpha \left(\frac{\dot{w}_{\text{p}} - \dot{w}_{\text{si}}}{v_{\text{o}}} \right)^{\beta} \right] \quad \text{(for the inner interface)} \tag{3.14}$$

where $\tau_{\text{max\_out}}$ and $\tau_{\text{max\_in}}$ are the maximum static shaft resistances at the outer and inner interfaces. $\dot{w}_{\text{p}}, \dot{w}_{\text{so}}$, and $\dot{w}_{\text{si}}$ are the velocities of the pile, the outer, and the inner soil nodes,

respectively. v_0 is a reference velocity (= 1 m/s for convenience). α varies from 0.1 (for sand) to unity (for clay) and β = 0.2 (for all soils) (Randolph and Deeks 1992).

The mobilised outer and inner shaft resistances, $\tau_{\text{mob-out}}$ and $\tau_{\text{mob-in}}$, are calculated by:

$$\tau_{\text{mob\_out}} = k_{\text{so}} w_{\text{so}} + c_{\text{ro}} \dot{w}_{\text{so}} \tag{3.15}$$

$$\tau_{\text{mob\_in}} = k_{\text{si}} (w_{\text{si}} - w_{\text{sp}}) + c_{\text{ri}} (\dot{w}_{\text{si}} - \dot{w}_{\text{sp}}) \tag{3.16}$$

where k_{so} and k_{si} are the spring stiffnesses, c_{ro} and c_{ri} are the radiation dampings of the outer and inner soil, respectively. w_{so}, w_{si}, and w_{sp} are the displacements of the outer soil, inner soil, and soil plug, respectively. $\dot{w}_{\text{sp}}$ is the velocity of the soil plug node.

If the absolute value of the mobilised soil resistance exceeds the corresponding maximum dynamic soil resistance at the interface, slippage occurs, resulting in relative displacements between the pile and the soil.

To take into account the non-linearity of the soil stiffness shown in Fig. 3.4, the empirical relation introduced by Chow (1986) is used in the proposed method to calculate the soil stiffness in the loading stage at the pile shaft, k_{s}, or at the pile tip, k_{b}, in the current step from the initial values, $k_{\text{s-ini}}$ or $k_{\text{b-ini}}$, as follows:

$$k_{\text{s}} = k_{\text{s-ini}} \left(1 - R_{\text{fs}} \frac{\tau}{\tau_{\text{max}}^{\text{pos}} \text{ or } \tau_{\text{max}}^{\text{neg}}} \right) \tag{3.17}$$

$$k_{\text{b}} = k_{\text{b-ini}} \left(1 - R_{\text{fb}} \frac{q_b}{q_{\text{max}}^{\text{comp}} \text{ or } q_{\text{max}}^{\text{tens}}} \right) \tag{3.18}$$

in which R_{fs}, τ, $\tau_{\text{max}}^{\text{pos}}$ and $\tau_{\text{max}}^{\text{neg}}$ are the non-linearity coefficient, mobilised static soil resistance, maximum shear resistance in positive friction and maximum shear resistance in negative friction at the pile shaft, respectively. R_{fb}, q_{b}, $q_{\text{max}}^{\text{comp}}$ and $q_{\text{max}}^{\text{tens}}$ are the non-linearity coefficient, mobilised static soil resistance, end-bearing resistance in compression and end-bearing resistance in tension at the pile tip, respectively.

For the unloading and reloading stages, the initial soil stiffness was used to calculate the soil response. This behaviour could be regarded as hysteretic damping.

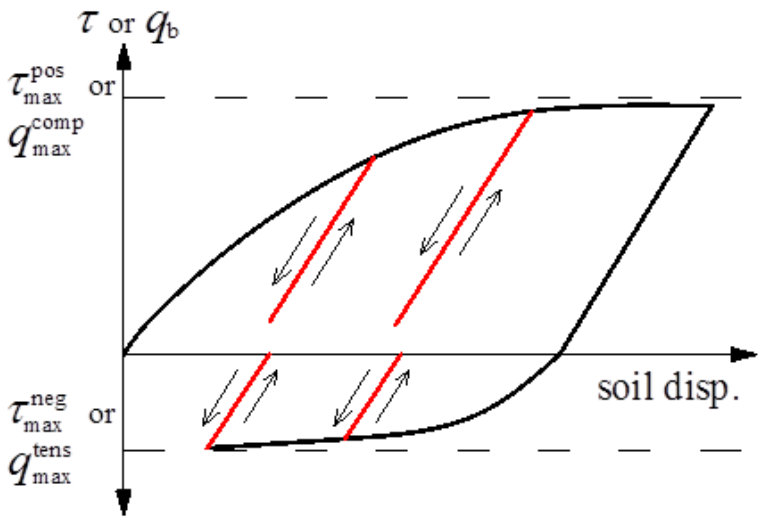

Figure 3.4. Non-linear soil response.

In the case of a non-linear behaviour of the soil stiffness, k_s or k_b, it may be appropriate to consider non-linear damping. According to Eq. (3.2) and Eq. (3.3) or Eq. (3.8), Eq. (3.9), and Eq. (3.10), non-linearity is related to the reduction of the shear modulus, G, of the soil. Hence, based on the above equations as well as Eq. (3.17) and Eq. (3.18), the following non-linear damping is considered:

$$c_r = \left(1 - R_{fs} \frac{\tau}{\tau_{max}^{pos} \text{ or } \tau_{max}^{neg}}\right)^{0.5} c_{r\text{-ini}} \tag{3.19}$$

$$c_{b1} = c_{b2} = \left(1 - R_{fb} \frac{q_b}{q_{max}^{comp} \text{ or } q_{max}^{tens}}\right)^{0.5} c_{b\text{-ini}} \tag{3.20}$$

where $c_{r\text{-ini}}$ and $c_{b\text{-ini}}$ are the initial values of c_r and $c_{br1} = c_{br2}$, respectively.

In order to calculate the responses of the outer and inner soils at the same time as the responses of the pile and the soil plug, a plastic slider in the rational soil models is connected to an interface spring with a great enough stiffness to minimise the relative displacement between the pile and the adjacent soil before slippage.

3.3 Formulation of calculations

By writing the force equilibrium equation at each pile node, soil plug node, outer soil node, and inner soil node, the pile motion can be expressed by the well-known matrix form as follows:

$$[K]\{w\}+[C]\{\dot{w}\}+[M]\{\ddot{w}\}=\{F\} \tag{3.21}$$

in which [K], [C] and [M] are the global stiffness, damping, and mass matrices, respectively. $\{w\}$, $\{\dot{w}\}$, $\{\ddot{w}\}$ and $\{F\}$ are the displacement, velocity, acceleration and the applied force vectors, respectively. Such matrix form calculation scheme was first used in geotechnical engineering by Idriss and Seed (1969) to calculate the seismic response of horizontal soil layers.

Matrix [K] consists of the spring stiffness of the pile, the soil plug, the interface spring, the outer shaft soil, the inner shaft soil, the base soil beneath the pile tip and the soil plug base. If a slip failure occurs at a node, the value of the interface spring stiffness, k_{inter}, is set to zero at that node. When the pile and the soil re-join, the value of the interface spring stiffness is recovered.

Matrix [C] includes the damping values of the outer shaft soil, the inner shaft soil, the base soil, and the additional soil masses. Matrix [M] involves the mass of each pile node, the mass of each soil plug node, and the mass of additional soil masses beneath the pile tip and the soil plug base.

In order to solve Eq. (3.21), it is convenient to rewrite it as an incremental form over time.

$$\sum_{0}^{t}[K]_t\{\Delta w\}_t+[K]_t\{\Delta w\}_{t+\Delta t}+[C]_t\{\dot{w}\}_{t+\Delta t}+[M]_t\{\ddot{w}\}_{t+\Delta t}=\{F\}_{t+\Delta t} \tag{3.22}$$

where $\{F\}_{t+\Delta t}$ is the applied force vector at the current step. $[K]_t\{w\}_t$ is the static node force vector existing in the pile, soil plug, outer soil and inner soil in the previous step. $\{\Delta w\}_{t+\Delta t}$ is the increment of the displacement vector during a time interval of Δt.

From the Newmark's β method (Newmark 1959), the acceleration, $\{\ddot{w}\}_{t+\Delta t}$, and the velocity, $\{\dot{w}\}_{t+\Delta t}$, at the current time, $t+\Delta t$, can be given by the following equations using $\{w\}_{t+\Delta t}$ for the current step, and $\{w\}_t$, $\{\dot{w}\}_t$ and $\{\ddot{w}\}_t$ for the previous step:

$$\{\dot{w}\}_{t+\Delta t}=\frac{\gamma}{\beta\Delta t}\left(\{w\}_{t+\Delta t}-\{w\}_t\right)+\left(1-\frac{\gamma}{\beta}\right)\{\dot{w}\}_t+\frac{\Delta t}{2}\left(2-\frac{\gamma}{\beta}\right)\{\ddot{w}\}_t \tag{3.23}$$

$$\{\ddot{w}\}_{t+\Delta t}=\frac{\{w\}_{t+\Delta t}-\{w\}_t}{\beta\Delta t^2}-\frac{\{\dot{w}\}_t}{\beta\Delta t}-\left(\frac{1}{2\beta}-1\right)\{\ddot{w}\}_t \tag{3.24}$$

in which γ = 1/2 and β varies from 0 to 1 (β = 1/4 for the constant average acceleration method, and β = 1/6 for the linear acceleration method). β = 1/6 was adopted in the proposed method because of its high accuracy (Edward 2000) in short time intervals.

Substituting Eqs. (3.23) and (3.24) into Eq. (3.22) gives us:

$$\left[[K]_t + \frac{[C]_t}{2\beta\Delta t} + \frac{[M]_t}{\beta\Delta t^2}\right]\{\Delta w\}_{t+\Delta t} = \left[\{F\}_{t+\Delta t} - \sum_0^t [K]_t \{\Delta w\}_t\right] + \left[\left(\frac{1}{2\beta} - 1\right)[C]_t + \frac{[M]_t}{\beta\Delta t}\right]\{\dot{w}\}_t$$

$$+\left[\left(\frac{1}{2\beta} - 2\right)\frac{\Delta t}{2}[C]_t + \left(\frac{1}{2\beta} - 1\right)[M]_t\right]\{\ddot{w}\}_t \tag{3.25}$$

The coefficient terms of the matrix in the left hand side of the Eq. (3.25) are known. Therefore, the increment of the displacement vector, $\{\Delta w\}_{t+\Delta t}$, for the pile, soil plug, outer soil, and inner soil can be solved readily. Using these results, the total displacement vector $\{w\}_{t+\Delta t}$ at the current step is calculated by Eq. (3.26):

$$\{w\}_{t+\Delta t} = \{w\}_t + \{\Delta w\}_{t+\Delta t} \tag{3.26}$$

The velocities and accelerations are then promptly derived from Eqs. (3.23) and (3.24).

If the values of $[C]$, $[M]$, α, and β are set at zero, the above approach can be applied to a fully static problem.

3.4 Verification of the proposed method

3.4.1 Comparison with theoretical solution

A homogeneous pile without soil resistance subjected to a vertical triangle impact force was calculated using the proposed numerical method. The calculated results were then compared with the theoretical values. The properties of the pile and the impact force are shown in Fig. 3.5. The pile was divided into 50 elements in order to have a pile element length, ΔL, of 0.2 m, and the time step was set at $0.1\Delta t_{\text{cri}}$, $0.5\Delta t_{\text{cri}}$, $1\Delta t_{\text{cri}}$, $2\Delta t_{\text{cri}}$ and $4\Delta t_{\text{cri}}$ in order to evaluate the stability of Newmark's β approach, which is used in the proposed method. Here, Δt_{cri} is defined as $(\Delta L/c)/2$ where c is the theoretical bar wave velocity, $c = \sqrt{E/\rho}$. When time steps were greater than $2\Delta t_{\text{cri}}$, a solution could not be obtained.

Figures 3.6a and 3.6b compare the theoretical solutions and the results from the proposed method, respectively, for the axial force and the velocity versus time at the middle point of the pile (z = 5 m). Although a good agreement between the theoretical and calculated

results can be seen in both figures for the different time steps, the calculation results using $\Delta t = 0.5\Delta t_{cri}$ gave the solutions which were the closest to the theoretical values in the figures. The calculation results using $\Delta t = 0.1\Delta t_{cri}$ were almost equal to those using $\Delta t = 0.5\Delta t_{cri}$. Although $\Delta t = 0.5\Delta t_{cri}$ can be used in dynamic analysis, in case of nonlinear analysis, calculation time step should be selected to be smaller than $0.5\Delta t_{cri}$ in order to achieve an acceptable accuracy with reasonable calculation time.

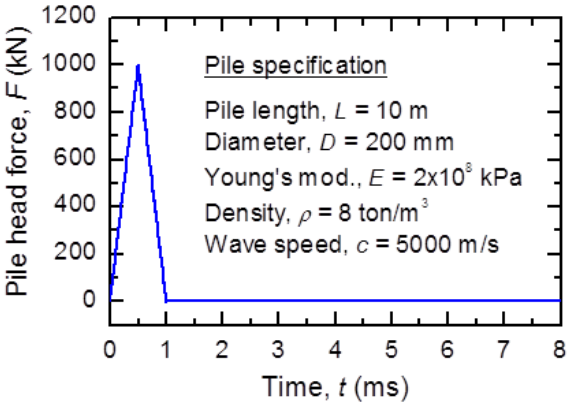

Figure 3.5. Head force and specification of the pile.

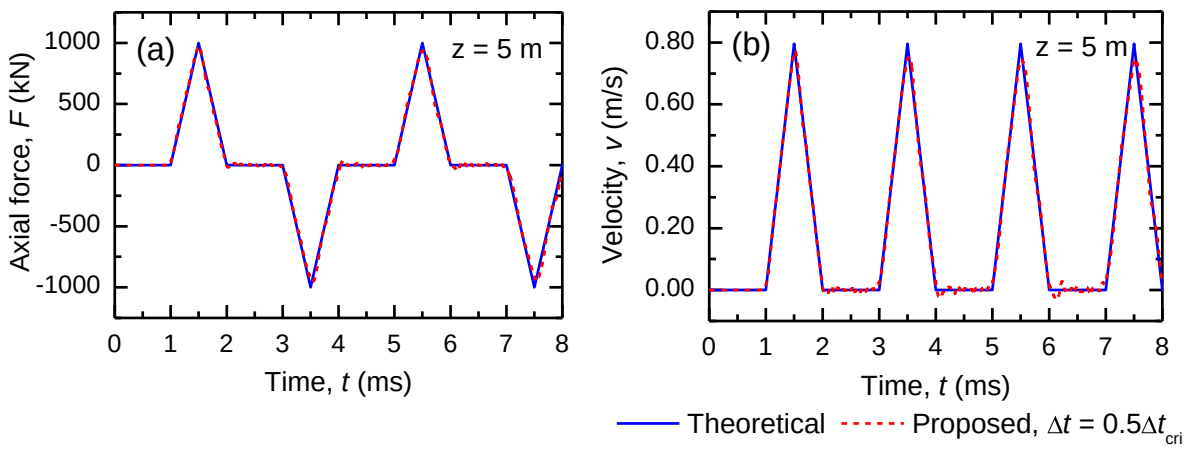

Figure 3.6. Comparison of the pile response at the middle point of the pile between the proposed method and the theoretical solution. (a) Pile axial force. (b) Pile velocity.

It should be noted that the above verification was conducted for a pile without soil resistance. No theoretical solution is available for wave propagation in a pile with soil resistance. Hence, the proposed approach is further verified for a pile with soil resistance.

3.4.2 Comparison with the Smith method

In order to compare the calculated results obtained from the proposed method with those from the Smith method in which rational soil models were employed, an open-ended pipe pile

having a length, L, of 21 m and a wave speed, c, of 4000 m/s in a uniform ground with the specifications as shown in Fig. 3.7 was analysed. The pile was divided into 42 elements for the two methods, and the same time interval, 0.01 ms, was used for both. Sinusoidal-shaped impact loads with a peak value of 2500 kN, and various loading durations, t_L = 2, 4, 6, 8, 80, 100, 120 and 140 ms as shown in Fig. 3.8, were applied on the pile head. The corresponding relative loading duration, $T_R = t_L/(2L/c)$, varied from about 0.2 to 14.

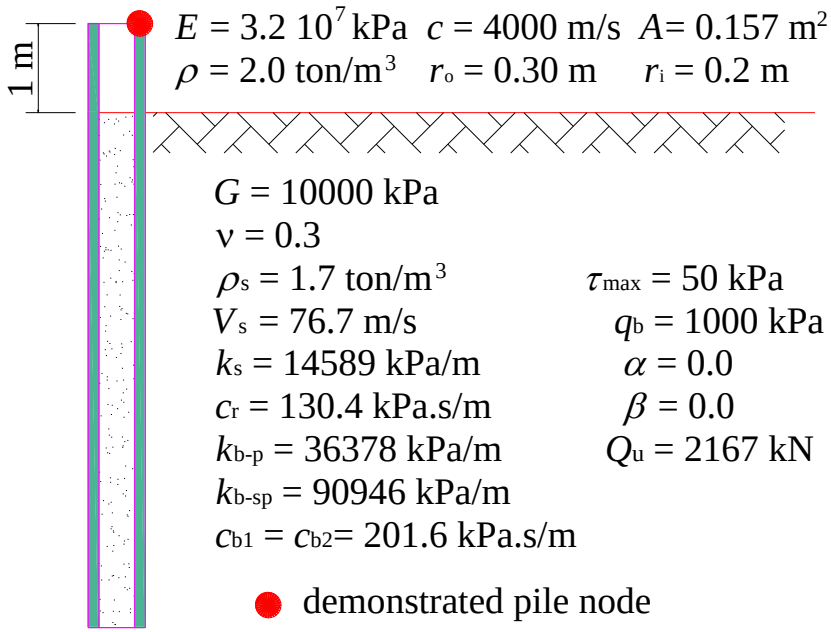

Figure 3.7. Specifications of the pile and soil.

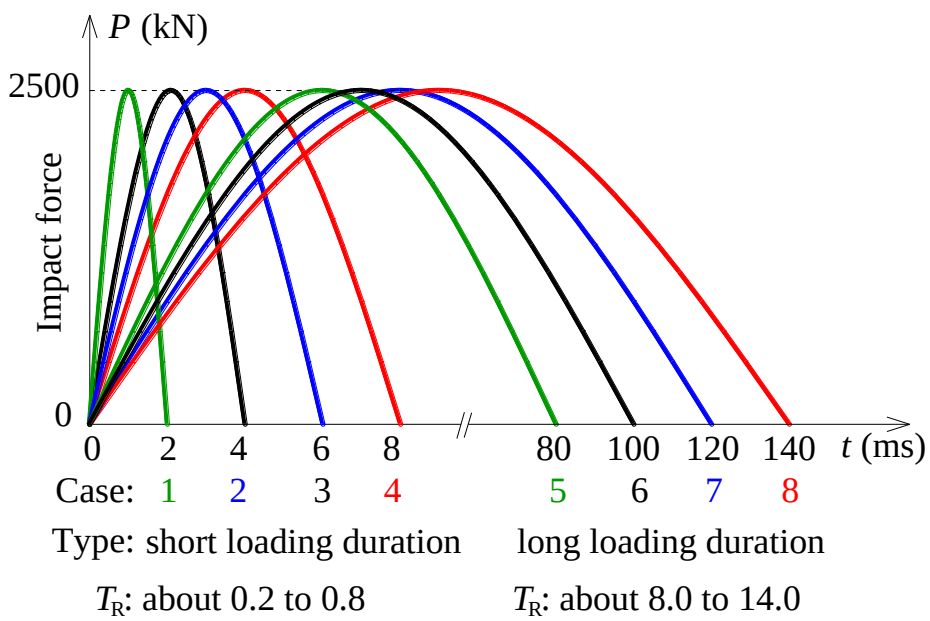

Figure 3.8. Impact force with different loading durations.

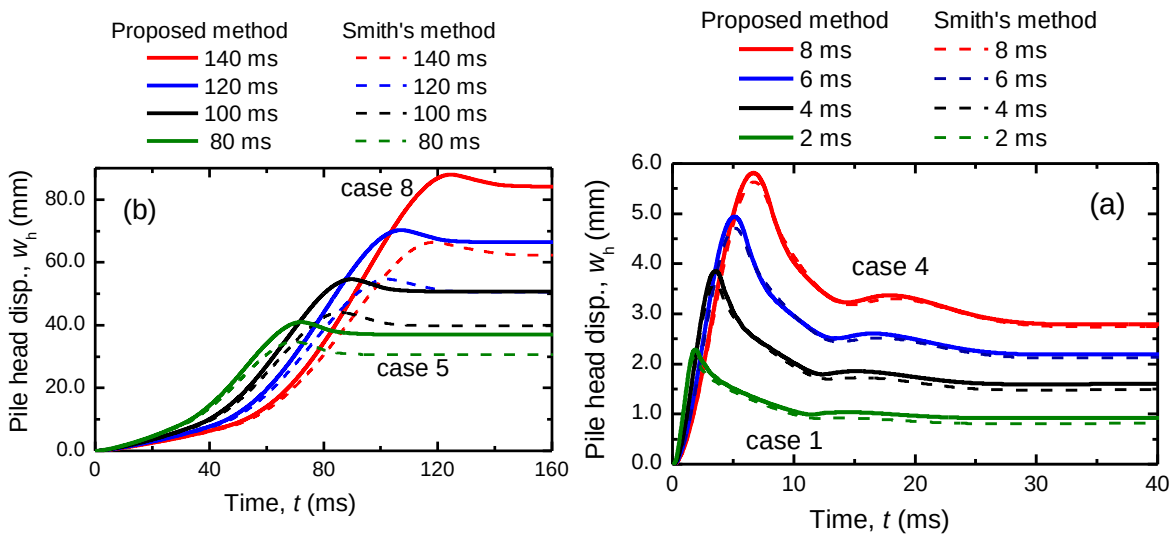

Figure 3.9. Pile head displacements vs. time.

(a) short loading duration. (b) long loading duration.

Figures 3.9a and 3.9b compare the pile head displacements versus time between the proposed and the Smith method for all the loading durations. In the cases with short loading durations, with t_L varying from 2 to 8 ms, as usual in DLTs, the results obtained from the Smith method are comparable with those from the proposed method, although the Smith method tends to slightly underestimate the pile displacement (Fig. 3.9a). In the cases with long loading durations, with t_L ranging from 80 to 140 ms, as usual in RLTs, the results obtained from the proposed method are always greater than those obtained from the Smith method, and this discrepancy becomes larger with the increase in loading duration.

In order to verify the proposed method in more detail, case 6 (t_L = 100 ms) was analysed again using the rigorous method FLAC^{3D} to compare the calculated results with those from the proposed and the Smith methods in the next section.

3.4.3 Comparison with results calculated using FLAC^{3D}

FLAC^{3D} is a three-dimensional explicit finite difference program for engineering mechanics computation simulating the behaviour of three-dimensional structures constructed on soil, rock or other materials that undergo plastic flow when their yield limits are reached (Flac^{3D} manual, Itasa 2000). Materials are represented by polyhedral elements within a three-dimensional grid.

Comparison analyses were made between the proposed method, the Smith method and the FLAC calculation for the case of an open-ended pipe pile. It was assumed that the inside of the pipe pile was filled with soil.

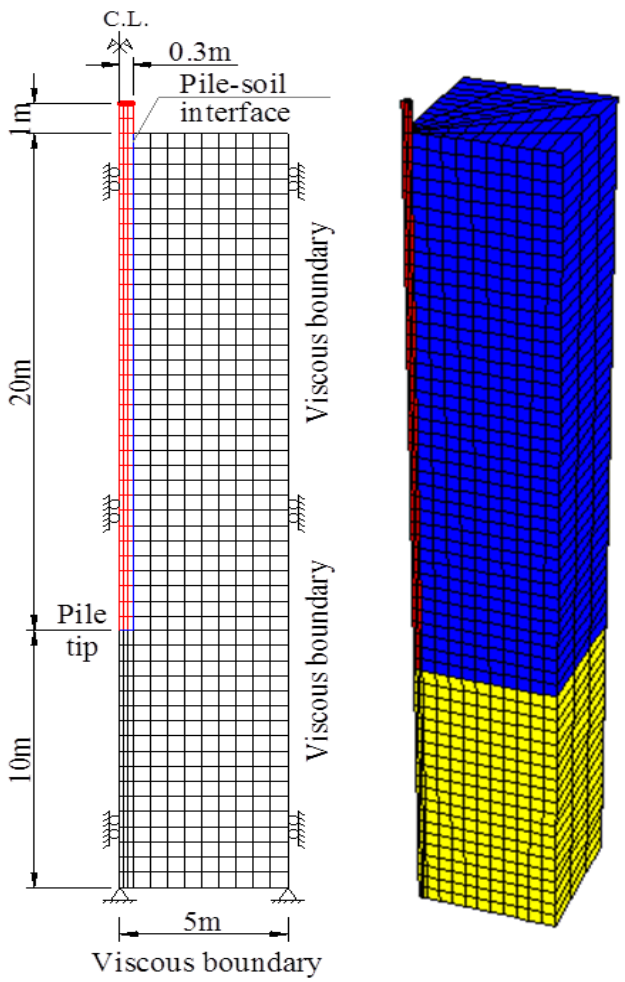

Figure 3.10. Modelling of the pile and ground using FLAC^{3D}.

Figure 3.10 shows the numerical model used in FLAC^{3D} to analyse the behaviour of an open-ended pile under vertical dynamic loading. In the present analysis, the pile is modelled by linear elastic elements surrounded by a linear elastic continuum media of soil. To take into account the slippage between the pile and soil, interface elements characterised by Coulomb sliding were employed at the pile-soil interfaces. In order to compare the results from the FLAC^{3D}, the Smith method and the proposed method, a cohesion strength of 50 kPa for soil surrounding the pile, a cohesion strength of 1000 kPa for soil beneath the pile tip and the zero friction coefficient were used in the FLAC^{3D} calculations, and $\alpha = 0$ (refer to Eqs. (3.13) and (3.14)) and $R_{fs} = R_{fb} = 0$ (refer to Eqs. (3.17) and (3.18)) were used in the proposed and the Smith methods.

In the FLAC^{3D} calculations, to minimise the influence of shear waves and longitudinal waves reflected from the outer boundaries of the ground, viscous boundaries were employed in the quarter-symmetry numerical model as shown in Fig. 3.10. The impact load of case 6 (t_L = 100 ms) (see Fig. 3.8) was applied on the pile head.

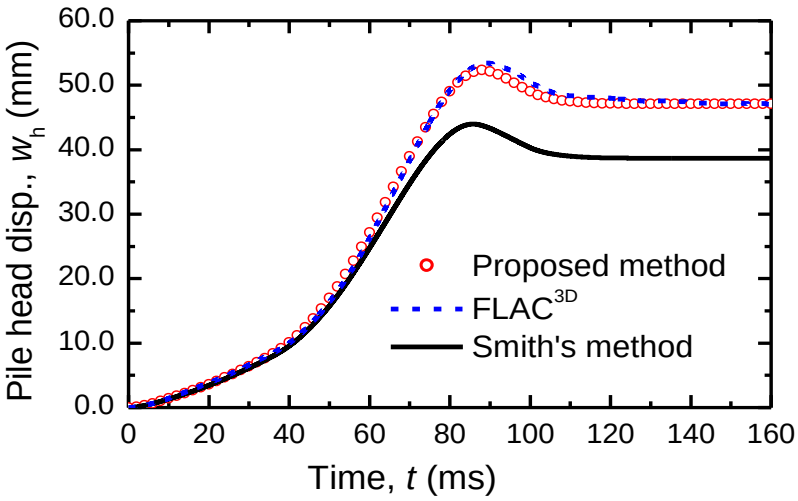

Figure 3.11. Pile head displacements of the open-ended pile obtained from the three methods.

Figure 3.11 compares the pile head displacement between the proposed method, the Smith method and the FLAC^{3D}. The figure shows that the calculated results obtained from the proposed method agree with those from the FLAC^{3D}, while the Smith method underestimates the pile displacements obtained from the FLAC calculation.

Based on the comparison of the results from three methods, it is obvious that the proposed numerical method is consistent with the FLAC^{3D} and more accurate than the Smith method for a wide range of loading durations. Moreover, the computational time using the proposed method is substantially shorter than the rigorous method, the FLAC^{3D}. In order to obtain the results in Fig. 3.11, for example, the calculation time using the proposed method was only a few seconds while the calculation time using the FLAC^{3D} required more than 30 minutes. Therefore, in terms of precision and computation time, the proposed method is a useful tool in pile driving analysis.

3.4.4 Sensitivity analyses of the example pile driving problem

In order to investigate the sensitivity of the analysed results in pile driving to variation of the soil parameters, the example pile driving problem in Fig. 3.7 with a loading duration of 6 ms (case 3 in Fig. 3.8) was analysed using the proposed numerical method. Since the linear elastic behaviour of the ground is assumed, α values (refer to Eqs. (3.13) and (3.14)) and R_{fs} = R_{fb} = 0 (refer to Eqs. (3.17) and (3.18)) are set as 0 in the example problem, shear modulus and maximum soil resistances are main soil parameters that influence the pile response. Let the values of G, τ_{max} and q_{max} shown in Fig. 3.7 be regarded as the reference soil parameters.

In addition to the analysis with the reference soil parameters (called reference case), twelve cases of analyses were carried out, changing the values of G, τ_{max} and q_{max}. In cases 1 to 4, shear moduli, G, alone were varied, while in cases 5 to 12, τ_{max} and q_{max} were varied. The reference soil parameters were factored from 0.5 to 1.5 in the sensitivity analyses.

It is a common practice in the monitoring of pile driving to measure strains and accelerations near the pile head. Time variations of force, F, velocity, v, and displacement, w, are obtained from these dynamic signals. Hence, the pile responses at the ground level (1 m below the pile head) are compared in this sensitivity analysis. It is well known from the one-dimensional stress-wave theory that the upward travelling force, F_u, is obtained using the following equation.

$$F_u = \frac{1}{2}\left(F - \frac{EA}{c}v\right) \tag{3.27}$$

where A is the cross-sectional area of the pile.

Calculated pile head displacement and F_u are compared below, because F_u tends to be largely influenced by the soil resistance.

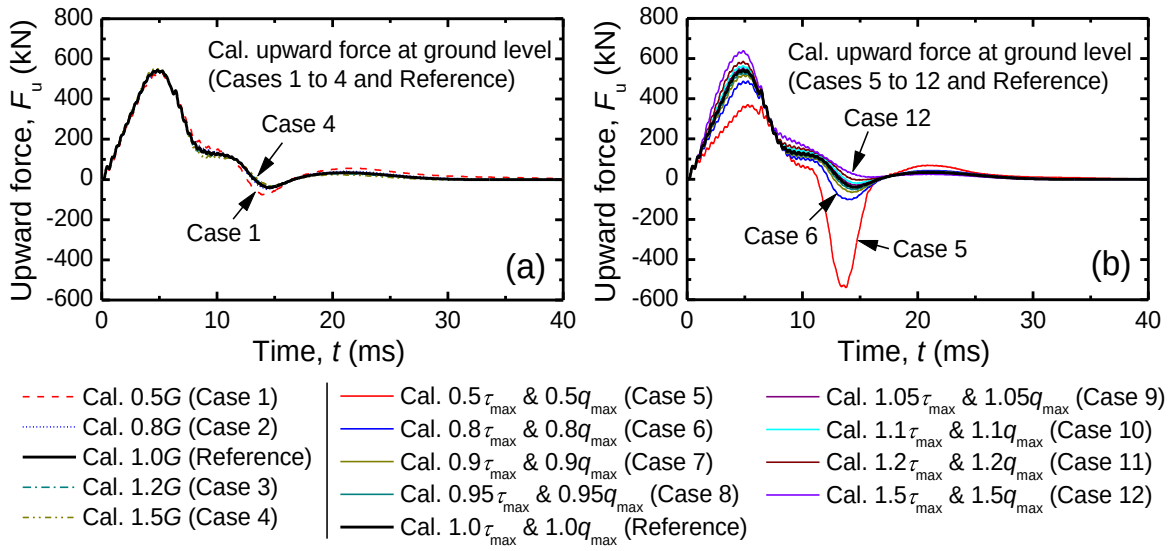

Figure 3.12. Sensitivity of upward force at ground level due to (a) Variation of G. (b) Variation of τ_{max} and q_{max}.

The calculated F_u are shown in Fig. 3.12: (a) in cases 1 to 4 where G alone was varied, (b) in cases 8 to 12 where τ_{max} and q_{max} were varied. It is seen that F_u is very sensitive to the variation of soil resistance, compared to the sensitivity of F_u to the variation of G. Approxi-

mately describing, variation of 5% in the soil resistance causes variation of 20% in F_u, while variation of 20% in the shear modulus causes variation of 15% in F_u.

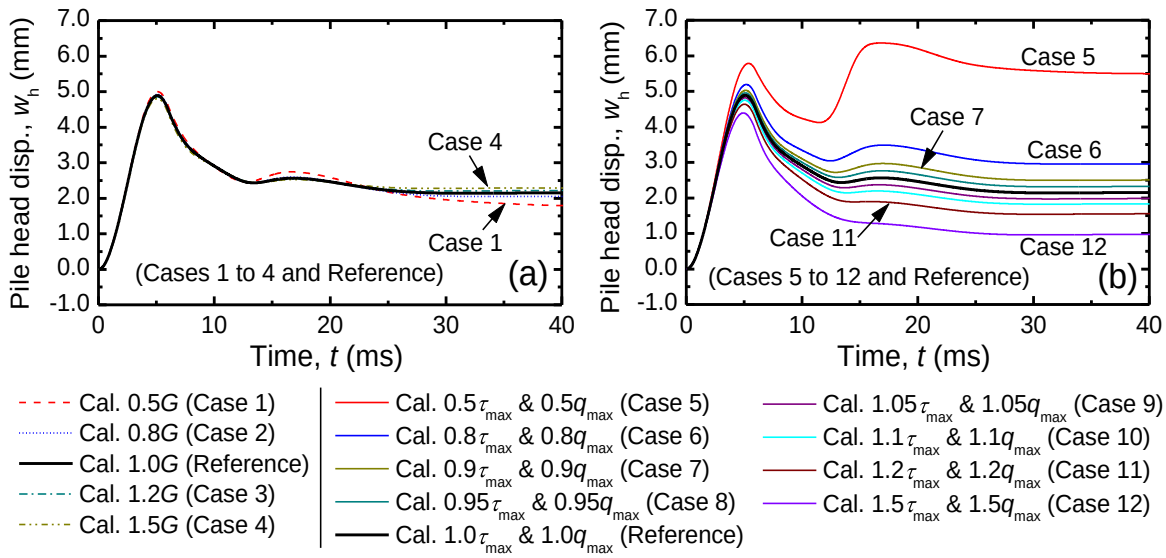

Figure 3.13. Sensitivity of the pile head displacement due to (a) Variation of G. (b) Variation of τ_{max} and q_{max}.

The calculated pile head displacements, w_h, are shown in Fig. 3.13: (a) in cases 1 to 4 where G alone was varied, (b) in cases 8 to 12 where τ_{max} and q_{max} were varied. It is seen that w_h is very sensitive to the variation of soil resistance, compared to the sensitivity of w_h to the variation of G. With a variation of 20% in shear modulus (cases 2 and 3 in Fig. 3.13a), final pile head displacement differs from the reference value by 4%, while only variation of 5% in the soil resistances (cases 8 and 9 in Fig. 3.13b) results in a difference of 8% from the reference value.

Low sensitivity of the dynamic pile responses to G may be explained as follows. In pile driving, soil resistance due to radiation damping (velocity-dependent soil resistance) is predominant, compared to static component in the soil resistance. Hence, maximum soil resistance is mobilised with very small soil displacement in pile driving, compared to the case of static loading. After the occurrence of the slippage failure at the pile shaft or failure of the ground below the pile tip, the soil resistance predominantly influence the pile response, resulting in low sensitivity of the dynamic pile responses to G.

The calculated static load-displacement curves are shown in Fig. 3.14: (a) in cases 1 to 4 where G alone was varied, (b) in cases 8 to 12 where τ_{max} and q_{max} were varied. As expected, pile head stiffness is sensitive to G, while yield load and bearing capacity are sensitive to the soil resistance.

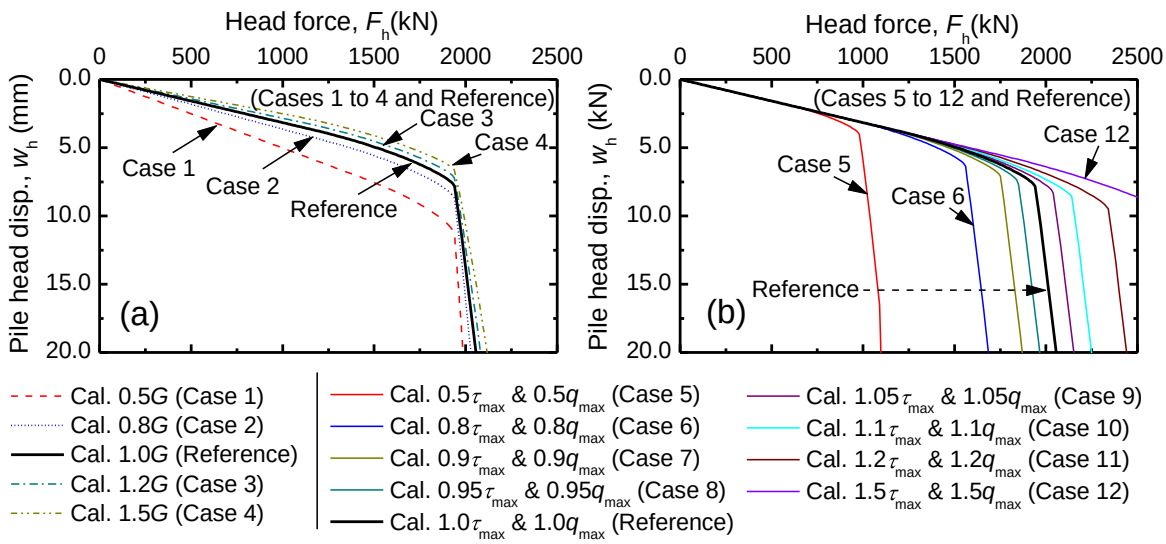

Figure 3.14. Sensitivity of derived load-displacement curve due to (a) Variation of G. (b) Variation of τ_{max} and q_{max}.

It can be said from the sensitivity analyses that the results of WMA (dynamic pile responses) are dominantly governed by the assumption of the soil resistance distribution. The soil resistance distribution could be estimated with an acceptable accuracy within a variation of 5 % if the differences between calculated and measured values of the peak upward travelling force and final pile head displacement in WMA are in range of 20 % and 5 %, respectively. Similar criteria could be used in WMA to obtain the distribution of shear modulus with an accuracy of 20 %. If measurements of elastic shear wave velocities of the ground are available we could improve the accuracy of the identified shear modulus form wave matching analysis.

3.5 Conclusions

In this chapter, a matrix method using a finite difference scheme to analyse the phenomenon of stress wave propagation in an open-ended pipe pile under both static and dynamic loading conditions has been proposed. In this method, the influence of stress wave propagation in the soil plug was considered, and the nonlinearity of the soil stiffness and damping coefficient were also taken into account. The proposed method was verified by comparing the analysed results with those from a theoretical solution, the conventional Smith method, and a rigorous continuum method, the FLAC^{3D}.

The following conclusions and findings were drawn from the numerical analyses and experiments with limited conditions:

(1) The results obtained from the proposed method are comparable with those obtained from the rigorous continuum method, the $FLAC^{3D}$.

(2) The proposed method has a fast computation time when compared to the rigorous method.

(3) The proposed method is precise when compared with the Smith method for a wide range of loading durations.

Although the validity of the proposed method was examined through numerical analysis, it is needed to verify the proposed numerical method through experiments and field tests.

References

Bermingham P. and Janes M. (1989). An innovative approach to load testing of high capacity piles. Proc. of Int. Conf. on Piling and Deep Foundations; 409-413.

Chow Y.K. (1986). Analysis of vertically loaded pile groups. Int. Jour. for Numerical and Analytical Methods in Geomechanics; 10: 59-72.

Chow Y.K. and Smith I.M. (1984). A numerical model for the analysis of pile drivability. Proc. 2nd Int. Conf. on the Application of Stress waves to Piles, Sweden; 319-325.

Edward L.W. (2000). Dynamic analysis using numerical integration. Three-dimensional static and dynamic analysis of structures. Computers and Structures, Inc., Berkeley, California, USA; 20.1-20.11.

Goble G.G. and Rausche F. (1976). Wave equation analysis of pile driving – WEAP program. FHWA; 1 to 4: FHWA IP-76-14.1 to76-14.4.

Goble G.G. and Rausche F. (1979). Pile driveability prediction by CAPWAP. Numerical method in offshore piling, ICE, London; 29-36.

Heerema E.P. and de Jong A. (1979). An advanced wave equation computer program which simulates dynamic pile plugging through a coupled mass-spring system. Proc. Int. Conf. on Num. Methods in Offshore Piling, ICE, London; 37-42.

Idriss I.M. and Seed H.B. (1969). Seismic response of horizontal soil layers. Journal of the Soil Mechanics and Foundation Division ASCE; 94(SM4): 1003-1031.

Itasa (2002). Fast lagrangian analysis of continua in three dimensions ($FLAC^{3D}$), version 3.0. Itasca Consulting Group, Inc. Minesota.

Kusakabe O. and Matsumoto T. (1995). Statnamic test of Shonan test program with review of signal interpretation. Proc. of 1st Int. Stanamic Seminar, Vancouver; 113-122.

Liyanapathirana D.S., Deeks A.J. and Randolph M.F. (2001). Numerical modelling of the driving response of thin-walled open-ended piles. Int. Journal for Numerical and Analytical Methods in Geomechanics; 25: 933-953.

Matsumoto T. and Takei M. (1991). Effects of soil plug on behaviour of driven pipe piles. Soils and Foundations; 31(2): 14-34.

Matsumoto T., Tsuzuki M. and Michi Y. (1994). Comparative study of static loading test and Statnamic on steet pipe pile driven in a soft rock. Proc. of 5th Int. Conf. on Exhibition on Piling and Deep Foundations, Bruges, Belgium; 5.3.1-5.3.7.

Matsumoto T., Wakisaka T., Wang F.W., Takeda K. and Yabuuchi N. (2004). Development of a rapid pile load test method using a hammer mass attached with spring and damper. Proc. of 7th Int. Conf. on Application of Stresswave Theory to Piles, Selangor, Malaysia; 351-358.

Middendorp P. and van Weele A.F. (1986). Application of characteristic stress wave method in offshore practice. Proc. 3rd Int. Conf. on Numerical Methods in Offshore Piling, Nantes, Supplement; 6-18.

Newmark N.M. (1959). A method of computation for structural dynamics. Journal of Engineering Mechanics, ASCE; 85 (EM3): 67-94.

Paikowsky S.G. and Chernauskas L.R. (2008). Dynamic analysis of open-ended pipe pile. Proc. 8th Int. Conf. Application of Stress Wave Theory to Piles, Lisbon; 59-76.

Rausche F., Moses F. and Goble G.G. (1972). Soil resistance predictions from pile dynamics. Journal of the Soil Mech. and Found. Div., ASCE; 98 (SM9): 917-937.

Randolph M.F. and Simon H.A. (1986). An improved soil model for one dimensional pile driving analysis. Proc. 3rd Int. Conf. Num. methods in Offshore Piling, Nantes; 1-17.

Randolph M.F. and Deeks A.J. (1992). Dynamic and static soil models for axial response. Proc. 4th Int. Conf. Application of Stress Wave Theory to Piles, The Hague; 3-14.

Smith E.A.L. (1955). Impact and longitudinal wave transmission. Trans., ASME; 963-955.

Smith E.A.L. (1960). Pile Driving Analysis with the wave equation. Journal of Soil Mechanics and Foundation Eng., ASCE; 86: 35-64.

Wakisaka T., Matsumoto T., Kojima E. and Kuwayama S. (2004). Development of a new computer program for dynamic and static pile load tests. Proc. 7th Int. Conf. on the Appl. of Stress-Wave Theory to Piles, Selangor, Malaysia; 341-350.

Chapter 4

Validation of the proposed numerical method through laboratory test.

4.1 Introduction

The proposed numerical method for analysing the wave propagation in an open-ended pipe pile based on the one-dimensional stress-wave theory has been developed in Chapter 3. In this chapter, two series of static and dynamic pile load tests on an open-ended pipe pile (OP) and a close-ended pipe pile (CP) in a model ground of dry sand were carried out to validate the proposed numerical method. The main objective of these experiments was placed on the wave matching analysis (WMA) of the piles subjected to impact forces due to falling hammer masses. The static response of the pile derived from the WMA was compared with that obtained from the static load test.

4.2 Test description

4.2.1 Model soil

Silica sand No.6 was used for the model ground throughout the experiments. The physical properties of the sand are summarised in Table 4.1. The internal friction angles, ϕ', were estimated by conducting direct shear tests (DSTs) for dense (relative density $D_r \approx 90\%$) and medium ($D_r \approx 70\%$) packing states of the sand. Peak and residual strengths of the dense and medium packing states were plotted against the effective normal stress, σ', in Fig. 4.1. As can be seen, cohesion, c', was negligible. The values of ϕ' at the peak and the residual strengths are listed in Table 4.2.

The silica sand was prepared in a 600 mm stainless steel cubic container. The model ground was 550 mm in height. In order to make a uniform ground, a model ground was prepared with 11 layers, each 50 mm thick. In every layer, an amount of soil corresponding to a prescribed relative density (D_r = 70 %) and a given height of 50 mm was first poured into the chamber and then compacted by tapping to make a layer of 50 mm thick. This procedure was iterated until a model ground of 550 mm in height was obtained. The dry density, ρ_d, of the model ground was 1.45 ton/m^3.

Table 4.1. Physical properties of the Silica sand.

Properties	Value
Density of soil particles, ρ_s (ton/m^3)	2.680
Max. dry density, $\rho_{d,max}$ (ton/m^3)	1.554
Min. dry density, $\rho_{d,min}$ (ton/m^3)	1.249
Max. void ratio, e_{max}	1.145
Min. void ratio, e_{min}	0.720

Table 4.2. Internal friction angle of the Silica sand.

Packing state of the Silica sand	ϕ'(deg.)
Dense (at peak)	39.4
Dense (at residual)	33.8
Medium (at peak)	33.9
Medium (at residual)	32.0

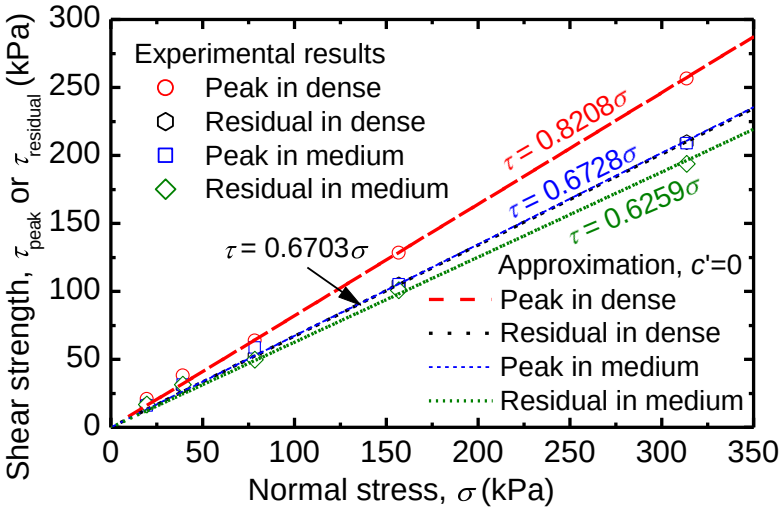

Figure 4.1. Test results of DSTs and its approximations with c'=0

4.2.2 Model piles

Aluminium pipe pile was used for the model piles, the properties of which are listed in Table 4.3. Young's modulus, E_p, and Poisson's ratio, ν_p, were estimated from a bending test of the

model pile. Two model piles were prepared. One of them was an open-ended pipe pile (OP), and the other was a close-ended pipe pile (CP) equipped with a flat cap at the pile toe.

Table 4.3. Properties of the model pile.

Properties	Value
Length, L (mm)	595
Outer diameter, D_o (mm)	32.0
Inner diameter, D_i (mm)	29.3
Young's modulus, E_p (GPa)	65.4
Density, ρ_p (ton/m^3)	2.636
Wave speed, c (m/s)	4981
Poisson's ratio, ν_p	0.33

In order to measure the distribution of the axial forces in the pile as well as the soil resistance during the tests, 24 strain gauges were mounted on the outer surface of the pile at six levels labelled SG1 to SG6, as shown in Fig. 4.2. At each level, the strain gauges were attached symmetrically through the central axis of the pile. Each location had two gauges to measure the vertical and horizontal strains. In order to protect the strain gauges from damage and to increase the friction between the pile and the outer soil, the pile was first covered by a protective material, followed by a thin layer of the same silica sand as the model ground.

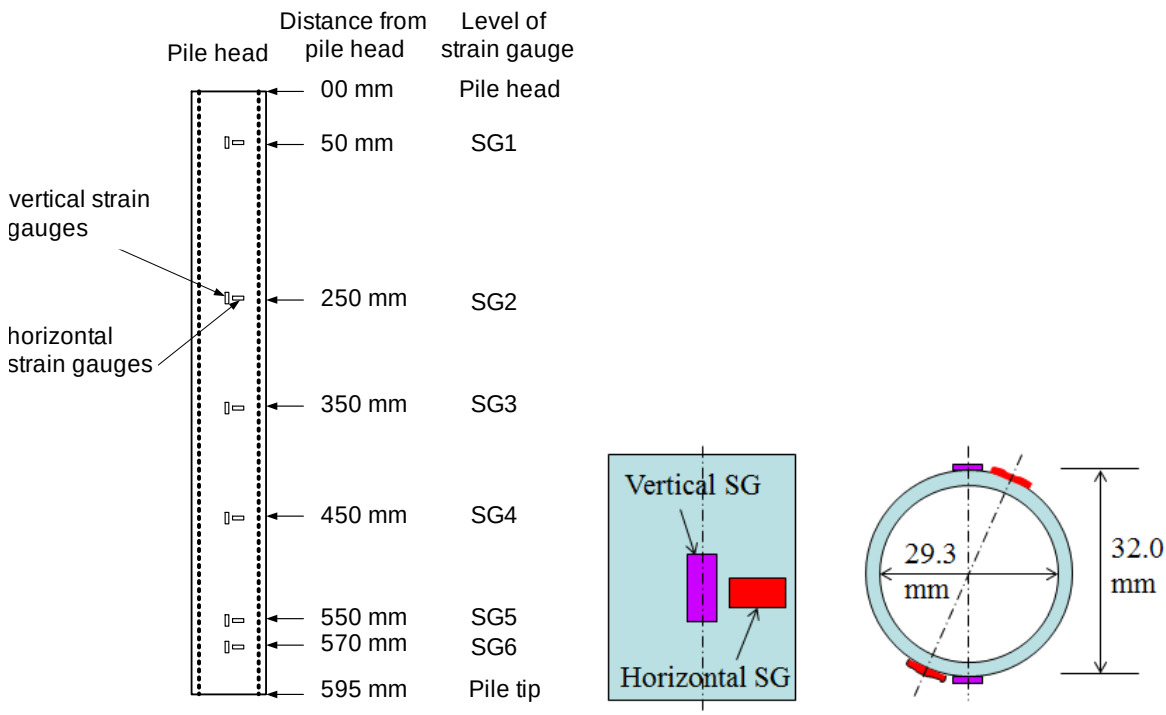

Figure 4.2. Arrangement of the strain gauge.

During the static load tests, both vertical and horizontal strains were measured in order to eliminate the influence of temperature change. Only vertical strains were measured in the

pile driving tests since the loading duration was less than 20 ms and the influence of temperature change was negligible.

At the SG1 level, two accelerometers having a range of 10,000g and a response frequency of 20 kHz were mounted next to the strain gauges on opposite sides.

4.3 Test procedure

After preparing the model ground, the pile was set at the centre location of the soil container with a support of horizontal bars at two levels to keep the model pile vertical. All the instrumentation of the SLTs including a jack, a load cell, a dial gauge, an encoder, and the measuring systems were arranged as shown in Fig. 4.3, and those of the DLTs are shown in Fig. 4.4. A series of pile load tests were carried out in four stages as below:

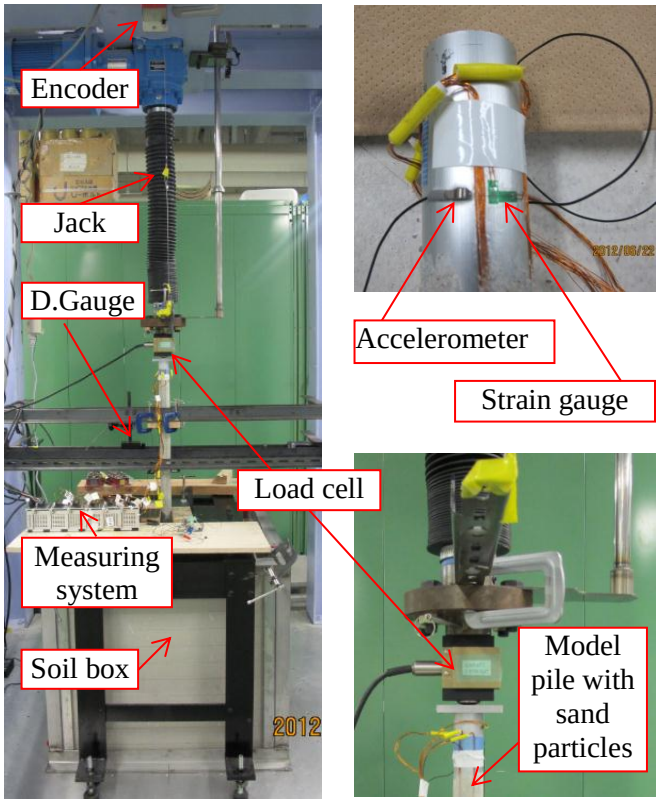

Figure 4.3. Photo of the static load test system.

1) The pile was pressed into the model ground to a depth of 400 mm by a screwed jack with a loading speed of 0.5 mm/s. The applied force, the pile head displacement and the strains were recorded during the test.
2) The SLT (SLT1 hereafter) was carried out with a maximum displacement of about 40 % of the outer pile diameter. The loading speed was fixed at 0.05 mm/s.

3) The pile driving system was arranged to carry out the DLTs. The DLTs were conducted using falling hammers with masses of 0.96 kg and 1.62 kg. Accelerations and strains were recorded for each blow with a sampling frequency of 1 MHz. Permanent settlement of the pile per blow, *S*, was also measured after the driving.

4) The SLT (SLT2 hereafter) was carried out again with the same specifications as the previous static load test to evaluate the influence of the pile driving process on the static response, and to compare its load-displacement relation to the relation obtained from the wave matching analysis (WMA).

In the case of the OP, to study the plugging mode, the soil plug height was obtained by measuring the distance between the pile head and the top of soil plug after each stage.

For the CP, an additional test was carried out in the same soil conditions. The close-ended pipe pile was pressed into the model ground to a depth of 400 mm and then pulled out to measure the difference in the outer shaft resistance between compression and tension loading conditions.

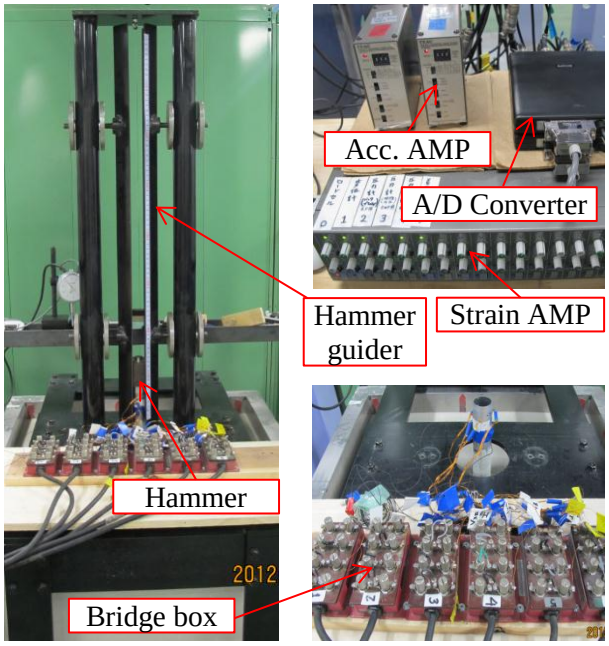

Figure 4.4. Photo of the pile driving system.

4.4 Results of the close-ended pipe pile

4.4.1 Results of the SLTs

Figure 4.5 shows the load-displacement curves obtained from the SLT1 and SLT2 for the open-ended pipe pile. If a yield load is defined as the load at the maximum curvature of the static load-displacement curve, the yield load of SLT2 is lower than that of SLT1. This

difference could be because the soil surrounding the pile was disturbed due to the pile driving tests between SLT1 and SLT2, resulting in a reduction of the total shaft resistance in SLT2.

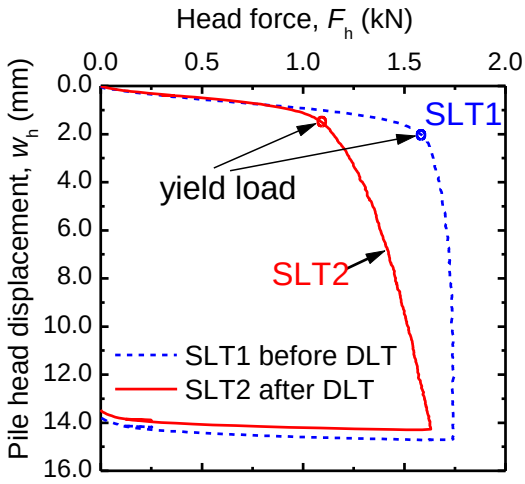

Figure 4.5. Load-displacement curves of the CP.

Figure 4.6a shows the relation between the mobilised shear resistance and the local pile displacement for the pile sections between the strain gauge levels obtained from SLT2. The results of the WMA for the final blow in the pile driving tests just prior to SLT2 will be compared with the results of SLT2 later. The local pile displacement at the middle point of each pile section was obtained from the measured pile head displacement and the measured strains. The relation between the mobilised tip resistance and the pile tip displacement is plotted in Fig. 4.6b.These figures demonstrate that the mobilisation of the shaft resistance can be modelled by slight nonlinear responses and the mobilisation of the tip resistance by a higher nonlinear response.

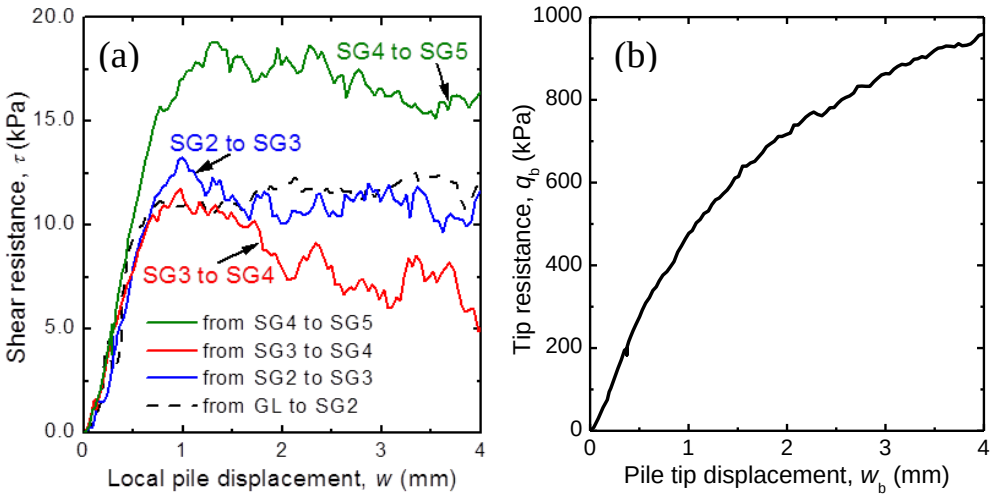

Figure 4.6. Mobilised soil resistance vs. local pile disp. of the CP in SLT2 at.

(a) Pile shaft. (b). Pile tip

The axial force distributions will be presented later with the results of the wave matching analyses for the DLTs.

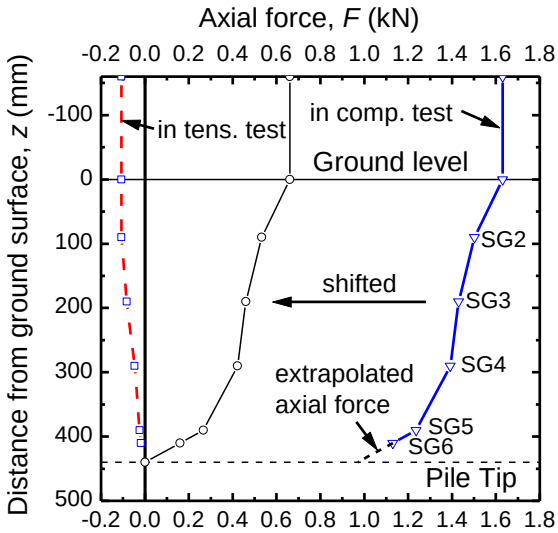

Figure 4.7. Comparison of the axial forces between the compression and tension tests.

Figure 4.7 shows the distributions of the axial forces of the pile at the maximum compression load of 1.62 kN in SLT2 and at the maximum tension force of 0.1 kN in the pull out test of the CP. The tension force is almost equal to the total outer shaft resistance in tension, because the tension tip resistance is not mobilised and the weight of the pile is negligible compared to the maximum tension force. For the compression test, the tip force was estimated by extrapolation as indicated by the dashed line in Fig. 4.7. In order to compare the distributions of the axial forces caused by the outer shaft resistance alone, the axial force distribution obtained in the compression test (SLT2) is shifted so that it has zero value at the pile tip level. It is clearly seen from the comparison of the axial force distribution in the tension test and the shifted distribution that the maximum outer shaft resistances along the pile shaft became remarkably smaller when compared to those in the compression loading. This phenomenon is clearly seen at a section 50 mm (about 1.5D_o) above the pile tip. It can be said that a similar phenomenon occurs in the open-ended pile (OP), although a pull out test was not carried out for the OP. Such a dramatic reduction in the outer shaft resistance during tension loading could be caused by the small size of the experiments, where effective stress levels are very low compared to those in actual piles.

It should be noted that the modelling of the shaft resistance response shown in Fig. 3.4 (Chapter 3) is reasonable, based on the experimental results in Fig. 4.7.

4.4.2 Wave matching analysis of the DLT

A total of 5 blows were conducted from various falling heights with the small and big hammers as listed in Table 4.4. No cushion was used between the hammer and the pile head in blows 1 to 4, while a rubber cushion, 1 mm in thickness, was used in blow 5. The results of the WMA of the last blow (the fifth blow) are presented in this study, because SLT2 was carried out right after this blow.

Table 4.4. Driving conditions and measured set per blow of DLTs of the CP.

Blow	1	2	3	4	5
Falling height (mm)	400	600	400	650	650
Measured set (mm)	0.8	1.1	2.0	2.6	3.3
Hammer	S	S	B	B	B

S: small steel hammer with a mass of 0.96 kg, *D* of 54.9 mm, height of 51.4 mm.
B: large steel hammer with a mass of 1.62 kg, *D* of 60.1 mm, height of 73.0 mm

Due to the high frequency of the acceleration generated while driving a very short pile and the limited response frequency of the accelerometers, the measured accelerations were not reliable enough to calculate the velocity and displacement of the pile. Therefore, the pile axial forces obtained from the measured strains were used as targets in the wave matching analysis (WMA).

In the WMA, assumptions about the distributions of the outer shaft resistance and the tip resistance, as well as the shear moduli of the soil layers, were needed. The authors are aware that SLT results are not usually available in practice. The main objective of the WMA in this chapter is to examine the validity of the proposed method. Hence, the shear resistances obtained from the SLT2 results were used for the first assumptions concerning the soil properties in the WMA.

In order to roughly estimate the distribution of the shear modulus, G, of the model ground with the depth used in the WMA as the first assumption value, one-dimensional compression tests of the silica sand No.6 with $D_r \approx 70$ % were conducted to obtain the relationship between the confined modulus, E_c, and the overburden stress, σ_v'. The oedometer test device was used for the one-dimensional compression tests. The applied pressure, σ_v', and the vertical strain, ε, were measured. The value of E_c at a given stress level was estimated as $E_c = \Delta\sigma_v' / \Delta\varepsilon$. Thus, the estimated E_c was plotted against σ_v' in Fig. 4.8. Note that σ_v' in Fig. 4.8 is the average value of each loading step. The measured relations are approximated using the following relation:

$$E_c = E_{cref}\left(\frac{\sigma_v'}{\sigma_{ref}}\right)^n \tag{4.1}$$

where σ_{ref} is the reference value of the vertical stress (100 kPa is used in this case), E_{cref} is the value of E_c at σ_{ref}, and n is an index number.

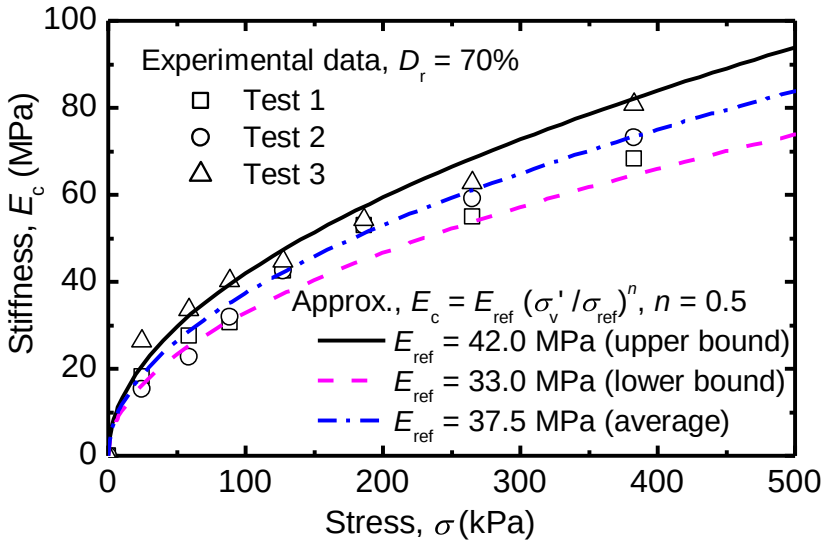

Figure 4.8. Relationship between the confined modulus, E_c, with overburden stress, σ_v'.

The mean values of E_c are closely approximated using E_{cref} = 37.5 MPa and n = 0.5 as shown in Fig. 4.8. The shear modulus, G, of the soil is estimated using the following equation of elasticity:

$$G = \frac{(1-2\nu)}{2(1-\nu)}E_c \tag{4.2}$$

where ν is Poisson's ratio of the soil, and assumed to be 0.3.

The first assumptions about the soil properties are shown in Fig. 4.9. The distribution of the shear modulus, G, with depth was estimated using Eqs. (4.1) and (4.2) with E_{cref} = 37.5 MPa and n = 0.5. The distribution of the outer shaft resistance was estimated from Fig. 4.6. Although the model ground was divided into 5 layers, the pile was divided into 55 elements in the analyses.

The measured pile force at SG1 (50 mm from the pile head) in the fifth blow (Fig. 4.10) was used as the input force in the WMA. Hence, the pile section below the level of SG1 was modelled in the analysis.

In the first WMA with the soil properties shown in Fig. 4.9, a good matching was not obtained. The soil properties were then changed until a good matching between the calculated and the measured responses was obtained.

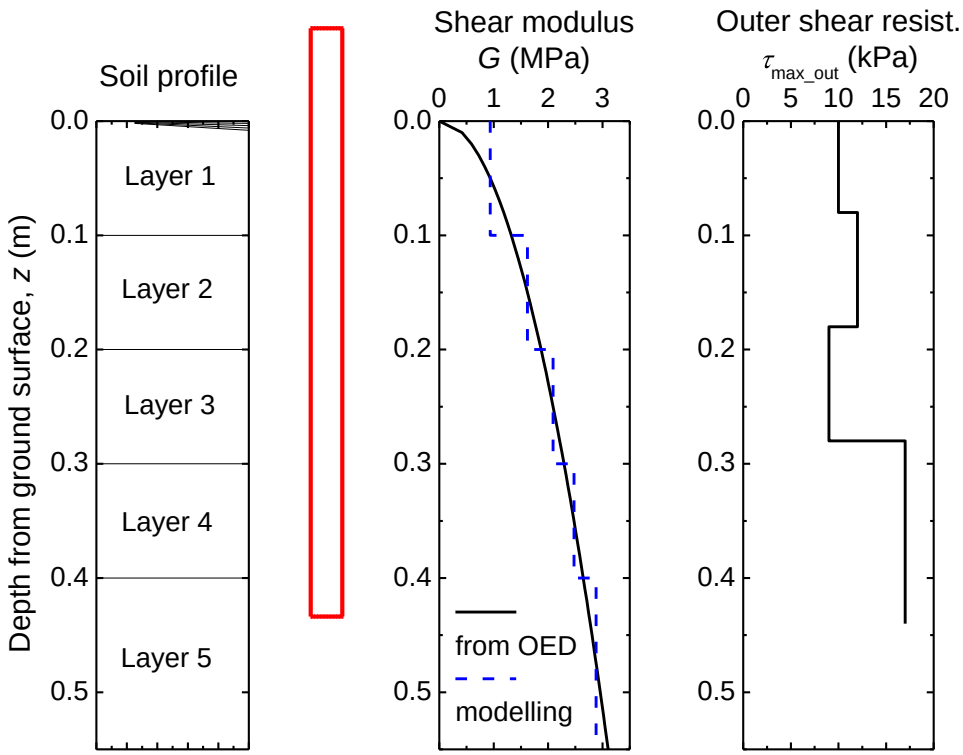

Figure 4.9. Soil properties used in the first WMA of the CP.

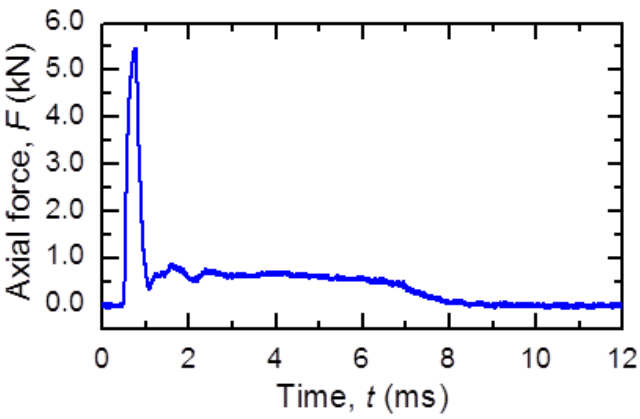

Figure 4.10. Measured axial force at SG1 of blow 5 of the CP.

Figure 4.11 shows the results of the final WMA. The calculated changes in the axial pile forces over time are compared with the measured values at SG3, SG4 and SG5. At every level, the calculated axial forces were in close agreement with the measured forces. It is seen from Fig. 4.11, that both of the calculated and measured pile axial forces returned to zero after

about 9 ms, indicating that residual axial forces are negligible in this driving. It also can be seen from the calculated results in Fig. 4.12 that the driving event terminates at 9 ms.

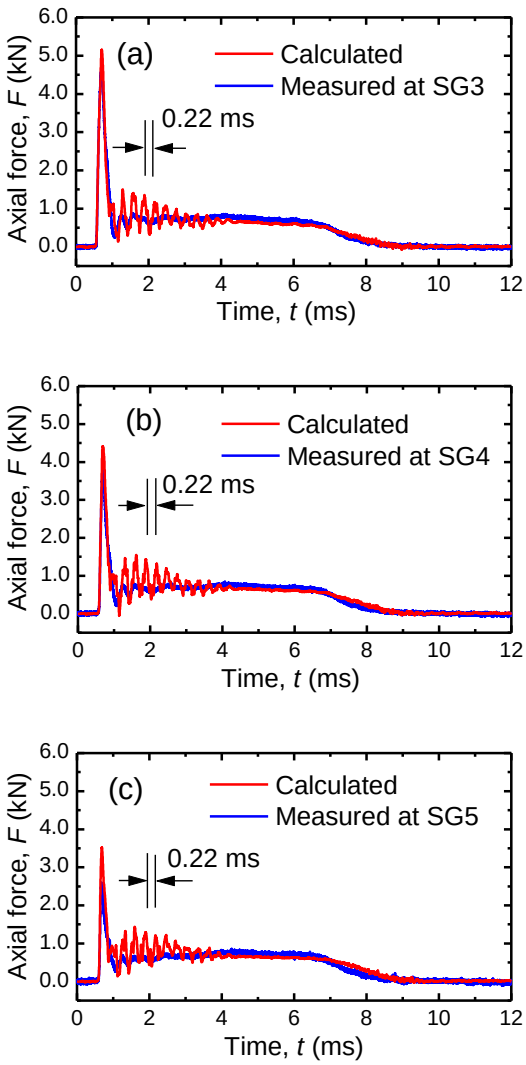

Figure 4.11. Results of the final WMA of the CP for the axial forces.
(a) at SG3. (b) at SG4. (c) at SG5.

It should be noted that oscillation axial forces are found in the calculated results and the magnitude of the oscillation decreases over time without divergence. The period of the oscillation corresponds to the return travelling time, $2L/c$ = 0.22 ms, of the stress wave in the pile. This means that the proposed numerical method is capable of calculating the wave propagation in a pile. Oscillation with a period of 0.22 ms is not seen in the measured forces. A possible reason for this might be due to the low frequency response of the amplifier used for the strain measurement. The oscillation of the calculated pile forces seems to be reduced for longer piles. Analyses of the case histories of longer piles would be useful for a more detailed discussion in a future study.

Furthermore, a reasonable agreement in the final settlements between the calculated and the measured values was obtained as indicated in Fig. 4.12.

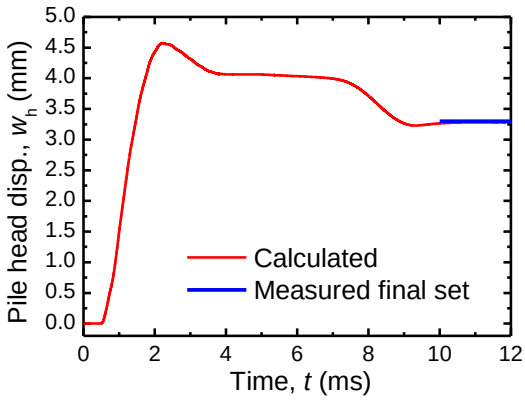

Figure 4.12. Pile head displacement calculated from the final WMA of the CP.

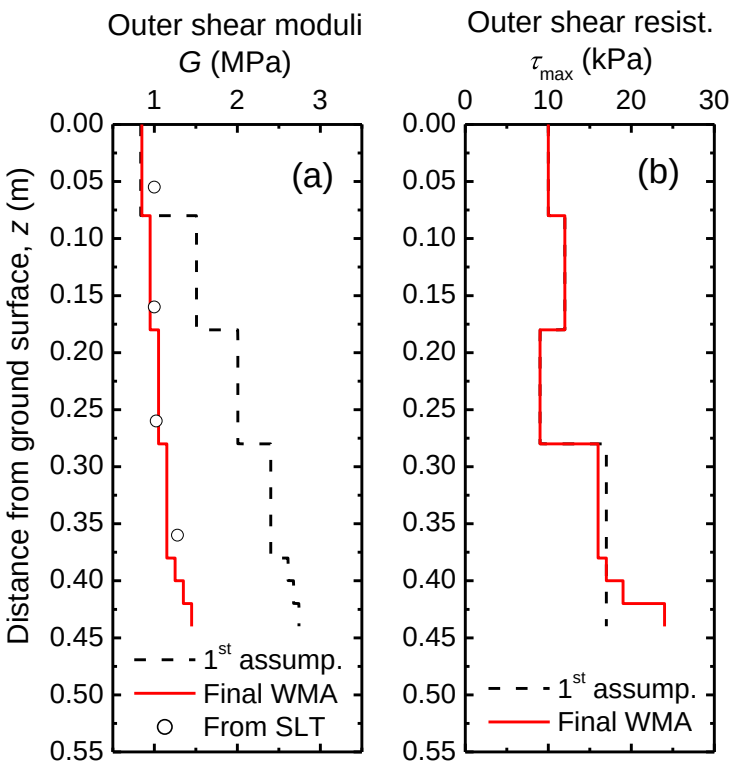

Figure 4.13. Distribution of the shear moduli and shear resistances.

(a) Shear moduli. (b) Shear resistances

The soil properties identified from the final WMA are shown in Fig. 4.13. The soil properties used in the first assumption are also indicated for comparison. The other soil properties identified from the final WMA are; $\alpha = 0$ (refer to Eqs. (3.13) and (3.14) in Chapter 3), $R_{fs} = 0.3$ (refer to Eq. (3.17) in Chapter 3), $R_{fb} = 0.9$ (refer to Eq. (3.18) in Chapter 3), end-bearing resistance at the pile tip = 1410 kPa, and shear modulus of the soil beneath the pile tip

= 3000 kPa. Note that β (refer to Eqs. (3.13) and (3.14) in Chapter 3) has no influence on the WMA results when $\alpha = 0$. The identified non-linearity coefficients of the soil at the pile shaft, R_{fs}, and at the pile tip, R_{fb}, are consistent with the soil responses as mentioned earlier in Figs. 4.6a and 4.6b. The maximum negative shear resistances, τ_{max}^{neg}, were 30 % of the maximum positive shear resistance, τ_{max}^{comp} ,and q_{max}^{tens} was set to zero in the final WMA.

Figure 4.13a shows that the values of the shear modulus, G, of the soil layers identified from the final WMA are smaller than those used in the first WMA. It should be noted that the effective overburden pressures, σ_v', in the model ground were less than 10 kPa. Estimation of the G of soil subjected to such small effective overburden pressures from the OED test results (Fig. 4.8) using Eqs. (4.1) and (4.2) may not be so reliable. Hence, the shear moduli were estimated from the static load test results in Fig. 4.6a. The spring stiffness, $k_{s(static)}$, was obtained from the initial stiffness of each curve in Fig. 4.6a, and then G was estimated using the relations in Eqs. (4) and (5). Thus, the estimated values of G are also indicated by circles in Fig. 4.13a. The values of G identified from the final WMA are comparable with those from the SLT.

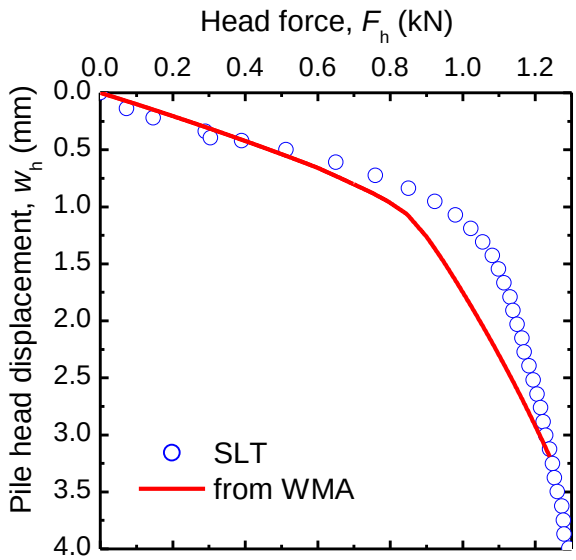

Figure 4.14. Derived and measured static load-displacement curves of the CP.

Figure 4.14 shows the static load-displacement curve derived from the soil properties identified in the final WMA when compared with the static load test results. Although the derived curve overestimates the pile displacement for applied loads greater than 0.5 kN, an overall agreement between the derived and the measured results was obtained. The overestimation of the pile displacement in the derived curve is attributed to the underestimation of G

in the final WMA compared to that in SLT2 (see Fig. 4.13a). It should be noted that the load-displacement curve could be calculated until the pile head force reached 1.2 kN, because the set per blow, *S*, was about 3.3 mm in the pile driving test, and the identified pile tip resistance during pile driving was used in the calculation of the static response.

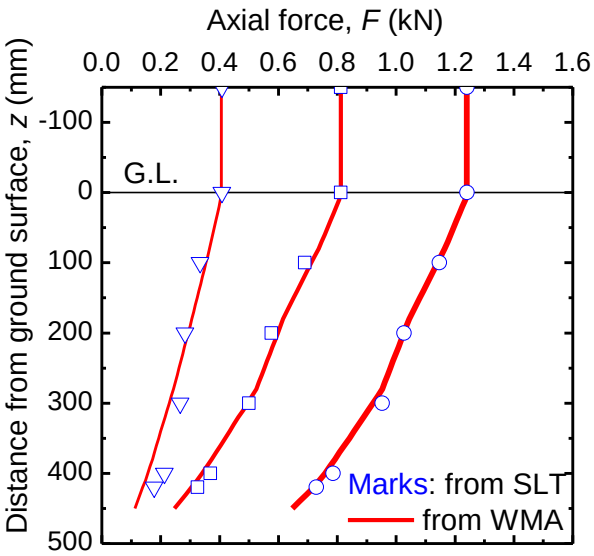

Figure 4.15. Derived and measured distributions of the axial forces of the CP.

Figure 4.15 shows the derived axial force distributions of the pile at different pile head loads, together with the SLT results. Fairly good agreements between the derived and the measured results were obtained.

4.4.3 Discussion on the influence of the boundary of the soil box on the pile response

The usefulness of the WMA to derive the static behaviour of the model pile in the model ground was demonstrated in the previous section. However, the influence of the size of the model ground on pile behaviour needs to be discussed.

The propagation of shear waves in the horizontal direction is prevailing in the ground surrounding the pile shaft during driving. The shear waves generated by pile driving reach the side walls of the soil box and are reflected. The reflected waves then propagate in the ground and return to the pile shaft at a given time instant after the impact of the pile. Similar phenomena occur in the ground below the pile tip. In the ground below the pile tip, the radial propagation of longitudinal waves (body waves) is predominant. Pile behaviour is not influenced by the size of the soil box until the reflection waves return to the pile from the side wall or the bottom of the soil box.

In order to estimate the typical value of the shear wave velocity, c_s, the shear modulus G = 2.80 MPa at the pile tip level (see Fig. 4.9) was selected. The reason for this selection is that the c_s estimated using G= 2.80 MPa is the highest value for the ground surrounding the pile shaft. For the estimation of c_p, G = 2.96 MPa at the midpoint (z = 0.5 m) between the pile tip and the bottom of the soil box was selected.

The values of c_s and c_p were estimated using the following equations:

$$c_s = \sqrt{G / \rho_d} \tag{4.3}$$

$$c_p = \sqrt{\frac{K}{\rho_d}} = \sqrt{\frac{1}{\rho_d}\frac{2(1+\nu)G}{3(1-2\nu)}} \tag{4.4}$$

in which K is the bulk modulus.

With the measured value of ρ_d = 1.45 ton/m^3 and an assumption of ν = 0.3, c_s = 45.2 m/s and c_p = 66.5 m/s are estimated.

The distance from the outer pile surface to the side wall of the soil box, d_s, is about 0.284 m. The return travelling time for the shear wave in the ground between the pile shaft and the side wall is 12.6 ms (= $2d_s/c_s$ = 0.0126 s). As mentioned earlier, the driving event terminates at about 8.5 ms after the impact, as shown in Figs. 4.11 and 4.12. Hence, it can be said that the side wall has no influence on the pile behaviour during the pile driving test.

The distance from the pile tip to the bottom of the soil box, d_b, is about 0.11 m. The return traveling time for the longitudinal wave in the ground between the pile tip and the bottom of the soil box is about 3.3 ms ($2d_b/c_p$ = 0.0033 s). This means that after 3.52 ms ($2L$/c + $2d_p/c_p$ = 0.00352 s) from the start of impact, or at the time of 3.98 ms in Fig. 4.10, the measured force at SG1 should instantly be influenced by the reflection wave from the bottom of the soil box. However, at this instant, the influence of the stress wave reflected from the bottom of the soil box was not found, indicating that the influence of the reflected wave from the bottom of the soil container might be negligible.

Hence, verification using the laboratory scale model in this experiment is acceptable.

4.4.4 Sensitivity analysis of the WMA results

In order to investigate the sensitivity of the WMA results to variations in the soil parameters, sensitivity analyses are presented in this section. Since it was estimated in the final WMA that the non-linearity of the ground is small and α = 0 (see Eqs. (3.13) and (3.14) in Chapter 3),

pile response sensitivity to variations in shear moduli and maximum soil resistance was investigated. The values of G, τ_{max} and q_{max} identified in the final WMA shown in Fig. 4.13 are regarded as the reference soil parameters.

In addition to the analysis with the reference soil parameters (the reference case), 8 cases of analyses were carried out, changing the values of G, τ_{max} and q_{max}. In cases 1 to 4, the shear moduli, G, alone was varied, while in cases 5 to 8, the τ_{max} and q_{max} were varied. The reference soil parameters were multiplied by factors ranging from 0.5 to 1.5 in the sensitivity analyses.

Figs. 4.16a and 4.16b show the variations of axial forces at the SG4 due to the variations of the shear modulus and soil resistances, respectively. It can be seen from these figures that the axial force in the pile is not so sensitive to variations of G, τ_{max} and q_{max}.

It is well known from the one-dimensional stress-wave theory that the upward travelling force, F_u, is obtained by the following equation.

$$F_u = \frac{1}{2}\left(F - \frac{EA}{c}v\right) \tag{4.5}$$

where A is the cross-sectional area of the pile.

The calculated F_u are shown in Fig. 4.17: (a) in cases 1 to 4 where the G alone was varied, (b) in cases 5 to 8 where the τ_{max} and q_{max} were varied. It is seen from these figures that the upward force, F_u, is relatively sensitive to variations of G, τ_{max} and q_{max}.

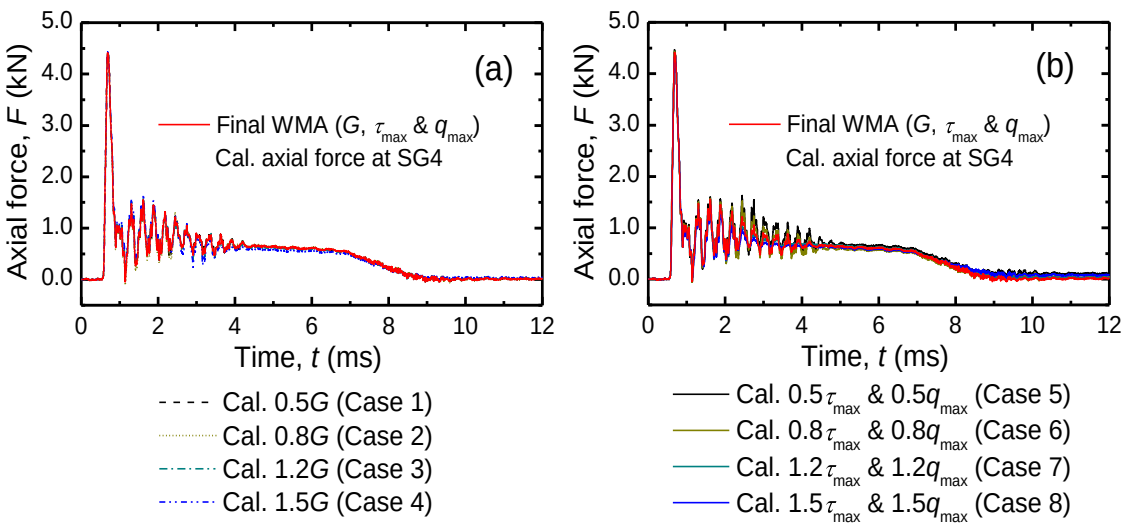

Figure 4.16. Sensitivity of the axial force at SG4 due to.

(a) Variation of G. (b) Variation of τ_{max} and q_{max}.

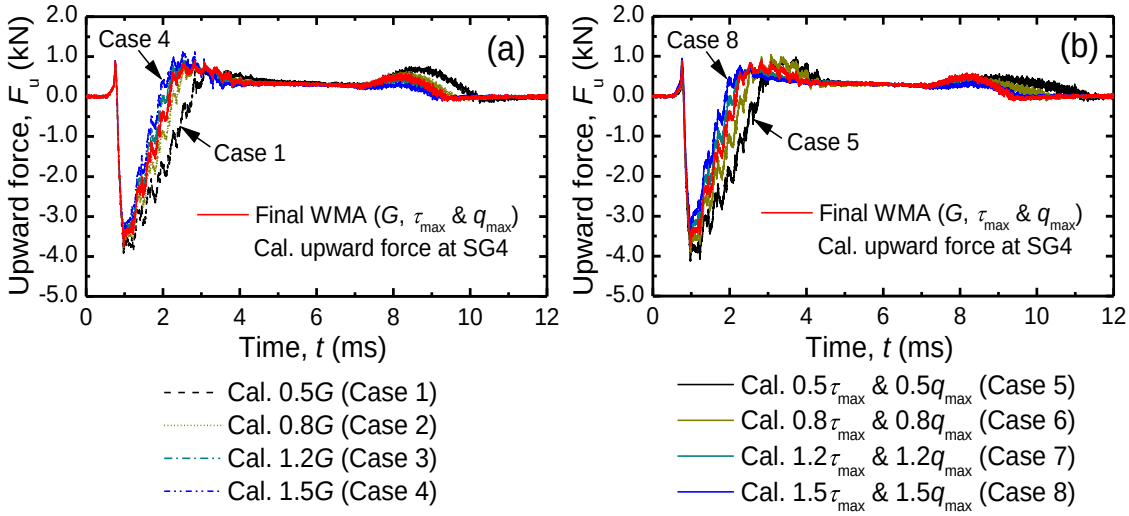

Figure 4.17. Sensitivity of the upward force at SG4 due to.

(a) Variation of G. (b) Variation of τ_{max} and q_{max}.

High sensitivity was also seen in the pile head displacement as shown in Figs. 4.18a and 4.18b. Pile head displacement decreases with the increase in G or soil resistance (τ_{max} and q_{max}), and vice versa. With a variation of 20 % in the shear modulus (see cases 2 and 3 in Fig. 4.18a) and in the soil resistance (see cases 6 and 7 in Fig. 4.18b), the final pile head displacement differs from the reference value by 10% and 13%, respectively.

Figure 4.19 shows the corresponding static load-displacement curves in the 8 cases. It can be seen that the load-displacement curves are also highly sensitive to variations of G and soil resistance (τ_{max} and q_{max}).

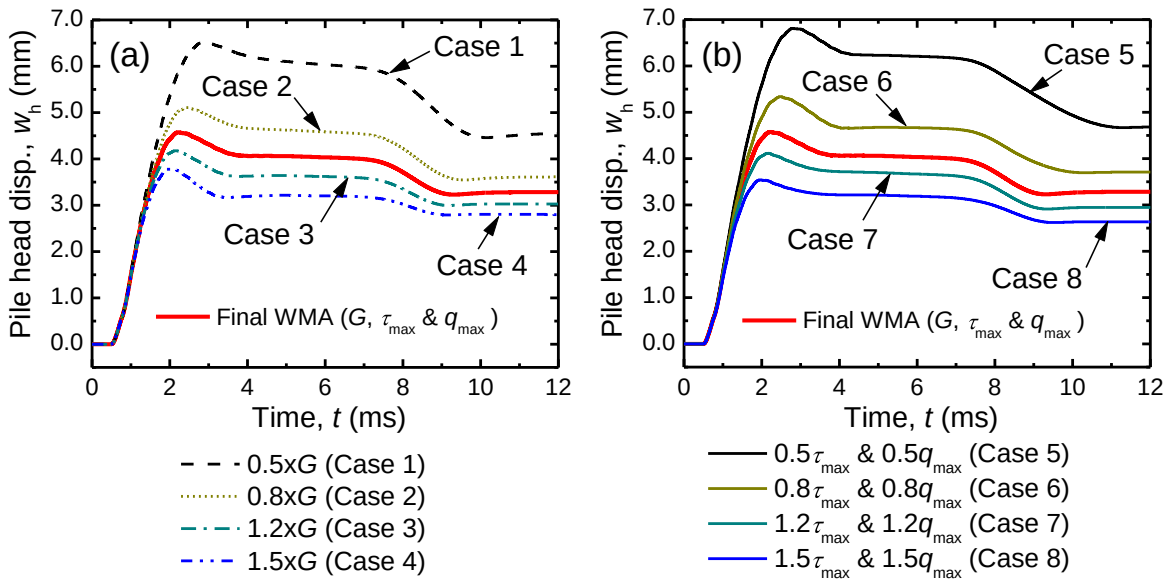

Figure 4.18. Sensitivity of the pile head disp. due to

(a). Variation of G (b). Variation of τ_{max} and q_{max}

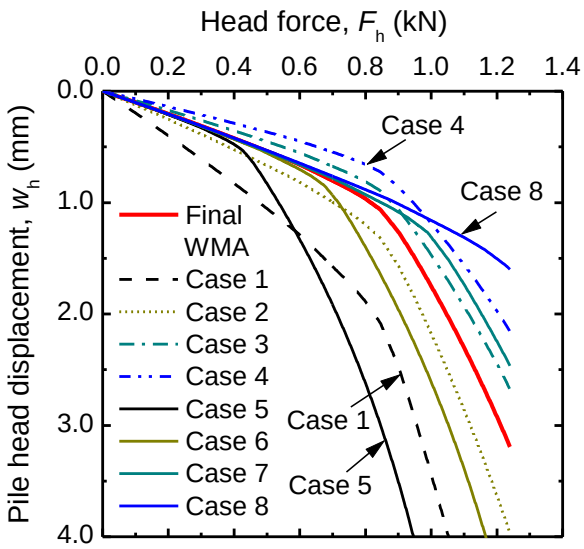

Figure 4.19. Variation of the static load-displacement curves of the CP.

It should be noted here that the upward travelling force, F_u, could not be obtained from the pile driving test of the CP because, as mentioned earlier, the acceleration measurement was not successful. In the WMA of the CP, the distribution of the soil resistance obtained from the static load test was used for the first assumption. Hence, the shear moduli of the ground were mainly changed in the consecutive analyses. As a result, it can be judged that the distribution of the G identified in the final WMA (see Fig. 4.13a) is reasonably precise, resulting in an accurate prediction of the static load-displacement curve (see Fig. 4.14).

Static load test results are not usually available in most practices. Hence, the results of soil investigations, such as the measurements of the elastic shear wave velocities of the ground, would be useful to narrow down the possible range of G when conducting the WMA.

4.5 Results of the open-ended pipe pile

4.5.1 Plugging modes of the soil plug

Figure 4.20 shows the changes in the pile location and the soil plug height at the end of each stage. In the pile penetration in stage 1, the pile penetration was terminated at a depth, L_d, of 257 mm and the height of the soil plug, H, was measured as 133 mm. The Incremental Filling Ratio (Lehane et al. 2002), $IFR = \Delta H / \Delta L_d$, was 52 %. The pile was further penetrated to a depth of 394 mm, and the soil plug height increased to 143 mm. The IFR for the 2nd penetration was 7.3 %. In SLT1, the pile was further penetrated 14 mm into the ground. The soil plug height did not change, however, demonstrating the perfect plugging mode. These results correspond to the findings of Paikowsky et al. (1989) and Paik et al. (2003). Hence, it can be

judged that the open-ended pipe pile reached the perfect plugging mode at a penetration depth of between257 mm to 394 mm. During the DLTs after SLT1, the pile was further penetrated 35 mm and the soil plug height increased to 158 mm, showing *IFR* = 43 %, i.e. the partially plugging mode occurred. During SLT2 after the DLTs, the soil plug height was constant at 158 mm, indicating again the perfect plugging mode. As pointed out by Matsumoto and Takei (1991), the occurrence of the partially plugging mode during the DLTs may be caused by the inertial force of the soil plug.

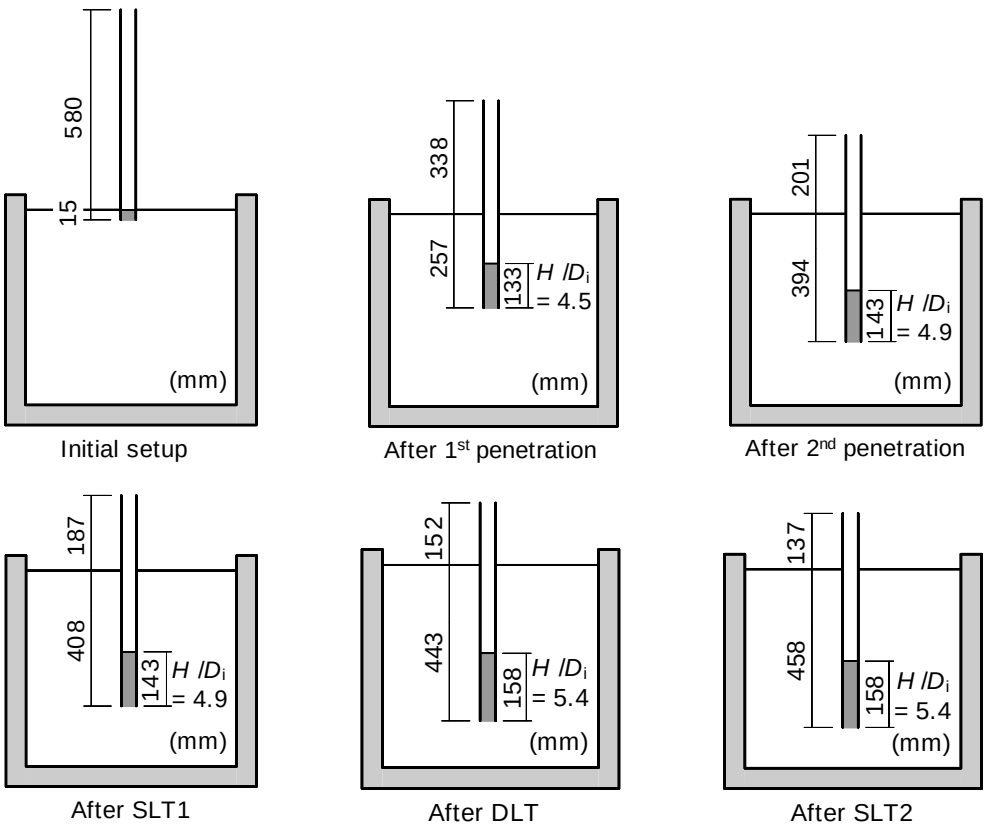

Figure 4.20. Location of the pile and change of the soil plug height at the end of each stage.

4.5.2 Results of the SLTs

Figure 4.21 shows the load-displacement curves obtained from SLT1 and SLT2 for the open-ended pipe pile (OP). Similar to the CP, the yield load in SLT2 is lower than that in SLT1 due to the disturbance of the soil surrounding the pile during driving.

Figure 4.22 shows the relation between the mobilised shear resistance and the local pile displacement for pile sections between the strain measurement levels. The local pile displacement at the middle point of each pile section was also calculated from the measured pile head displacement and the measured strains. Note here that the outer shaft resistance alone

acts on the pile shaft up to the depth of SG4, and that both the outer and inner shaft resistances act on the pile shaft below the level of SG4. However, the mobilised shaft resistance for the pile section between SG4 and SG5 was estimated assuming that the inner shaft resistance was negligible. This is because the separation of the outer and inner shaft resistances in this experiment was not possible. It was found from Fig. 4.22 that the mobilisation of the shaft resistance could also be modelled by slight nonlinear responses.

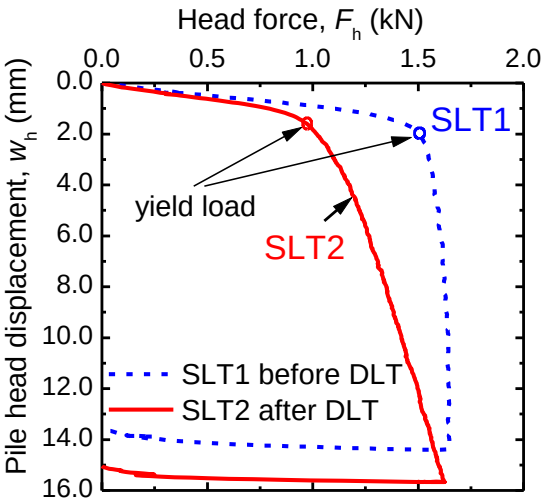

Figure 4.21. Load-displacement curves of the OP.

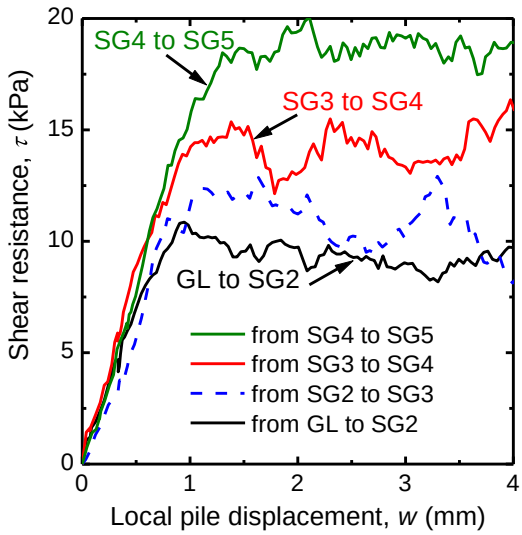

Figure 4.22. Relationship between the shear resistance, τ, and the local pile displacement, w, of the OP in SLT2.

The axial force distributions will be presented later with the results of the wave matching analyses of the DLT.

4.5.3 Wave matching analysis of the DLT

In case of the open-ended pile (OP), a total of 10 blows were conducted in the DLTs after the first static load test (SLT1) subsequent to the penetration stage to a depth of 394 mm. The test procedure and ground conditions were the same as those for the close-ended pipe pile. The driving conditions and driving records are listed in Table 4.5. Only a small hammer with mass of 0.96 kg was used in the DLTs. The second static load test (SLT2) was carried out after the completion of the tenth blow. The results of the WMA of this blow are presented and compared with the results of SLT2.

Table 4.5. Driving conditions and measured set per blow of DLTs of the OP.

Blow	1	2	3	4	5	6	7	8	9	10
Falling height (mm)	200	300	400	500	600	200	300	400	500	600
Measured set (mm)	0.8	1.1	2.0	2.6	3.3	0.8	1.4	2.2	2.8	2.8
Hammer	S	S	S	S	S	S	S	S	S	S

The first assumptions concerning the soil properties for the WMA are shown in Fig. 4.23. The distribution of the shear modulus, *G*, was the same as those of the CP while the distribution of the outer shaft resistance was estimated from Fig. 4.22 with assumption that there was no inner shaft resistance between the soil plug and the pile.

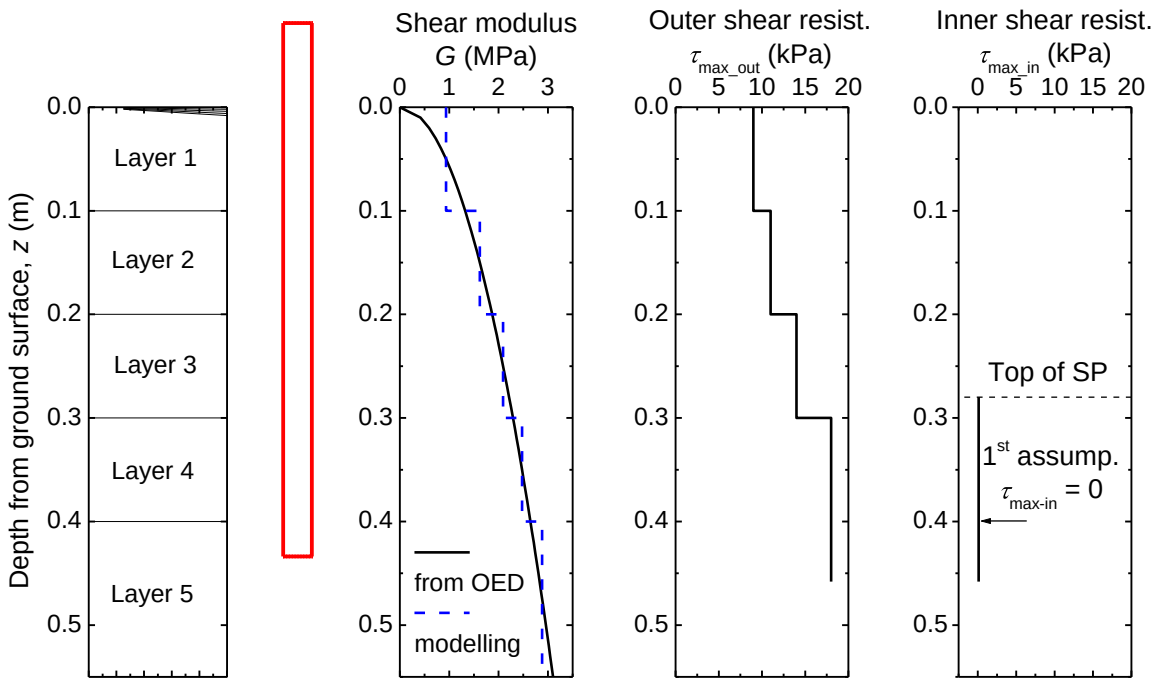

Figure 4.23. Soil properties used in the first WMA of the OP.

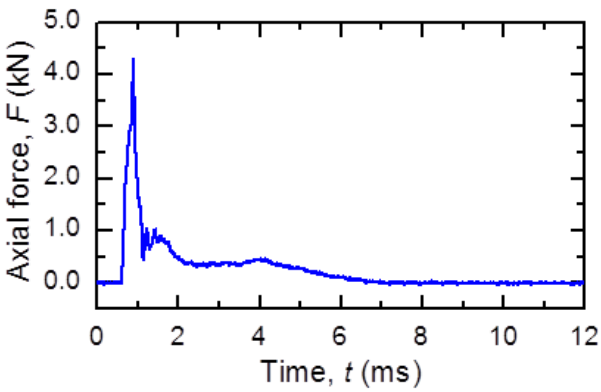

Figure 4.24. Measured axial force at SG1 of blow 10 of the OP.

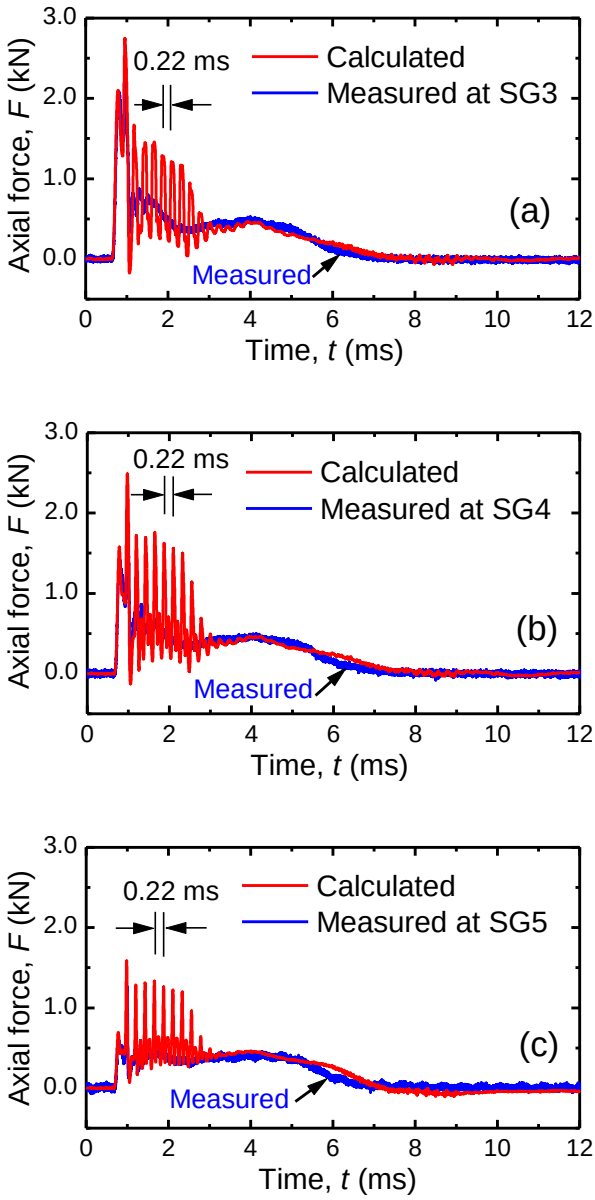

Figure 4.25. Results of the final WMA of the OP for the axial forces.

(a) at SG 3. (b) at SG4. (c) at SG5.

The measured pile force at the SG1 in the tenth blow (Fig. 4.24) was used as the input force in the WMA. The results of the final WMA are shown in Fig. 4.25 for the axial forces in the pile, and in Fig. 4.26 for the pile head displacement. Although the calculated axial forces exhibit oscillation with an interval of $2L/c$ = 0.22 ms, as discussed in the WMA of the CP, the overall trend of the calculated results agree with the measured results. Furthermore, the calculated and the measured final settlements are also in agreement, as indicated in Fig. 4.26. The calculated displacement at the top of the soil plug is also shown in this figure. The final settlement of the soil plug is smaller than that of the pile, showing that "imperfect" plugging occurs during pile driving. These calculation results correspond to the measured plugging mode presented in Fig. 4.20.

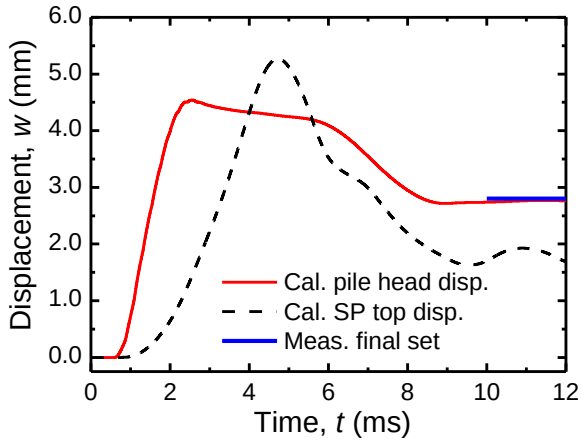

Figure 4.26. Displacements of the pile head and the top of soil plug calculated in the final WMA of the OP.

The soil properties identified from the final WMA are shown in Fig. 4.27. The values of the shear modulus, G, of the ground estimated from the results of SLT2 (Fig. 4.22) with the relations of Eqs. (3.4) and (3.5) in Chapter 3 are also plotted in Fig. 4.27a. The values of G identified from the final WMA are comparable with those from the SLT.

Consideration of the inner shaft resistance was necessary to get good matching results. Large values for the inner shaft resistance were identified for a pile section from the pile tip to a level of about two times the inner pile diameter, as shown in Fig. 4.27d. The inner shaft resistance tended to increase exponentially from the top of the soil plug to the bottom. These results, for example, correspond to the theoretical solution for soil plug capacity proposed by Yamahara (1964) and the results of the push-up load tests of sand soil plugs in an model open-ended pipe pile by Thongmunee et al. (2011). The distribution of the G of the soil inside

the pipe pile (soil plug) displayed a similar trend to the distribution of the inner shaft resistance (see Fig. 4.27c), indicating that the soil plug from the pile tip to a level of about two times the inner pile diameter was subjected to great pressure.

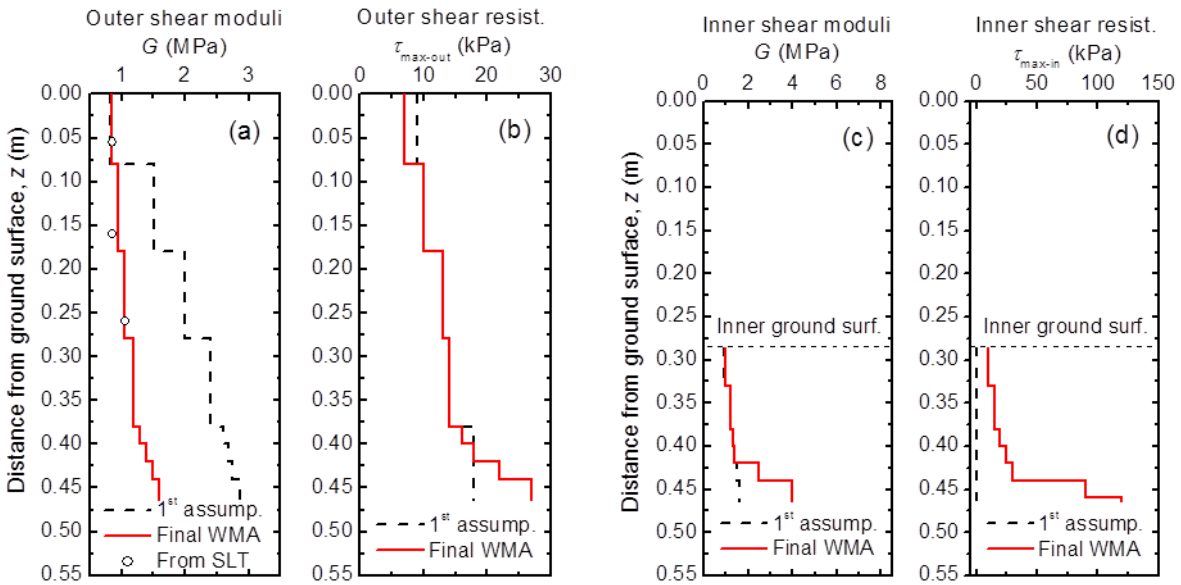

Figure 4.27. Distribution of the shear moduli and shear resistances. (a) Outer shear moduli. (b) Outer shear resistances. (c) Inner shear moduli. (d) Inner shear resistances.

The other soil properties identified from the final WMA are; $\alpha = 0$ (refer to Eqs. (3.13) and (3.14) in Chapter 3), $R_{fs} = 0.3$ (refer to Eq. (3.17) in Chapter 3), $R_{fb} = 0.7$ (refer to Eq. (3.18) in Chapter 3), the mobilised end-bearing resistance at the pile tip = 3525 kPa, the mobilised end-bearing resistance at the soil plug base = 255 kPa, and the shear modulus of the soil beneath the pile tip = 15000 kPa and beneath the soil plug base = 3000 kPa. The maximum tension shear resistances, τ_{max}^{tens}, were identified as 25 % of τ_{max}^{comp}, and q_{max}^{tens} was also set to zero in this analysis. Similar to the case of the CP, the identified non-linearity coefficients of the soil at the pile shaft, R_{fs}, and at the pile tip, R_{fb}, indicated that slight and high non-linear responses of the soil were found at the pile shaft and at the pile tip, respectively.

The static load-displacement curve and the axial force distributions derived using the soil properties identified from the final WMA are shown in Figs. 4.28 and 4.29, respectively, when compared with the SLT results. The agreement between the derived and the measured values are seen in both figures. Fig. 4.28 also shows that the shaft resistance was fully mobilised when the applied head force reached a value of about 0.84 kN, while the soil plug base

resistance reached its peak when the head force increased to 1.02 kN, indicating that the perfect plugging mode occurred at this applied force.

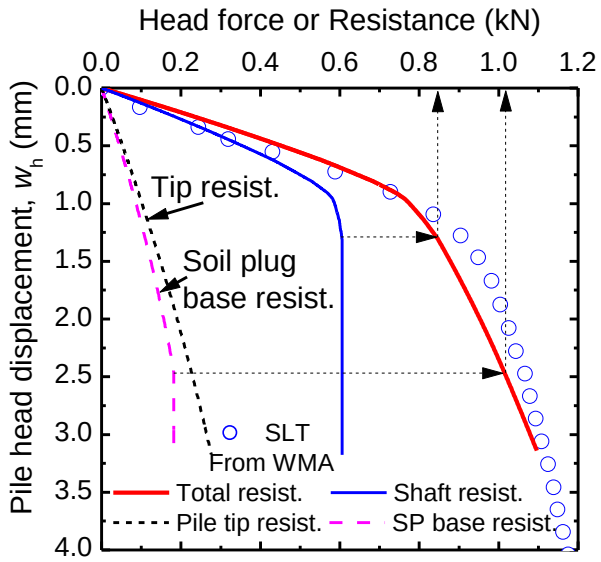

Figure 4.28. Derived and measured static load-displacement curves of the OP.

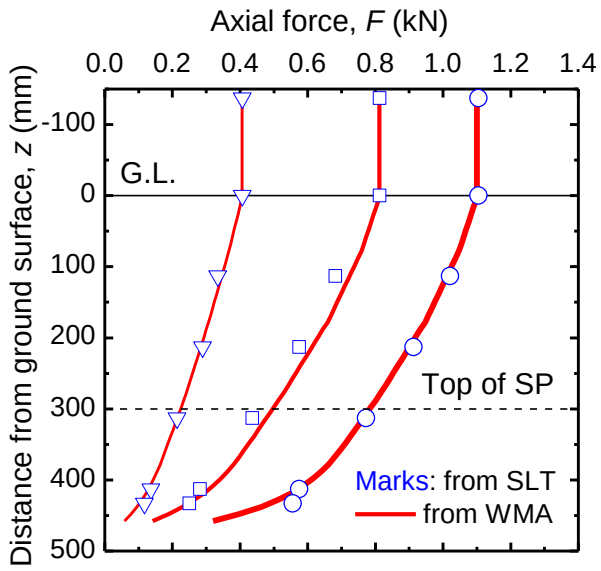

Figure 4.29. Derived and measured distributions of the axial forces of the OP.

4.5.4 Comparison of the static response between the OP and CP

Figure 4.30 shows the derived and measured load-settlement curves of the OP and CP. It is seen from the measured load-displacement curves that the CP has a greater yield load than the OP. These measured results are correctly predicted through the WMAs using the proposed numerical method.

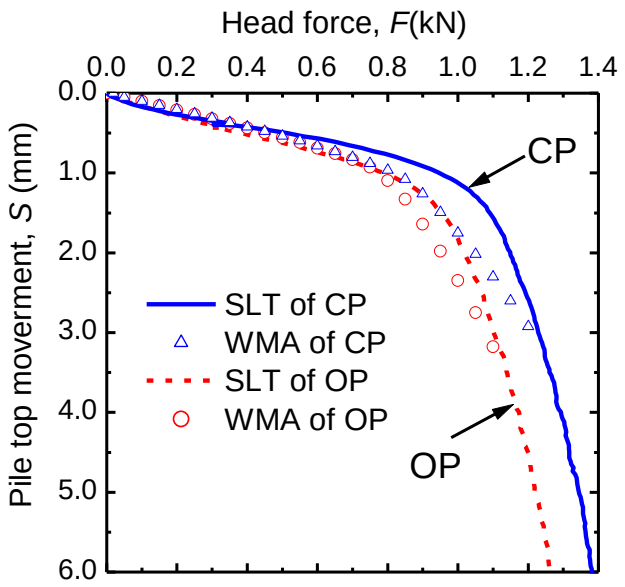

Figure 4.30. Derived and measured static load-displacement curves of the OP and CP.

4.6 Conclusions

In this chapter, the static and dynamic load testing of an open-ended pipe pile and a close-ended pipe pile were carried out in a model ground of dry sand to examine the applicability of the proposed method to dynamic pile load testing. Wave matching analyses (WMA) of the dynamic load tests were conducted to derive the static load-displacement relations and distribution of axial forces in the piles.

The following conclusions and findings were drawn from experiments with limited conditions:

(1) The wave matching analysis using the proposed method has the potential to estimate static responses of open-ended pipe piles as well as close-ended piles with a reasonable accuracy.

(2) Partially plugging mode occurs during penetration and dynamic load test while perfectly plugging mode happens in static load test.

(3) Shear modulus estimated from one-dimensional compression test could be used as the first assumption in WMA.

Although the validity of the proposed method was examined using the small scale experiments in this study, analyses of full scale pile load tests using the proposed method would be useful for further verification.

References

Lehane B.M. and Randolph M.F. (2002). Evaluation of a minimum base resistance for driven pipe piles in siliceous sand. J. Geotech. Geoenviron. Eng.; 128(3): 198–205.

Matsumoto T. and Takei M. (1991). Effects of soil plug on behaviour of driven pipe piles. Soils and Foundations; 31(2): 14-34.

Paikowsky S.G., Whitman R.V. and Baligh M.M. (1989). A new look at the phenomenon of offshore pile plugging. Marine Georesources Geotech.; 8: 213-230.

Paik K., Salgado R., Lee J. and Kim B. (2003). Behaviour of open- and closed-ended piles driven into sand. Journal of Geotechnical and Geo-environmental Engineering, ASCE; 129(4): 296-306.

Thongmunee S, Matsumoto T., Kobayashi S., Kitiyodom P. and Kurosawa K. (2011). Experimental and numerical studies on push-up load tests of sand plug in a steel pipe pile. Soil and Foundations; 51(5): 959-974.

Yamahara H. (1964). Plugging effects and bearing mechanism of steel pipe piles. Transaction of the Architectural Institute of Japan; 96: 28-35 (in Japanese).

Yamahara H. (1964). Plugging effects and bearing mechanism of steel pipe piles (Part 2). Transaction of the Architectural Institute of Japan; 97: 34-41 (in Japanese).

Chapter 5

Comparative SLTs and DLTs on steel pipe piles and spun concrete piles: A case study at Thi Vai International Port in Viet Nam

In Chapter 3, the accuracy of the proposed numerical program has been verified by comparing the calculated results with those obtain form the theoretical solution, Smith's method and FLAC^{3D}. In Chapter 4, two series of static and dynamic load tests of small-scale model piles carried out in model ground of dry sand were used to further verify the proposed numerical program. In this chapter, static and dynamic load test of the four test piles were carried out in a construction site in Viet Nam. The proposed numerical method was used to perform the wave matching analysis WMA of dynamic load tests (DLTs) in order to identify soil parameters used for determining the pile performance, to obtain information for selecting pile driving system and to examine the applicability of wave matching analysis (WMA).

5.1 Introduction

Thi Vai International Port located on the bank of the Cai Mep River in Viet Nam (Fig. 5.1) is under construction, with the scheduled start of operation at the end of 2013. A berth structure, 600 m long and 60 m wide, has been completed in the project as shown in Fig. 5.2. The berth is a quay structure supported by 885 driven spun concrete piles (SC pile hereafter) and 156 driven steel pipe piles (SP pile hereafter). Test piling was conducted at the project site in 2011 to obtain design parameters, to select appropriate driving system, and to seek for driving control and quality assessment methods for constructed piles.

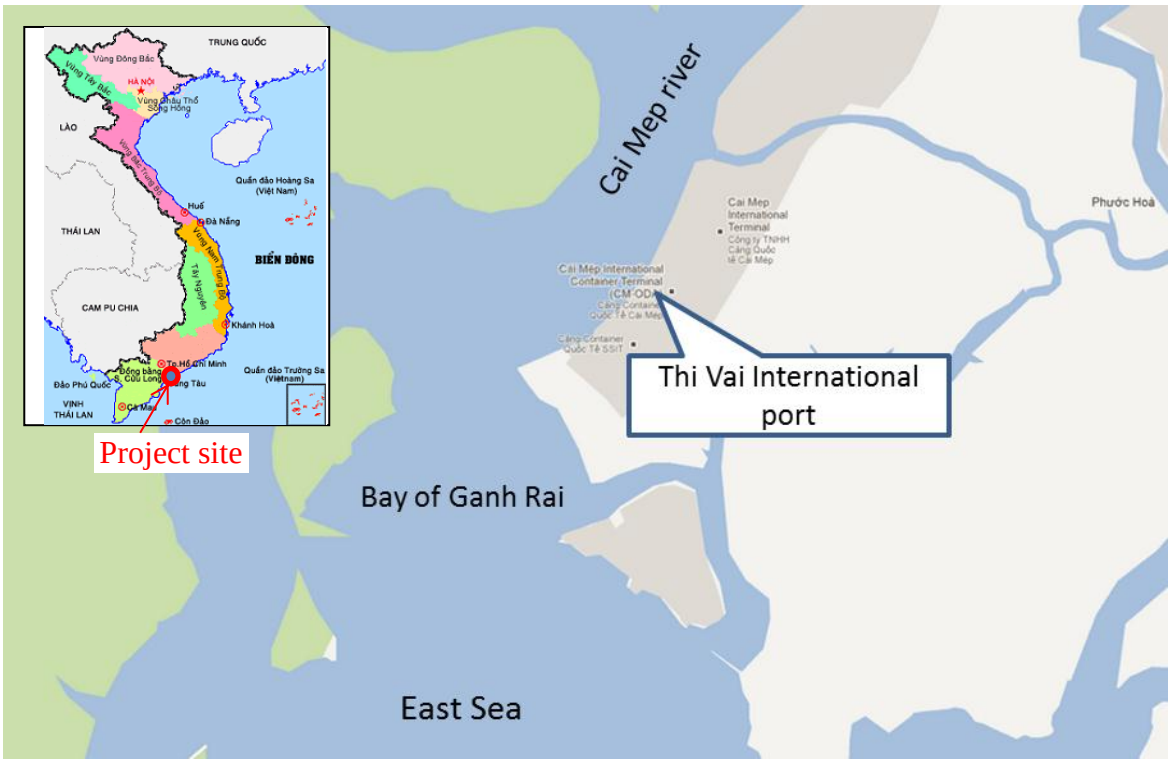

Figure 5.1. Location of the site.

Figure 5.2. Photo of the berth area prior to in use.

Four test piles were driven prior to construction of working piles. Two of them were spun concrete piles designated as TSC1 and TSC2, and the other two piles were open-ended

steel pipe piles designated as TSP1 and TSP2. The TSC1 and TSC2 had outer diameters of 0.7 m and 0.8 m, wall thicknesses of 100 mm and 110 mm, lengths of 54 m and 48.7 m, respectively. The TSP1 and TSP2 had outer diameters of 1.0 m and 0.9 m, respectively, a wall thickness of 12 mm, and lengths of 60 m and 49.9 m, respectively. All the test piles were driven using a diesel hammer having a ram mass of 10 tons. Dynamic load tests (DLTs) were carried out at the end of initial driving (EOD) and re-striking tests were conducted after curing periods of 7 days for the TSC1 and 34 days for the TSP1. Static load tests (SLTs) were carried out 10 days later for the TSC1 and 14 days later for the TSP1. SLT was also carried out for the TSC2 and TSP2 after the corresponding curing time of 17 days and 27 days from the completion of the driving work.

This study first describes the test piling in detail including objectives, site conditions, preliminary pile design and results of the SLTs. Then, wave matching analysis (WMA) of the DLTs at initial driving and re-striking are conducted using a numerical approach developed by the authors, in order to derive the corresponding static load-displacement relations and soil resistance distributions. The derived load-displacement relations clearly showed so-called "set-up" phenomena. The derived load-displacement relations of the TSC1 and TSP1 were good estimates for the results of the SLTs. Static load-displacement relations of the TSC2 and TSP2 were predicted using the soil parameters identified from the WMA of the TSC1 and TSP1, respectively. The predicted results were comparable to the measured results, indicating that DLT with the WMA is a good alternative to SLT.

5.2 Site and test description

5.2.1 Site conditions

a. Locations of the boreholes, working piles and test piles, and geological sections at the four test piles

A total of the 30 borehole investigations were conducted in this area (Fig. 5.3) to obtain the profiles of the soil layers and SPT *N*-values. Typically, very soft clay exists from the seabed to depths of 6 m to 20 m. Below this top layer, a clayey sand of about 25 m thick with loose state at the top to medium dense state at the bottom exists, being underlain by hard silt clay that could be regarded as a bearing stratum.

Locations of the boreholes are shown in Fig. 5.3, together with the locations of the test piles and the working piles. Of the four test piles, only the TSP1 and TSP2 were re-used as the working piles. The geological sections of the four test piles are shown in Fig. 5.4 for the

TSP1 and TSC1, and in Fig. 5.5 for the TSC2 and TSP2. Note that the high water level (HWL), mean water level (MWL) and low water level (LWL) using the Vietnamese national standard elevation system are +3.97 m, +2.67 m and +0.58 m, respectively. The elevation of the working floor of the berth structure is +5.50 m.

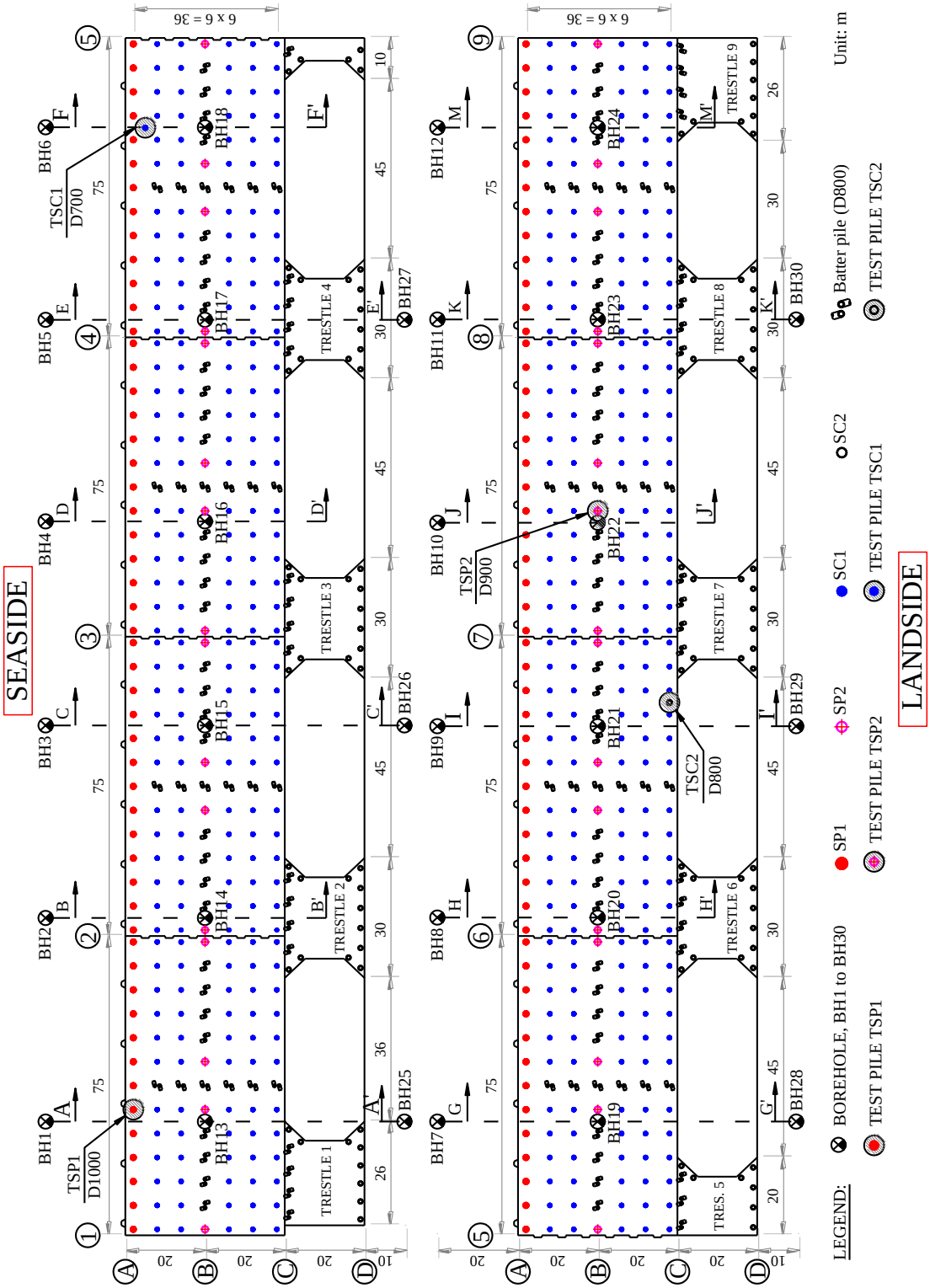

Figure 5.3. Locations of the boreholes, test piles and working piles.

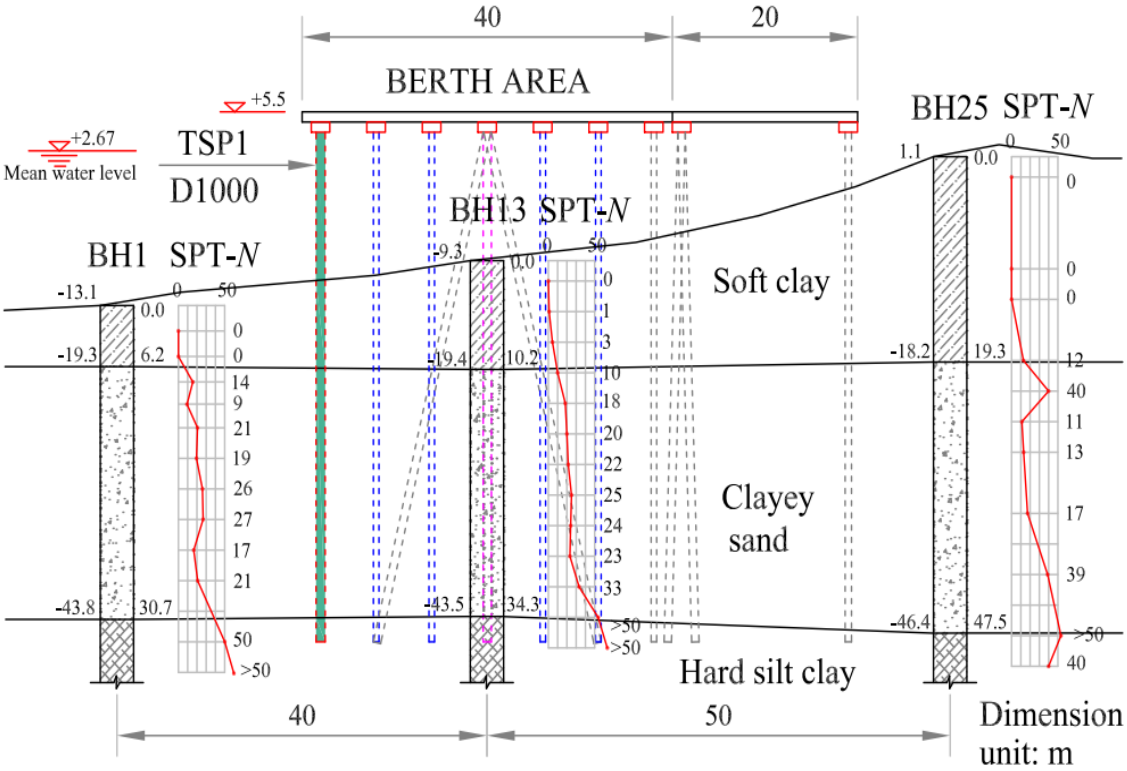

SECTION A-A'

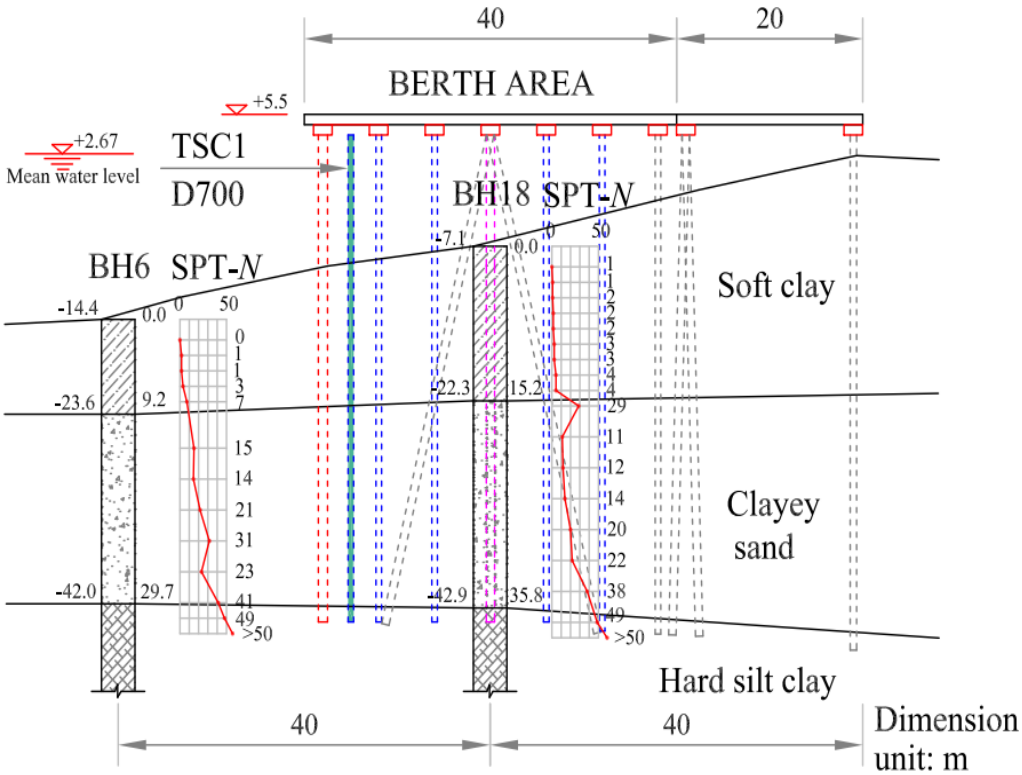

SECTION F-F'

Figure 5.4. Geological sections at locations of the test piles. (a) TSP1. (b) TSC1.

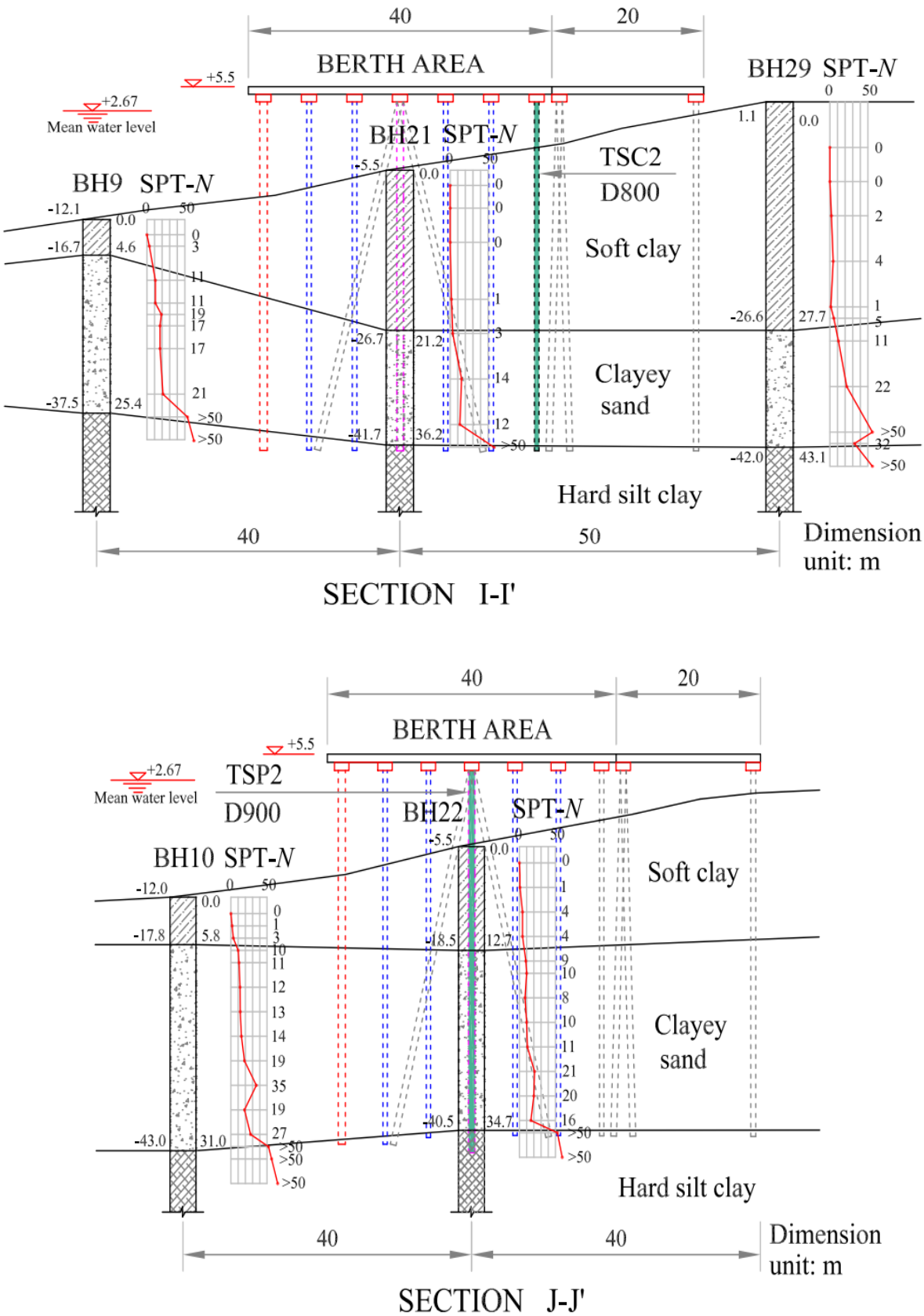

Figure 5.5. Geological sections at locations of the test piles.

(a) TSC2. (b) TSP2.

b. Estimation of the shear modulus of the ground

Load-displacement relation of a pile is strongly influenced by shear moduli of the surrounding ground as well as the distribution of shaft resistance and tip resistance. The shear moduli of the ground need to be assumed in WMA of the DLTs of the TSC1 and TSP1 in the later section. Hence, it may be appropriate here to approximately estimate the shear moduli of the ground at the locations of the test piles.

The soil shear modulus, G_0, at small strain level was estimated using the following empirical equation proposed by Imai (1977), regardless of soil type.

$$G_0 = 98 \times 120 \times N^{0.737} \quad \text{(kPa)} \tag{5.1}$$

The distribution of the SPT *N*-value with depth at the location of each test pile was interpolated from the SPT *N*-values of the two nearest boreholes, e.g., the SPT *N*-values at the location of the TSP1 was estimated from those of the two boreholes BH1 and BH13 (see Fig. 4a).

Figure 5.6 shows thus estimated distributions of the G_0 with depth at each location of the test piles. These values will be used as the first assumptions of the shear moduli in the wave matching analysis of the DLTs.

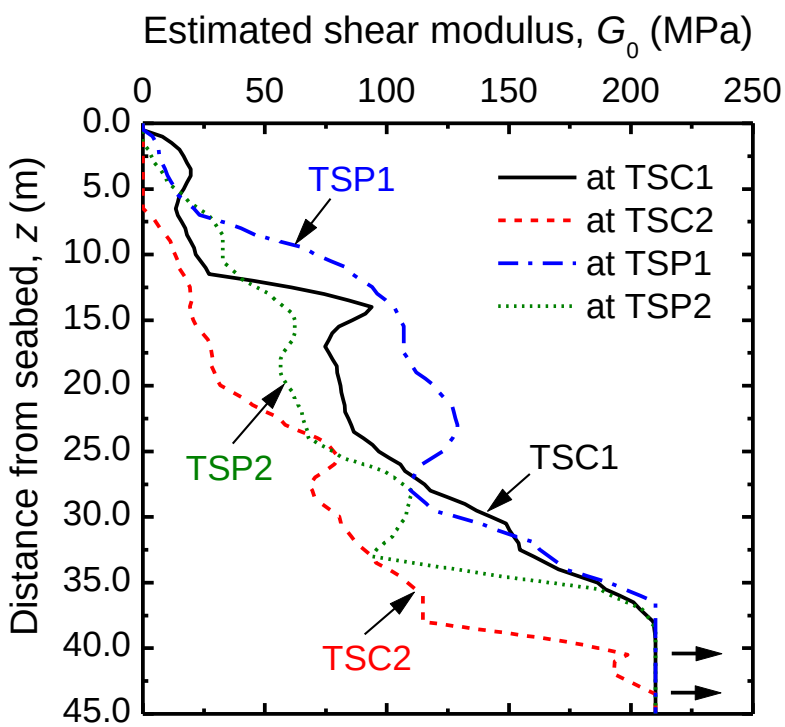

Figure 5.6. Estimated shear modulus at the four test piles.

5.2.2 Preliminary pile design

a. Design of the working piles

The berth structure was subjected to various types of loads including vertical loads (self-weight, live load caused by goods) and horizontal loads (earthquake, wind, wave and collision of the ship to its structure). Different combinations of loading conditions are applied to the berth structure with the pile location as shown in Fig. 5.3. The maximum compressive forces are varied in location from pile to pile, ranging from 1800 kN to 4002 kN. High potential of tensile forces are found at the sea-side row (axis A) and at the middle row (axis B) of the working piles. Hence, the steel piles were used at the axes A and B while the concrete piles (spun piles) were used for the remaining locations in order to have an effective solution for foundation of this structure. Due to the wide range of the pile head force, it was decided to use four pile types which have different diameters and have strong enough to support the above forces. The locations of each pile type were shown in Fig. 5.3.

The design working vertical load for each pile type is listed in the Table 5.1. Under these loads, the allowable settlements of the piles without taking into account the pile elastic shortening is 20 mm.

According to TCVN 205-1998, selection of the factor of safety, *FS*, for determining the required capacity depends on the method used for estimating the ultimate capacity, Q_u, e.g., FS = 3.0 is employed if Q_u is calculated from the empirical equations, FS = 2.5 to 6.0 is employed if Q_u is estimated from the driving formulas, and FS = 2 can be employed if Q_u is obtained from SLT. In this study, the required capacity was first estimated from the empirical equation to select the embedment pile length, and then the required capacity was confirmed through the static load test. The required capacities of the four test piles in accordance with SLT (FS = 2) and without SLT (FS = 3) are listed in Table 5.2.

Table 5.1. Working load and corresponding allowable set.

Pile type	Diameter	Working load	Allowable settlement
	D (mm)	P_a (kN)	S_a (mm)
SC1 (SCP)	700	1800	20
SC2 (SCP)	800	2585	20
SP1 (SPP)	1000	4002	20
SP2 (SPP)	900	3858	20

SPP: Steel Pipe Pile, SCP: Spun Concrete Pile

Table 5.2. Required capacity.

Pile type	Required capacity (kN)	
	with SLT	w/o SLT
SC1	3600	5400
SC2	5170	7755
SP1	8004	12006
SP2	7716	11574

b. Design of the test piles

To adapt the requirement of the capacity, the ultimate capacity, Q_u, of the test piles was estimated using the following equation:

$$Q_u = q_{max} A_p + \sum \tau_{max,i} A_{s,i} \tag{5.2}$$

in which, q_{max} is the maximum base resistance, $\tau_{max,\,i}$ is the maximum shaft resistance of soil layer i, A_p is the pile tip area with an assumption that perfect plugging mode occurs at the pile tip, and $A_{s,\,i}$ is the circumferential area of the pile along soil layer i. According to Vietnamese pile design standard code, TCVN 205-1998, the strength parameters, τ_{max} and q_{max}, can be estimated from SPT N-value using the following empirical equations:

$\tau_{max} = 2N$ (kPa) for sand (limit value = 100 kPa) (5.3)

$\tau_{max} = c_u$ or $10N$ (kPa) for clay (limit value = 150 kPa) (5.4)

$q_{max} = 300N_p$ (kPa) for both sand and clay soils (N_p is limited to 50) (5.5)

where N_p is the average SPT N-value of the soil at the pile tip within a range of $4D$ above and $1D$ below the pile tip.

Distributions with depth of the ultimate capacity of the test piles are shown in Figs. 5.7a, 5.7b, 5.7c and 5.7d for the TSC1, TSC2, TSP2 and TSP1, respectively. The required pile tip levels are shown by the red circles in the figures. In case of the TSC1, the required pile tip level does not reach the hard silt clay. However, it was decided to penetrate the pile tip of the TSC1 into the hard silt clay, since TCVN 205-1998 prescribes that the pile tip should be penetrated at least 0.5 m into a hard bearing stratum to ensure the pile capacity under both vertical and horizontal loading conditions. The selected embedment lengths at this preliminary design stage of the test piles were 34.6 m, 40.4 m, 34.0 m and 37.4 m for the TSC1, TSC2, TSP1 and TSP2, respectively.

Distance from the seabed to the top level of the test piles (+6.5 m, 1 m above the working floor of the berth structure) are 15.7 m for the TSC1, 7.5 m for the TSC2, 17.1 m for the TSP1 and 12.5 m for the TSP2. Hence, the minimum length of the TSC1, TSC2, TSP1 and TSP2 are 50.3 m, 47.9 m, 51.1 m and 49.9 m, respectively, as shown in Table 5.3 together with the other pile specifications. Note that allowable stress and forces in both tension and compression are also indicated in the table for evaluating the appropriateness of the driving system in following part (Section 5.3.2).

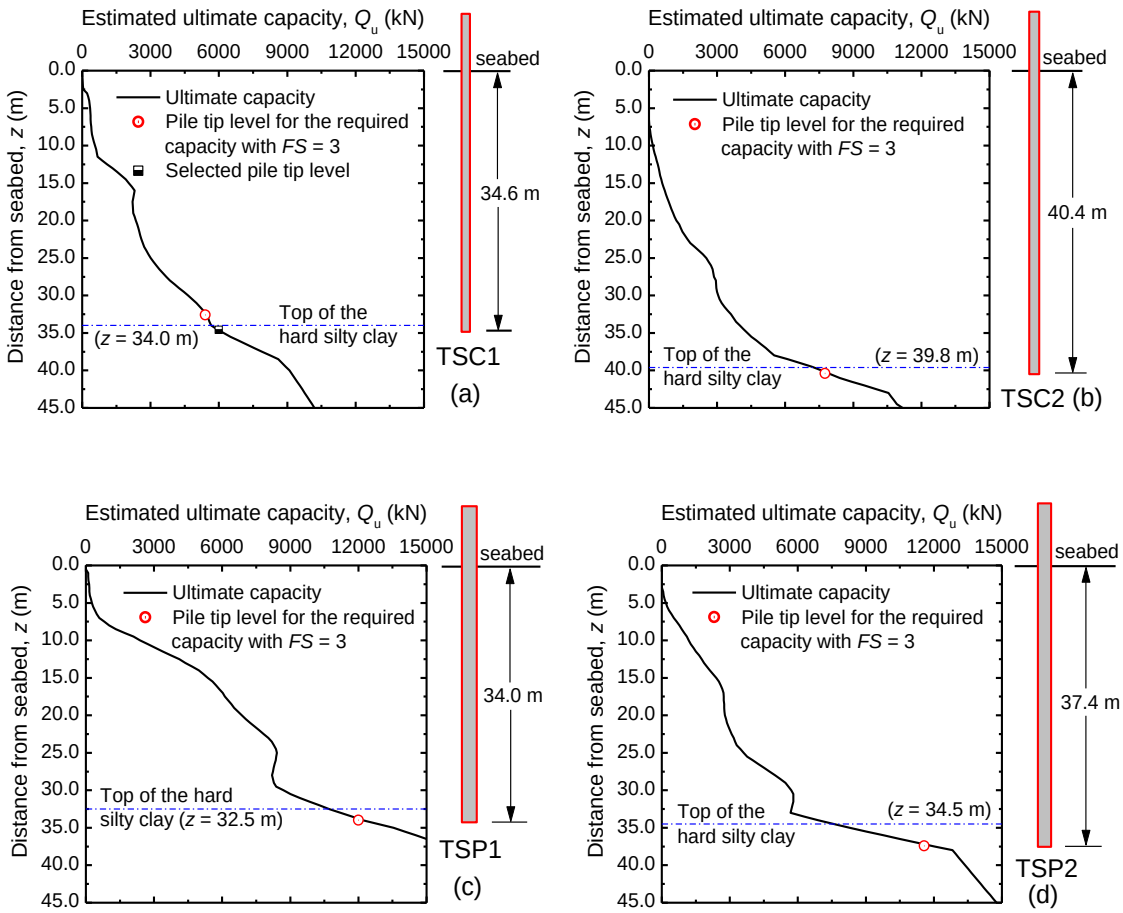

Figure 5.7. Estimated ultimate capacity with depth and selection of the pile tip level. (a) TSC1. (b) TSC2. (c) TSP1. (d) TSP2.

Table 5.3. Specification of test piles.

Item	TSC1	TSC2	TSP1	TSP2
Diameter, D (mm)	700	800	1000	900
Wall thickness, t_w (mm)	100	110	12	12
Cross-sectional area, A (mm^2)	188495	238447	37247	33477
Young's modulus, E (kPa)	4.3×10^7	4.3×10^7	2.0×10^8	2.0×10^8
Pile density, ρ (ton/m^3)	2.5	2.5	7.88	7.88
Wave speed, c (m/s)	4148	4148	5038	5038
Minimum pile length, L_{min} (m)	50.3	47.9	51.1	49.9
Allowable compressive stress, σ_{com} (MPa)	64.16	64.16	360	360
Allowable tensile stress, σ_{ten} (MPa)	7.85	7.85	360	360
Allowable compressive force, F_{com} (kN)	12090	15299	13409	12051
Allowable tensile force, F_{ten} (kN)	1480	1872	13409	12051

5.2.3 Driving work of the test piles

In order to drive a pile to the designed depth without any damage to the pile, selecting the pile driving system with adequate energy is very important. This selection involves several factors

such as: the size and type of the pile, the properties and topography of the ground, the location of the project (whether driving on land or in water) and the pile driving cost. In order to have an economical and efficient solution when driving a very long pile (L ~ 50 m) with a large diameter (D = 700 to 1000 mm) through a sandy soil of medium packing state in offshore condition, a diesel hammer was selected for this project. The required energy of the hammer and the driving work of the test piles are presented below.

a. Selecting the pile driving hammer

According to TCVN 286-2003, the minimum required energy, E_h (Nm), of each blow is estimated based on the following empirical equation:

$$E_h = 1.75 \times a \times P_a \tag{5.6}$$

in which a = 25 Nm/kN is empirical constant, P_a (kN) is the design working load of the pile.

In case of a single-acting diesel hammer, the hammer mass, M_h (kg), must be consistent with the following empirical conditions:

$$M_h + M_p \leq \frac{5E_h}{g} \tag{5.7}$$

where M_p (kg) is the mass of the pile including masses of the helmet and cushions, and g is the gravity acceleration.

Table 5.4 lists the minimum driving energy and the maximum hammer mass required for the four test piles. From these requirements, a diesel hammer, Delmag D100-13, was selected for the driving work of the test piles in this construction site. The main specifications of the hammer indicated in Table 5.5 satisfy the requirements of driving of all the test piles. Selection of the pile driving hammer for the working piles will be reconsidered, if the driving stresses predicted by the wave propagation analysis presented in a later part in this research exceed the allowable values of the axial stresses or axial forces of the test piles (see Table 5.3).

Table 5.4. Required energy for pile driving hammer and condition for hammer mass.

Item	TSC1	TSC2	TSP1	TSP2
Design working load, P_a (kN)	1800	2585	4002	3858
Mass of pile, M_p(ton) including helmet and cushions	26.5	32.1	18.2	15.5
Minimum required energy, E_h (kNm)	78.7	113.1	175.1	168.8
Maximum mass of hammer, M_h (ton)	13.6	25.5	71.0	70.5

Table 5.5. Specification of the pile driving hammer.

Item	Specification
Pile driving hammer	Delmag, D100-13
Hammer mass, M_h (ton)	10.0
Drop height of hammer, H (m)	2.8
Energy per blow, E_h (kNm)	213.9 to 333.6
Number of blows per minute	36 to 45
Suitable for driving pile with mass, M_p, up to (ton)	40.0

b. Requirements for driving the test piles

Based on the minimum required pile length, L of about 50 m, the maximum manufactured pile segment length, L_{seg} (not longer than 30 m) as well as the limitation of transport, the TSC1 and TSC2 consisted of two segments in which the lower segment is 30 m and the upper segment is 26 m (Fig. 5.8a). The reason for the longer lower segment is to ensure that the pile tip is driven though the soft clay and is laid in the clayey sand at the end of the driving work of the lower segment. Meanwhile, the test steel pipe piles, the TSP1 and TSP2, consisted of three segments with 20 m length for each. Like the above purpose, the Seg. 1 and Seg. 2 of the TSP piles were spliced on the barge to form the lower segment of 40 m length (Fig. 5.8b). The lower and upper segments of all the test piles were welded at the site.

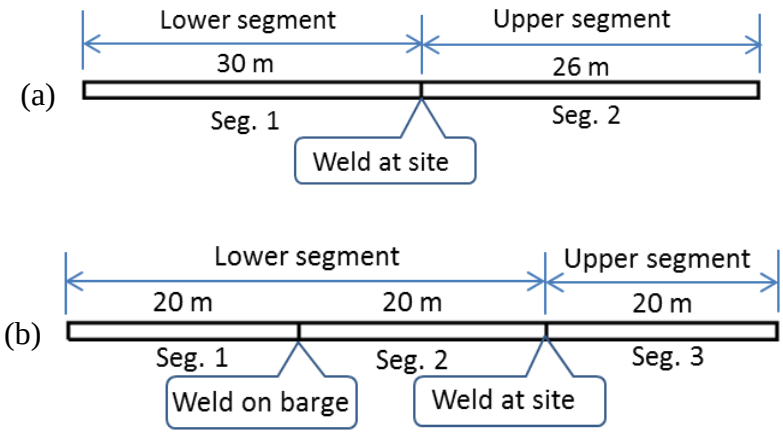

Figure 5.8. Pile combination from its segments.

(a) TSC1 and TSC2. (b) TSP1 and TSP2.

In order to possibly reach the required capacity, the piles have to be driven to the designed depths with an appropriate penetration per blow. According to TCVN 286-2003, when driving a pile using a diesel hammer, the average settlement per blow, S, obtained from the last 10 blows has to be smaller than the required value, S_d, calculated from Eq. (5.8). The values of S_d for the four test piles are listed in Table 5.6.

$$S_d = \frac{e_f M_h gH}{Q_d} - 0.5\sqrt{\frac{2e_f M_h gHL_p}{EA}} \tag{5.8}$$

in which: e_f is the hammer fall efficiency, e_f = 0.8 for a single-acting diesel hammer.

Q_d is the total dynamic pile resistance which can be estimated from the design working load, P_a, with the safety factor of more than 3. FS = 4.5 was chosen for this particular case because of a safe side pile driving termination. L_p is the pile length, L_p = 56 m for SC piles, L_p = 60 m for SP piles. E is the Young's modulus of the pile material. A is the net cross-sectional area of the pile calculated from the outer diameter. H is the falling height of the hammer mass, H = 2.5 m for SC piles, H = 2.8 m for SP piles.

Table 5.6. The maximum settlement per blow of the four test piles.

Item	TSC1	TSC2	TSP1	TSP2
Maximum penetration per blow, S_d (mm)	4.8	2.0	4.7	4.5

The sequence of the driving work of the test piles are as follows:

1. The lower segment is first driven into the ground to the given depth.
2. The welding work of upper and lower segments shall be carried out immediately at the site right after the completion of the driving work of the lower segment.
3. Further driving is conducted as soon as the welding work is completed and approved.
4. The pile is driven to the designed depth with the penetration per blow being smaller than the required value.

Note that, settlement per blow, S, and rebound, R, was measured at the end of driving manually using "paper and pencil method".

c. Results of driving work of the four test piles

All the test piles were driven into the bearing stratum of the hard silt clay with final embedment lengths as follows: 34.6 m for the TSC1, 41.2 m for the TSC2, 34.9 m for the TSP1 and 37.4 m for the TSP2. The embedment pile length of the TSC1 and the TSP2 were similar to those estimated from the empirical equation, while the penetration length of the TSC2 and the TSP1 were 0.8 m and 0.9 m greater than the expected values, respectively. The average settlement per blow calculated from the last 10 blows of the four test piles, TSC1, TSC2, TSP1 and TSP2, were 2.3 mm, 1.3 mm, 0.6 mm and 1.6 mm, respectively. All these values satisfied the requirements indicated in Table 5. The final embedment pile length of the working piles will be decided after analysing the results of the static and dynamic load tests of the test piles.

To prepare for the dynamic load test, except for the TSP1, the other three test piles were cut to the cut-off level, as illustrated in Fig. 5.9.

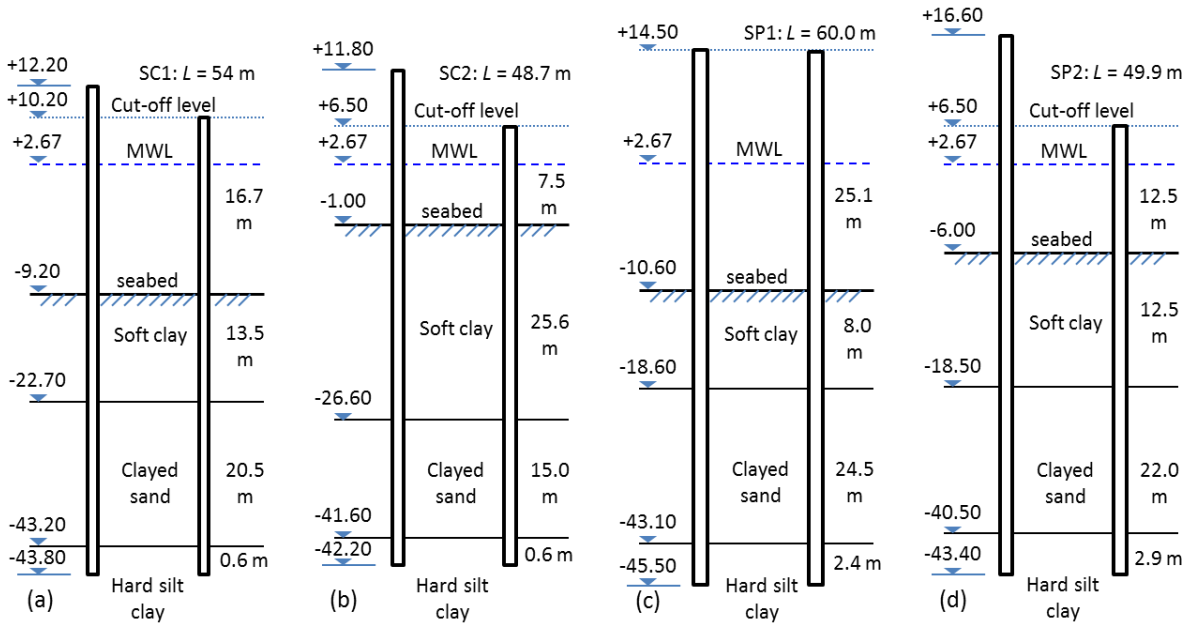

Figure 5.9. Illustration of the four test pileS before and after cutting the pile to the cut-off level. (a) TSC1. (b) TSC2. (c) TSP1. (d) TSP2.

5.2.4 Test procedure

Table 5.7 shows the testing schedule for each test pile including dynamic load test at the end of the driving work (EOD), dynamic load test at the beginning of re-striking (BOR) after rest period (7 days for the TSC1, 34 days for the TSP1), and static load test after further rest period (10 days for the TSC1 and 14 days for the TSP1). Static load tests only were carried out for the TSC2 and TSP2 after rest periods of 17 days and 27 days, respectively, from the day of driving.

Table 5.7. Schedule for the test piles.

Test date	TSC1	TSC2	TSP1	TSP2
DLT at end of driving (EOD)	21-Feb-2011	16-Mar-2011	26-May-2011	7-May-2011
Rest period before re-striking	**7 days**		**34 days**	
DLT at beginning of re-striking (BOR)	28-Feb-2011	**17 days**	26-Jun-2011	**27 days**
Rest period before static load test	**10 days**		**14 days**	
Static load test (SLT)	10-Mar-2011	2-Apr-2011	13-Jul-2011	3-Jun-2011

a. Dynamic load tests of the TSC1 and TSP1

Dynamic load tests were carried out at the end of driving (EOD) and at the beginning of re-striking (BOR) to investigate the "set-up" phenomenon, to check the driveability of the driving system and to identify the soil parameters. In order to measure the dynamic signals, two strain gauges and two accelerometers were attached to the pile at a distance of 2.7 m for the TSC1 and 3.5 m for the TSP1 from the pile top. At the dynamic measurement location, each pair of strain gauges and accelerometers were attached to the pile at symmetrical positions to the pile centre. The same driving hammer in the stage of driving the test piles was used. Illustration of the driving work in DLT is shown in Fig. 5.10. The monitoring devices were placed at a distance of about 7 to 10 m from the test pile to minimise the possible influence of the pile response on the measured signals.

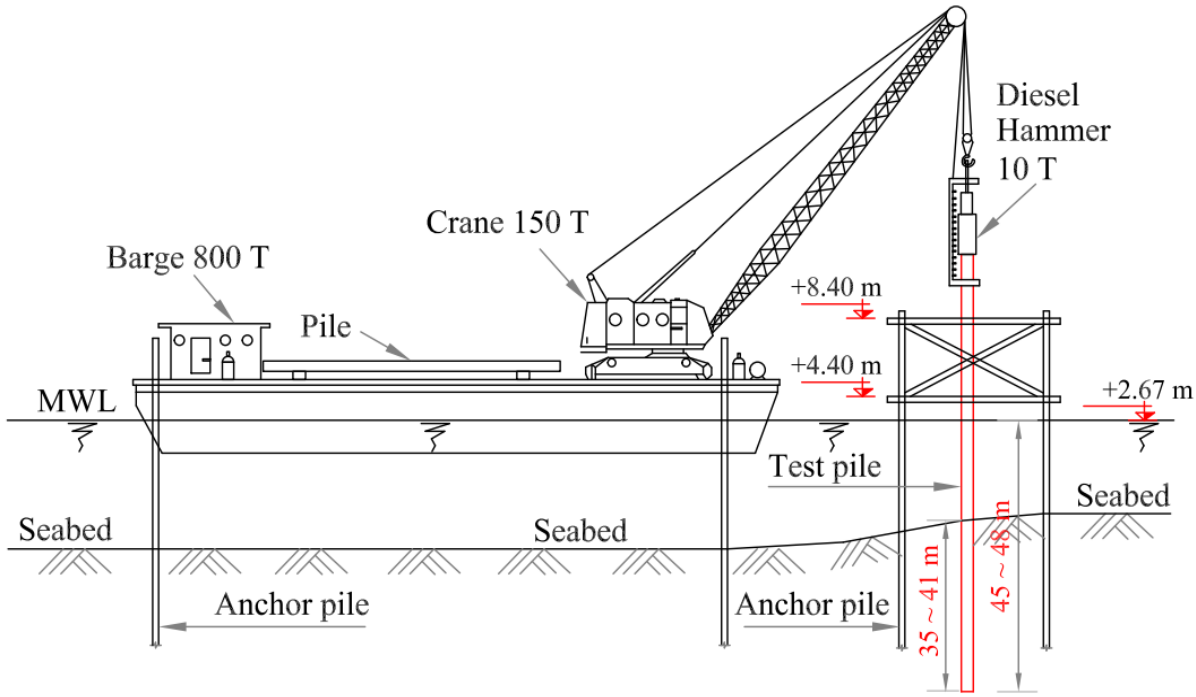

Figure 5.10. Illustration of the test pile driving by diesel hammer.

Dynamic load tests were conducted in accordance with ASTM-D4945-00 for PDA pile testing by high strain method. A PDA software suite was used to measure the dynamic signals including strains and accelerations. Using this software, velocity and force signals are automatically obtained from the measured values. The settlement per blow of the pile head was also manually measured at the end of driving.

b. Static load tests of the four test piles

The static load test was carried out after a given rest period from the BOR test in order to obtain the static load-displacement relation. The maximum load, P_{max}, for each test is listed in Table 5.8.

Table 5.8. The maximum test load.

Item	TSC1	TSC2	TSP1	TSP2
Design working load, P_a (kN)	1800	2585	4002	3858
Maximum test load, $P_{max} = 2 \times P_a$ (kN)	3600	5170	8004	7716

Static load tests were conducted in accordance with ASTM-D1143-81 for piles under static axial compressive load. The tests were carried out in offshore condition where the conventional static load test method using steel or concrete blocks as reaction force is very complicated. Hence, the reaction force for these tests was created by 8 anchor steel pipe piles with diameter of 700 mm and 4 pairs of reaction beams, I No. 900, as shown in Fig. 5.11.

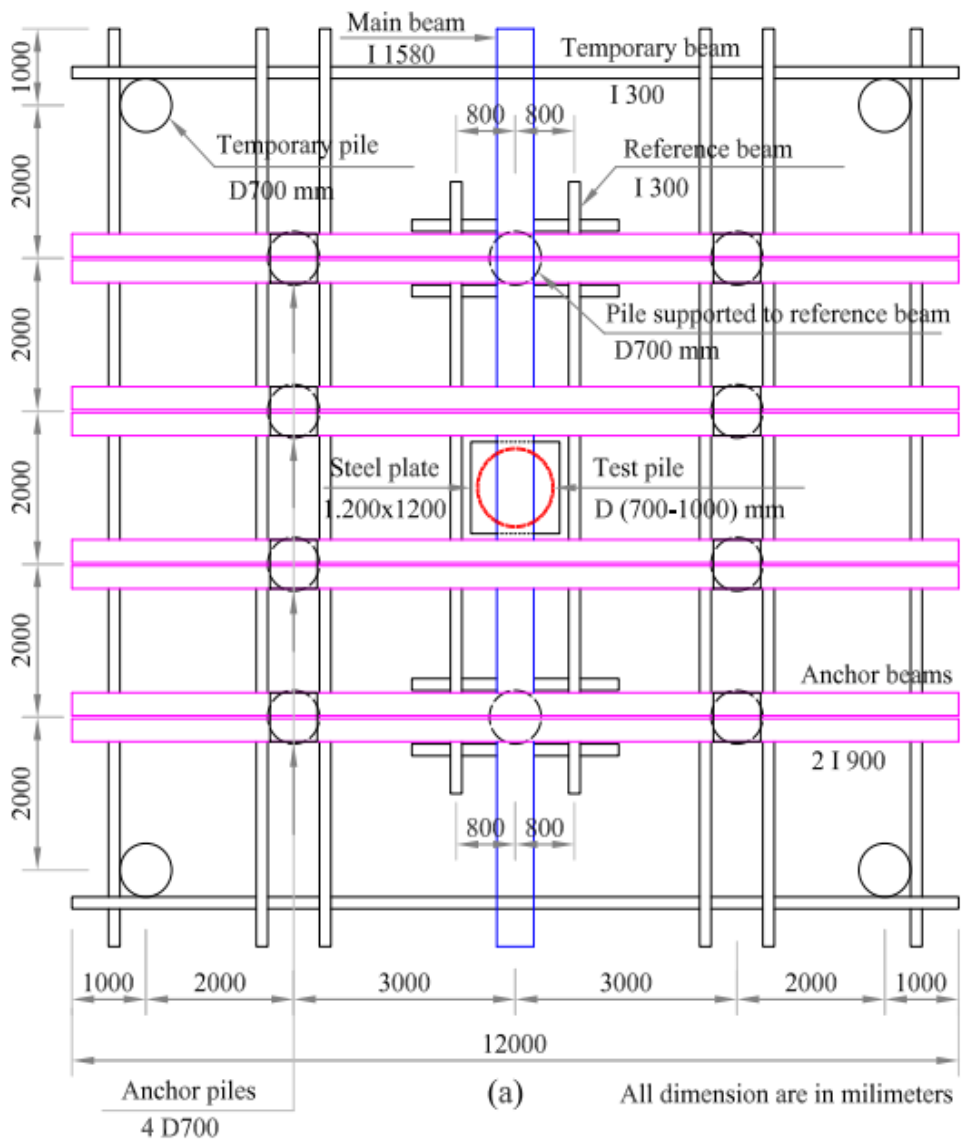

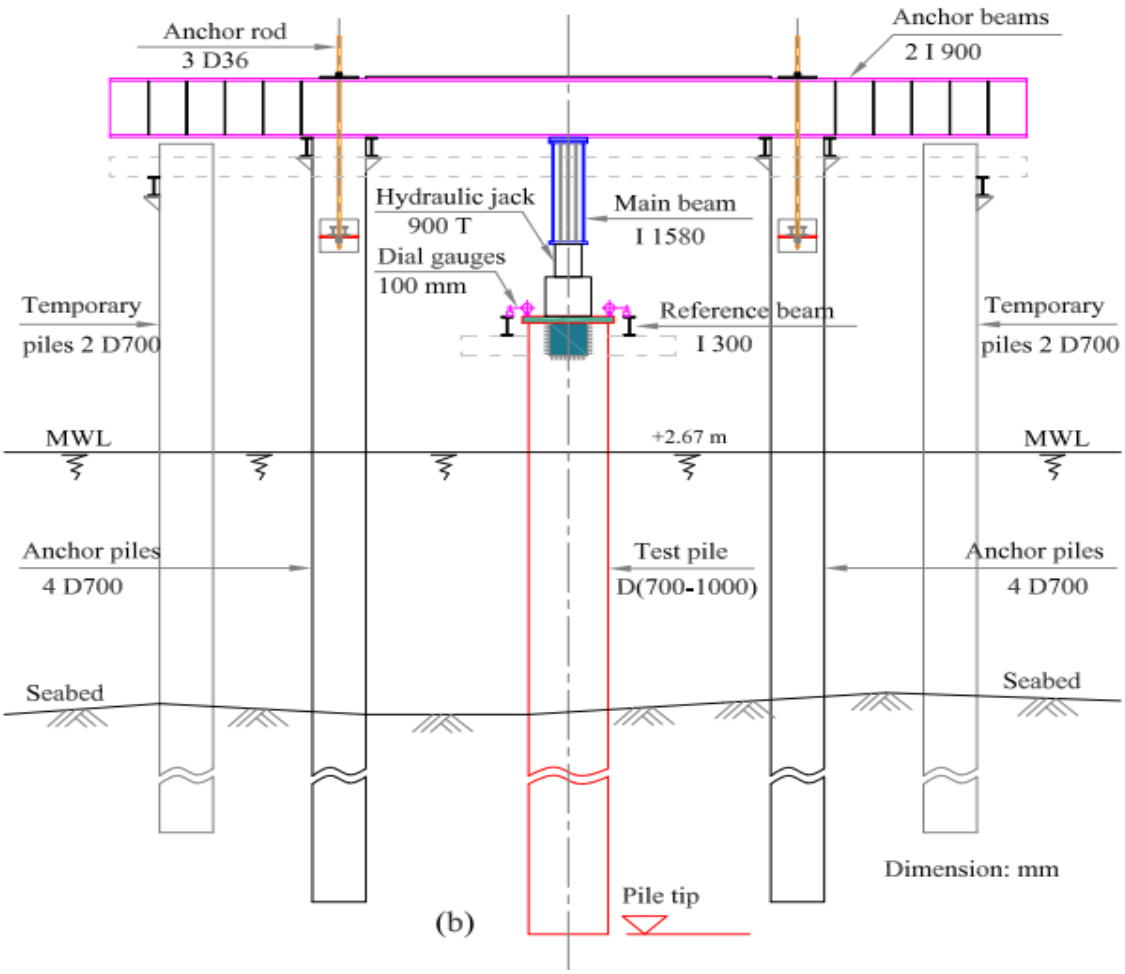

Figure 5.11. Illustration of the SLT. (a) Layout of the test piles and reaction system. (b) Front view of the SLT.

Regardless of the self-weight of the reaction system, reaction anchor piles were designed to have a tension resistance 3 times P_{max}. As the 8 anchor piles were used for the reaction system, each anchor steel pile for SLT of the TSC1, TSC2, TSP1 and TSP2 had to have the uplift capacity of 1350, 1939, 3002 and 2894 kN, respectively. The uplift capacity with depth of the anchor piles at the locations of the test piles calculated from Eq. (5.3) with assumption of q_{max} = 0, are shown in Fig. 5.12. The pile tip level for the required uplift capacity is indicated by dot symbol in the figure. The selected pile tip level indicated by triangle symbol corresponding to the embedment length of the anchor piles in SLT of the TSC1, TSC2, TSP1 and TSP2 were 28, 39, 35 and 40 m, respectively. As seen from Fig. 5.12, the uplift capacities of the anchor piles at the selected pile tip levels are greater than the required capacity. The nearest centre-to-centre distance, L_c, from the anchor piles to the test pile was 3.2 m, corresponding to the ratio L_c/D ranging from 3.2 to 4.6. This distance is large enough to minimise the influence of the anchor pile on the test pile.

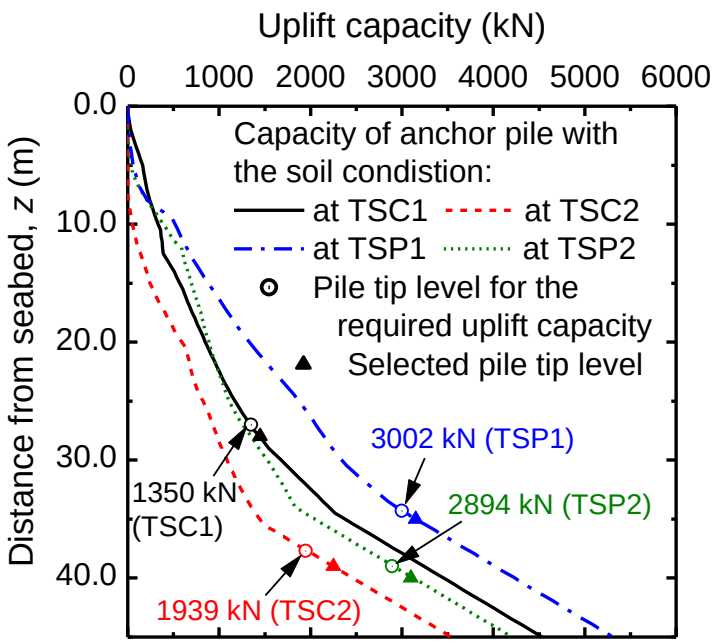

Figure 5.12. Uplift capacity of the anchor piles with the soil conditions at the TSC1, TSC2, TSP1 and TSP2.

In the static load test, in order to measure the applied force and the corresponding pile head settlement, the testing system consisted of a hydraulic jack with a capacity of 9 MN and 4 dial gauges of 100 mm in range. The jack was placed on the pile top and under the main beam I No. 1580 as shown in Fig. 5.11b. The dial gauges were placed firmly on two stable reference beams supported by the two additional anchor piles to minimise the influences of soil movement and deformation of the equipment on the measurement data.

The loading and unloading processes indicated in Fig. 5.13 were employed in the SLT including two cycles with 21 steps as follows:

1. First cycle (8 steps, from step 1 to step 8): Loading to the design working load, P_a, then unloading to zero. Increment of the applied load at each loading step was set at 25% of the design working load and load maintaining time of each step was 1 hour. Each unloading step was the same as that in the loading step and the load maintaining time of each step was 10 minutes.
2. Second cycle (13 steps, from step 9 to step 21): After 1 hour of unloading to zero in the 1st cycle, reloading to the design working load and maintaining the load for 6 hours at step 9. Further load was applied until the maximum load, P_{max}. At the maximum load, the load maintaining time was also 6 hours at step 13, and thereafter unloading procedure like in the 1st cycle was used to unload to zero.

For measuring the pile head displacement, after every 15 minutes in loading process and 10 minutes in unloading the settlement of the pile was recorded.

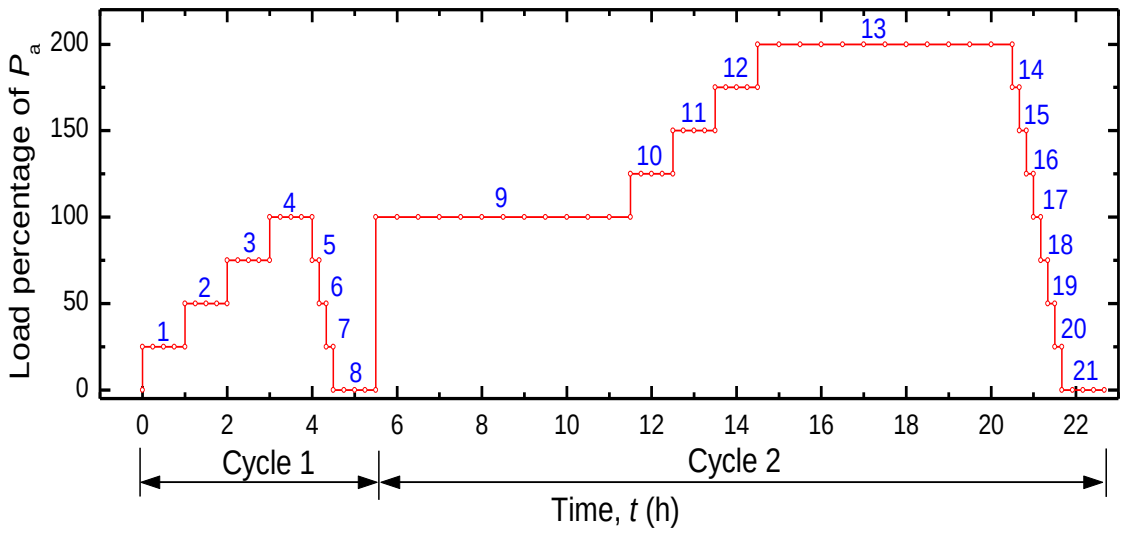

Figure 5.13. Loading process in SLTs.

The pile is considered to reach the failure (ultimate) state if one of the followings occurs:

1. Under the working load, the pile displacement without taking into account the pile compression exceeds 20 mm.
2. When unloading the working load to zero, the residual settlement exceeds the limit value, S_{ar} = 10 mm.
3. Under the maximum load, the total displacement of the pile head including the pile compression exceeds 10% of the pile diameter.
4. During the test, the pile is found to be away from its original position or to be damaged.

The first criterion can be expressed by means of the allowable pile head displacement including the pile compression under the working load. In accordance with TCVN 269-2002, elastic pile compression, ΔL, of a friction pile with a length, L, subjected to a vertical pile head load, P, can be calculated using the following equation:

$$\Delta L = \frac{2}{3}\frac{PL}{EA} \tag{5.9}$$

in which E and A are the Young's modulus and the cross-sectional of the pile, respectively.

The elastic shortening of the pile and the corresponding allowable pile head displacements under the working load, and the allowable pile head displacement under the maximum test load are listed in Table 5.9.

Table 5.9. Elastic shortening of the pile and the allowable pile head displacements.

Item	TSC1	TSC2	TSP1	TSP2
Pile compression, ΔL(mm) at working load P_a	8.4	9.3	18.6	18.2
Allowable pile head settlement S_a(mm) with taking into account the elastic shortening of the pile subjected to the working load P_a	28.4	29.3	38.6	38.2
Allowable pile head settlement S_{max}(mm) with taking into account the elastic shortening of the pile subjected to the maximum test load P_{max}	70.0	80.0	100.0	90.0

Results of the static load test will be presented later along with the results of WMA.

5.3 Wave matching analysis and test results

5.3.1 Wave matching procedure

a. Numerical approach

The numerical approach for the analyses of the dynamic load tests is similar to that in Section 3.3 of Chapter 3.

b. Modelling of the test ground and the pile

Figures 5.14 and 5.15 show the profiles of SPT *N*-values, the soil stratification, location of the pile and the distributions with depth of the shear moduli, G_0, and shear resistances, τ_{max}, for the TSC1 and TSP1, respectively. Note that the values of G_0 and τ_{max} are the first assumption of the soil properties for both the outer and inner soils in the wave matching analysis. Although the 3-layer ground at both the test piles was divided into 5 sub-layers in the analysis, the test pile TSC1 with the length of 54 m was divided into 54 elements and the test pile SP1 with the length of 60 m was divided into 60 elements. Because the top level of the soil plug was not measured during driving, the soil plug height was assumed to be 70 % to 80 % of the embedment pile length. This assumption is reasonable to the research of Paik et al. (2003) and Paikowsky et al. (1989). Hereafter, the distance from the seabed to the top of the soil plug was assumed to be 9 m for the TSC1 and 7 m for the TSP1. Discussion of the influence of the soil plug height on the wave matching analysis results will be made later.

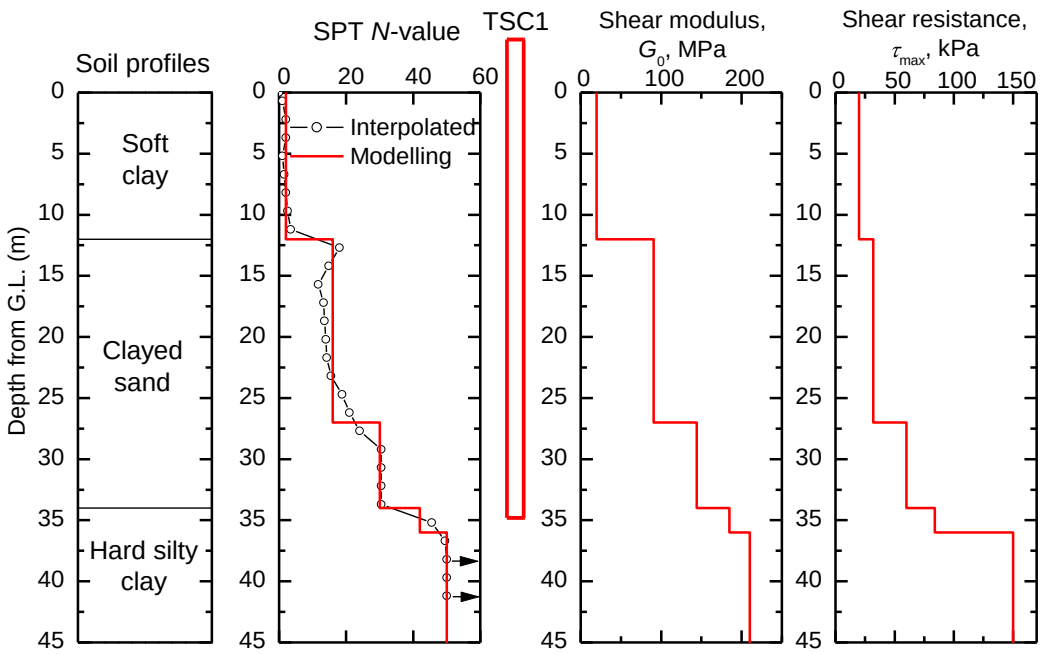

Figure 5.14. Modelling of the test ground at the test pile TSC1.

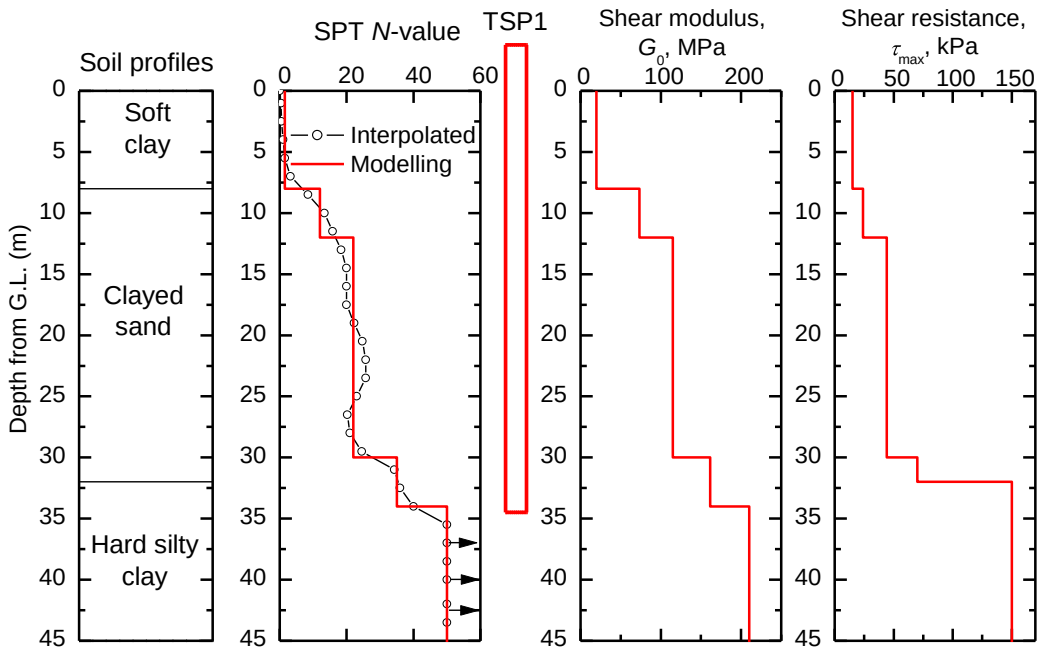

Figure 5.15. Modelling of the test ground at the test pile TSP1.

c. Calculation of impact force at the pile head from the measured force and velocity

The forces and velocities are usually measured near the pile head, about 1.0 to 2.0 times diameter of the pile. However, in these field tests, distance from the pile head to the strain gauges level, L_m, were 2.7 m for the TSC1 and 3.5 m for the TSP1, corresponding to 3.8D for the TSC1 and 3.5D for the TSP1. In order to model the full pile length in the analysis, it is needed to estimate the impact force acting on the pile head. Since there was no soil resistance

from the measurement level to the pile head, the one-dimensional stress-wave theory was employed to calculate the impact force acting on the pile head from the measured force and measured velocity.

The impact head force, $F(0,t)$, is calculated from the measured downward travelling force, $F_{\mathrm{d}}(L_{\mathrm{m}}, t)$, and the upward travelling force, $F_{\mathrm{u}}(L_{\mathrm{m}}, t)$, based on the one-dimensional stress-wave theory, as follows:

$$F(0,t) = F_{\mathrm{d}}(L_{\mathrm{m}}, t + L_{\mathrm{m}}/c) + F_{\mathrm{u}}(L_{\mathrm{m}}, t - L_{\mathrm{m}}/c) \tag{5.10}$$

in which $F_{\mathrm{d}}(L_{\mathrm{m}}, t + L_{\mathrm{m}}/c)$ and $F_{\mathrm{u}}(L_{\mathrm{m}}, t - L_{\mathrm{m}}/c)$ are calculated from the measured force, F_{meas}, and the measured velocity, v_{meas}, as the following equations:

$$F_{\mathrm{d}}(L_{\mathrm{m}}, t + L_{\mathrm{m}}/c) = \frac{1}{2}\left\{F_{\mathrm{meas}}(L_{\mathrm{m}}, t + L_{\mathrm{m}}/c) + \frac{E}{c} v_{\mathrm{meas}}(L_{\mathrm{m}}, t + L_{\mathrm{m}}/c)\right\} \tag{5.11}$$

$$F_{\mathrm{u}}(L_{\mathrm{m}}, t - L_{\mathrm{m}}/c) = \frac{1}{2}\left\{F_{\mathrm{meas}}(L_{\mathrm{m}}, t - L_{\mathrm{m}}/c) - \frac{E}{c} v_{\mathrm{meas}}(L_{\mathrm{m}}, t - L_{\mathrm{m}}/c)\right\} \tag{5.12}$$

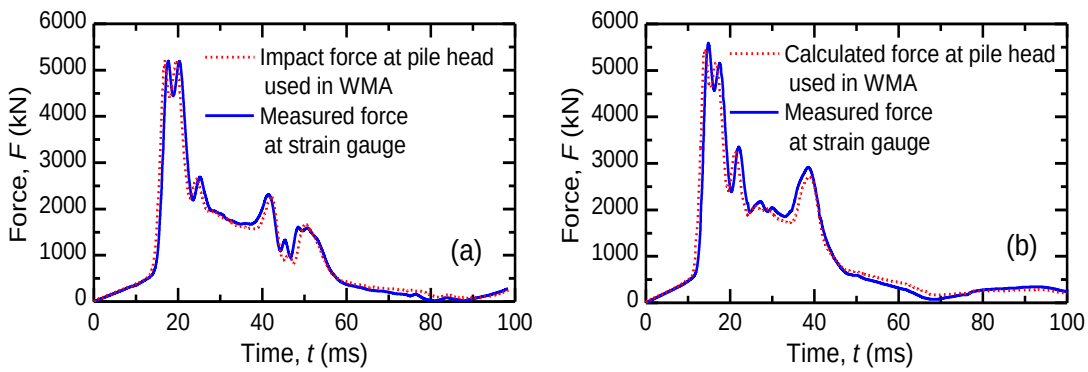

Figure 5.16. Calculated impact forces at the pile head, together with measured forces of the TSC1 at (a) EOD. (b) BOR.

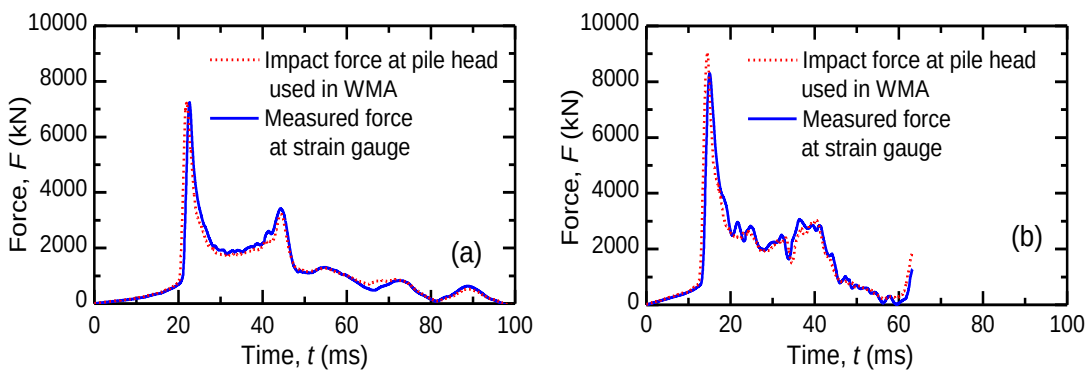

Figure 5.17. Calculated impact forces at the pile head, together with measured forces of the TSP1 at (a) EOD. (b) BOR.

The calculated impact forces at the pile head in the EOD and BOR tests are shown in Figs. 5.16a and 5.16b for the TSC1 and in Figs. 5.17a and 5.17b for the TSP1. The measured forces at the strain gauge level are also shown in the figures for comparison.

5.3.2 Results of wave matching analyses

a. Results of the TSC1

Under the impact force caused by a hammer mass of 10 ton with a falling height of 2.5 m, the measured settlement per blow of the pile head were 2.3 mm in the EOD test and 1.5 mm in the BOR test. These values along with pile axial force, downward and upward traveling forces, velocities and displacements obtained from the measured dynamic signals at the strain gauge level were used as targets in the wave matching analysis (WMA).

As mentioned earlier, the distance from the seabed to the top of the soil plug was assumed to be 9 m for TSC1. In the first WMA with the soil properties shown in Fig. 5.14, good matching was not obtained. Then, the soil properties were changed until getting a good matching between the calculated and the measured responses. The results of the final WMA for both EOD and BOR tests of the pile axial force, downward and upward travelling forces, velocity and displacement at the pile head are shown in Figs. 5.18 and 5.19, respectively.

Note that, the calculated downward and upward travelling forces shown in Figs. 5.18b and 5.19b were calculated from the calculated axial force, F, and the calculated velocity, v, at the strain gauge level using Eqs. (5.11) and (5.12), respectively.

As seen from the figures, the analysed results of the final WMA are comparable with the measured values for both EOD and BOR tests. The return travelling time of stress wave in the pile is about 26.0 ms ($2L/c$ = 0.0260 s). The rise time of the axial forces was 17.5 ms in EOD test and 14.5 ms in BOR test. Therefore, the peak of the force was reflected to the strain gauge level at t = 43.5 ms (26 + 17.5 ms) in EOD test and at t = 40.5 ms (26 + 14.5 ms) in BOR test. From Fig. 5.19a, the axial force at the instant of 40.5 ms obtained in BOR test is substantially greater than that in EOD test (see axial force at t = 43.5 ms in Fig. 5.18a), indicating that higher soil resistance was mobilised in BOR test than in EOD test due to the "set-up" phenomenon during the rest period between EOD and BOR tests. Of course, influence of the soil resistance can be found more clearly when we compare the calculated upward travelling forces with the measured values as shown in Figs. 5.18b and 5.19b. Note that, the final calculated pile head displacement in BOR test shown in Fig. 5.19d was 1.28 mm which was in good agreement with the measured value of 1.5 mm.

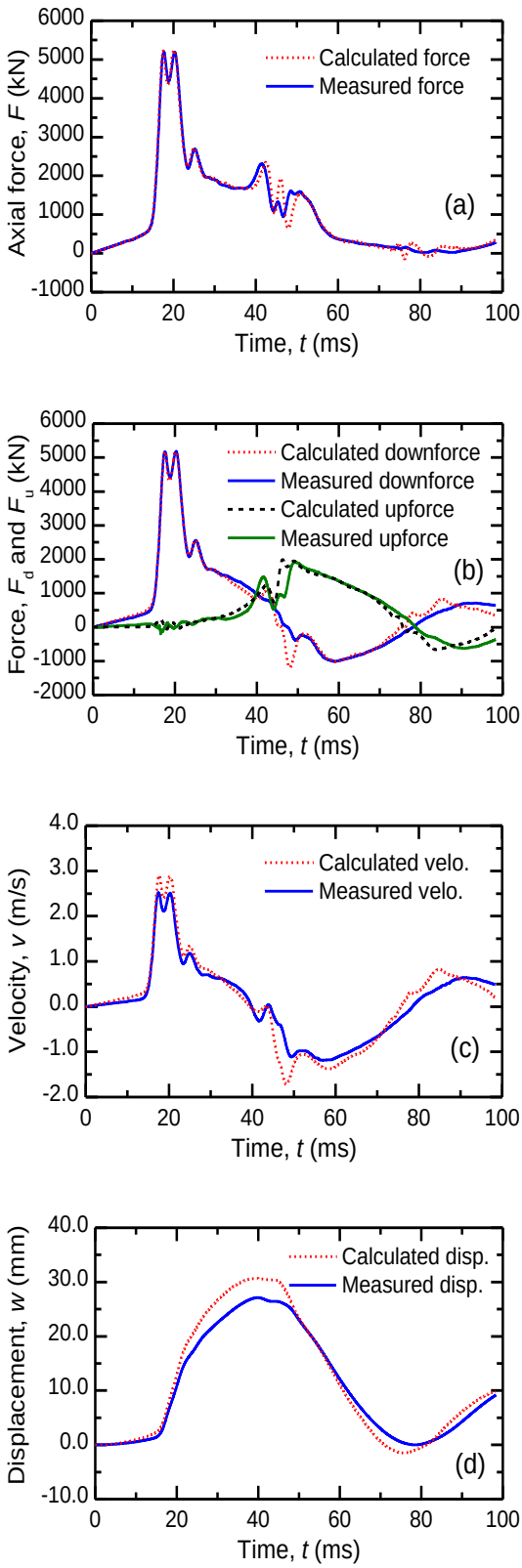

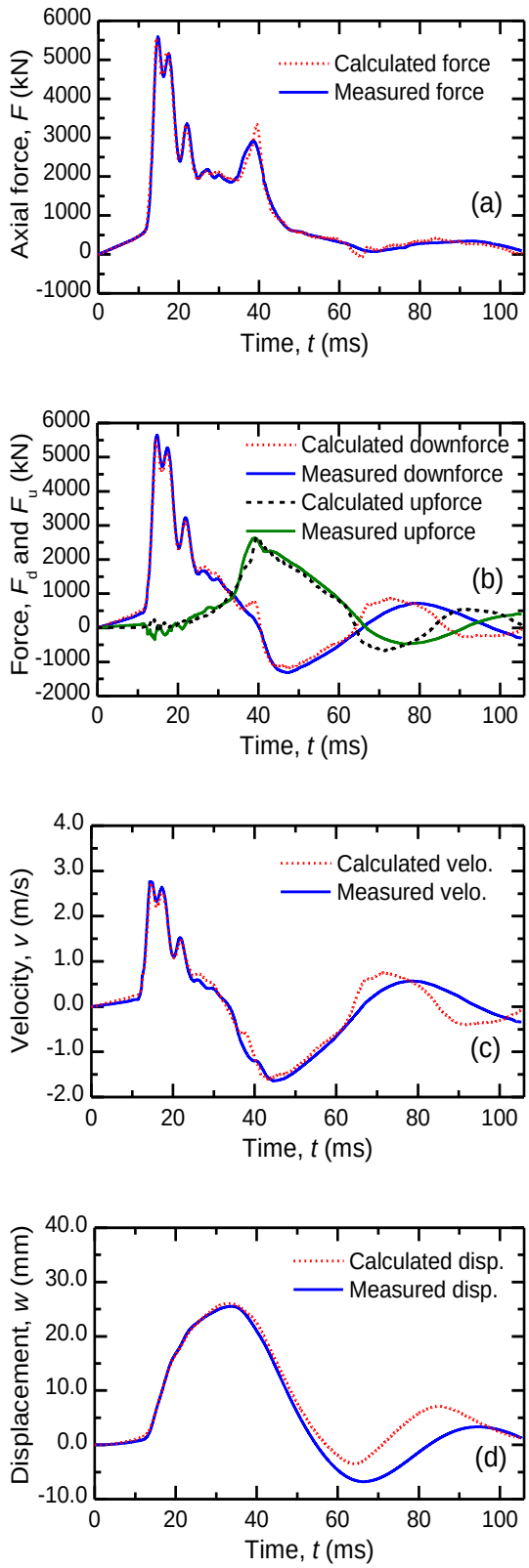

(a) Force. (b) Downward and upward travelling forces. (c) Velocity. (d) Displacement.

Figure 5.18. Results of the final wave matching analysis of EOD test of the TSC1.

Figure 5.19. Results of the final wave matching analysis of BOR test of the TSC1

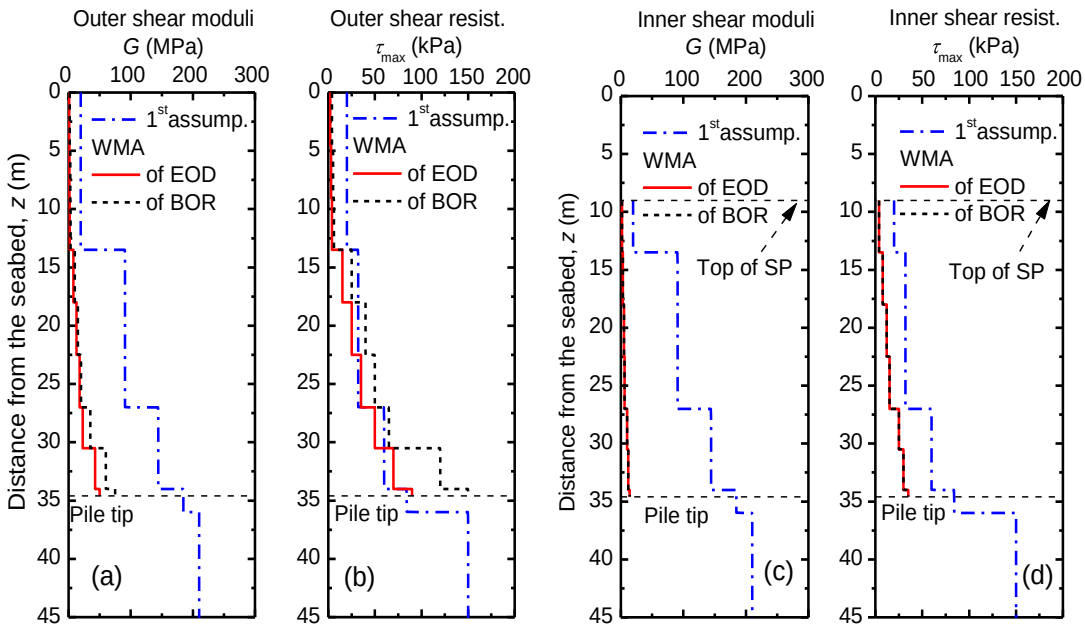

Figure 5.20. Soil properties obtained from the final WMA of the TSC1 in the EOD and BOR tests.

The soil properties identified from the final WMA are shown in Fig. 5.20 for the soil surrounding the pile shaft and in Table 5.10 for the soil beneath the pile tip and the soil plug base. The soil properties in the first assumption are also indicated for comparison.

Table 5.10. The soil parameters at the pile tip and soil plug base obtained from the final WMA.

Item	Unit	EOD test	BOR test	1st assumption
Shear modulus at the pile tip, G_b	MPa	1700	7000	210
Shear modulus at the soil plug base, G_{sp}	MPa	1000	2000	210
End bearing resistance at the pile tip, $q_{b,max}$	kPa	30700	33500	15000
End bearing resistance at the soil plug base, $q_{sp,max}$	kPa	1000	2000	15000

Figure 5.20 shows that the values of shear modulus, G, and the shear resistance, τ_{max}, of the soil layers identified from the final WMA of the EOD test are smaller than those of the BOR test, indicating again that the "set-up" phenomenon occurred after the rest period. As seen from the figures, the identified values of G for both tests are smaller than the first assumptions for the soils. The outer shear resistance, however, are smaller than the firstly assumed values for the weak soils (the top soil layer of soft clay and the upper part of the second soil layer of clayey sand with loose packing state). For the harder soils (the lower part of the second soil layer of clayey sand with medium packing state and the third soil layer of

hard silt clay), the outer shear resistance identified from the final WMA of the EOD test are comparable with the first assumptions of τ_{max}, but those identified from the final WMA of the BOR test are greater than the firstly assumed values. Comparison of the shear modulus between the identified and the firstly assumed values suggests that reduction factor of 0.1 for soft soils, 0.15 to 0.20 for medium soils and 0.25 to 0.40 for hard soils can be used to estimate the shear moduli of soils at this particular site.

Consideration of the inner soil parameters (τ_{max} and G) was indispensable to get good matching results. The identified inner soil parameters obtained from the final WMA are smaller than both the first assumption and the values of the outer soils. The smaller soil parameter values of the soil plug could be attributed to the soil disturbance when driving the pile in the saturated condition. Furthermore, it could be supposed that the excess-pore water pressure generated in the soil plug during driving was not easy to dissipate after the short rest period.

As for the identified shear moduli and the end bearing resistances of the soil at the pile tip and the soil plug base indicated in Table 5.10, the values obtained from the final WMA of EOD test are also smaller than those from BOR test. For both tests, all the identified values are substantially greater than the firstly assumed values. One reason is that the first assumption of soil parameters were estimated based on the limit of SPT N-values of the soil at the pile tip, $N_p = 50$, which was smaller than the actual value at this site. Another reason might be that the empirical equations are only crude approach to estimate G and q_{max} for the hard soil beneath the pile tip. Note that the identified end bearing resistance of the soil beneath the soil plug base was substantially smaller than that of the soil below the pile tip. This could be explained that the mobilised inner soil resistances were very small during driving, resulting in the small mobilised end-bearing resistance of the soil beneath the soil plug base.

In order to investigate the influence of the assumed soil plug height on the analysed results, the top of soil plug from the seabed level was varied from 0 to 13 m within three more cases (Cases 1 to 3) in which Cases 1 and 2 have higher heights of the soil plug while Case 3 has a shorter height of the soil plug compared to the previously analysed case (the reference case) with the distance from the seabed to the top of the soil plug of 9 m. The identified soil parameters obtained from the final WMA of the BOR test were used in these analyses. Note that, the inner soil parameters at the top of the soil plug (z = 9 m) identified from the final WMA of the BOR test were used for the shallower depths from z = 0 to 9 m in Case 1 and Case 2. Results of the pile head displacements obtained from the three additional analyses are compared with that in the final WMA of the BOR test in Fig. 5.21.

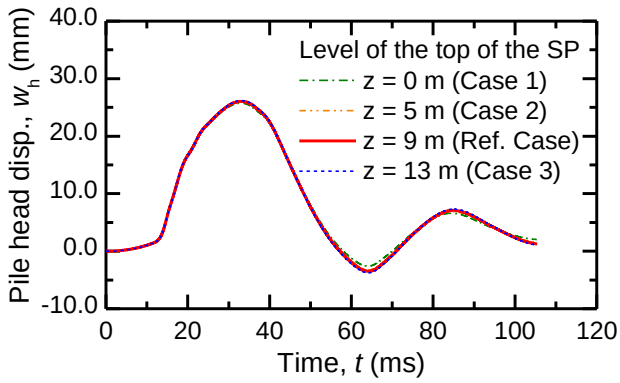

Figure 5.21. Calculated pile head displacement with different heights of the soil plug.

As seen from the figure, although the soil plug height changed widely, the calculated result varied slightly, indicating that the influence of the soil plug height in these particular analyses was negligible. One of the reasons could be that the soil near the top of the soil plug was very weak with SPT *N*-values ranging from 0 to 4 and the identified values of τ_{max} was only 4 kPa for depths from 0 to 13.5 m. Therefore, assumption of the top of the soil plug height in this study could be acceptable. All of the identified soil parameters were then used to derive the static load displacement curves, as presented later.

Selection of an appropriate pile driving hammer in pile driving is obligatory to ensure that pile is not damaged during driving. In order to evaluate the appropriateness of the selected pile driving hammer, the distributions with depth of the maximum compressive and tensile stresses calculated from the final WMA of the EOD and BOR tests are compared with the allowable values in Fig. 5.22.

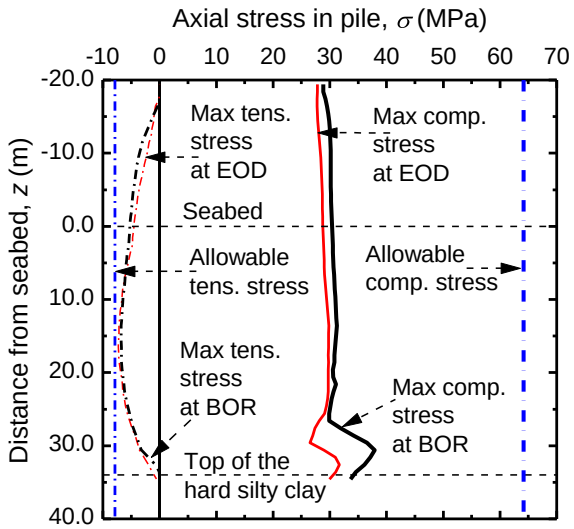

Figure 5.22. Distribution with depth of the maximum tensile and compressive stresses in the pile during driving of the TSC1.

It can be seen from the figure that the maximum compressive stress occurred at about 4 m above the pile tip while the tensile stress reached the maximum value at the middle of the embedment pile length. All the calculated stresses in the pile generated during driving were smaller than the allowable stresses, indicating that the selected pile hammer was suitable for the TSC1. Similar evaluation of the suitability to the pile driving hammer will be made for the TSP1 in the later part.

Figure 5.23 shows the static load-displacement curves derived from the soil properties identified in the final WMA of the EOD and BOR tests, compared with the static load test result in two cycles of loading process. As seen from the figure, the stiffness of the derived static response obtained from the BOR test is higher than that obtained from the EOD test, indicating the "set-up" phenomenon discussed previously. The derived static response obtained from the final WMA of the BOR test is comparable with the SLT, compared to that obtained from the EOD test. As indicated in Table 5.10, the EOD test was carried out 17 days before the SLT and the BOR test was conducted 10 days before the SLT. The three load-displacement curves in Fig. 5.23 clearly indicate the "set-up" phenomenon during the period from the EOD test via the BOR test to the SLT.

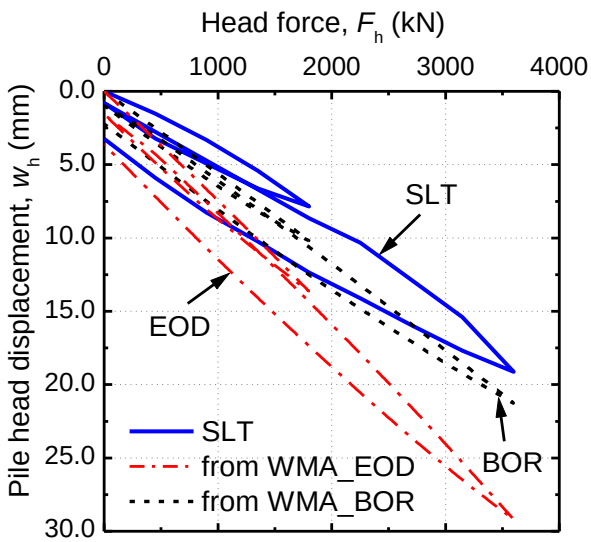

Figure 5.23. Comparison of the static load displacement curves of the TSC1.

From the result of the SLT, the measured settlement S = 9.0 mm at the working load of 1800 kN was sufficiently smaller than the allowable value S_a = 28.4 mm. The measured settlement S = 19.0 mm at the maximum load of 3600 kN was also smaller than 70 mm that is 10% of the pile diameter. And the residual settlement S = 1.0 mm after the full unloading process from the working load was also below the limit value S_{ar} = 10.0 mm. All of these

values indicated that the pile did not reach the ultimate bearing state. Hence, the TSC1 has a factor of safety greater than 2 against the working load of 1800 kN.

As mentioned earlier, the pile head load and the pile head displacement alone were measured in the SLT. The load-displacement curve derived from the final WMA of the BOR test was comparable with the SLT result (Fig. 5.23). Therefore, let us discuss more the static response of the TSC1 based on the calculated results of the BOR test including the loading and unloading processes.

Figure 5.24 shows the calculated changes of distributions with depth of the axial forces in the TSC1, including the first loading process (steps 1 to 4), the first unloading process (steps 5 to 8) and the second loading process (steps 9 to 13, see Fig. 5.13). The axial force at the pile tip can be regarded as the mobilised pile tip resistance. As seen from the figure, in the first loading process from step 1 to step 4, the mobilised shaft resistance and tip resistance increase with increase in the applied head force. At the working load, P_a = 1800 kN, the mobilised tip resistance, Q_b, and the total mobilised shaft resistance, Q_s, share almost the same force, about 50% of the applied force. When unloading to zero at step 8, axial forces remain along the embedment pile length. These residual forces increase with depth and reach a maximum value of about 400 kN at the pile tip. When reloading to the working load at step 9, the axial forces along the pile deeper than 15 m are greater than those in step 4 because of the residual forces in the pile generated in the previous loading steps. When further loads are applied on the pile head in steps 10 to 13, the mobilised shaft resistance and end-bearing resistance continue to increase, indicating that the pile does not reach the ultimate bearing state at the maximum applied force of 3600 kN.

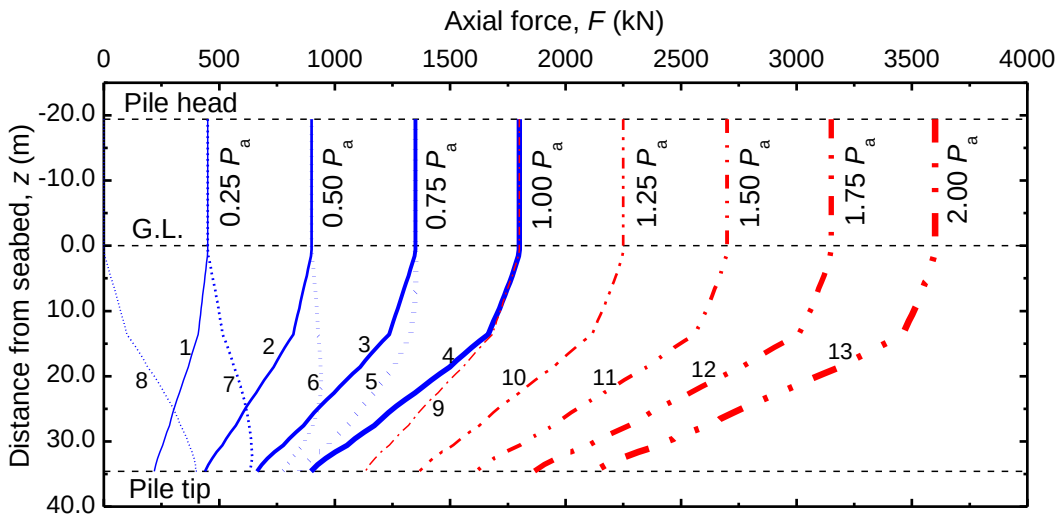

Figure 5.24. Calculated distributions with depth of the pile axial forces of the TSC1 at the BOR test.

The TSC1 was not used for the working pile after the completion of the SLT. However, it may be interesting to calculate the pile response, supposing that the TSC1 were loaded to the working load again after the completion of the SLT. For this purpose, the third loading process was fictitiously added to the previous analysis.

Figure 5.25 shows the calculated distribution of the axial forces in the pile at the end of the third loading process, together with those at the working load in step 4 of the first loading process and in step 9 of the second loading process, and those at the maximum load (step 13) and full unloading step of the second loading process. The figure indicates that when unloading to zero from the maximum load, the residual axial force is again caused along the embedment pile length with a maximum value of 1000 kN at the pile tip which is much greater than 400 kN in the first full unloading step (step 8 in Fig. 5.24). At the working load, the axial forces decrease with depth in the first and second loading processes, however, the axial force in the third loading process increases with depths to 25 m (neutral plane) and then decreases with increasing depth. It is clearly seen from comparison of the axial forces in the pile at the working load in three loading processes that the mobilised shear resistances decrease while the mobilised tip resistances increase with increase in the number of the loading processes. Such aspect should be considered when evaluating the pile capacity after the SLT, because the safety margin of the pile tip resistance decreases with increasing the number of loading processes in which magnitude of the maximum applied force increases in each process. This aspect will be discussed again in later part for the TSP1, which was reused as a working pile in this site.

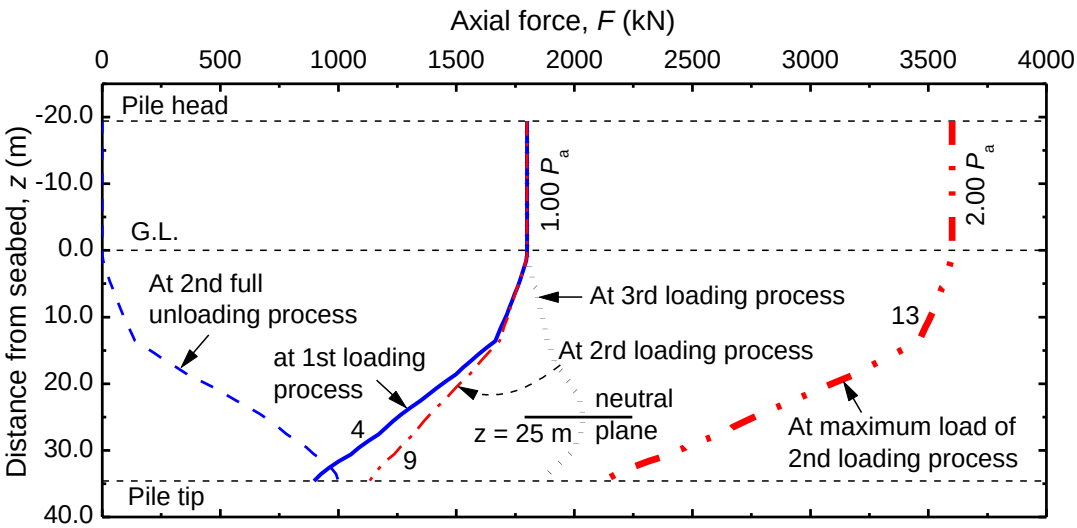

Figure 5.25. Calculated distributions with depth of the pile axial forces of the TSC1 at the BOR test for three loading processes.

b. Results of the TSP1

Similar to the TSC1, wave matching analysis was conducted for the TSP1, and the results of the final WMA at the strain gauge level including axial forces, downward and upward travelling forces, velocities and displacements are shown in Fig. 5.26 for the EOD test and in Fig. 5.27 for the BOR test. As seen from these figures, the calculated results were comparable with the measured values, when the soil parameters shown in Fig. 5.28 and Table 5.11 were assumed.

Note that under the impact force caused by a hammer mass of 10 ton with a falling height of 2.8 m, the measured settlement per blow of the pile head were 0.6 mm in the EOD test and 0.3 mm in the BOR test. As seen from Fig. 5.27d, the calculated pile head settlement in the BOR test was comparable with the measure value of 0.76 mm.

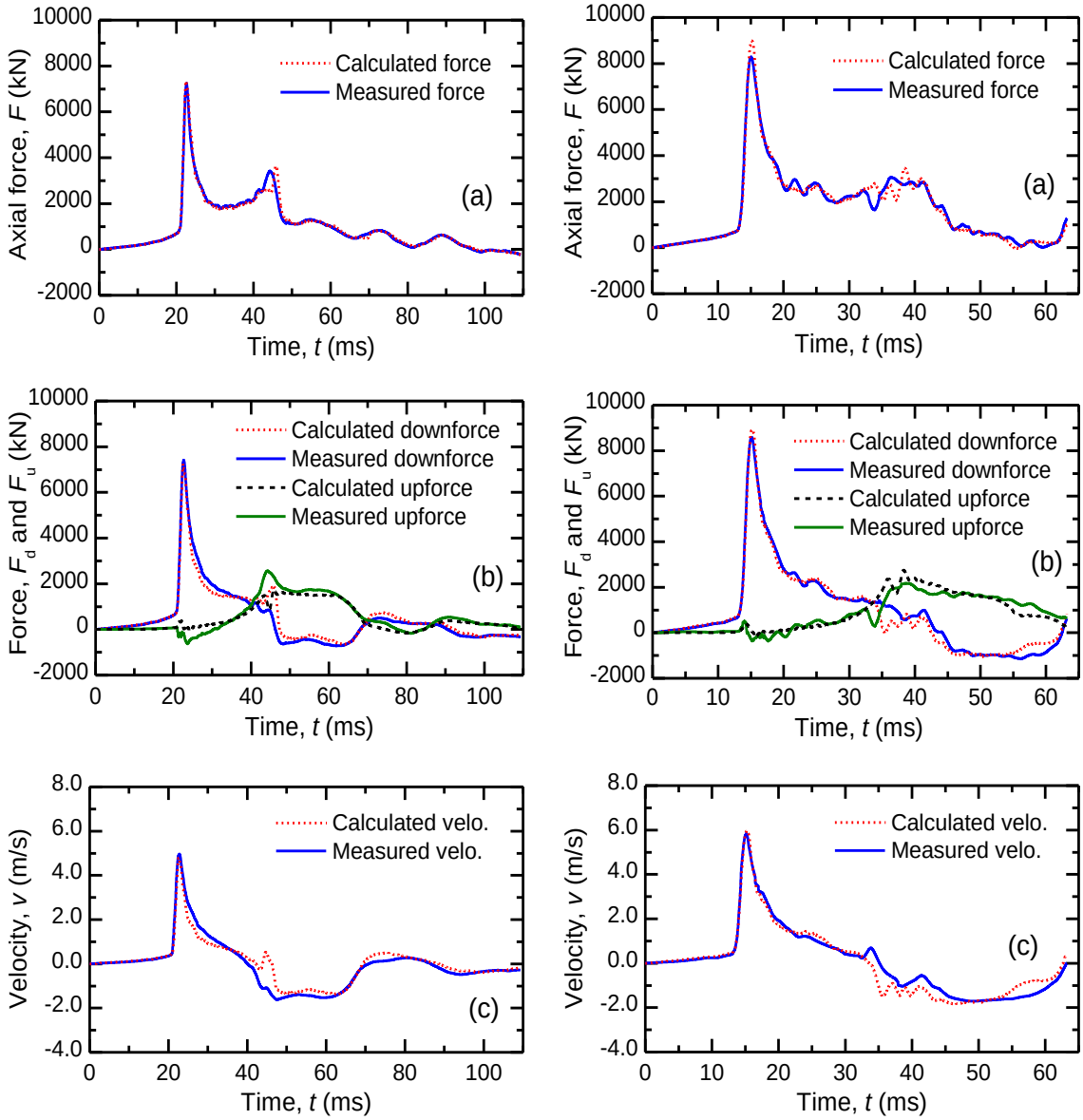

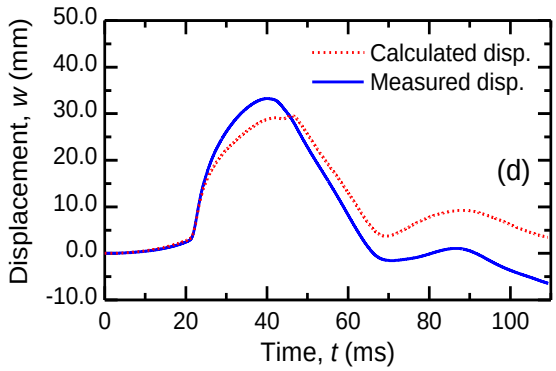

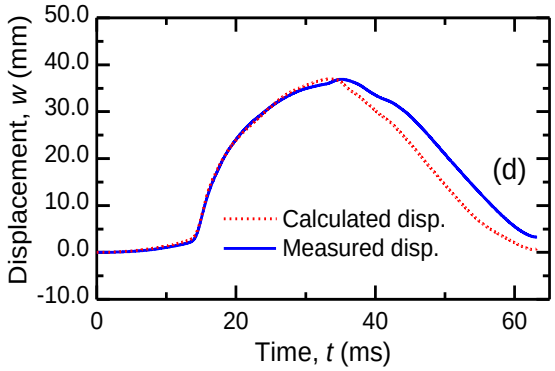

(a) Force. (b) Downward and upward travelling forces. (c) Velocity. (d) Displacement.

Figure 5.26. Results of the final wave matching analysis of EOD test of the TSP1.

Figure 5.27. Results of the final wave matching analysis of BOR test of the TSP1

The soil parameters in the first assumption are also indicated in Fig. 5.28 for comparison. The values of shear modulus, G, and the shear resistance, τ_{max}, of the soil layers identified from the final WMA of the EOD test were smaller than those from the WMA of the BOR test, indicating again that the "set-up" phenomenon occurred after the rest period. Such phenomenon was also obtained for the soil at the pile tip by comparison of the identified values, G_b and $q_{b,max}$, between the EOD and BOR tests shown in Table 5.11.

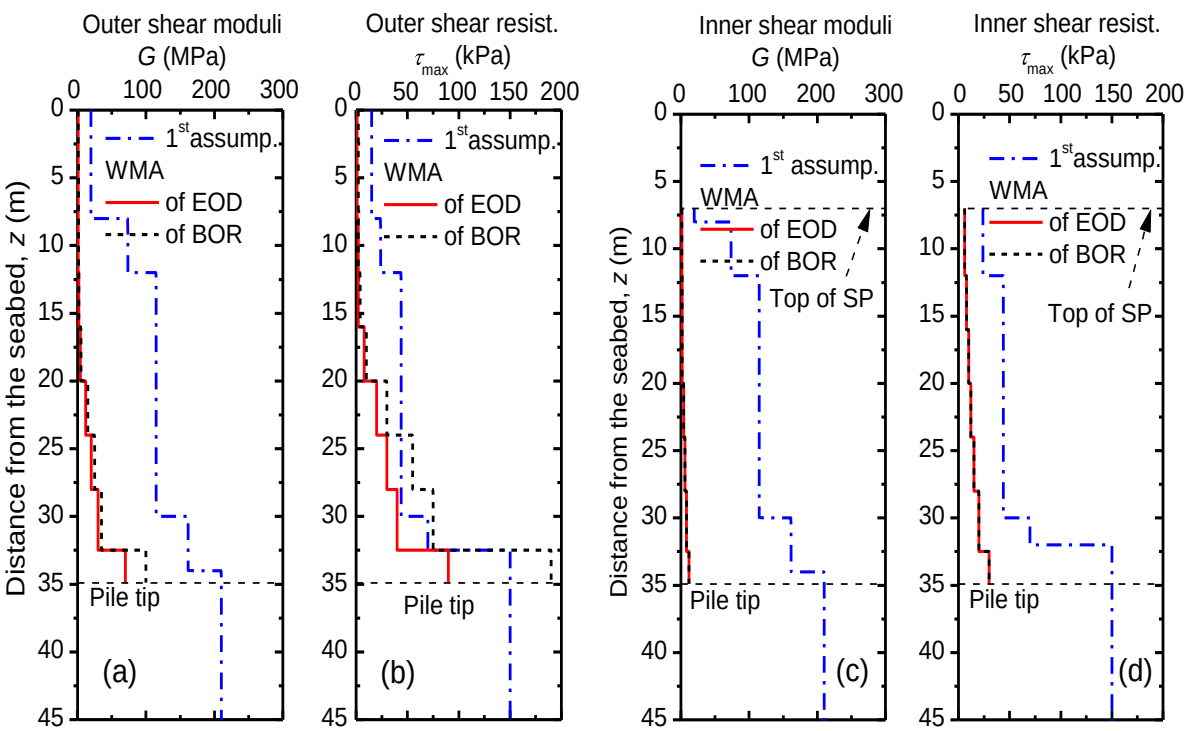

Figure 5.28. Soil properties obtained from the final WMA of the TSP1 in the EOD and BOR tests.

Table 5.11. Soil parameters at the pile tip and soil plug base obtained from the final WMA.

Item	Unit	EOD test	BOR test	1st assumption
Shear modulus at the pile tip, G_b	MPa	20000	22000	210
Shear modulus at the soil plug base, G_{sp}	MPa	2000	2000	210
End bearing resistance at the pile tip, $q_{b,max}$	kPa	120000	140000	15000
End bearing resistance at the soil plug base, $q_{sp,max}$	kPa	1000	1000	15000

For the EOD and BOR tests, similar to the case of the TSC1, the first assumption of the shear modulus estimated from empirical equation Eq. (1) were overestimated, compared to the finally identified values (Figs. 5.28a and 5.28b). For the BOR test, the empirical equations (5.4) and (5.5) overestimated the identified shear resistances for the soft soil layers (the first layer of the soft clay and the upper part of the second layer of clayey sand with loose packing state), while underestimated the identified shear resistances for the hard soil layers (the lower part of the second layer of clayey sand with medium packing state and the third layer of hard silt clay).

Let us discuss the suitability of the selected hammer for the TSP1. The calculated maximum compressive and tensile stresses in the pile during driving in the EOD and BOR tests shown in Fig. 5.29 do not exceed the allowable stresses. Therefore, the selected pile driving hammer is suitable for driving the working piles.

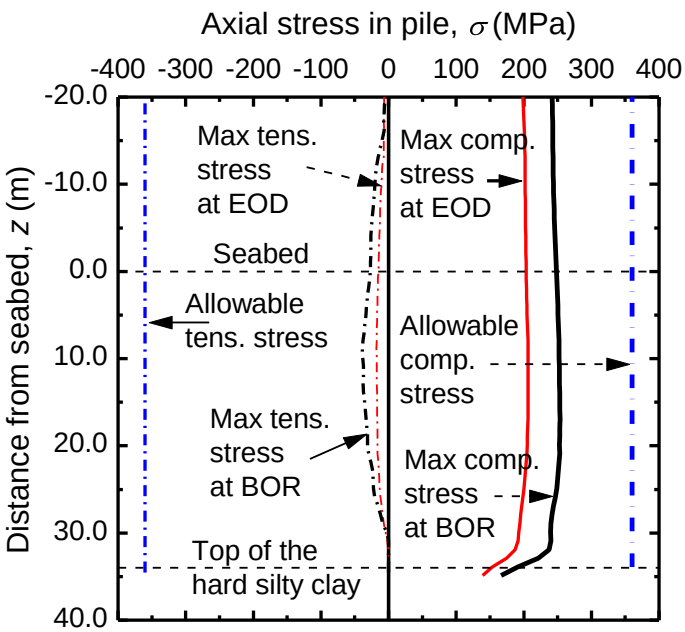

Figure 5.29. Distributions with depth of the maximum tensile and compressive stresses in the pile during driving of the TSP1.

Figure 5.30 shows the static load-displacement curve derived from the soil properties identified in the final WMA, compared with the static load test result in two cycles of loading process. The stiffness of the static response derived from the final WMA of the BOR test was a little bit higher than that of the static response in the EOD test. Although the rest period between the EOD and the BOR in this test (34 days) was longer than that in the TSC1 (14 days), the difference of the derived static responses between the EOD and the BOR is not remarkable compared to the case of TSC1. Similar to the case of the TSC1, the static response derived from the final WMA of the BOR test was comparable with the SLT result, indicating that the identified soil parameters were reasonable. It is noted that the derived static curve underestimated the measured curve because the “set-up” phenomenon continues occurring for further rest period, 14 days from the BOR test.

The different degrees of the "set-up" between the TSC1 and the TSP1 might be explained by different configurations of the test piles. The TSC1 had an outer diameter of 700 mm and a wall thickness of 100 mm, while the TSP1 had an outer diameter of 1000 mm and a wall thickness of 12 mm (see Table 3). It is reasonable to think that the TSC1 pushed away the surrounding ground outward during driving much more, compared to the case of the TSP1. Hence, greater excess pore-water pressures might have been generated in the ground during driving of the TSC1. If these suppositions are adequate, it is reasonable to state that the TSC1 had a higher degree of the "set-up" phenomenon.

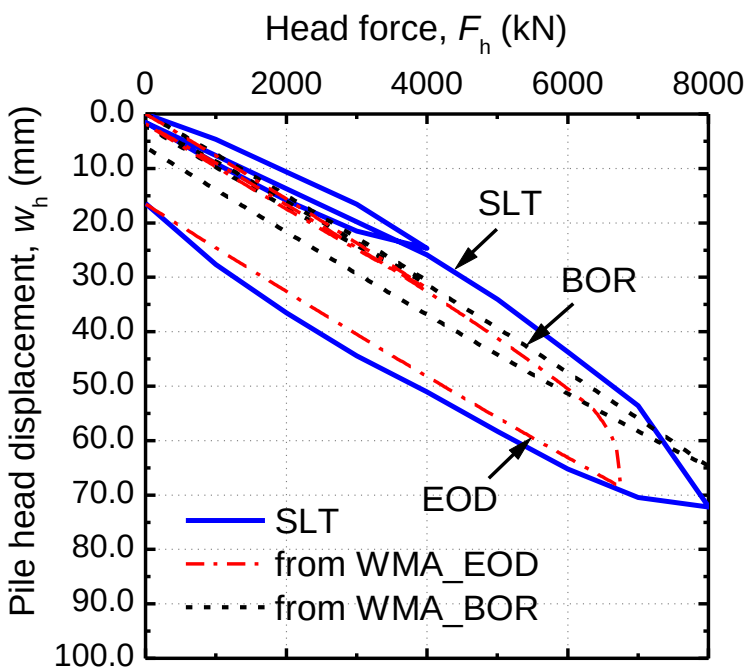

Figure 5.30. Comparison of static load displacement curves of the TSP1.

From the results of the SLT, the measured settlement S = 25.0 mm at the working load of 4002 kN was sufficiently smaller than the allowable value S_a = 38.6 mm. The measured settlement S = 72.0 mm at the maximum test load of 8004 kN was also smaller than 100 mm that is 10% of the pile diameter. And the residual settlement S = 1.5 mm after the full unloading process from the working load was also below the limit value S_{ar} = 10.0 mm. All of these values indicated that the pile did not reach the ultimate bearing state. Hence, the TSP1 has a factor of safety greater than 2 against the working load of 4002 kN.

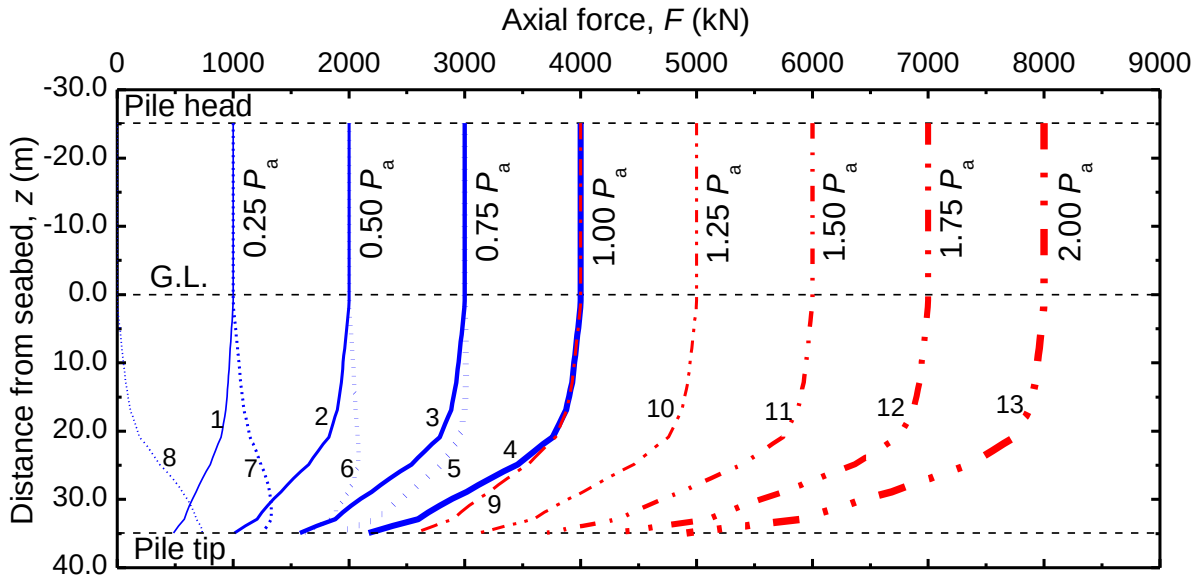

Figure 5.31. Distribution with depth of pile axial forces at different applied load of the TSP1.

Similar to the case of the TSC1, the calculated distributions of the pile axial forces at different pile head forces ranging from 0.25 to 2.00 times of the working load P_a within 13 steps of the loading and unloading processes for the BOR test are shown in Fig. 5.31. As seen from the figure, the mobilised shaft resistance and tip resistance increase with increase in the applied head force in the first loading process from steps 1 to 4. At the working load, P_a = 4002 kN, the mobilised tip resistance, Q_b, and the total mobilised shaft resistance, Q_s, were 2174 kN and 1928 kN, respectively, corresponding to about 55 % and 45 % of the applied force. When unloading to zero at step 8, axial forces remain along the embedment pile length. These residual forces increase with depth and reach a maximum value of about 735 kN at the pile tip. When reloading to the working load at step 9, the axial forces along the pile deeper than 20 m are greater than those in step 4 because of the residual forces in the pile generated in the previous unloading steps. At this applied force, the mobilised tip and shaft resistances were 2565 kN and 1437 kN, respectively, corresponding to 65 % and 35 % of the applied force. When further loads are applied on the pile head in the second loading process from

steps 10 to 13, the mobilised shaft resistance and tip resistance continue to increase, indicating that the pile does not reach the ultimate bearing state at the maximum applied force of 8004 kN.

As previously mentioned, the TSP1 was actually used as a working pile after the SLT. Hence, in the analysis, the TSP1 was reloaded to the working load after completion of the SLT to predict the pile response when it is used as the working pile. The pile response at the end of the third loading process is indicated by the dot line in Fig. 5.32. At the working load of the third loading process, P_a = 4002 kN, the pile axial force reaches a maximum value of 4552 kN at a depth z = 30.8 m (neutral plane) and the mobilised tip and shaft resistance are 3837 kN and 165 kN, respectively. At this applied force, the mobilised tip resistance reaches about 96 % of the applied load, which is greater than that in the first loading process at step 4 (55 % of P_a) and the second loading process at step 9 (65 % of P_a). Because of the higher mobilised tip resistance during multiple loading process, the TSP1 will have smaller safety factor at the pile tip compared to that of the non-tested working piles with the same pile configuration, the same soil and driving conditions.

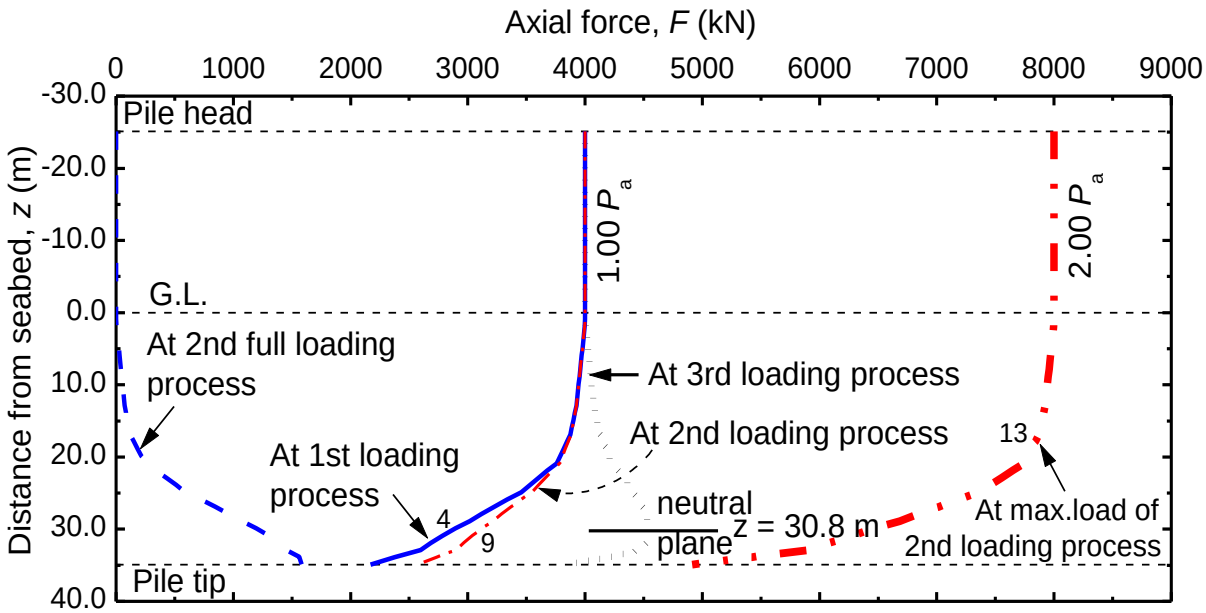

Figure 5.32. Calculated distributions with depth of the pile axial forces of the TSC1 at BOR test at the working load for three loading processes.

In order to estimate the load-displacement behaviour of the TSP1 when it is reused as a working pile after the two loading processes of the SLT, the TSP1 was further loaded in the analysis from the working load in the third loading process until the pile reaches the ultimate

bearing capacity. The calculated curve is shown in Fig. 5.33, together with the SLT result. For a comparison purpose, the calculated load-displacement curve of the TSP for a monotonic loading is also shown in the figure.

It can be seen from the figure that the yield load and the ultimate bearing capacity of the TSP1 after the two cycle of loading process are similar to those of the TSP1 subjected to only monotonic loading. This means that cyclic loading has little influence on the load-displacement curve at the pile head, if reduction of the shaft resistance due to cyclic loading does not occur.

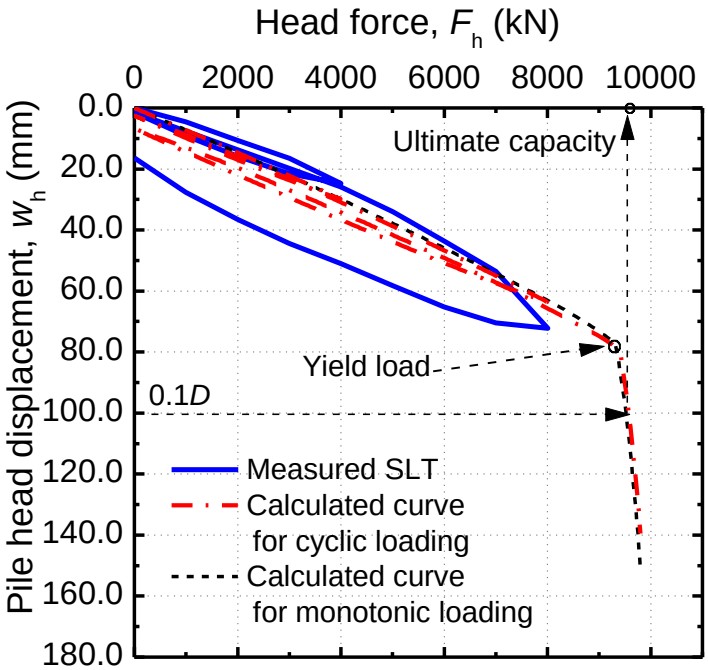

Figure 5.33. Calculated load-displacement curves with and without cyclic loading, together with the result of SLT of the TSP1.

5.3.3 Prediction of static load-displacement curves for other test piles

In this part, the static responses of the other two test piles, the TSC2 and TSP2, are predicted using the soil parameters identified from the final WMA analyses of the TSC1 and TSP1, respectively. The predicted curves are then compared with the load-displacement relations obtained from the static load tests. The specifications of the TSC2 and TSP2 have been indicated in Table 5.2 and the soil profiles have been shown in Fig. 5.9. The loading and unloading processes were similar to that of the static load test described previously in Fig. 5.13, with the maximum test loads, P_{max}, of 5170 kN for the TSC2 and 7716 kN for the TSP2, which are two times of the design working load for each pile (see Table 5.8).

Although the ground at each location of the test piles consisted of three soil layers of the soft clay, clayey sand and hard silt clay, thicknesses of the soil layers vary location to location as shown in Fig. 5.9. Hence, for the analyses of the TSC2 and the TSP2, the soil parameters were estimated as follows. In each layer, the average values of the identified soil parameters surrounding the TSC1 and the TSP1 were used for the soil parameters of the TSC2 and the TSP2, respectively, while the identified soil parameters at the pile tip and the soil plug base of the TSC1 and the TSP1 were used for the TSC2 and the TSP2, respectively.

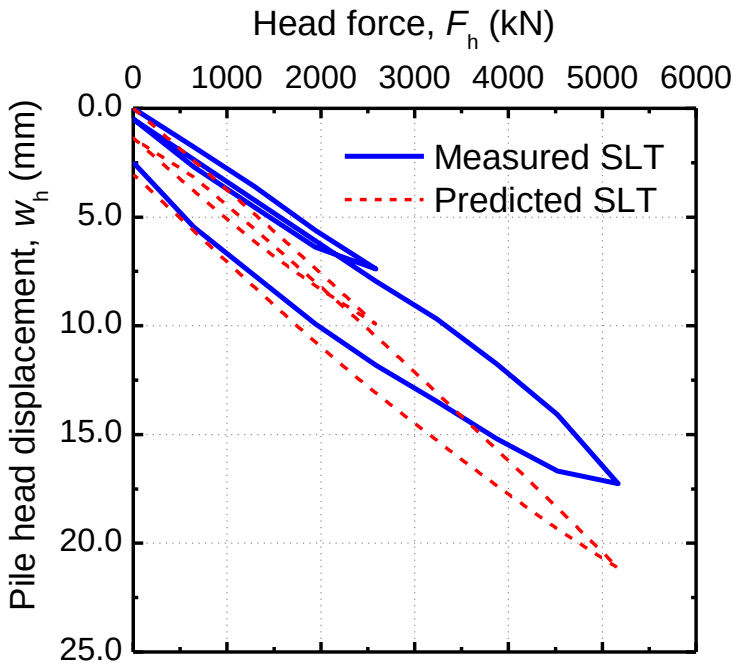

Figure 5.34. Comparison of the static load displacement curves of the TSC2.

The predicted and measured curves are shown in Fig. 5.34 for the TSC2 and in Fig. 5.35 for the TSP2. Similar to the TSC1 and TSP1, the ultimate states of these two test piles are not reached at the applied load of $2\times P_a$ in both the measurements and the calculations. Hence, it can be judged that the TSC2 and TSP2 have a factor of safety greater than 2 against the working loads of 2585 kN and 3858 kN, respectively.

As seen from these two figures, the predicted curves are comparable with the measured ones, indicating that the identified soil parameters of the two tested piles, the TSC1 and TSP1, are reasonable. The soil parameters identified from the WMA could be used to adequately estimate the static responses of the other non-tested working piles in this construction site. This means that the WMA of DLTs using the proposed approach can be a practical alternative to the conventional static load test.

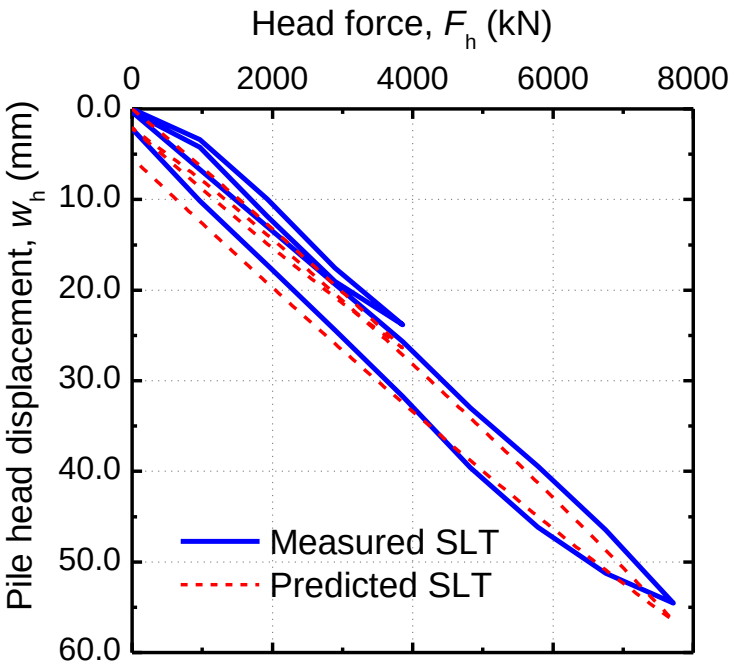

Figure 5.35. Comparison of the static load displacement curves of the TSP2.

5.4 Conclusions

Dynamic and static load tests were conducted on the four test piles with different specifications at the construction site of Thi Vai International Port in Vung Tau province, Viet Nam with the purposes of obtaining the design parameters, selecting the appropriate driving hammer and seeking for quality assessment methods for the constructed piles.

This chapter first described the test piling in detail including objectives, site conditions, preliminary pile design and results of the SLTs. Then, wave matching analyses (WMAs) of the DLTs of the two test piles, the TSC1 and TSP1, at initial driving and re-striking were conducted using the numerical approach developed by the authors, to identify the soil resistance distributions and to derive the corresponding static load-displacement relations using the soil parameters identified in the final WMA. Furthermore, the influence of cyclic loading process on the pile response was analytically examined.

The soil parameters identified from the WMAs of the BOR tests were also used to predict the load-displacement relations of the other test piles, the TSC2 and TSP2, having different pile configurations and soil profiles from those of the TSC1 and TSP1.

The major results of the SLTs and the driving work of the TSC1 and TSP1 are as follows:

(1) The bearing capacities of the two test piles exceed two times the design working loads.

(2) Termination criteria based on the maximum value of settlement per blow estimated from the Hiley type formula with an ultimate bearing capacity estimated from an empirical equation based on SPT *N*-values can be adequately used for controlling the driving work.

From the WMAs of the TSC1 and TSP1, the following findings and implications were drawn:

(3) The static load-displacement curves derived from the final WMAs of DLTs were comparable with the results obtained from the SLTs.

(4) The piles which have been subjected to cyclic loading have similar yield and ultimate capacities to those of the piles subjected to monotonic loading.

(5) WMA using the proposed numerical approach can be used to predict the static load-displacement curves of the non-tested working piles based on the identified soil parameters of the tested piles.

(6) The "set-up" phenomenon was clearly found from the EOD test, through the BOR test, to the SLT. The thickness of the pile wall might have a great influence on the degree of "set-up" phenomenon.

(7) Shear moduli of soils to be used in WMA of piles at this particular site can be estimated from shear moduli at small strain level with reduction factors, about 0.1 for soft soils, 0.15 to 0.20 for medium soils and 0.25 to 0.40 for hard soils.

(8) Selection of the pile driving hammer based on the empirical equation in this study is reasonable, because the maximum compressive and tensile stresses along the pile calculated in the WMAs do not exceed the allowable values.

From the SLT results, the TSC2 and TSP2 also had the bearing capacities more than two times the design working loads. Load-displacement curves of the TSC2 and TSP2 predicted using the soil parameters identified from the WMAs of the TSC1 and TSP1 were comparable with the measured ones. This encourages the use of the WMA procedure proposed by the authors as a practical alternative to the conventional static load test.

Although the applicability of the WMA to quality assessment of constructed piles was demonstrated in this study, it is desired to collect more case histories in Viet Nam for improving the current pile design and pile driving control methods.

References

Imai T. (1977). P- and S-wave velocities of the ground in Japan. Proc. 9th ICSMFE, Tokyo; 2: 257-260.

Newmark N.M. (1959). A method of computation for structural dynamics. Journal of Engineering Mechanics, ASCE; 85(EM3): 67-94.

Paikowsky S.G., Whitman R.V. and Baligh, M.M. (1989). A new look at the phenomenon of offshore pile plugging. Marine Geo-resources Geotech.; 8: 213-230.

Paik K., Salgado R., Lee J. and Kim B. (2003). Behaviour of open- and closed-ended piles driven into sand. Journal of Geotechnical and Geo-environmental Engineering, ASCE; 129(4): 296-306.

Phan T.L., Matsumoto T. and Kobayashi S. (2012). A matrix method of wave propagation analysis in an open-ended pipe pile based on equation of motion. Proc. 9th Int. Conf. on Testing and Design Methods for Deep Foundations, Kanazawa, Japan; 105-112.

Randolph M.F. and Deeks A.J. (1992). Dynamic and static soil models for axial response. Proc. 4th Int. Conf. Application of Stress Wave Theory to Piles, The Hague; 3-14.

ASTM D1143-81. Standard test method for piles under axial compressive load.

ASTM D4945-00. Standard test method for high-strain dynamic testing of piles.

TCXDVN 205-1998. Pile foundation- Specifications for design.

TCXDVN 286-2003. Pile driving and static jacking works - Standard for construction, check and acceptance.

TCXDVN 269-2002. Piles- Standard test method for piles under axial compressive load.

Chapter 6

Application of the proposed wave matching procedure to penetration tests with dynamic measurements

In this chapter, measurement of driving energy of 13 penetration tests in Shiga prefecture in Japan is summarised. Application of the proposed wave matching analysis to dynamic cone penetration test (DCPT) and standard penetration test (SPT) are presented. The proposed method is used to analyse dynamic signals obtained from two blows of one dynamic cone penetration test with dynamic measurement to obtain the soil resistance acting on the cone and driving rod, and then compare with the cone resistance obtained from cone penetration test. Additionally, a simple method based on the conservative energy concept was used to estimate the total dynamic soil resistance.

6.1 Introduction

In site investigation, standard penetration test (SPT) and cone penetration test (CPT) are the two most common in-situ tests. SPT results are usually expressed in terms of number of blow per 30 cm, N_{30}, used for estimating the soil strength index. It has another advantage with the collection of disturbed soil samples used for determine other soil properties such as soil density, soil fabric. SPT is useful to soil types with fine-grained sands or soil types with coarser sands and silt sands, but very poor to clays and gravelly soils. In addition, SPT results do not provide continuous data due to large sampling interval, typically about 1.5 m, resulting in a low reliability of the soil profile with depth, e.g., important data such as weak seams may

be missed. Such situation can be overcome by using CPT to obtain the cone resistance, q_c, with sampling interval reduced up to 2 cm, resulting in the high reliability of soil properties with depth. However, CPT is unable to penetrate through gravels and cobbles, and difficult penetrate through hard clays or very dense sandy soils, resulting a limited investigated depth. CPT also requires reaction force during carrying the test.

In terms of mobility, low cost and quickness in operation, dynamic cone penetration test (DCPT) seem to be a promising method for determining soil strength index compared to SPT and CPT. It is common practice that DCPT results at certain depths are expressed in terms of blow count, N_d, for a given penetration length or set per blow, S, at depth interval of about 20 cm. These values are then converted into SPT N-value using empirical relation (SPT, ASTM D1586-64) in order to estimate various soil parameters like SPT method. In DCPT, in addition to the cone resistance, skin friction of the rod is also estimated with additional measurement of the rotational torque of the rod. Although distribution with depth of the soil strength is estimated using the value of N_d, improvement of the estimation accuracy is also useful in practice. Because penetration mechanism of DCPT is quite similar to driving a pile except for tip shapes, if dynamic measurements are associated with DCPT, we have possibility of estimating the dynamic soil resistances acting on the cone and the driving rod by conducting the wave matching analysis. Besides that, we also estimate the total dynamic resistance using the simple conservative energy concept.

In this study, dynamic cone penetration test and standard penetration test with dynamic measurements carried out in Moriyama city, Shiga prefecture, Japan in 2012 were used to demonstrate the advantages of the penetration test with dynamic measurements and also to further validate the proposed numerical program.

6.2 Test description

A total of 13 penetration tests (12 DCPTs and 1 SPT) with dynamic measurements were conducted for measuring impact energy in Shiga prefecture in 2012 as shown in Table 6.1. Driving rods including hollow and solid with different outer diameters varying from 16 to 32 mm and various cone diameters ranging from 25 to 51 mm were used. The wave speed in the driving rod are in range from 4900 to 5200 m/s. Specification of each test device including dimension of hammer, anvil, driving rod, cone and potential impact energy are summarised in Table 6.2. Rubber cushion could be used at the top of driving rod to investigate its influence on the energy efficiency.

Table 6.1. Specifications of driving rods of various DCPTs and SPT.

Test No.	Device name	O.D. (mm)	I.D. (mm)	Area (mm^2)	Length (m)	Mass (kg)	Density (ton/m^3)	Young's mod. E (kPa)	Wave velo. c (m/s)	Cone diameter (mm)
1	Lamda	32.0		804.2	1.0	6.150	7.647	2.06E+08	5190.3	45.0
2	MRS	28.0		615.8	1.0	4.720	7.665	2.06E+08	5184.0	36.6
3	SRS	32.0		804.2	1.0	6.374	7.925	1.93E+08	4934.8	45.0
4	Penny	20.0		314.2	1.0	2.410	7.671	2.00E+08	5106.0	35.7
5	PDC (MiniRam)	19.0	7.0	245.0	1.0	1.860	7.590	2.06E+08	5209.5	25.0
6	SRS	32.0		804.2	1.0	6.150	7.647	2.06E+08	5190.3	45.0
7	PDC (MRS)	28.6	18.6	370.7	1.0	3.040	8.201	2.06E+08	5012.0	36.6
8	SRS (Hollow Rod)	32.0	16.0	603.2	1.0	4.783	7.930	1.93E+08	4933.5	45.0
9	MRS (DPM-HT)	28.0		615.8	1.0	4.68	7.600	2.06E+08	5206.1	36.6
10	DSPT	19.0		283.5	1.0	2.19	7.724	2.06E+08	5164.3	33.0
11	PDCPT	16.0		201.1	1.0	1.57	7.809	2.06E+08	5136.3	25.0
12	SH	16.0		201.1	1.0	1.58	7.858	1.93E+08	4955.8	25.0
13	SPT	40.5	31.0	533.5	1.0	4.55	8.529	2.00E+08	4842.5	51.0

Table 6.2. DCPT and SPT with various hammers, anvils, rods, cones and impact energies.

Test / Device	SRS	Lamda	MRS	DPM-HT	Penny	DSPT	PDCPT	SH	SPT	
Hammer guide rod diameter (mm)	101.6	40.5	20	40.5	30	19	16	16	40.5	
Hammer diameter D_h (mm)	246	180	160	180	178	95	60		180	
Anvil diameter D_a (mm)	175	97	90	75	51	50	50		71	
Hammer mass m (kg)	63.5		30		30	10	5	3, 5	63.5	
Falling height H (mm)	500		350		200	500	500		750	
Cone-tip angle (°)	90		90		60	S.P.	60		*1Open-tip	*2Close-tip
Cone mantle length (mm)	90		69		9	-	0		D_o = 51	D_o = 51
Cone diameter D_c (mm)	45		36.6		35.7	33	25		D_i = 35	D_i = 0
Cone cross-sectional area A_c ($\times 10^{-4}$ m^2)	15.9		10.5		10.0	8.6	4.9		10.8	20.4
Rod diameter D_r (mm)	32		28		20	19	16		40.5	
Diameter cone / rod diameter D_c/D_r	1.41		1.31		1.79	1.74	1.56		-	
Energy per unit area, $E_n = mgH/A$ (kJ/m^2)	195.8		97.9		58.8	57.3	50.0		432.6	229.0
Penetration interval for blow count measurement, L (m)	0.20		0.20		0.10	0.25	0.10		0.30	0.30

*1: soil can enter in the SPT sampler, *2: the tip of the SPT sampler is close

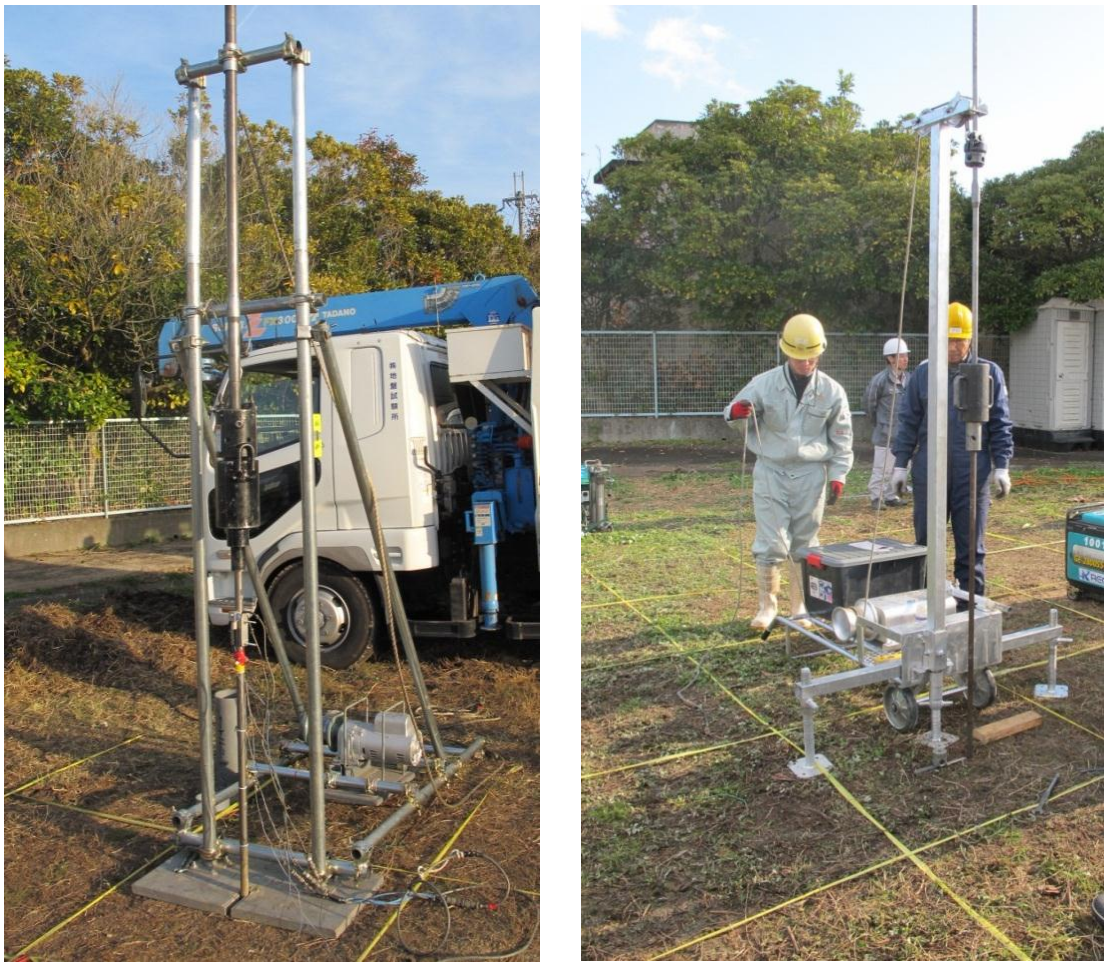

Figure 6.1.Various types of DCPT devices

For each penetration test with dynamic measurement, a corresponding driving rod was prepared and instrumented by accelerometers and strain gauges as shown in Fig. 6.2. At a location of 100 mm downward from the anvil, two accelerometers having a range of 5000 g and two vertical strain gauges were attached symmetrically to the driving rod in order to eliminate the effects of bending. The accelerations, α, and strains, ε, are the average value of these measurements. Sampling frequency is 1 MHz. By multiplying the cross-sectional area, A, the Young's modulus of the rod, E, and the measured strain, ε, the axial force, F, in the driving rod was determined. The velocity of driving rod was calculated as follows. From the start of impact to the rise time (at the time of maximum measured force), velocity was estimated from downward travelling force in Eq. (6.1) with assumption that upward travelling force has minor influence on the velocity. From the rise time to the end of impact, by integrating the acceleration with respect to time, velocity of the driving rod, v, was obtained.

$$v(t) = v_{\mathrm{d}}(t) = \frac{\sigma_{\mathrm{d}}(t)}{E} c = \frac{F(t)}{A \times E} c \tag{6.1}$$

In each test, the driving rod was first penetrated to the depth of about 5.5 to 6.0 m, and then connected with the instrumented rod and start to measure the dynamic signals. For the first several blows, dynamic signals and settlement were measured for each blow called "initial blow". After that, the driving rod was penetrated continuously by multiple blows (called "successive blow") with penetration depth of about 100 to 250 mm. The settlement per blow in this case was the average value of the penetration length.

The driving energy transferred to the driving rod, E_{drv}, can be estimated by the following equation (Matsumoto et al. 1992):

$$E_{\mathrm{drv}}(t) = \int_0^t F(t) \cdot v(t) \cdot \mathrm{d}t \tag{6.2}$$

where $F(t)$ and $v(t)$ are the force and velocity at location of strain gauge, respectively.

Figure 6.2.Various types of driving rods of DCPTs and SPT instrumented with strain gauges

The driving efficiency, e_{f}, is defined as a ratio of the transferred energy to the potential energy, $E_{\mathrm{po}} = mgH$:

$$e_{\mathrm{f}}(\%) = \frac{E_{\mathrm{drv}}}{E_{\mathrm{po}}} \tag{6.3}$$

From the energy conservation law, the total dynamic cone resistance, R_{dyn}, under a set per blow, S, can be estimated using a simple equation as below:

$$R_{dyn} = \frac{E_{drv}}{S} \tag{6.4}$$

The total dynamic cone resistance, R_{dyn}, is the sum of the frictional force acting on the driving rod and resistance acting at the cone tip. With assumption of no friction acting on the rod, the dynamic cone resistance, q_{dyn}, can be determined by the following equation.

$$q_{dyn} = \frac{R_{dyn}}{A_c} \tag{6.5}$$

where A_c is the cross-sectional area of the cone tip.

6.3 Results of measured driving energy for various types of DCPTs & SPT

Figure 6.3 and 6.4 show results of calculation of measured driving energy for a blow of Test No.12 (DCPT) and a blow of test No. 13 (SPT), respectively.

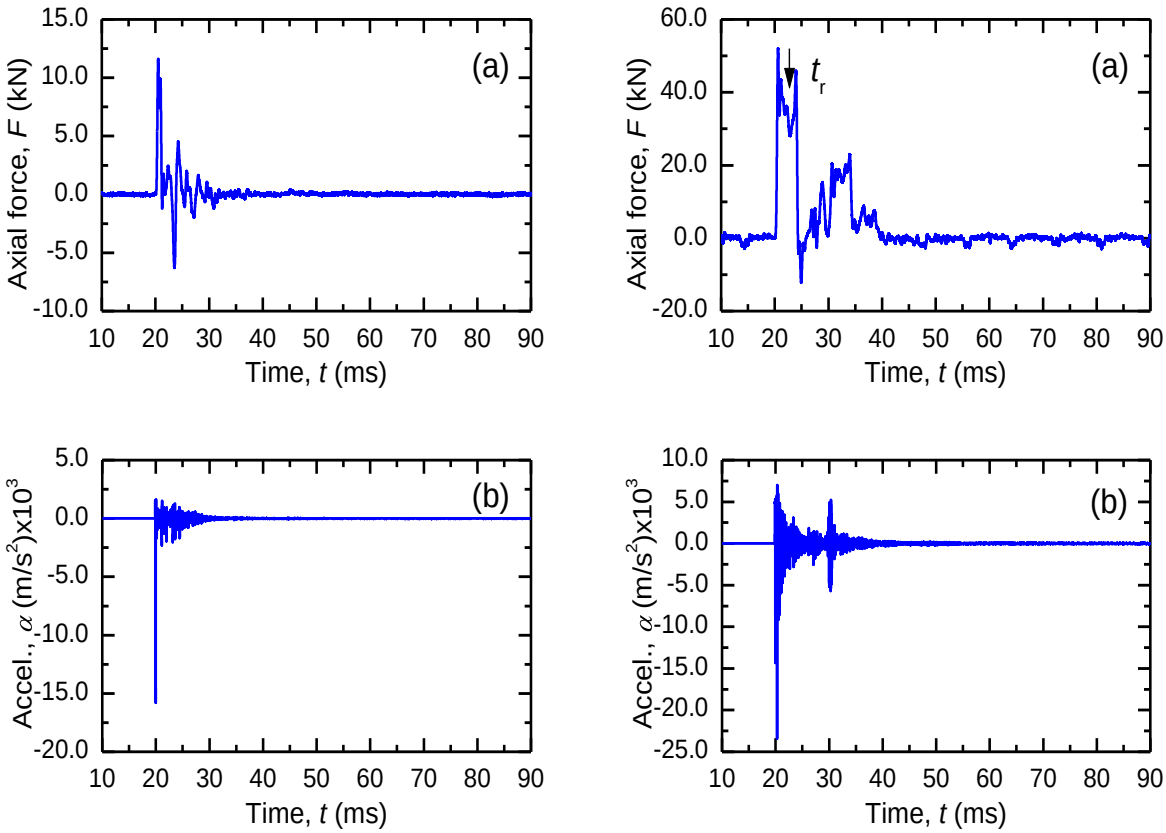

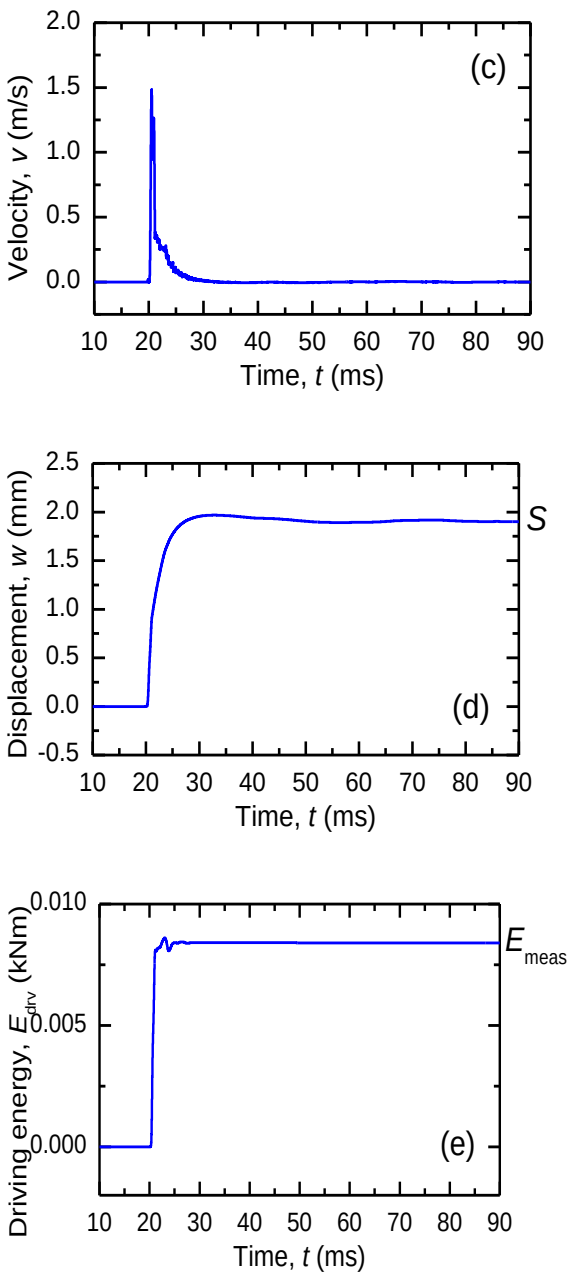

Fig. 6.3. Results of measured driving energy of a blow in a DCPT with dynamic meaurement

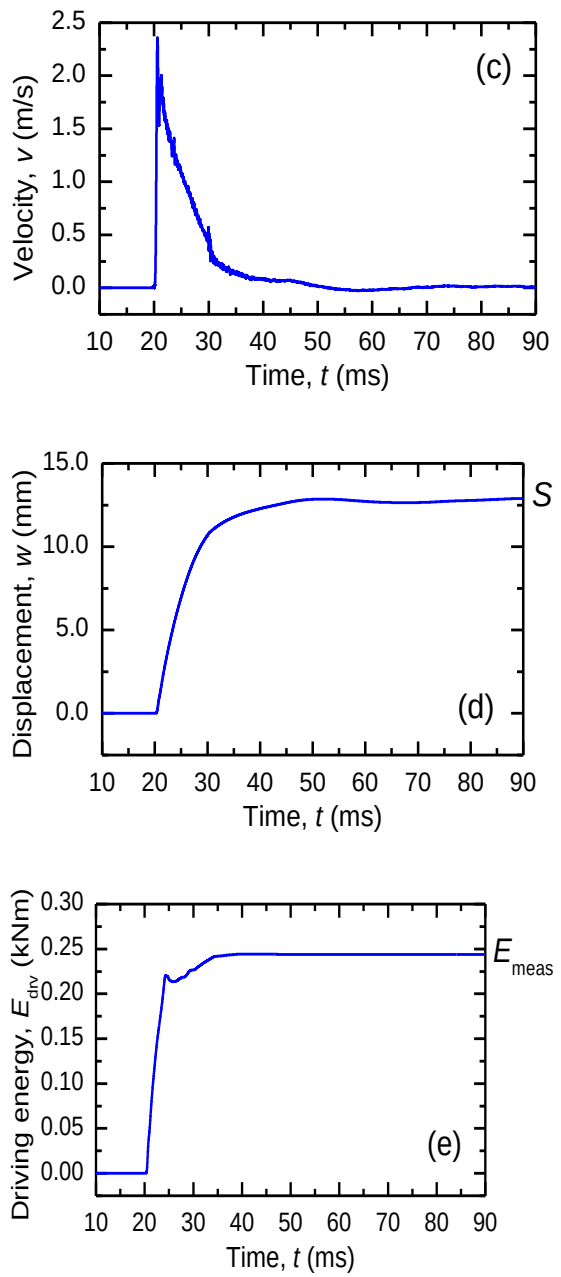

Fig. 6.4. Results of measured driving energy of a blow in SPT with dynamic meaurement

Similar calculation was conducted for several blows of various DCPTs and SPT. Except for the Test No.6 (a, b and c), 5 blows of each test was used to calculate the driving energy. Note that cushion was put on the top of the driving rod in Test No.1, No. 4 and No. 6 to investigate its influence on the driving efficiency. The minimum, the average and the maximum values of the driving efficiency transferred to the driving rod for various DCPTs and SPT are indicated in Table 6.3. The table indicates that the energy efficiencies vary from 56 to 93 % in case of no cushion, and reduce 20 % in case of using 2 cushions of rubber, 1mm thickness for each.

Reduction of the driving efficiency due to the existing of the cushion can be clearly seen in the Test No. 6 (a, b and c) which 3 blows for each test were analysed. The test results indicated that increase in numbers of cushion resulted in the reduction of driving efficiency.

Table 6.3. Summary of driving efficiency of various types of DCPTs and SPT.

Test No.	Device Name	Number of tests analysed	Driving energy efficiency, e_f (%)			Comment
			Min	Ave.	Max	
1	LAMDA	5	40.21	57.95	77.89	2 cushions
2	MRS	5	73.48	77.11	84.20	
3	SRS	5	65.61	71.00	80.93	
4	PENNY	5	30.99	44.30	67.49	2 cushions
5	PDC (μRS)	5	59.20	70.39	86.15	
6a	SRS (OYO)	3	48.35	55.34	60.66	2 cushions
6b		3	65.94	73.83	77.87	1 cushions
6c		3	74.73	79.09	86.26	No cushions
7	PDC (MRS)	5	59.99	73.42	93.10	
8	SRS	5	60.43	68.08	76.47	
9	DPM-HT	5	56.31	62.00	68.31	
10	DSPT	5	62.17	67.30	71.55	
11	PDCPT	5	73.34	74.46	76.14	
12	SH	5	57.12	63.55	66.63	
13	SPT	5	49.83	58.84	69.06	

Distribution with depth of the analysed results in Table 1 is shown in Figure 6.5a. Except for the Test No. 1 and Test No. 4, the energy efficiency for each blow is mostly in range of 60 to 80 %.

Figure 6.5b indicates the distribution with depth of dynamic cone resistance, q_{dyn}, together with static cone resistance, q_t, obtained from CPT which was carried out in the same test site. It can be clearly seen from the figure, although the dynamic cone resistance had higher values than the static ones, the trend was comparable between them. The higher value of the dynamic cone resistance is reasonable because it includes the dynamic component. Most of results as shown here were calculated from the dynamic signals of the "successive blows". Test No. 5 (Blows 5.1, 5.4 and 5.5) and Test No. 9 (Blow 9.1) have the large values compared to other blows as well as the static ones because they are the "initial blows" which were greatly influenced by the "set-up" phenomenon after the rest period of the preparation works for connecting the instrumented rod or after the rest period between different series of successive blows.

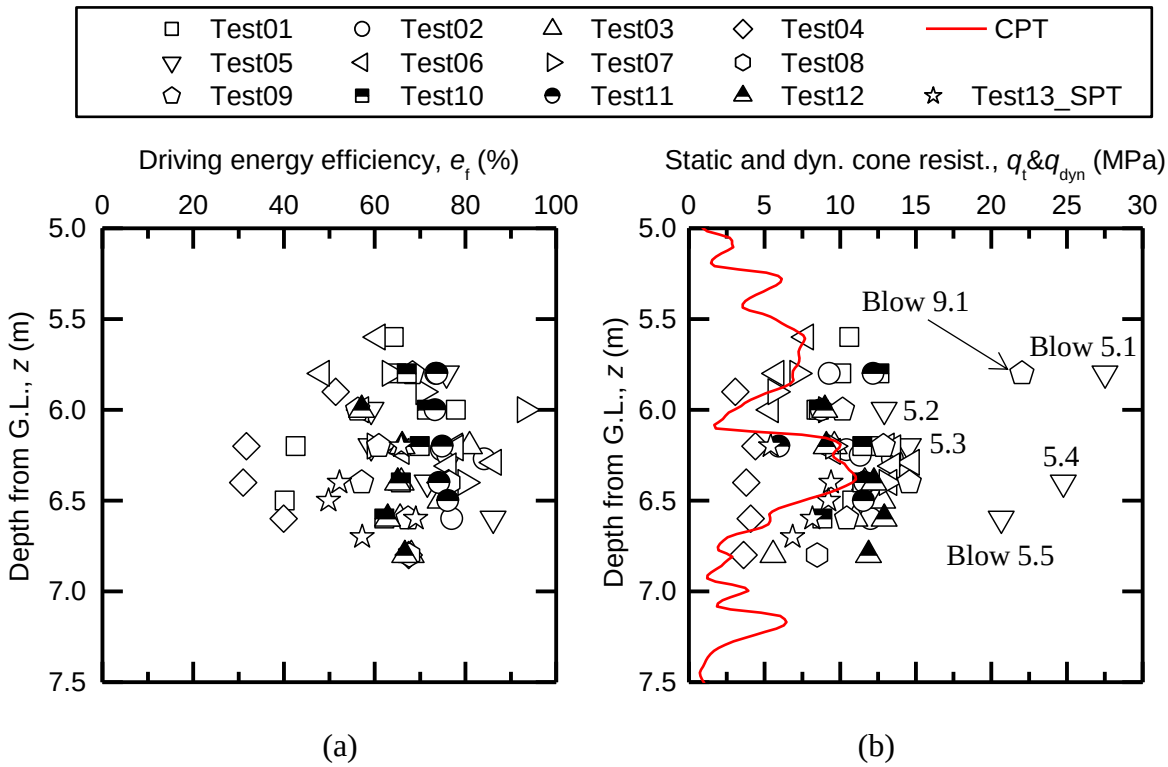

Figure 6.5. Results of DCPTs and SPT with dynamic measurement.

(a) Driving efficiency. (b) Comparison of static cone resistance, q_t, obtained from CPT with dynamic cone resistance calculated from energy conservation law.

The test results as shown in these figures were obtained from limited blows, about 5 blows for each test. Therefore, increase in the numbers of test analyses would be useful for further discussion.

6.4 Wave matching analysis and test results

In this part, proposed WMA was conducted to identify the static resistances acting on the driving rod and that at the cone tip of one example of the DCPT, and then compare with the static cone resistance obtained from CPT as presented previously. In this analyses, WMA of two blows of Test No. 12 were conducted, Blow 12.1 with cone tip level at depth of 5.8 m and Blow 12.2 at depth of 6.0 m. Illustration of the DCPT No. 12 with dynamic measurement is shown in Fig. 6.6.

6.4.1 Numerical modelling

Driving rod of the DCPT No.12 is shown in Fig. 6.7. The driving rod has a total length, L, of 7 m and a diameter, D, of 16 mm. The pile is modelled from the strain gauge level to the pile tip and divided into 45 elements. The cone tip was modelled as a flat tip with the same cross-sectional area, A_c, and the same mass, m_c. The embedment length, L_{emb}, was 5.8 m for analysis

of Blow 12.1 and 6.0 m for Blow 12.2. The ground was divided into three layers. Linear soil response was used in WMA. That is, R_{fs}, R_{fb} and α were set to be zero in the analysis.

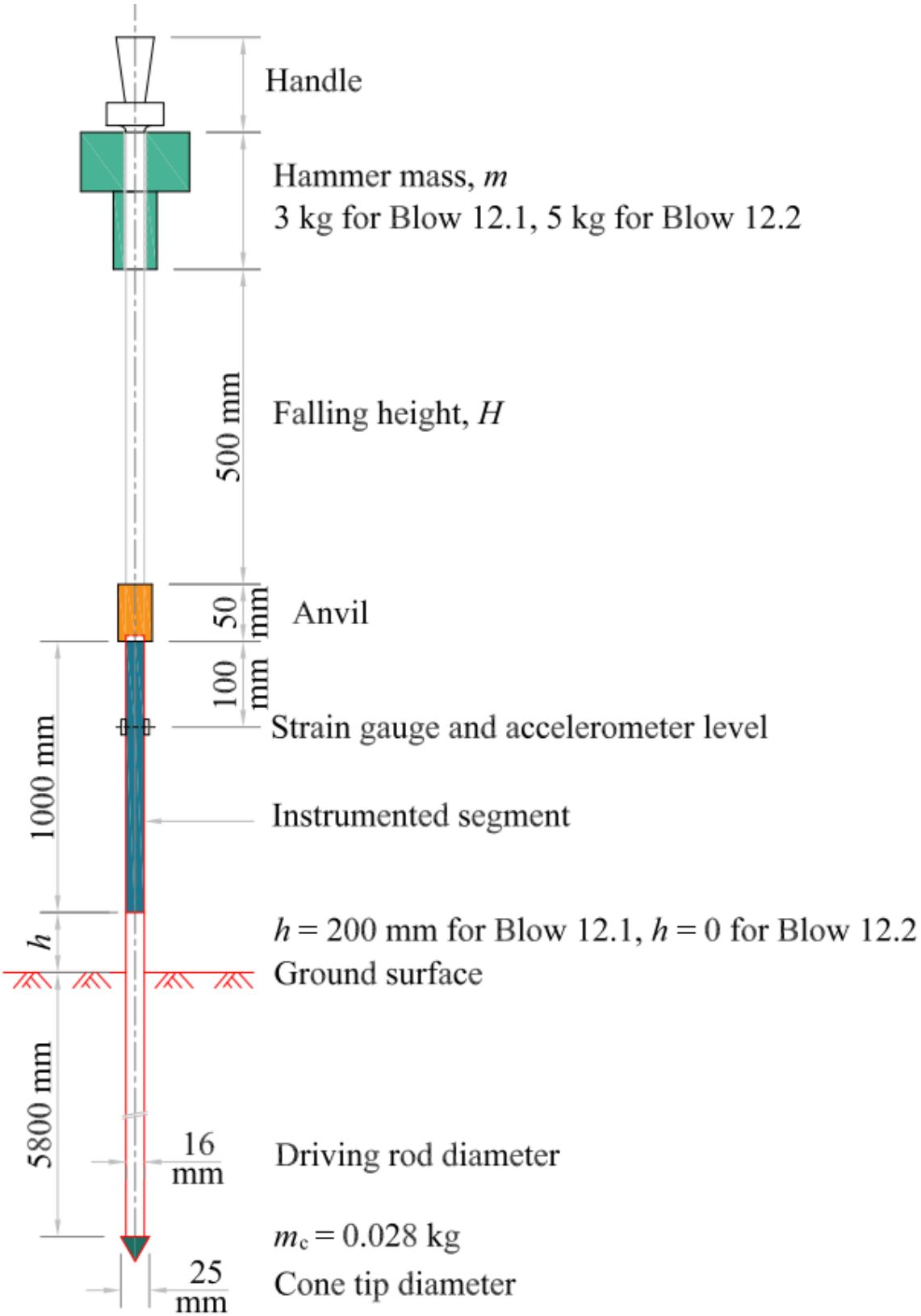

Figure 6.6. Illustration of a DCPT with dynamic measurement.

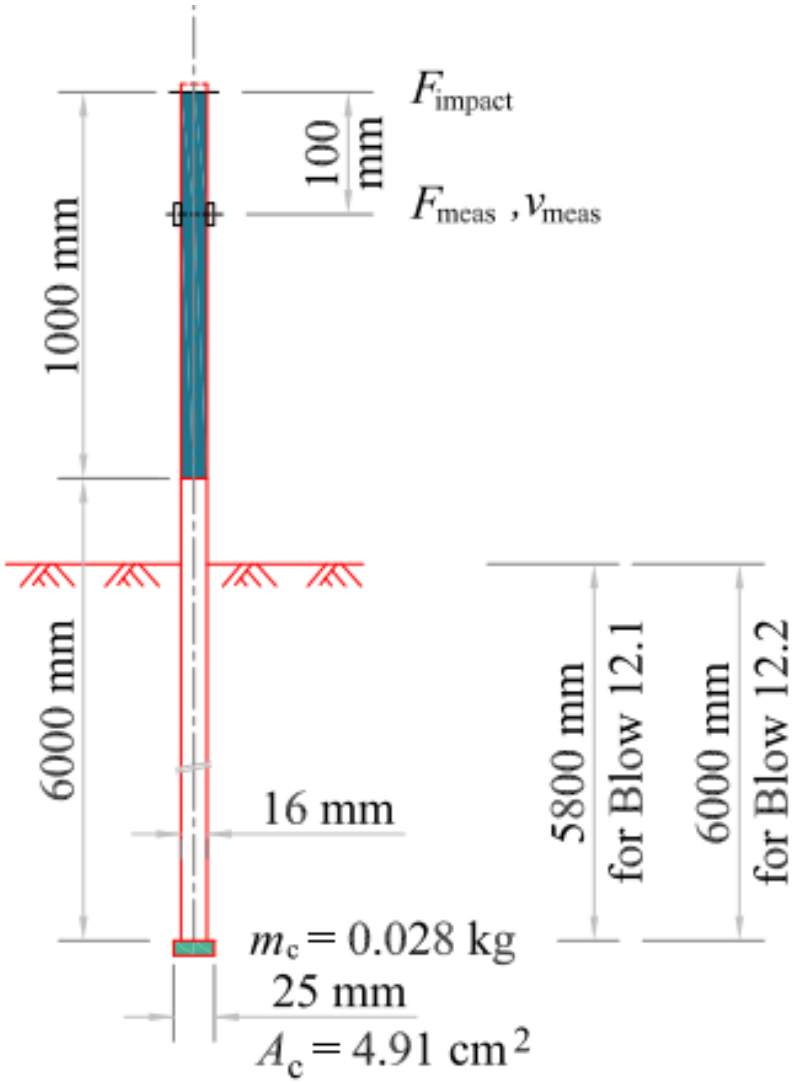

Figure 6.7. Modelling of the driving rod in WMA.

The first assumptions of soil parameters are as below:

1. The outer soil resistance, τ_{max}, was estimated based on the vertical effective stress.

$$\tau_{max} = \sigma_n' \times \tan\delta = K \times \sigma_v' \times \tan\delta = K \tan\delta \times (\gamma_{sat} - u) \times z \qquad (6.6)$$

where σ_n' is the normal effective stress acting around the pile shaft during installation, δ is the angle of friction between pile and soil and u is the excess pore-water pressure generated during driving. The normal effective stress maybe taken as some ratio K of the vertical effective stress, σ_v', resulting in the second form of the expression in Eq. (6.6). The appropriate value of K will depend on (a) the in-situ earth pressure coefficient, K_0, (b) the method of installation of the pile and (c) the initial density of the sand. $K \tan\delta = 0.3$ to 0.5 (Thongmunee et al., 2011) and $\sigma_v' = \gamma_{sat} - u =$

5 kN/m^3 could be used for initial assumption of the soil parameter in WMA of a DCPT in this site.

2. According to Randolph and Deeks (1992), the outer shear modulus, G, can be taken from 400 to 1000 times the outer shear resistance, τ_{max}; end-bearing resistance, q_{max}, can be estimated at 50 to 100 times τ_{max} and the shear modulus, G_b, are in range 5 to 10 times the end-bearing resistance, q_{max}.

Modelling of the driving rod and the ground surrounding the rod and at the tip for the Blows 12.1 and 12.2 of DCPT No.12 are shown in Fig. 6.8.

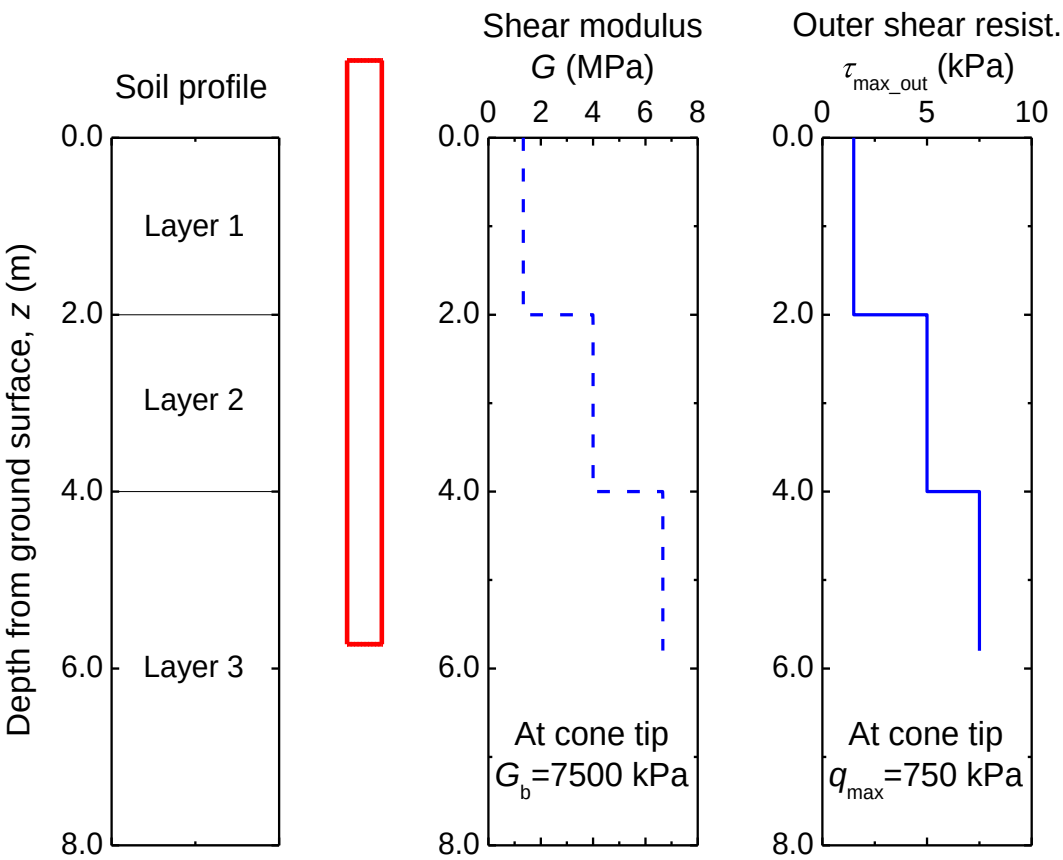

Figure 6.8. Modelling of the driving rod and soil.

The measured dynamic signals including axial forces and accelerations of the Blows 12.1 and Blow 12.2 are shown in the following figures.

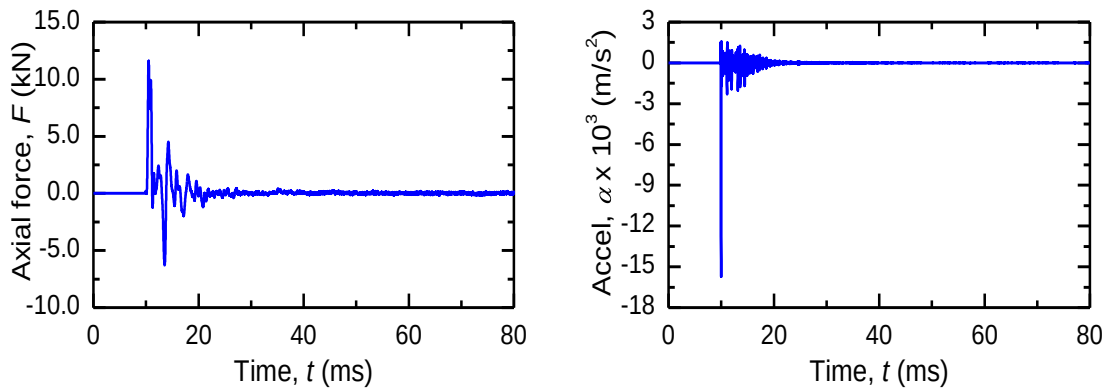

Figure 6.9. Measured dynamic signals of Blow 12.1 using hammer mass of 3 kg.

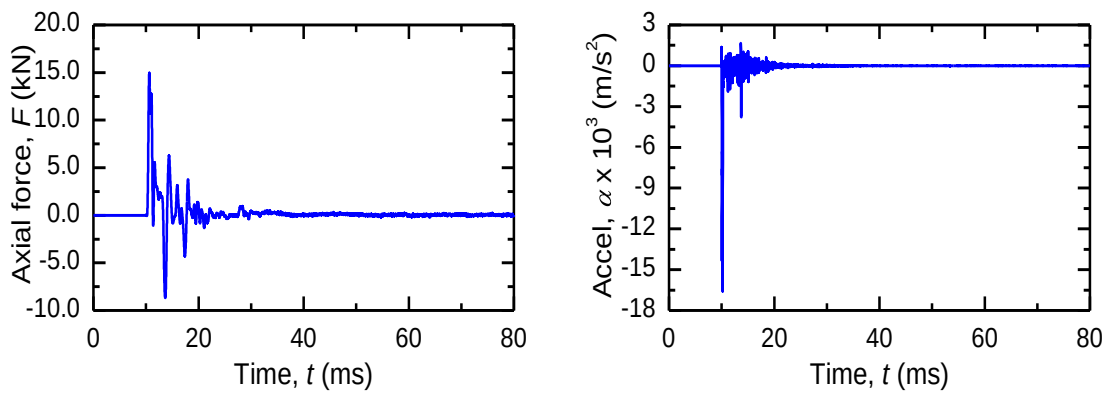

Figure 6.10. Measured dynamic signals of Blow 12.2 using hammer mass of 5 kg.

Measured force at the strain gauge level was used as the impact force, F_{impact}, acting on the top of the driving rod. The measured downward and up travelling force was calculated using Eq. (5.11) and (5.12), respectively.

Sets per blow were average values of penetration length on the number of the "successive blows", 1.9 mm for the Blow 12.1 and 3.7 mm for the Blow 12.2. Set per blow, together with downward travelling force at strain gauge level, were used as targets in wave matching analysis.

6.4.2 Results of WMA of the DCPT

In the first WMA with the first assumption of soil properties, a good matching was not obtained. The soil properties were then changed until a good matching between the calculated and the measured responses was obtained. Results of the final WMA at the strain gauge level are shown in Fig. 6.11 for the Blow 12.1 and in Fig 6.12 for the Blow 12.2.

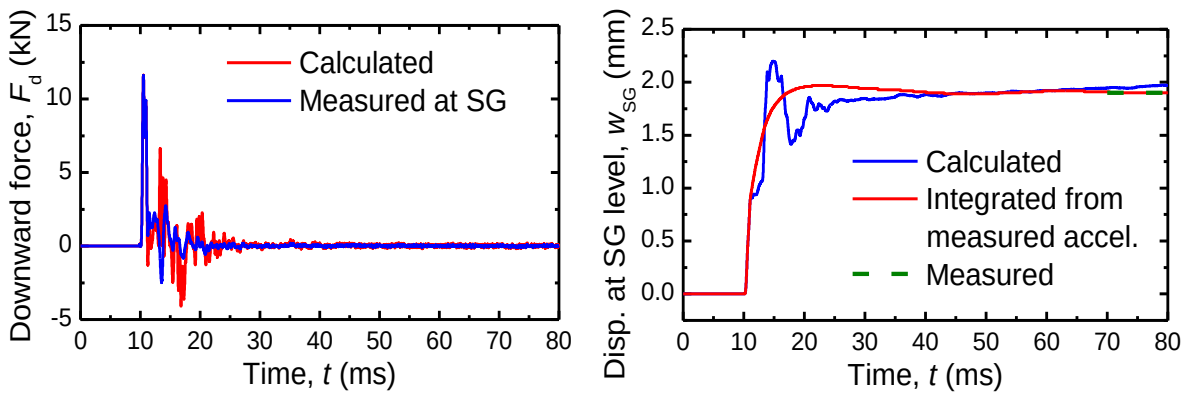

Figure 6.11. Results of the final WMA of Blow 12.1.
(a) Downward traveling force. (b) Displacement at SG level.

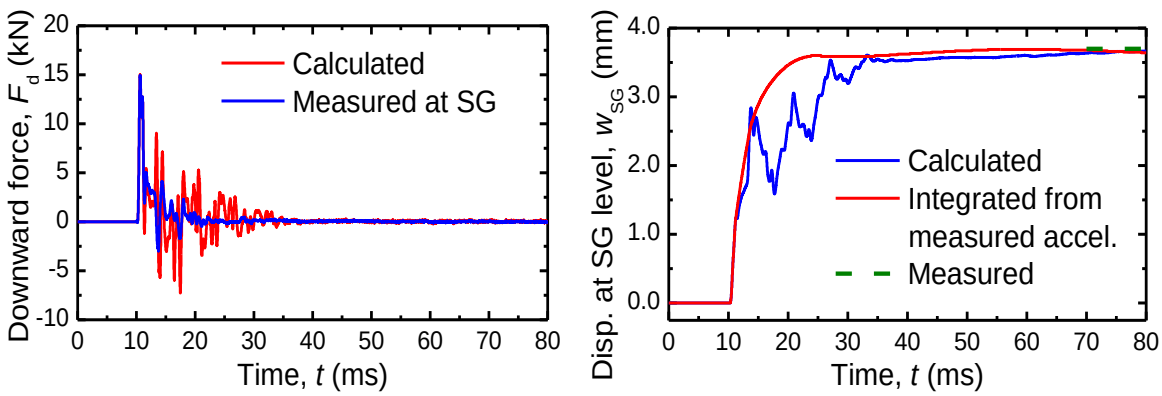

Figure 6.12. Results of the final WMA of Blow 12.2

(a) Downward traveling force. (b) Displacement at SG level.

Although oscillation was found in the calculated axial forces for both blows, the trend of calculated and measured axial forces were comparable. In addition, the displacement wave-form at the top of the driving rod are reasonable compared to that integrated from the measured acceleration, and the final calculated displacements were in good agreement with the measured values.

Soil identified from the final WMA for both blows are shown in Fig. 6.13. It can be clearly seen that, outer shear moduli and outer shear resistances obtained from WMA of the Blow 12.1 were greater than those of the Blows 12.2. This could be explained that the Blows 12.1 was treated as “initial blow” while the Blows 12.2 was a “successive blow”. Therefore, “set-up” phenomenon of the soil surrounding the rod before conducting the Blow 12.1 was higher than that of the Blow 12.2. However, the cone tip resistance of the Blow 12.2 was greater than that of the Blow 12.1. This means, soil at the depth of 6.0 m was harder than that at depth of 5.8 m.

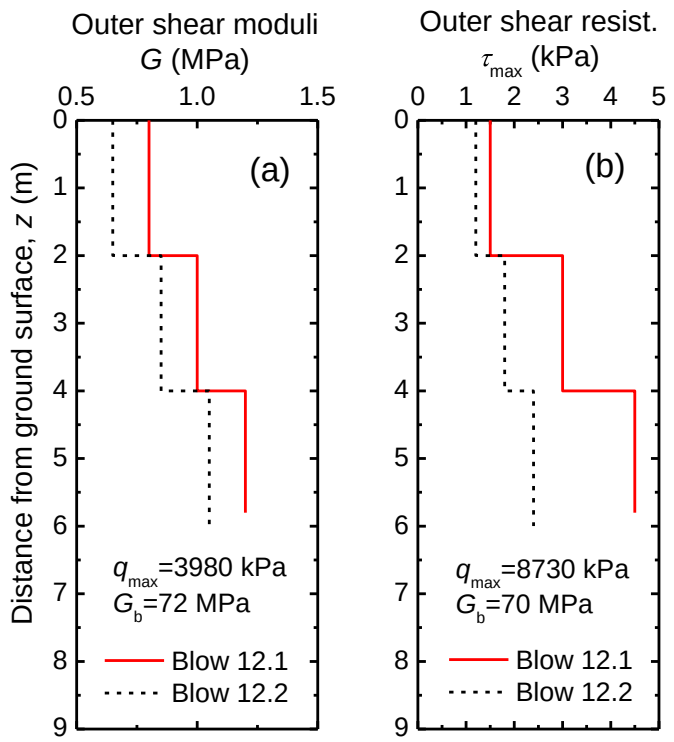

Figure 6.13. Results of the final WMA of Blow 12.2
(a) Outer shear moduli. (b) Outer shear resistances.

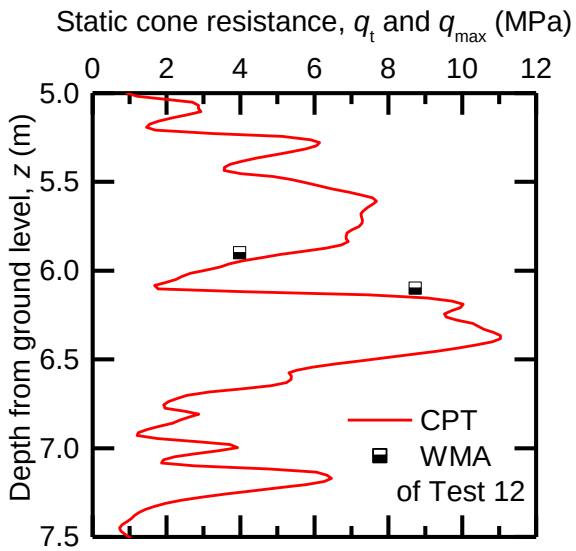

Figure 6.14. Comparison of static cone resistance from CPT and from WMA

The cone tip resistance identified from WMA of Blows 12.1 and 12.2 were then compared to the static cone tip resistance obtained from CPT in Fig. 6.14. The figure indicates that the values identified from the final WMA of DCPT were comparable with that obtained from CPT, indicating that the proposed WMA properly predicted the cone tip resistance of DCPT with dynamic measurement.

6.5 Conclusions

In this chapter, dynamic measurements of 12 DCPTs and 1 SPT carried out in Shiga prefecture were summarised. First, dynamic signals obtained from these test were used to estimate driving efficiency of each DCPT, and then to calculate the total dynamic cone resistance based on the conservation of energy. Finally, the proposed wave matching analysis was used to identify the static cone resistance.

The following conclusions and findings were drawn from the limited analyses as follows:

(1) Driving efficiency of DCPTs and SPT varies from 60 to 80 %.

(2) Dynamic cone resistance estimated from measured energy based on the law of energy conservation are comparable with static cone resistance.

(3) "Set-up" phenomenon can be seen clearly between "initial blows" and "successive blows" due to their different rest periods.

(4) Static cone resistance identified from the final WMA are reasonable with static cone resistance obtained from CPT.

Although advantages of the various DCPTs and SPT with dynamic measurements were demonstrated in this study, increase in the numbers of tests with various soil conditions would be useful for further study.

References

Matsumoto, T., Sekiguchi, H., Yoshida, H., Kita, K. (1992). Significance of two-point strain measurements in SPT, Soil and Foundations, JSSMFE, 32(2); 67-82.

Randolph M.F. and Deeks A.J. (1992). Dynamic and static soil models for axial response. Proc. 4th Int. Conf. Application of Stress Wave Theory to Piles, The Hague; 3-14.

Thongmunee S, Matsumoto T., Kobayashi S., Kitiyodom P. and Kurosawa K. (2011). Experimental and numerical studies on push-up load tests of sand plug in a steel pipe pile. Soil and Foundations; 51(5): 959-974.

Chapter 7

Summary

7.1 Introduction

In this thesis, a proposed numerical approach on dynamic load testing of open-ended pipe piles based on the one-dimensional stress-wave theory were developed with the principle objectives as follows:

1. Improve the limitations in the current pile dynamic analysis by proposing a numerical method using a matrix form to analyse the phenomenon of wave propagation in an open-ended pipe pile within a framework of one-dimensional stress-wave theory.
2. Reveal the reliability and higher accuracy of the proposed method compared to the conventional methods through verification work which starts from numerical analysis to analyses of small-scale model tests and full-scale tests.
3. Demonstrate the advantage of dynamic cone penetration tests (DCPTs) with dynamic measurements as well as use the proposed numerical method for identifying the soil resistance acting on the driving rod and cone tip of DCPTs.

7.2 Summary of each chapter

The contents of each chapter are summarised in the following.

In **Chapter 1**, the background and motivation of the research, the objectives and organisation of the research report were presented.

Chapter 2 first deals with related research works on dynamic pile analysis method. Then, the mechanism of soil resistance mobilised along pile shaft and base is briefly presented. After that reaction soil models for dynamic pile analysis are summarised. Finally,

information obtained from the related researches encourages the author developing a numerical method to analyse the one-dimensional stress-wave propagation in an open-ended pipe pile.

In **Chapter 3**, a numerical method using a matrix form with Newmark's b method was developed to analyse the phenomenon of wave propagation in an open-ended pipe pile within the framework of one-dimensional stress-wave theory. In this method, the rational soil resistance models suggested by Randolph and Deeks (1992) were implemented. Nonlinearity of soil stiffness and radiation damping are considered using the empirical relation proposed by Chow (1986). Maximum values of shaft soil resistances are distinguished when the pile move downward called maximum positive shear resistance, $\tau_{\max}^{\text{pos}}$, and when the pile moves upward (maximum negative shear resistance, $\tau_{\max}^{\text{neg}}$. A plastic slider in the rational soil model was replaced by a slider connected to an interface spring stiffness to calculate the soil response at the same time with the pile response. In this method, if damping matrix, mass matrix and viscous parameters of the rational soil model are set to be zero, the proposed approach can be applied to a fully static problem.

Based on the numerical analyses, the following findings are as follows:

(1) The results obtained from the proposed method are comparable with those obtained from the rigorous continuum method, the FLAC^{3D}.

(2) The proposed method has a fast computation time when compared to the rigorous method.

(3) The proposed method is precise when compared with the Smith method for a wide range of loading durations.

In addition, the sensitivity of the analysed results in pile driving due to variation of shear moduli and soil resistances are investigated. The analysed results showed that the shear modulus has a lower sensitivity to pile response compared to the soil resistance. It can be said from the sensitivity analyses that the results of WMA are dominantly governed by the assumption of the soil resistance distribution. The soil resistance distribution could be estimated with an acceptable accuracy within a variation of 5 % if the differences between calculated and measured values of the peak upward travelling force and final pile head displacement in WMA are in range of 20 % and 5 %, respectively. Similar criteria could be used in WMA to obtain the distribution of shear modulus with an accuracy of 20 %. If measurements of elastic shear wave velocities of the ground are available we could improve the accuracy of the identified shear modulus from wave matching analysis.

In **Chapter 4**, two series of static and dynamic pile load tests on an open-ended pipe pile (OP) and a close-ended pipe pile (CP) in a model ground of dry sand were carried out to validate the proposed numerical method. Although oscillation of pile axial force was found in WMA due to small-scale model test, overall agreement between calculated and the measured dynamic signals were obtained. Main findings from experimental study are listed as below:

(1) The wave matching analysis using the proposed method has the potential to estimate static responses of open-ended pipe piles as well as close-ended piles with a reasonable accuracy.

(2) Partially plugging mode occurs during penetration and dynamic load test while perfectly plugging mode happens in static load test. They can be found from analyses using the proposed numerical method.

(3) Shear modulus estimated from one-dimensional compression test could be used as the first assumption in WMA.

(4) Yield and ultimate capacity of the open-ended pipe pile is smaller than those of the close-ended pipe pile.

(5) Higher maximum shear resistance when the pile move downward was found from compression test of the close-ended pile, compared to maximum shear resistance in tension test when the pile move upward.

In **Chapter 5**, static and dynamic load test of the four test piles were carried out in a construction site in Viet Nam. Two of them were spun concrete piles designated as TSC1 and TSC2, and the other two piles were open-ended steel pipe piles designated as TSP1 and TSP2. The proposed numerical method was used to perform the wave matching analysis WMA of dynamic load tests (DLTs) in order to identify soil parameters used for determining the pile performance, to obtain information for selecting pile driving system and to examine the applicability of wave matching analysis (WMA). First, the test piling in detail including objectives, site conditions, preliminary pile design and results of the SLTs was described. Then, wave matching analyses (WMAs) of the DLTs of the two test piles, the TSC1 and TSP1, at initial driving and re-striking were conducted using the numerical approach developed by the authors, to identify the soil resistance distributions and to derive the corresponding static load-displacement relations using the soil parameters identified in the final WMA. Furthermore, the influence of cyclic loading process on the pile response was analytically examined. The soil parameters identified from the WMAs of the BOR tests were also used to predict the load-displacement relations of the other test piles, the TSC2 and TSP2, having different pile configurations and soil profiles from those of the TSC1 and TSP1.

The major results of the SLTs and the driving work of the TSC1 and TSP1 are as follows:

(1) The bearing capacities of the two test piles exceed two times the design working loads.

(2) Termination criteria based on the maximum value of settlement per blow estimated from the Hiley type formula with an ultimate bearing capacity estimated from an empirical equation based on SPT *N*-values can be adequately used for controlling the driving work.

From the WMAs of the TSC1 and TSP1, the following findings and implications were drawn:

(3) The static load-displacement curves derived from the final WMAs of DLTs were comparable with the results obtained from the SLTs.

(4) The pile which has been subjected to cyclic loading has similar yield and ultimate capacities to those of the piles subjected to monotonic loading.

(5) WMA using the proposed numerical approach can be used to predict the static load-displacement curves of the non-tested working piles based on the identified soil parameters of the tested piles.

(6) The "set-up" phenomenon was clearly found from the EOD test, through the BOR test, to the SLT. The thickness of the pile wall might have a great influence on the degree of "set-up" phenomenon.

(7) Shear moduli of soils to be used in WMA of piles at this particular site can be estimated from shear moduli at small strain level with reduction factors, about 0.1 for soft soils, 0.15 to 0.20 for medium soils and 0.25 to 0.40 for hard soils.

(8) Selection of the pile driving hammer based on the empirical equation in this study is reasonable, because the maximum compressive and tensile stresses along the pile calculated in the WMAs do not exceed the allowable values.

From the SLT results, the TSC2 and TSP2 also had the bearing capacities more than two times the design working loads. Load-displacement curves of the TSC2 and TSP2 predicted using the soil parameters identified from the WMAs of the TSC1 and TSP1 were comparable with the measured ones. This encourages the use of the WMA procedure proposed by the authors as a practical alternative to the conventional static load test.

Chapter 6, application of the proposed wave matching analysis to dynamic cone penetration test (DCPT) and standard penetration test (SPT) were presented. The proposed method was used to analyses dynamic signals obtained from DCPTs with dynamic measurement carried out in Shiga prefecture in Japan in order to obtain the soil resistance acting on the cone

and driving rod. Additionally, a simple method based on the conservative energy concept was used to estimate the total dynamic soil resistance.

The following findings were drawn from the limited analyses as follows:

(1) Driving efficiency of DCPTs and SPT varies from 60 to 80 %.

(2) Dynamic cone resistance estimated from measured energy based on the law of energy conservation are comparable with static cone resistance.

(3) "Set-up" phenomenon can be seen clearly between "initial blows" and "successive blows" due to their different rest periods.

(4) Static cone resistance identified from the final WMA are reasonable with static cone resistance obtained from CPT.

7.3 Recommendations

Although the applicability of the proposed WMA was demonstrated in this study by analysing of small-scale model tests in laboratory and a case study in Viet Nam, further researches should be considered on the following aspects:

(1) Carry out the DLT of the model piles in model ground of saturated soil in order to investigate the influence of the excess pore-water pressure on the pile response during driving.

(2) Collect more case histories in Viet Nam for improving the current pile design and pile driving control methods.

(3) Develop a numerical method for analysing the stress-wave propagation in a pile subjected to the horizontal impact force.

Appendix

Formulation of stiffness, damping and mass matrices in the proposed method

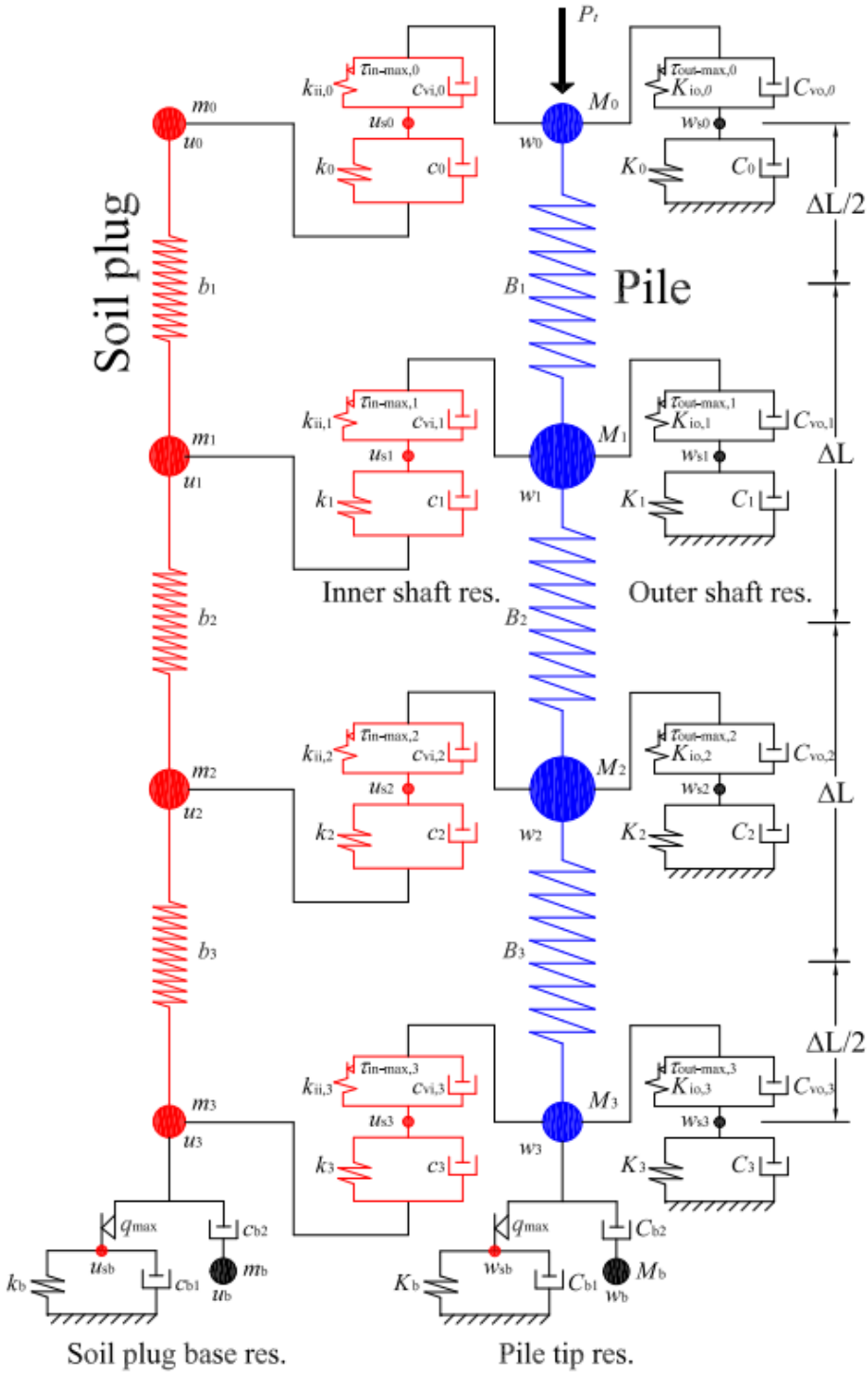

Modelling of the pile-soil system

Stiffness matrix, $[K]$

$\{U\}$	w_0	u_0	w_{s0}	u_{s0}	w_1	u_1	w_{s1}	u_{s1}	w_2	u_2	w_{s2}	u_{s2}	w_3	u_3	w_{s3}	u_{s3}	w_{sb}	u_{sb}	w_b	u_b
w_0	$B_1+K_{io,0}+k_{ii,0}$		$-K_{io,0}$	$-k_{ii,0}$	$-B_1$															
u_0		k_0+b_1		$-k_0$		$-b_1$														
w_{s0}	$-K_{io,0}$		$K_{io,0}+K_0$																	
u_{s0}	$-k_{ii,0}$	$-k_0$		$k_{ii,0}+k_0$																
w_1	$-B_1$				$B_1+B_2+K_{io,1}+k_{ii,1}$		$-K_{io,1}$	$-k_{ii,1}$	$-B_2$											
u_1		$-b_1$				$b_1+b_2+k_1$		$-k_1$		$-b_2$										
w_{s1}					$-K_{io,1}$		$K_{io,1}+K_1$													
u_{s1}					$-k_{ii,1}$	$-k_1$		$k_{ii,1}+k_1$												
w_2					$-B_2$				$B_2+B_3+K_{io,2}+k_{ii,2}$		$-K_{io,2}$	$-k_{ii,2}$	$-B_3$							
u_2						$-b_2$				$b_2+b_3+k_2$		$-k_2$		$-b_3$						
w_{s2}									$-K_{io,2}$		$K_{io,2}+K_2$									
u_{s2}									$-k_{ii,2}$	$-k_2$		$k_{ii,2}+k_2$								
w_3									$-B_3$				$B_3+K_{ib}+K_{io,3}+k_{ii,}$		$-K_{io,3}$	$-k_{ii,3}$	$-K_{ib}$			
u_3										$-b_3$				$b_3+k_{ib}+k_3$		$-k_3$		$-k_{ib}$		
w_{s3}													$-K_{io,3}$		$K_{io,3}+K_3$					
u_{s3}													$-k_{ii,3}$	$-k_3$		$k_{ii,3}+k_3$				
w_{sb}													$-K_{ib}$				$K_{ib}+K_b$			
u_{sb}														$-k_{ib}$				$k_{ib}+k_b$		
w_b																				
u_b																				

Damping matrix, $[C]$

$\{\dot{U}\}$	$\dot{w}_0$	$\dot{u}_0$	$\dot{w}_{s0}$	$\dot{u}_{s0}$	$\dot{w}_1$	$\dot{u}_1$	$\dot{w}_{s1}$	$\dot{u}_{s1}$	$\dot{w}_2$	$\dot{u}_2$	$\dot{w}_{s2}$	$\dot{u}_{s2}$	$\dot{w}_3$	$\dot{u}_3$	$\dot{w}_{s3}$	$\dot{u}_{s3}$	$\dot{w}_{sb}$	$\dot{u}_{sb}$	$\dot{w}_b$	$\dot{u}_b$
$\dot{w}_0$																				
$\dot{u}_0$		c_0		$-c_0$																
$\dot{w}_{s0}$			C_0																	
$\dot{u}_{s0}$		$-c_0$		c_0																
$\dot{w}_1$																				
$\dot{u}_1$						c_1		$-c_1$												
$\dot{w}_{s1}$							C_1													
$\dot{u}_{s1}$						$-c_1$		c_1												
$\dot{w}_2$																				
$\dot{u}_2$										c_2		$-c_2$								
$\dot{w}_{s2}$											C_2									
$\dot{u}_{s2}$										$-c_2$		c_2								
$\dot{w}_3$													C_{b2}						$-C_{b2}$	
$\dot{u}_3$														$c_{b2}+c_3$		$-c_3$				$-c_{b2}$
$\dot{w}_{s3}$															C_3					
$\dot{u}_{s3}$														$-c_3$		c_3				
$\dot{w}_{sb}$																	C_{b1}			
$\dot{u}_{sb}$																		c_{b1}		
$\dot{w}_b$													$-C_{b2}$						C_{b2}	
$\dot{u}_b$														$-c_{b2}$						c_{b2}

Mass matrix, $[M]$

$\{\ddot{U}\}$	$\ddot{w}_0$	$\ddot{u}_0$	$\ddot{w}_{s0}$	$\ddot{u}_{s0}$	$\ddot{w}_1$	$\ddot{u}_1$	$\ddot{w}_{s1}$	$\ddot{u}_{s1}$	$\ddot{w}_2$	$\ddot{u}_2$	$\ddot{w}_{s2}$	$\ddot{u}_{s2}$	$\ddot{w}_3$	$\ddot{u}_3$	$\ddot{w}_{s3}$	$\ddot{u}_{s3}$	$\ddot{w}_{sb}$	$\ddot{u}_{sb}$	$\ddot{w}_b$	$\ddot{u}_b$
$\ddot{w}_0$	M_0																			
$\ddot{u}_0$		m_0																		
$\ddot{w}_{s0}$																				
$\ddot{u}_{s0}$																				
$\ddot{w}_1$					M_1															
$\ddot{u}_1$						m_1														
$\ddot{w}_{s1}$																				
$\ddot{u}_{s1}$																				
$\ddot{w}_2$									M_2											
$\ddot{u}_2$										m_2										
$\ddot{w}_{s2}$																				
$\ddot{u}_{s2}$																				
$\ddot{w}_3$													M_3							
$\ddot{u}_3$														m_3						
$\ddot{w}_{s3}$																				
$\ddot{u}_{s3}$																				
$\ddot{w}_{sb}$																	M_b			
$\ddot{u}_{sb}$																		m_b		
$\ddot{w}_b$																				
$\ddot{u}_b$																				

Procedure of Wave Matching Analysis

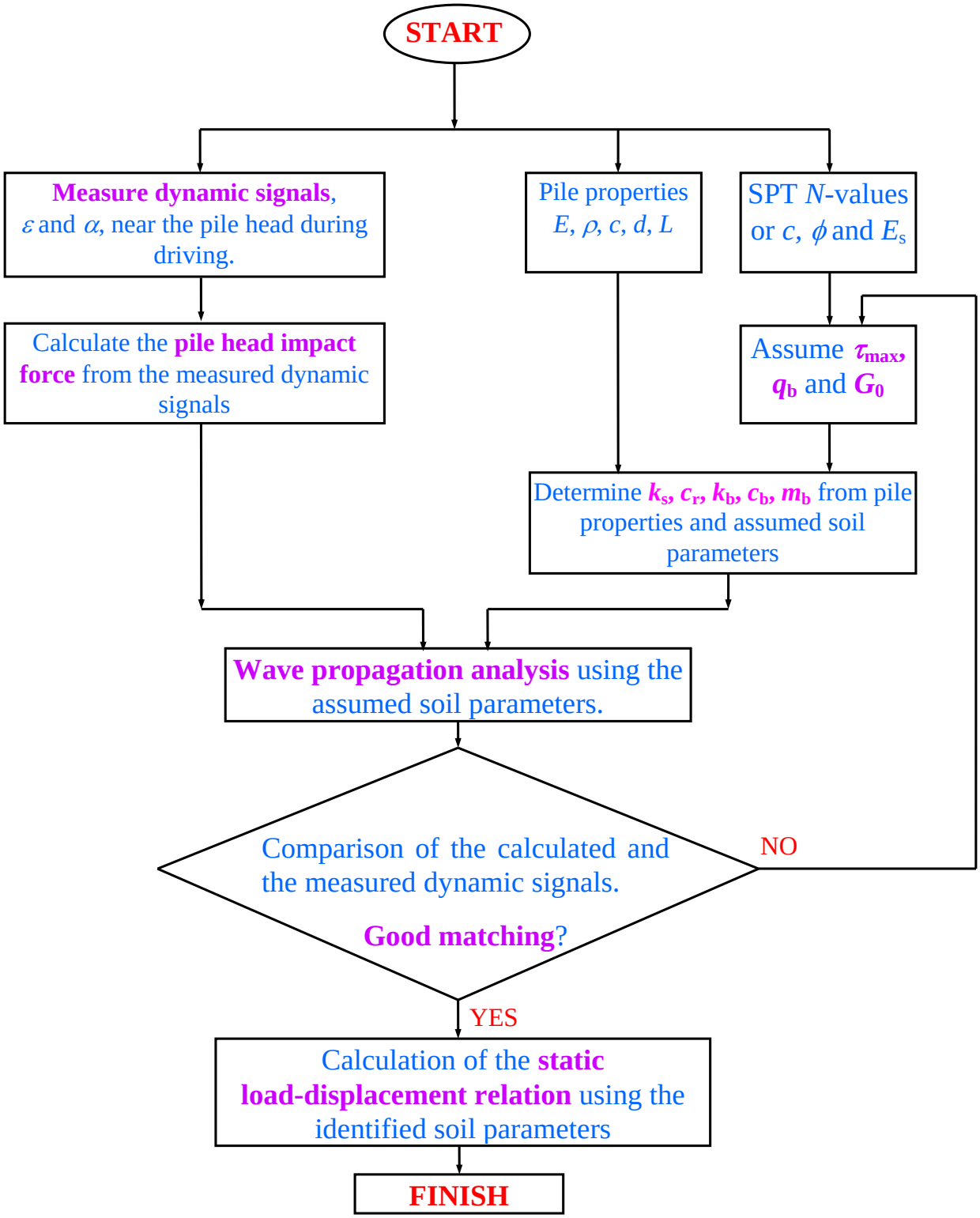

Guideline for Wave Matching Analysis

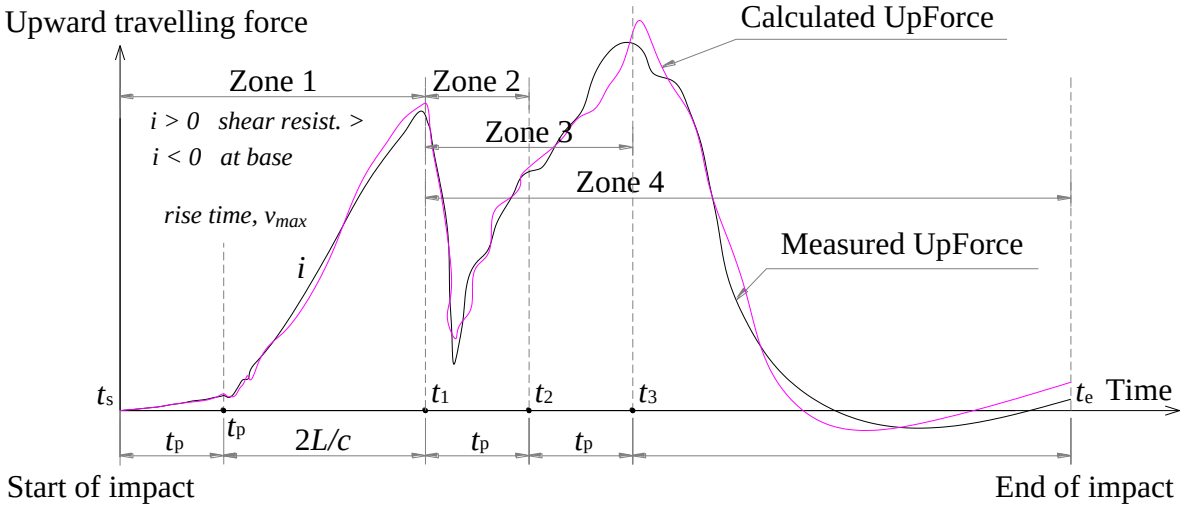

Wave Matching Analysis using upward travelling force

In WMA, the non-linear coefficients Rfs and Rfb can be assumed to be zero for promptly identifying soil resistances and shear moduli for each soil layer and soil at the pile tip. The following procedure is used:

In Zone 1: From t_s to $t_1 = t_p + 2L/c$: Shaft resistance develop.

τ_{max} are first changed to have similar inclination, i, and the peak upward travelling force. Then G varies in range of 400 to 1000 times τ_{max}.

In Zone 2. From $t_p + 2L/c$ to $t_2 = t_1 + t_p$: Tip resistance develop.

q_{max} are changed to get a reasonable value of bottom force, then G_b varies in range of 5 to 10 times q_{max}.

In Zone 4. From $t_p + 2L/c$ to t_e, end of impact: Unloading behaviour.

G_{unload} or τ_{max}^{neg} are changed to get a good matching of final displacement.

After identifying the soil properties from WMA, R_{fs} and R_{fb} can be used to calculate the static response. If the pile is treated as a friction pile, R_{fs} should vary from 0.5 to 0.9 while R_{fb} ranges between 0.2 and 0.5. If the pile is end-bearing pile, R_{fs} can vary from 0.2 to 0.5 while R_{fb} ranges between 0.5 and 0.9.

Input manual for KWAVE-MT program

FOR WAVE PROPAGATION ANALYSIS IN AN OPEN-ENDED PIPE PILE

PROGRAM STRUCTURE

1. Main menu of the KWaveMT

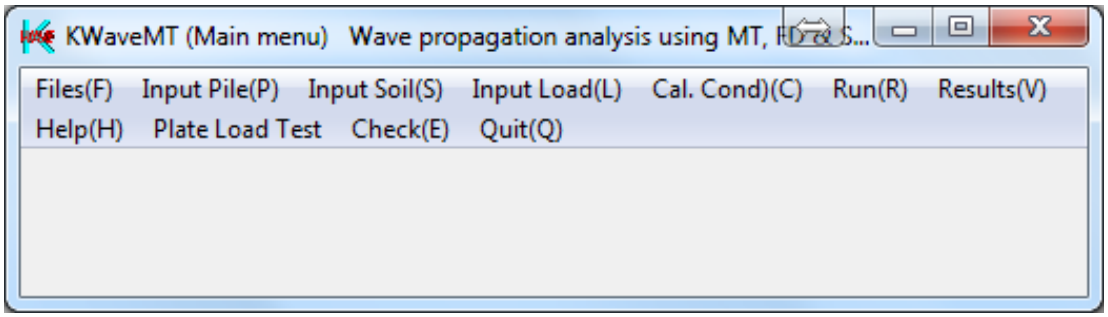

Files → **Read file** → **Pile & Soil**: Open input data from the input file (*.inp)

→ **Dynamic Signals**: Read data file from PDI measurements

→ **SLT Results**: Read data file from Static Load Test

→ **Save file** → **Save Input File**: Save input data to the input file (*.inp)

→**Save Extrapolated Head Force**: Save extrapolated head force calculated from measured signals to file

→ **Quit** : Quit program

Input Pile : Input pile properties

Input Soil → **Outer Soil** : Input outer soil parameters

→ **Inner Soil** : Input inner soil parameters

Input Load → **Measured Load** : Input impact head force from data file

→ **Simulate Load** : Create the input impact head force

→ **Static Load** : Create the static head force

Run → **DLT Analysis with Sine Load** (Smith's method)

→ **WMA with Measured Pile Head Force** (Smith's method)

→ **DLT Analysis with Sine Load** (Matrix method)

→ **WMA with Measured Pile Head Force** (Matrix method)

→ **DLT Analysis using a Falling Hammer** (Matrix method)

→ **SLT**: Calculate the static load-displacement curve

Results → **Waveforms**: Show the waveform of force, displacement, velocity and acceleration with time of each node and element.

→ **Distribution with time**: Show axial force, mobilised shaft resistance with depth at any time.

→ **Static curve or Driving Energy**: Calculate the static curve and show driving energy transferred to the pile

→ **Soil resistance mobilisation**: Show the mobilised soil resistances with time any depth.

→ **Distribution of the maximum resistances**: Show the maximum mobilised soil resistances with depth.

Check : Check the soil properties after modelling

Help : About KWaveMT

2. Example analysis of the pile TSC1 in Chapter 6.

2.1 "Input Pile" Menu

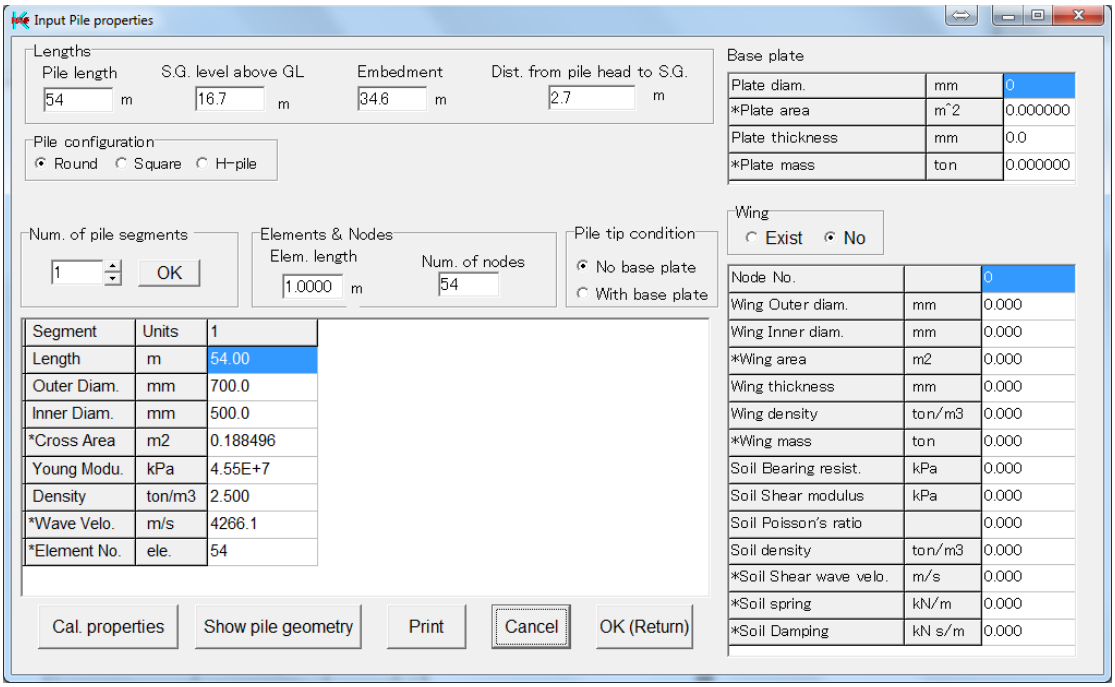

2.2 “Input Soil” Menu

Input Soil → Outer soil

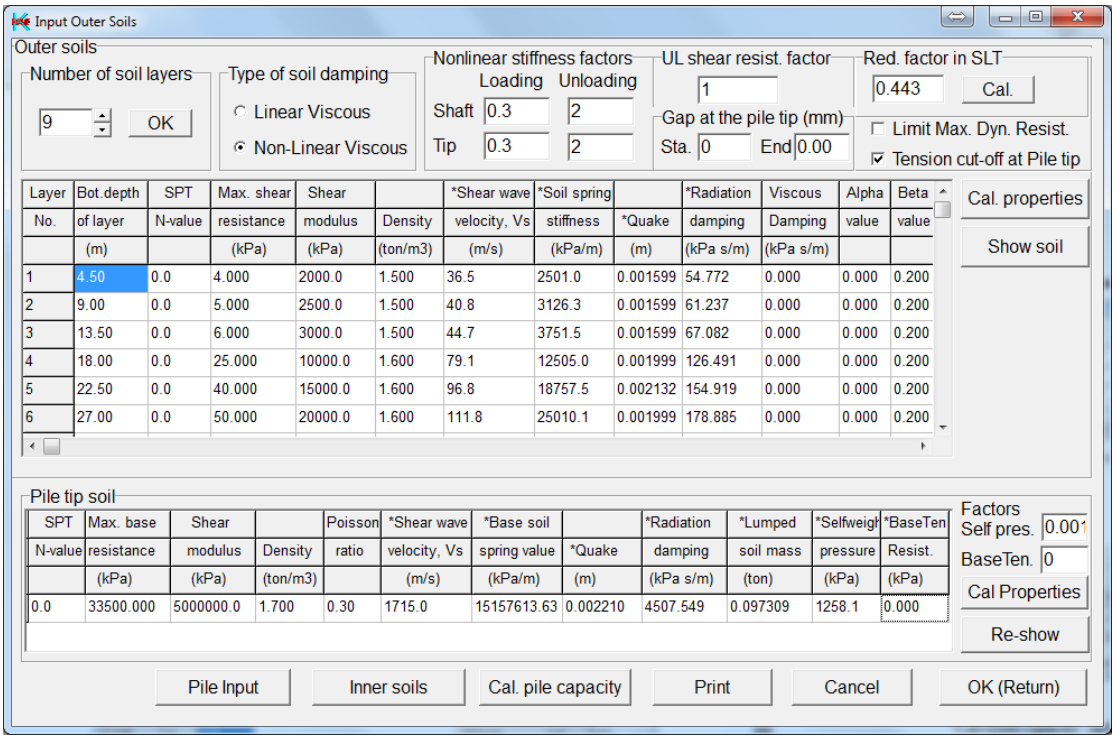

Input Soil → Inner soil

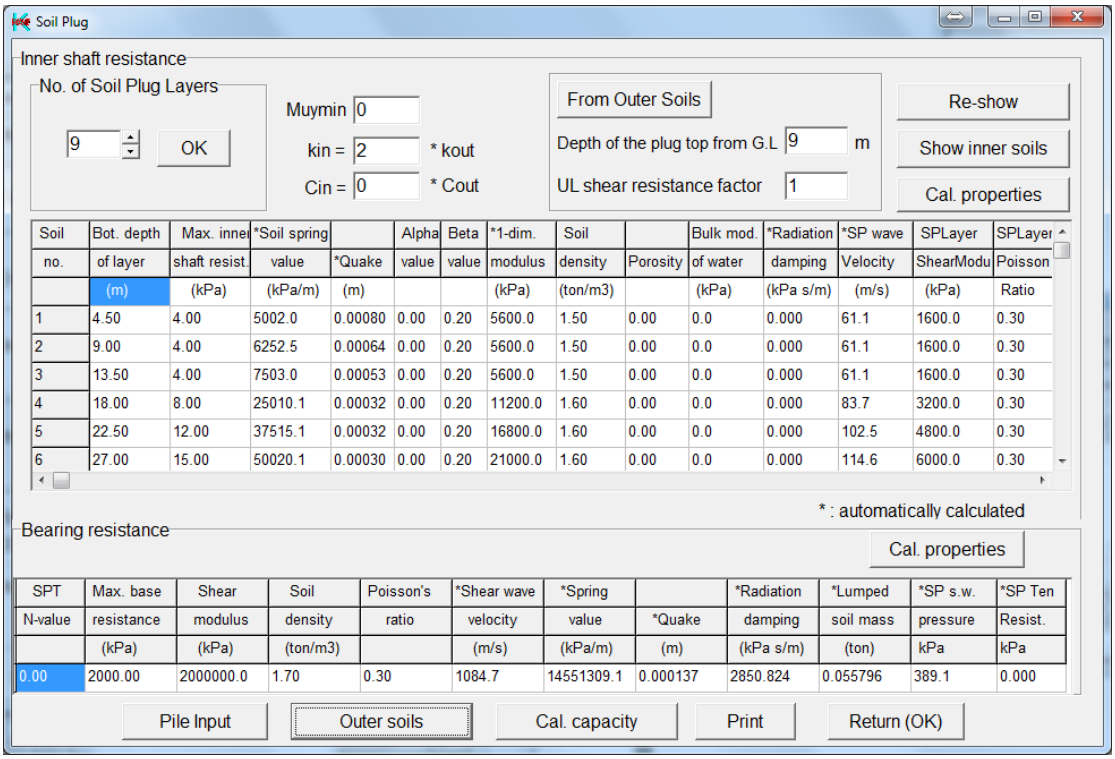

"**Calculate capacity**" option: to estimate the ultimate capacity

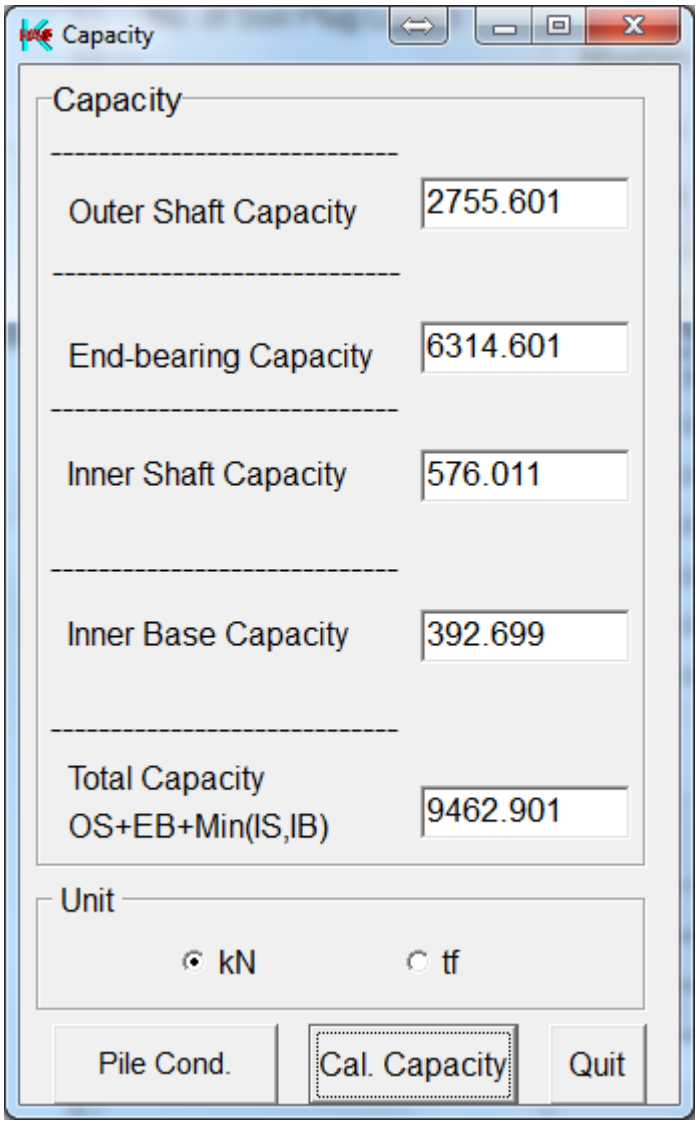

2.2 Input Head Load:

Files → Read file → Dynamic Signals: Read data file from PDI measurements

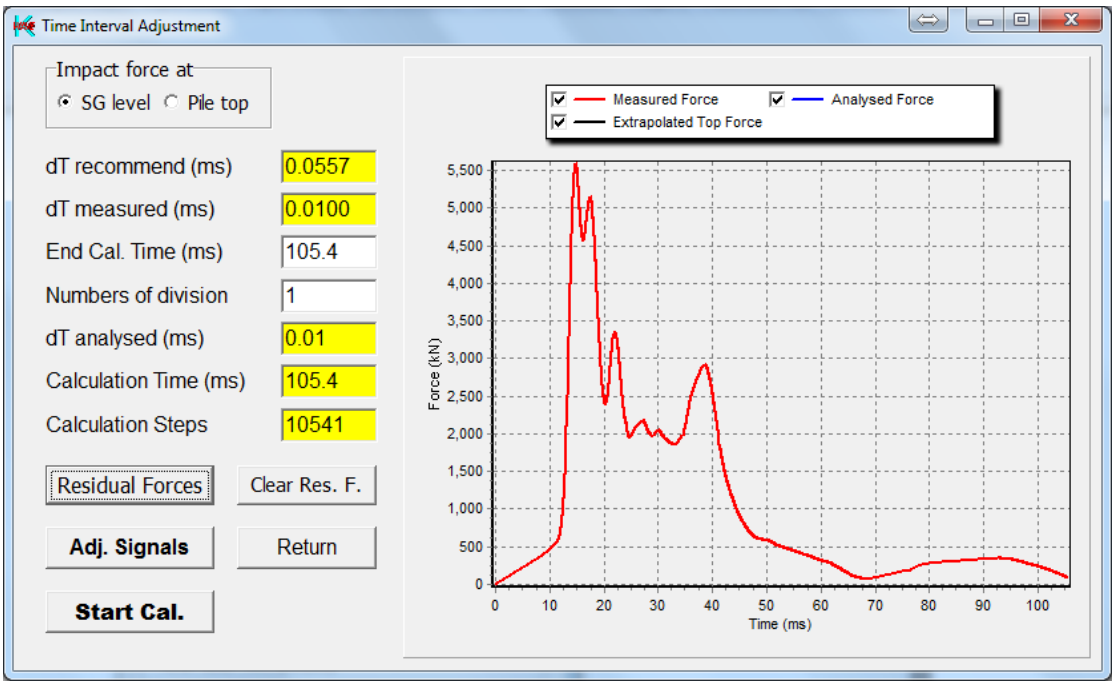

then **Start Cal.**

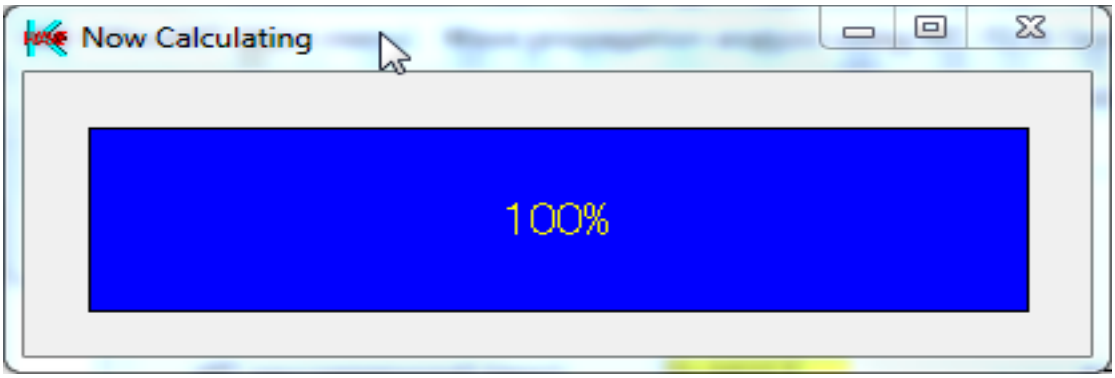

and **Finish**

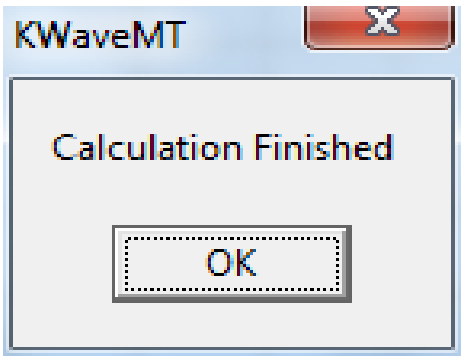

2.3 Results of dynamic analysis

Show WMA results:

Results → Waveforms

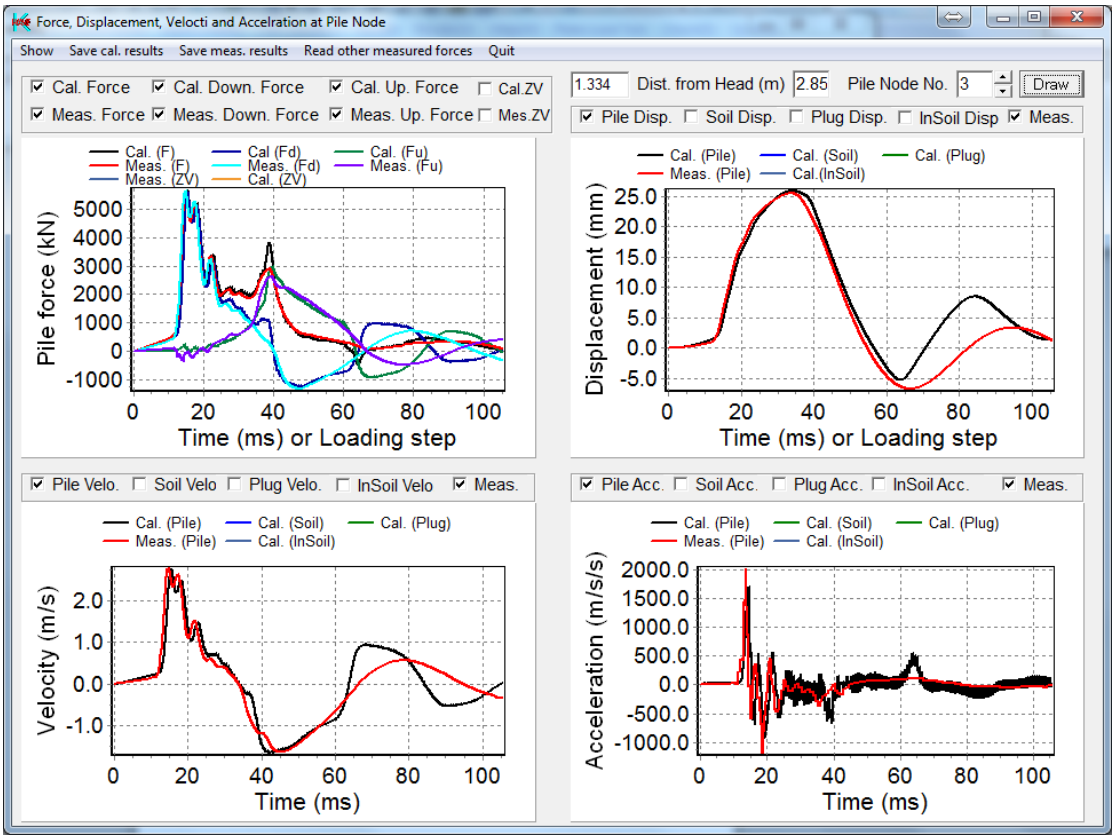

Show Distribution of pile axial force, soil plug force and shaft resistance

Results → Distribution with time

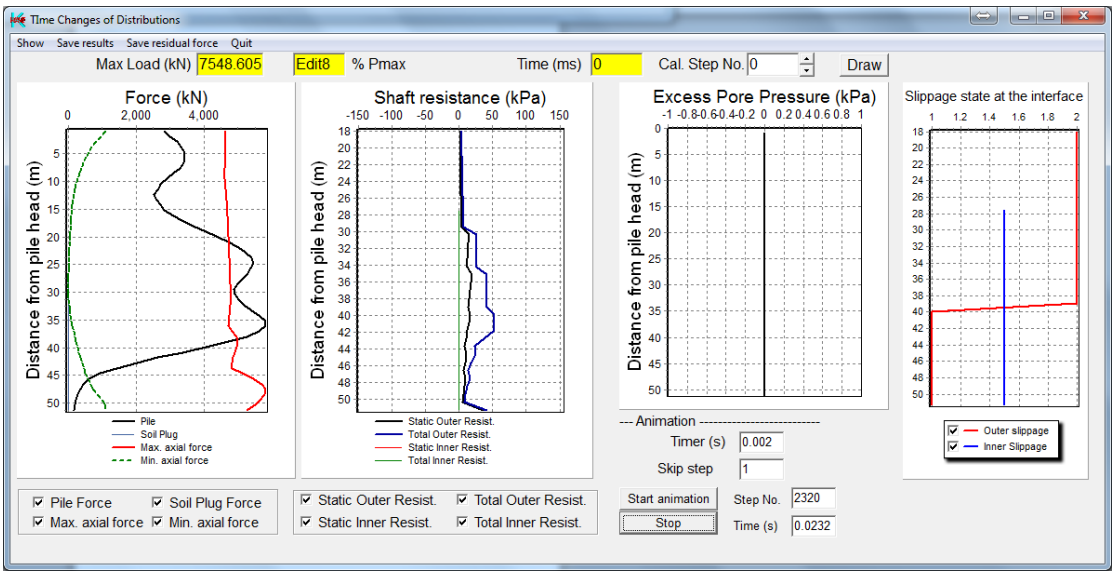

Show Mobilisation of soil resistances

Results → Soil resistance mobilisation

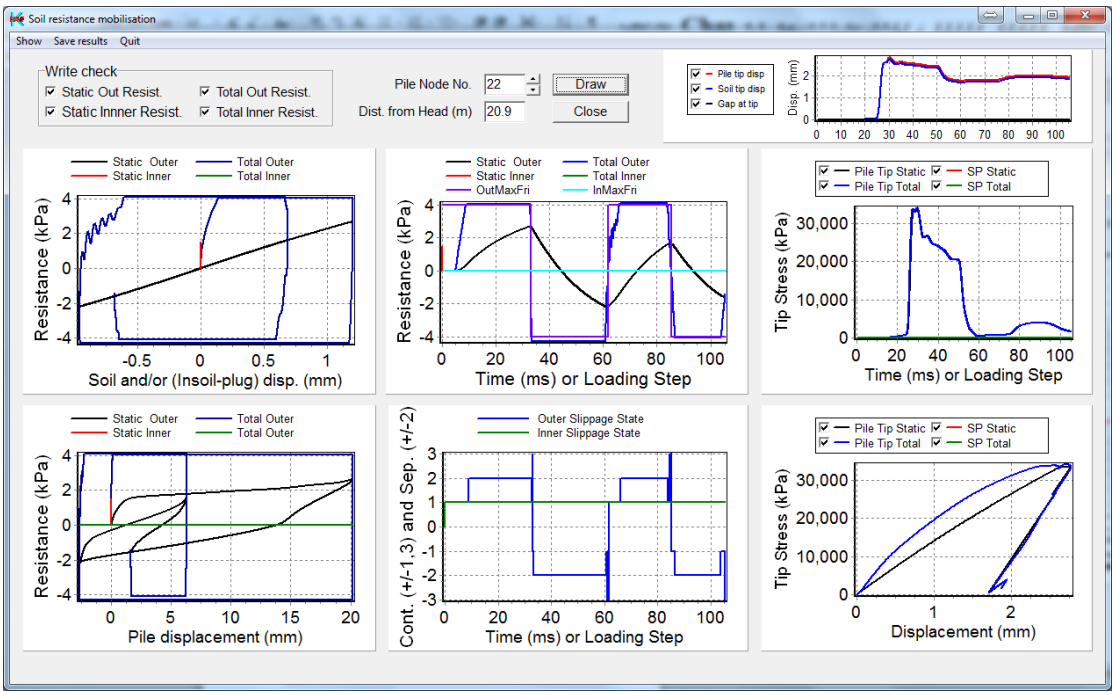

Show Driving energy

Results → Load vs displacement & Driving energy

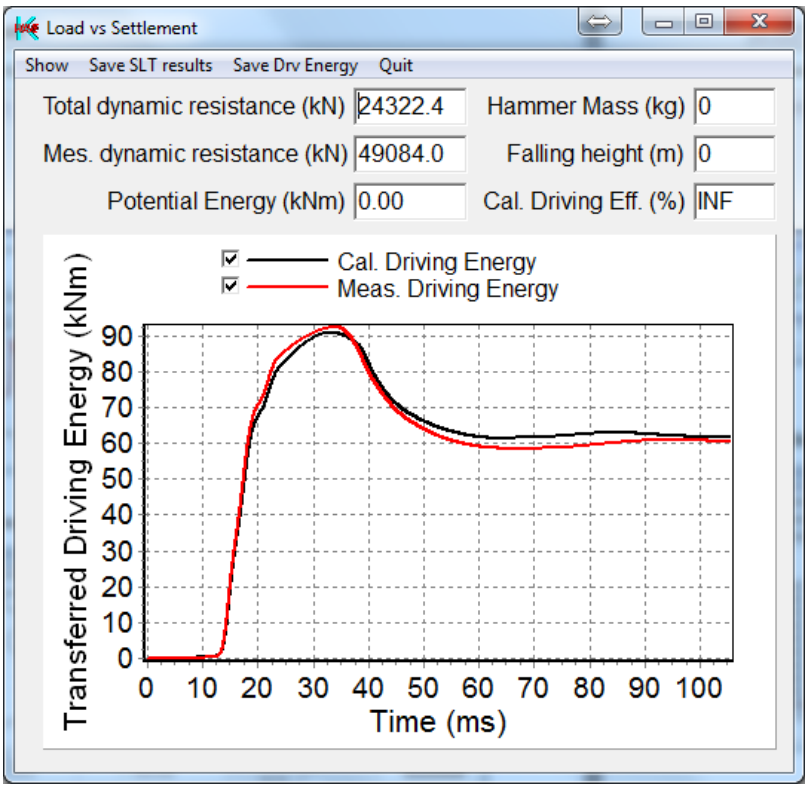

2.4 Static analysis

Input static force

Input Load → Static Load

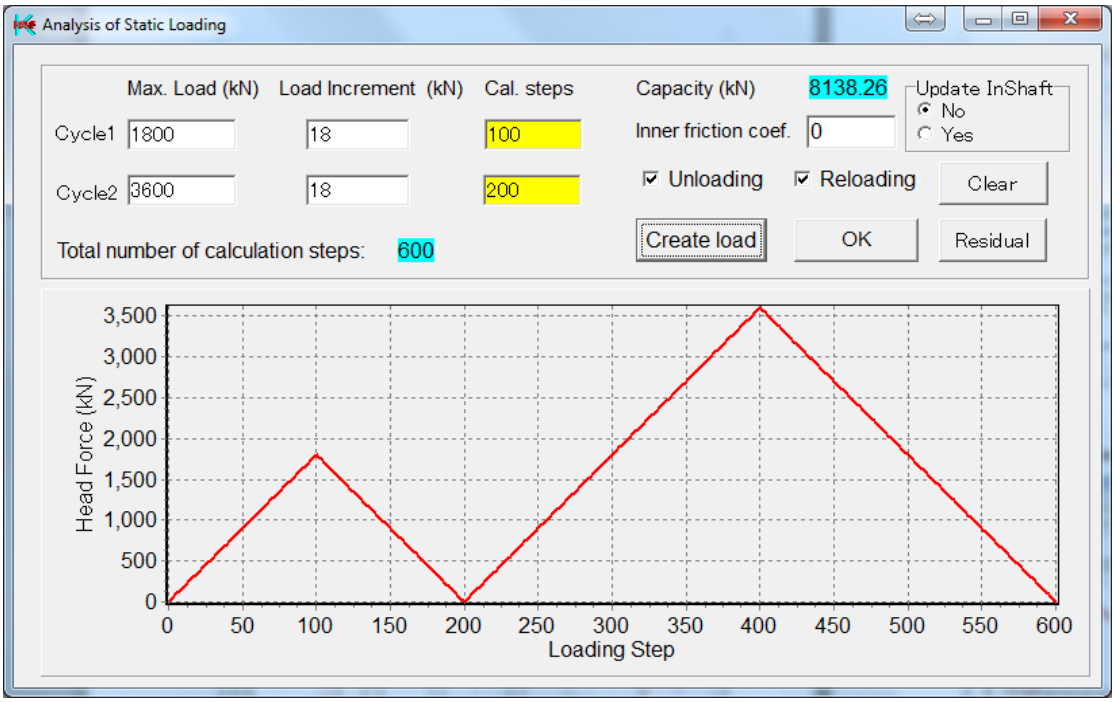

Calculate the static load-displacement curve

Run → SLT

Show the static load-displacement curve and compare with measured curve

Files → Read file → SLT Results: Read data file from Static Load Test

Results → Load vs displacement & Driving energy